POLITECHNIKA ŚLĄSKA

Wydział Chemiczny

Katedra Fizykochemii i Technologii Polimerów

mgr inż. Dominika Czerwińska-Główka

PRACA DOKTORSKA

Elektroaktywne powierzchnie polimerowe do sterowania wzrostem biofilmu bakteryjnego i komórkowego

Promotor: dr hab. inż. Katarzyna Krukiewicz, prof. Politechniki Śląskiej

GLIWICE 2022

Spis treści

Wykaz publikacji wchodzących w skład rozprawy

Rozprawę doktorską stanowi cykl pięciu przedstawionych poniżej publikacji. Doktorant jest pierwszym autorem wszystkich prac wchodzących w skład rozprawy doktorskiej.

A1. **Czerwińska-Główka D**., Krukiewicz K., *A journey in the complex interactions between electrochemistry and bacteriology: From electroactivity to electromodulation of bacterial biofilms,* Bioelectrochemistry 131 (2020) 1-14 (art. no. 107401)
IF: 5,373
Punktacja MNiSW: 100

A2. **Czerwińska-Główka D**., Przystaś W., Zabłocka-Godlewska E., Student S., Cwalina B., Łapkowski M., Krukiewicz K. *Bacterial surface colonization of sputter-coated platinum films,* Materials 13(12) (2020) 1-12 (art. no. 2674)
IF: 3,623
Punktacja MNiSW: 140

A3. **Czerwińska-Główka D**., Przystaś W., Zabłocka-Godlewska E., Student S., Cwalina B., Łapkowski M., Krukiewicz K., *Electrically-responsive antimicrobial coatings based on a tetracycline-loaded poly(3,4-ethylenedioxythiophene) matrix,* Materials Science and Engineering: C 123 (2021) 1-11 (art. no. 112017)
IF: 7,328
Punktacja MNiSW: 140

A4. **Czerwińska-Główka D**., Skonieczna M., Barylski A., Golba S., Przystaś W., Zabłocka-Godlewska E., Student S., Cwalina B., Krukiewicz K., *Bifunctional conducting polymer matrices with antibacterial and neuroprotective effects*, Bioelectrochemistry 144 (2021) 1-14 (art. no. 108030)
IF: 5,373
Punktacja MNiSW: 100

A5. **Czerwińska-Główka D**., Krukiewicz K., *Guidelines for a Morphometric Analysis of Prokaryotic and Eukaryotic Cells by Scanning Electron Microscopy*, Cells 10(12), (2021) 1-17 (art. no. 3304)
IF: 6,600
Punktacja MNiSW: 140

A6. Krukiewicz K, **Czerwińska-Główka D**., zgłoszenie patentowe krajowe nr P.434000 z dnia 19.05.2020, *Przewodząca powłoka polimerowa o właściwościach bakteriobójczych i działaniu neuroprotekcyjnym, sposób jej wytwarzania i zastosowania*

Udział autorski doktorantki

1. **Czerwińska-Główka D**., Krukiewicz K., *A journey in the complex interactions between electrochemistry and bacteriology: From electroactivity to electromodulation of bacterial biofilms,* Bioelectrochemistry 131 (2020) 1-14 (art. no. 107401)

   Mój udział w powstaniu tej pracy polegał na przeglądzie literatury oraz zredagowaniu tekstu manuskryptu.
   Mój wkład szacuję na 80 %.

2. **Czerwińska-Główka D**., Przystaś W., Zabłocka-Godlewska E., Student S., Cwalina B., Łapkowski M., Krukiewicz K. *Bacterial surface colonization of sputter-coated platinum films,* Materials 13(12) (2020) 1-12 (art. no. 2674)

   Mój udział w powstaniu tej pracy polegał na przeglądzie literatury, opracowaniu metodologii, przygotowaniu materiałów do badań, charakterystyce morfologii i zwilżalności powierzchni, przeprowadzeniu badań mikrobiologicznych, zebraniu i analizie wyników, opracowaniu wykresów i rysunków oraz zredagowaniu tekstu manuskryptu.
   Mój wkład szacuję na 65 %.

3. **Czerwińska-Główka D**., Przystaś W., Zabłocka-Godlewska E., Student S., Cwalina B., Łapkowski M., Krukiewicz K., *Electrically-responsive antimicrobial coatings based on a tetracycline-loaded poly(3,4-ethylenedioxythiophene) matrix,* Materials Science and Engineering: C 123 (2021) 1-11 (art. no. 112017)

   Mój udział w powstaniu tej pracy polegał na przeglądzie literatury, opracowaniu metodologii, polimeryzacji elektrochemicznej matryc polimerowych, pomiarach spektroskopowych, charakterystyce morfologii i zwilżalności powierzchni, przeprowadzeniu badań mikrobiologicznych, zebraniu i analizie wyników, opracowaniu wykresów i rysunków, zredagowaniu tekstu manuskryptu.
   Mój wkład szacuję na 65 %.

4. **Czerwińska-Główka D**., Skonieczna M., Barylski A., Golba S., Przystaś W., Zabłocka-Godlewska E., Student S., Cwalina B., Krukiewicz K., *Bifunctional conducting polymer matrices with antibacterial and neuroprotective effects*, Bioelectrochemistry 144 (2021) 1-14 (art. no. 108030)

   Mój udział w powstaniu tej pracy polegał na przeglądzie literatury, opracowaniu metodologii, polimeryzacji elektrochemicznej matryc polimerowych, pomiarach spektroskopowych, charakterystyce morfologii i zwilżalności powierzchni, przeprowadzeniu badań mikrobiologicznych, przeprowadzeniu badań z wykorzystaniem linii komórkowej, zebraniu i analizie wyników, opracowaniu wykresów i rysunków, zredagowaniu tekstu manuskryptu.
   Mój wkład szacuję na 55 %.

5. **Czerwińska-Główka D**., Krukiewicz K., *Guidelines for a Morphometric Analysis of Prokaryotic and Eukaryotic Cells by Scanning Electron Microscopy*, Cells 10(12), (2021) 1-17 (art. no. 3304)

   Mój udział w powstaniu tej pracy polegał na przeglądzie literatury, zaprojektowaniu rysunków oraz zredagowaniu tekstu manuskryptu.
   Mój wkład szacuję na 80 %.

6. Krukiewicz K, **Czerwińska-Główka D**., zgłoszenie patentowe krajowe nr P.434000 z dnia 19.05.2020, *Przewodząca powłoka polimerowa o właściwościach bakteriobójczych i działaniu neuroprotekcyjnym, sposób jej wytwarzania i zastosowania*

   Mój udział w powstaniu tej pracy polegał na opracowaniu metodologii, polimeryzacji elektrochemicznej matryc polimerowych, pomiarach spektroskopowych, charakterystyce morfologii i zwilżalności powierzchni, przeprowadzeniu badań mikrobiologicznych, przeprowadzeniu badań z wykorzystaniem linii komórkowej, zebraniu i analizie wyników, opracowaniu wykresów i rysunków.
   Mój wkład szacuję na 40 %.

Wykaz pozostałych publikacji

1. Krukiewicz K., Kowalik A., **Czerwińska-Główka D**., Biggs M..P., *Electrodeposited poly(3,4-ethylenedioxypyrrole) films as neural interfaces: Cytocompatibility and electrochemical studies*, Electrochimica Acta 302 (2019) 21-30
   IF: 6,215
   Punktacja MNiSW: 100
2. Skorupa M., Więcławska D., **Czerwińska-Główka D**., Skonieczna M., Krukiewicz K., *Dopant-Dependent Electrical and Biological Functionality of PEDOT in Bioelectronics*, Polymers 13(12) (2021) 1-15 (art. no. 1948)
   IF = 4,329
   Punktacja MNiSW: 100
3. Nyga A., **Czerwińska-Główka D**., Krzywiecki M., Przystaś W., Zabłocka-Godlewska E., Student S., Kwoka M., Data P., Blacha-Grzechnik A., *Covalent Immobilization of Organic Photosensitizers on the Glass Surface: Toward the Formation of the Light-Activated Antimicrobial Nanocoating*, Materials 14(11) (2021) 1-15 (art. no. 3093)
   IF = 3,623
   Punktacja MNiSW: 140

Wykaz skrótów

Ag/AgCl	elektroda chlorosrebrowa
CA	kąt zwilżania (ang. *contact angle*)
CIC	pojemność „wstrzykiwania" ładunku (ang. *charge injection capacity*)
CSC	pojemność matrycy (ang. *charge storage capacity*)
CV	woltamperometria cykliczna (ang. *cyclic voltammetry*)
EDOP	3,4-etylenodioksypirol
EDOT	3,4-etylenodioksytiofen
EIS	elektrochemiczna spektroskopia impedancyjna (ang. *electrochemical impedance spectroscopy*)
FTIR	spektroskopia w podczerwieni z transformacją Fouriera (ang. *Fourier-transform infrared spectroscopy*)
ISO	Międzynarodowa Organizacja Normalizacyjna (ang. *International Organization for Standarization*)
PBS	bufor fosforanowy (ang. *phosphate- buffered saline*)
PEDOP	poli(3,4-etylenodioksypirol)
PEDOT	poli(3,4-etylenodioksytiofen)
PI	jodek propidyny
S_a	chropowatość powierzchni (średnie arytmetyczne odchylenie wysokości nierówności powierzchni od płaszczyzny odniesienia)
SEM	skaningowa mikroskopia elektronowa (ang. *scanning electron microscopy*)
Tc	tetracyklina, $C_{22}H_{24}N_2O_8$ ((4S,4aS,5aS,6S,12aS)-4-(dimetyloamino)-3,6,10,12,12a-pentahydroksy-6-metylo-1,11-diokso-1,4,4a,5,5a,6,11,12a-oktahydrotetraceno-2-karboksyamid)

1. Wstęp

Jednym z największych wyzwań współczesnej medycyny jest walka z chorobami układu nerwowego. Choroby neurodegeneracyjne skutkują postępującym uszkodzeniem komórek nerwowych, prowadzącym do zaburzeń związanych z poruszaniem się, utratą pamięci oraz spadkiem sprawności umysłowej. Przykładem chorób neurodegeneracyjnych są choroby Parkinsona, Alzheimera czy Huntingtona. Choć diagnozowane są one od dawna, jednak wciąż brakuje metod umożliwiających skuteczną terapię. Na przełomie ostatnich lat obserwuje się tendencję wzrostową liczby pacjentów cierpiących na choroby neurodegeneracyjne. Co więcej, Światowa Organizacja Zdrowia na podstawie danych statystycznych przewiduje, że ze względu na wydłużającą się długość życia liczba zachorowań będzie stale wzrastać (Rys.1a) [1]. Wiąże się to również ze wzrostem liczby publikacji naukowych dotyczących chorób neurodegeneracyjnych i możliwości ich leczenia (Rys.1b).

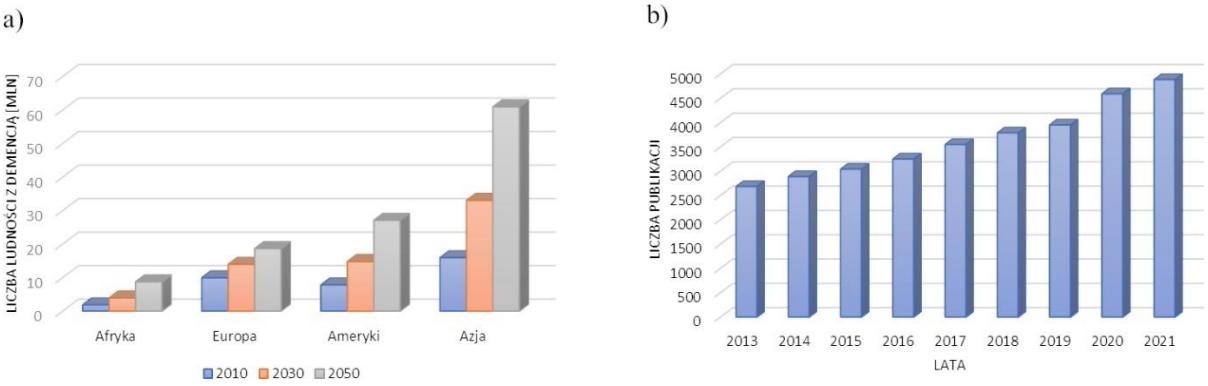

Rys. 1. a) Liczba ludzi z demencją (mln) w roku 2010 oraz przewidywana liczba chorych w latach 2030 i 2050 [2], b) liczba publikacji naukowych dotyczących chorób neurodegeneracyjnych opublikowanych w latach 2013-2021 według bazy Scopus.

Pomocą w diagnostyce i terapii chorób neurodegeneracyjnych służyć mogą urządzenia biomedyczne, w których kluczową rolę pełnią elektrody neurologiczne. Neuroelektrody stanowią znaczne osiągnięcie w neurotechnice, umożliwiając kontrolę nad elektrycznie aktywnym elementem budulcowym układu nerwowego - neuronami. Urządzenia biomedyczne umieszczone w centralnym lub obwodowym układzie nerwowym pozwalają zarówno na rejestrację potencjałów czynnościowych neuronów, jak również ich stymulację za pomocą zewnętrznych impulsów elektrycznych [3]. Elektrostymulacja układu nerwowego to metoda, której początki sięgają XVIII wieku i pionierskich badań L. Galvaniego oraz A. Volty. W ślad za wysiłkami włoskich uczonych, G. Duchenne w XIX wieku wykazał, że prąd

elektryczny może służyć do przezskórnego stymulowania mięśni [4,5]. Natomiast w 1920 roku W. Hess jako pierwszy wszczepił elektrody do mózgów kotów, demonstrując skuteczność neurostymulacji [6].

Współcześnie stymulacja elektryczna układu nerwowego jest wykorzystywana w leczeniu urazów rdzenia kręgowego [7], porażenia mózgowego [8–10], do zmniejszania częstości pojawiania się objawów choroby Parkinsona (głęboka stymulacja mózgu) [11] czy epilepsji (stymulacja nerwu błędnego) [12], a także w celu przywrócenia słuchu (implanty ślimakowe) [13] lub wzroku (protezy siatkówki) [14]. Niemniej jednak, stosowane implanty neuronowe mają szereg ograniczeń. Dla przykładu, wciąż trwają badania nad poprawą biokompatybilności na styku elektroda/tkanka nerwowa [15]. Obecnie biokompatybilność wyrobu medycznego jest oceniana zgodnie ze standardowymi normami Międzynarodowej Organizacji Normalizacyjnej (ISO) (ISO 10993) [16]. Uwzględniają one między innymi wpływ wyrobów medycznych na tkanki, badania cytotoksyczności *in vitro*, ocenę miejscowej reakcji po implantacji czy ocenę biozgodności. Podstawowym celem badań zgodnie z przedstawionymi normami jest obniżenie ryzyka biologicznego wynikającego z zastosowania nowych materiałów bioinżynieryjnych.

W celu opracowania odpowiedniego materiału elektrodowego należy wziąć pod uwagę zarówno skład chemiczny podłoża, jak również jego cechy fizykochemiczne, w tym topografię powierzchni, porowatość, hydrofobowość i ładunek powierzchniowy [17,18]. Ponadto, potencjalne elektrody powinny być niewielkich rozmiarów oraz powinny zapewniać sprawne przenoszenie ładunku elektrycznego, co związane jest z niską impedancją materiału i możliwością akumulowania ładunku [19,20]. Istotne jest również, aby materiał charakteryzował się stabilnością (elektryczną i mechaniczną) w warunkach fizjologicznych oraz podczas sterylizacji (sterylizacja etanolem, tlenkiem etylenu, autoklawowanie, promieniowanie UV, itp.).

Ze względu na bardzo dobre przewodnictwo, stabilność oraz wielokrotnie potwierdzoną biokompatybilność, obecnie jako neuroelektrody stosuje się metale szlachetne, zwłaszcza platynę i jej stopy [21,22]. Jednak w dłuższej perspektywie niedopasowanie mechaniczne między miękką, żywą tkanką, a twardą powierzchnią implantu nerwowego może prowadzić do powstawania chronicznego stanu zapalnego i aktywacji komórek glejowych, a w konsekwencji do degeneracji neuronów i powstania blizny glejowej, co prowadzi do utrudnienia rejestracji sygnałów komórkowych oraz zmniejszenia skuteczności stymulacji elektrycznej [3,23]. W związku z tym, w ostatnich latach pojawiło się wiele prac

badawczych nad alternatywnymi materiałami, które mogłyby sprostać wymaganiom stawianym elektrodom neurologicznym.

Istotnym problemem bezpośrednio związanym z wszczepialnymi urządzeniami biomedycznymi są infekcje bakteryjne [24]. Zakażenia szpitalne wiążą się z długotrwałym leczeniem, mogą prowadzić do obniżenia jakości życia, a w niektórych przypadkach nawet do śmierci. Co więcej, stanowią one powszechny problem w wielu oddziałach szpitalnych (Rys. 2).

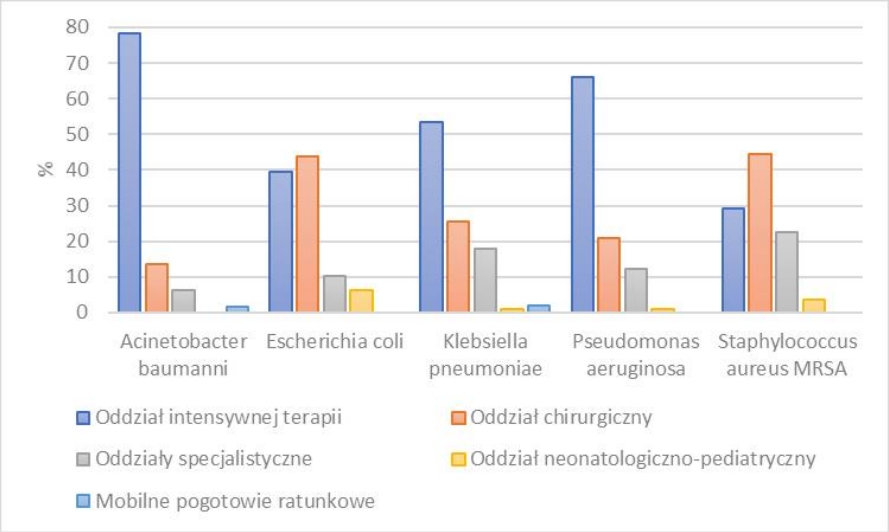

Rys. 2. Zakażenia bakteryjne zgłoszone w latach 2017-2018 w Hrabstwie Mures w Rumunii (1024 pacjentów) w poszczególnych oddziałach szpitalnych [25].

Oprócz ryzyka rozwinięcia się zakażenia okołowszczepowego, obecność biofilmu bakteryjnego osadzonego na powierzchni implantu znacznie utrudnia integrację komórek nerwowych z urządzeniem biomedycznym [26]. Rozwój biofilmu rozpoczyna się wraz z osadzeniem się bakterii na powierzchni materiału na skutek działania sił Van der Waalsa, oddziaływań kwasowo-zasadowych lub sił elektrostatycznych [27]. Następnie bakterie zaczynają wytwarzać pozakomórkowe substancje polimerowe, co daje im możliwość proliferacji. Funkcjonowanie bakterii w biofilmie możliwe jest dzięki komunikacji, która odbywa się na drodze sygnałów chemicznych [28,29] i elektrycznych [30,31] regulujących jego wzrost. Komunikacja na drodze sygnalizacji chemicznej (ang. *quorum sensing*) odbywa się poprzez produkcję i wyczuwanie określonych cząsteczek umożliwiających rozpoznanie otoczenia przez bakterie [32,33]. Natomiast sygnalizacja na drodze elektrycznej odbywa się poprzez przesyłanie impulsów elektrycznych za pomocą kanałów potasowych, w których zachodzi propagacja przestrzennie uporządkowanych fal [30,34]. Struktura biofilmu

bakteryjnego zapewnia mu przyczepność, trwałość i odporność na środowisko zewnętrzne, a tym samym możliwość przetrwania w najtrudniejszych warunkach [35,36]. Jedną z bakterii, które powszechnie powodują skażenie urządzeń medycznych oraz prowadzą do licznych zakażeń szpitalnych jest *Escherichia coli* [37,38]. Jest ona jedną z najbardziej znanych bakterii Gram-ujemnych i służy jako organizm modelowy dla badań w inżynierii biologicznej i mikrobiologii przemysłowej. Pałeczka *Escherichia coli* to bakteria o średniej długości 1–2 μm i szerokości 0,5–1,0 μm, ale jej wymiary mogą ulec zmianie w zależności od dostępności pożywki i jej bogactwa w składniki odżywcze [39,40].

Obecnie powszechną praktyką lekarską w walce z infekcjami bakteryjnymi jest terapia z wykorzystaniem antybiotyków. Wykazano jednak, że ze względu na utrudnioną zdolność dyfuzji dojrzały biofilm jest znacznie trudniejszy do usunięcia za pomocą antybiotyku niż pojedyncze bakterie. Jednocześnie zastosowanie zbyt wysokiego stężenia leku nie jest wskazane, ponieważ może okazać się toksyczne dla zdrowych komórek [41]. Jednym z czynników, które mogą regulować żywotność bakterii jest ładunek elektryczny. Jak wskazują liczne doniesienia literaturowe [42], równoczesne zastosowanie środków bakteriobójczych z polem elektrycznym zwiększa skuteczność działania antybiotyków, co znane jest jako efekt bioelektryczny. Zatem materiały elektroaktywne z unieruchomionymi cząsteczkami biologicznie czynnymi mogą umożliwić kontrolę wzrostu biofilmów bakteryjnych. Ponieważ bakterie osadzone na powierzchni implantu utrudniają kontakt pomiędzy komórkami nerwowymi a urządzeniem, zastosowanie powłoki antybakteryjnej może dodatkowo zwiększać skuteczność stymulacji elektrycznej.

Ze względu na ograniczenia obecnie stosowanych biomateriałów, w tym neuroelektrod, wzrasta zainteresowanie materiałami alternatywnymi do metali szlachetnych, które charakteryzowałyby się miękką powierzchnią, wysokim przewodnictwem i biokompatybilnością. Obiecujące do tego typu zastosowań są polimery przewodzące, które łączą niski moduł Younga oraz możliwość formowania w kształty dopasowane do potrzeb żywych tkanek [6]. Co więcej, charakteryzują się one wysoką pojemnością elektryczną, niską impedancją oraz możliwością efektywnego przenoszenia ładunku [43–45]. Wykazana biokompatybilność i zdolność do pełnienia funkcji nośników związków biologicznie aktywnych, takich jak antybiotyki [46], leki przeciwnowotworowe [47–49] czy przeciwzapalne [50,51] sprawia, że polimery przewodzące mają potencjalne zastosowanie w inżynierii biomedycznej [52] **[A3]**. Najczęściej badanymi polimerami przewodzącymi pod kątem zastosowań neurologicznych są polipirol (Ppy) [53,54] i poli(3,4-etylenodioksytiofen) (PEDOT) [55–58].

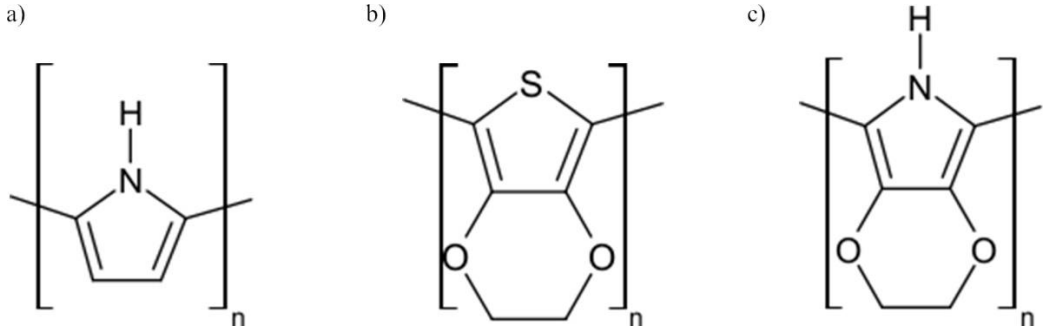

Rys. 3. Wzory strukturalne polimerów przewodzących: a) PPy, b) PEDOT, c) PEDOP.

Ppy ze względu na doskonałą biokompatybilność i stabilność środowiskową jest szeroko badany jako materiał do zastosowań biomedycznych [59]. Co więcej, dzięki dobrej przewodności elektrycznej badany jest jako materiał do otrzymywania warstw (mediatorów) pośredniczących w stymulacji elektrycznej komórek i tkanek [60]. Jednak PPy jest mało plastyczny i odporny na rozciąganie, dlatego prace badawcze przeważnie koncentrują się na połączeniu go z innymi polimerami w celu modyfikacji właściwości [61,62].

Podobnie jak PPy, również PEDOT wykazuje biokompatybilność zarówno *in vitro* jak i *in vivo* [63], stabilność środowiskową oraz elektrochemiczną, która jest wynikiem obecności mostka etylenodioksylowego w jego strukturze chemicznej. PEDOT stosowany jest jako materiał do otrzymywania implantów [64,65], systemów dostarczania leków [51,66,67], jak również rusztowań tkankowych [68,69]. PEDOT badany jest także pod kątem zastosowania w bakteriologii do kontrolowania adhezji bakterii [70], diagnozowania infekcji bakteryjnych [71] oraz zapobiegania tworzeniu się biofilmu [72] **[A3]**.

Obiecującą alternatywą dla PPy oraz PEDOT jest poli(3,4-etylenodioksypirol) (PEDOP), który należy do grupy polipiroli (PPy) i podobnie jak PEDOT posiada w swojej strukturze mostek etylenodioksylowy. Polimer ten w porównaniu z PPy i PEDOT charakteryzuje się niskim potencjałem polimeryzacji oraz wysoką stabilność elektrochemiczną [73]. W literaturze pojawiły się już pierwsze doniesienia na temat wysokiej biokompatybilności PEDOPu z komórkami nerwowymi [74] oraz pod kątem zastosowania jako nośnik leków [75,76].

2. Cel pracy

Celem niniejszej rozprawy doktorskiej jest opracowanie innowacyjnych materiałów dla zastosowań biomedycznych, opartych na wybranych polimerach przewodzących będących nośnikami antybiotyku. Powinny one umożliwiać jednoczesną kontrolę nad procesem powstawania biofilmu bakteryjnego oraz stymulację komórek nerwowych, a także zapewniać działanie neuroprotekcyjne. W ramach przeprowadzonych badań zastosowano matryce PEDOT oraz PEDOP do unieruchomienia antybiotyku: tetracykliny (Tc), który posiada właściwości antybakteryjne zarówno wobec bakterii Gram-dodatnich jak i Gram-ujemnych. Ponadto, istnieją doniesienia naukowe o neuroprotekcyjnym działaniu antybiotyków należących do grupy tetracyklin, które ograniczają aktywację mikrogleju, osłabiają zjawisko apoptozy oraz hamują produkcję reaktywnych form tlenu [77–79].

Pracę rozpoczyna przegląd literatury mający na celu określenie możliwości regulowania wzrostu biofilmu poprzez stymulację elektryczną oraz obecność materiałów elektroaktywnych **[A1]**. W kolejnym etapie prac określono w jakim stopniu powierzchnia platyny, czyli materiału powszechnie wykorzystywanego w projektowaniu elektrod neurologicznych, ulega procesowi kolonizacji bakteryjnej **[A2]**. Po eksperymentalnym potwierdzeniu podatności platyny na rozwój biofilmu bakteryjnego, zajęto się opracowaniem pokryć ochronnych na bazie wybranych polimerów przewodzących **[A3,A4]**. PEDOT i PEDOP osadzano metodą polimeryzacji elektrochemicznej na powierzchni szkła z napyloną cienką warstwą platyny. Immobilizację leku prowadzono równocześnie z procesem polimeryzacji elektrochemicznej, uzyskując powłoki o dobrych właściwościach elektrycznych i wysokiej zawartości leku. Ponadto, otrzymane powłoki scharakteryzowano z wykorzystaniem technik elektrochemicznych (woltamperometria cykliczna, elektrochemiczna spektroskopia impedancyjna, chronoamperometria), spektroskopowych (spektroskopia w podczerwieni, spektroskopia UV/Vis) i mikroskopowych (skaningowa mikroskopia elektronowa), a także określono ich zwilżalność i adhezję do powierzchni. Wytypowane matryce wykorzystano jako podłoża do hodowli modelowych szczepów bakteryjnych i komórkowych. Charakter antybakteryjny powierzchni oceniano wykorzystując szczep bakterii Gram-ujemnych *Escherichia coli*. Działanie neuroprotekcyjne analizowano z wykorzystaniem linii komórkowej szczurzego nerwiaka zarodkowego B35. Istotną częścią pracy była analiza morfometryczna bakterii oraz komórek nerwowych na podstawie obrazów otrzymanych za pomocą skaningowego mikroskopu elektronowego (SEM). W ramach pracy doktorskiej zoptymalizowano proces przygotowania próbek biologicznych do pomiarów

SEM, a także wyselekcjonowano parametry, które dostarczają informacji o stanie komórek (faza wzrostu, możliwość podziału, apoptoza, nekroza, itp.) **[A5]**.

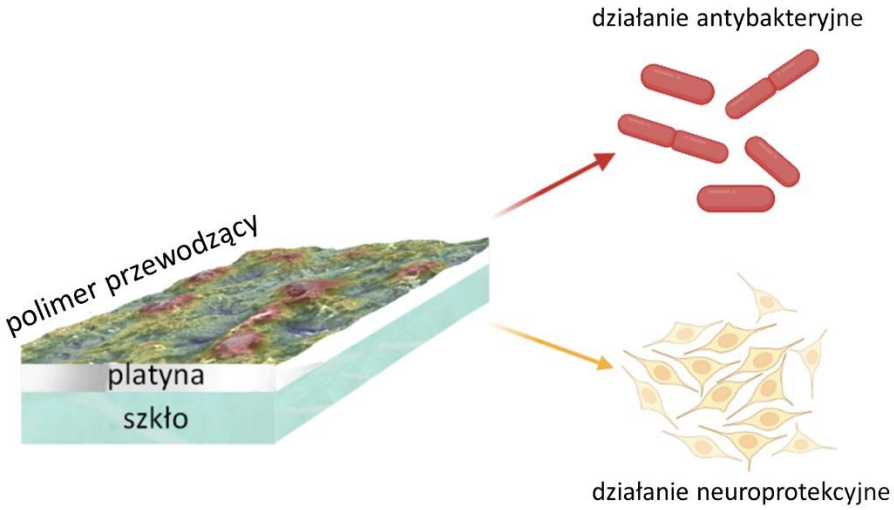

Rys. 4. Schemat przedstawiający cel pracy.

3. Część eksperymentalna

3.1. Elektrochemiczna synteza polimerów przewodzących i ich modyfikacja poprzez zastosowanie tetracykliny

Wybrane polimery przewodzące, PEDOT i PEDOP, osadzano na powierzchni szkiełek mikroskopowych (Labglass) z napyloną warstwą platyny. W celu naniesienia cienkiej warstwy metalu na powierzchnię szklaną zastosowano metodę napylania próżniowego stosując napylarkę Q150R Quorum Technologies pracującą przy 30 mA przez 120 s. Uzyskano warstwę Pt o grubości 4,8 nm **[A2]**.

Matryce polimerowe syntezowano na drodze polimeryzacji elektrochemicznej metodą woltamperometrii cyklicznej (CV) z wykorzystaniem potencjostatu CH Instruments 400c **[A3,A4]**. Proces prowadzono w układzie trójelektrodowym, w którym elektrodą pracującą była płytka szklana z napyloną warstwą Pt o powierzchni aktywnej równej 0,283 cm^2. Elektrodą pomocniczą była blaszka platynowa o powierzchni 1 cm^2, natomiast elektrodą odniesienia była elektroda Ag/AgCl (3M KCl).

Polimeryzację elektrochemiczną EDOT przeprowadzono z roztworu monomeru (10 mM) w PBS stosując zakres potencjałów od -0,9 V do 1,27 V (vs Ag/AgCl), przy szybkości skanowania 0,1 V/s w zakresie 15-100 cykli CV. Matryce polimerowe funkcjonalizowane chlorowodorkiem tetracykliny (PEDOT/Tc) otrzymano podczas polimeryzacji elektrochemicznej 10 mM EDOT w PBS wraz z Tc (od 0,5 mM do 50 mM). Podobnie jak w przypadku matrycy PEDOT, polimeryzacja elektrochemiczna była prowadzona w zakresie potencjałów od -0,9 V do 1,27 V (vs Ag/AgCl), przy szybkości skanowania 0,1 V/s w zakresie 15-100 cykli CV **[A3]**.

Polimeryzację elektrochemiczną EDOP przeprowadzono z roztworu monomeru (10 mM) w PBS stosując zakres potencjałów od -0,8 V do 1,0 V (vs Ag/AgCl), przy szybkości skanowania 0,1 V/s w zakresie 15-100 cykli CV. Matryce polimerowe funkcjonalizowane chlorowodorkiem tetracykliny (PEDOP/Tc) otrzymano podczas polimeryzacji elektrochemicznej 10 mM EDOP w PBS wraz z Tc (od 1 mM do 20 mM). Aby uzyskać matrycę z lekiem, prowadzono polimeryzację elektrochemiczną w zakresie potencjałów od -0,8 V do 1,0 V (vs Ag/AgCl), przy szybkości skanowania 0,1 V/s w zakresie 15-100 cykli CV **[A4]**.

3.2. Ocena właściwości fizykochemicznych otrzymanych materiałów

3.2.1 Właściwości elektryczne

Zdolność magazynowania ładunku (CSC)

Zdolność magazynowania ładunku, tj. CSC, badano z wykorzystaniem woltamperometrii cyklicznej. Pomiary prowadzono w trójelektrodowym układzie analogicznym jak w procesie syntezy elektrochemicznej polimerów na powleczonej polimerem elektrodzie platynowej w roztworze PBS, przy szybkości skanowania 0,1 V/s. Wartość CSC wyliczono korzystając ze wzoru:

$$CSC = \frac{1}{S}\int_{t1}^{t2} I(t)dt$$

gdzie: S to powierzchnia elektrody (cm^2), t_1 to początek cyklu CV a t_2 koniec cyklu CV, natomiast i to natężenie prądu (A) **[A3,A4]**.

Stabilność elektrochemiczna

Parametr CSC umożliwił również ocenę stabilności uzyskanych matryc polimerowych po kolejnych cyklach utlenienia i redukcji. Krzywe CV rejestrowane były w zakresie potencjałów od -0,9 V do 1,27 V (vs Ag/AgCl) dla PEDOT oraz PEDOT/Tc, natomiast od -0,8 V do 1,0 V (vs Ag/AgCl) dla PEDOP i PEDOP/Tc. Warstwy polimerowe porównywano w zakresie 15-100 cykli CV **[A3,A4]**.

Przewodnictwo i pojemność elektryczna matryc

Pomiary wykorzystujące elektrochemiczną spektroskopię impedancyjną (EIS) przeprowadzono w roztworze PBS o amplitudzie AC 40 mV (vs Ag/AgCl) i potencjale DC 0 V (vs Ag/AgCl), w zakresie częstotliwości od 100 mHz do 10 kHz. W celu dopasowania danych eksperymentalnych do równoważnego modelu obwodu zastosowano oprogramowanie EIS Spectrum Analyzer 1.0 oraz algorytm Powella **[A4]**.

Zdolność do „wstrzykiwania" ładunku (CIC)

W celu wyznaczenia profilów napięcia podczas wstrzykiwania ładunku zastosowano chronopotencjometrię z powtarzalnymi impulsami utleniania i redukcji o przeciwnej biegunowości, ale równym czasie (5 ms) i wielkości, równoważnym impulsowi dwufazowemu bez przerwy międzyfazowej. Pomiary prowadzono w PBS w układzie trójelektrodowym, z elektrodą pomocniczą z drutu platynowego i elektrodą odniesienia

Ag/AgCl (3M KCl). Stosowano cztery gęstości ładunku, tj. 3 μC/cm^2, 10 μC/cm^2, 36 μC/cm^2 i 50 μC/cm^2. Pełny impuls dwufazowy, składający się z jednego impulsu utleniania i jednego impulsu redukcji, powtórzono pięć razy **[A4]**.

3.2.2 Właściwości powierzchni

Struktura chemiczna powierzchni

Strukturę chemiczną otrzymanych filmów polimerowych, a także samego leku, określono za pomocą spektroskopii w podczerwieni FTIR (PerkinElmer Spectrum Two). Umożliwiło to określenie skuteczności wprowadzenia Tc w strukturę matryc polimerów przewodzących. Widma rejestrowano w zakresie od 500 cm^{-1} do 1800 cm^{-1} stosując 16 skanów przy użyciu kryształu UATR **[A3,A4]**.

Morfologia powierzchni

Obserwację morfologii wszystkich otrzymanych polimerów przewodzących **[A3,A4]**, a także szkła i napylonej warstwy platyny **[A2]** przeprowadzono wykorzystując skaningowy mikroskop elektronowy (SEM) (Phenom Pro X) pracujący przy napięciu przyspieszającym 10 kV lub 15 kV. Parametr chropowatości powierzchni (średnia arytmetyczna wysokość, S_a) określono przy użyciu oprogramowania 3D Roughness Reconstructions (Phenom ProSuite) **[A2,A3,A4]**.

Grubość matryc polimerowych

Pomiar grubości próbek wykonano za pomocą profilometru Profilm3D i 3D Optical Profiler (Filmetrics) **[A3,A4]**.

Zwilżalność powierzchni

Hydrofilowość materiałów wyrażoną przez kąt zwilżania (CA) określono za pomocą goniometru optycznego (DataPhysic OCA15) przeprowadzając pomiary w temperaturze pokojowej (~ 20°C) z użyciem wody dejonizowanej **[A2,A3,A4]**.

Adhezja matryc do powierzchni

Adhezję warstw PEDOP i PEDOP/Tc do płytek z napyloną warstwą Pt oraz warstwy Pt do płytki szklanej oceniano metodą testu zarysowania, za pomocą urządzenia Micro-Combi Tester (Anton Paar) zgodnie z normami ISO 19252, ISO 20502 i ASTM C1624. Do

wykonania rysy użyto diamentowego stożka Rockwella o średnicy 100 µm. Zarysowania próbek wykonano stosując wzrastające obciążenia od 0,03 N do 15 N dla warstw PEDOP oraz PEDOP/Tc, natomiast dla Pt od 0,03 N do 30 N przy prędkości 3 mm/min i długości zarysowania równej 3 mm. Wykonano "prescan" i "postscan", stosując stałe obciążenie 0,03 N, które miały na celu identyfikację profilu powierzchni **[A4]**.

3.2.3. Badanie matryc polimerowych jako nośników leku

Spontaniczne uwalnianie leku

W celu określenia ilości Tc uwalnianej w sposób spontaniczny z matrycy PEDOP/Tc wykorzystano trzy elektrody powleczone warstwą polimeru i umieszczono w oddzielnych kuwetach kwarcowych o ścieżce optycznej 2 mm wypełnionych 0,5 ml roztworu PBS. W celu zbadania kinetyki uwalniania leku zastosowano model kinetyczny Avramiego według równania:

$$\ln(-\ln(1-X)) = \ln k + n \ln t,$$

gdzie: X to ułamek leku uwolnionego w czasie t, n jest wykładnikiem uwalniania, a k jest stałą szybkości uwalniania **[A4]**.

Wymuszone uwalnianie leku

Aby uwolnić maksymalną dostępną ilość Tc z otrzymanych polimerów przewodzących, elektrody zanurzone w PBS poddano stymulacji elektrycznej poprzez chronoamperometryczny skok potencjału od -0,6 V (przyłożony przez 2 s) do -0,5 V (przyłożony przez 600 s) względem elektrody odniesienia Ag/AgCl (3M KCl) **[A3,A4]**.

Spektroskopia UV/Vis

Ilość Tc uwalnianego z matrycy polimerowej metodą chronoamperometryczną oceniano za pomocą spektrofotometrii UV-Vis (UV-Vis Hewlett Packard 8453). Stężenia Tc wyznaczono stosując krzywą kalibracyjną: $y=3{,}0461 \cdot x + 0{,}0326$ ($R^2 = 0{,}9969$), gdzie y jest wartością absorbancji przy długości fali równej 363 nm, natomiast x jest stężeniem Tc wyrażonym w mM. Przeprowadzono również badania dotyczące samoistnego uwolnienia antybiotyku z matryc polimerowych, zanurzając je w wodnym roztworze PBS i umieszczając w kuwetach kwarcowych. W tym przypadku widma UV-Vis rejestrowano w określonych punktach czasowych, a stężenie Tc oceniano za pomocą krzywej kalibracyjnej **[A3,A4]**.

3.3. Badania biologiczne z wykorzystaniem bakterii

3.3.1 Hodowla bakteryjna

W celu oceny właściwości antybakteryjnych otrzymanych warstw polimerowych zastosowano modelowy szczep bakterii Gram-ujemnych *Escherichia coli* (DSM 30083, U5/41). Bakterie hodowano na podłożu agarowym 23 g/L (BTL) w temperaturze 35°C przez 48 godzin w cieplarce. Po tym czasie skosy agarowe przemyto solą fizjologiczną (0,85% wodny roztwór NaCl; Acros Organics). Tak przygotowaną zawiesinę bakterii ($\approx 10{,}5 \cdot 10^8$ CFU/ml) wykorzystano do przeprowadzenia hodowli bakteryjnej na powierzchniach szkła, Pt, PEDOT, PEDOT/Tc, PEDOP oraz PEDOP/Tc **[A2,A3,A4]**. Wcześniejszą sterylizację materiałów osiągnięto poprzez ich umieszczenie na płytkach 12-dołkowych i zanurzenie na 1 godzinę w 70% etanolu **[A2]** lub pozostawienie ich na godzinę pod działaniem promieniowania UVC (253,7 nm) **[A3,A4]**. Na próbki wkraplano kolejno po 0,1 ml zawiesiny bakteryjnej w soli fizjologicznej i 2 ml pożywki hodowlanej (zawierającej 10 g/L tryptonu (BTL), 5 g/L ekstraktu drożdżowego (BTL) i 10 g/L soli fizjologicznej (Acros Organics) przy pH = 7). Hodowlę bakterii prowadzono przez 48 h w inkubatorze w temperaturze 35°C. Próbki do analiz pobierano po 3, 24 i 48 godzinach. W celu uzyskania wiarygodnych wyników, każdy z eksperymentów wykonano trzykrotnie dla wszystkich materiałów w identycznych warunkach. W celu określenia istotności statystycznej przeprowadzono test t-Studenta ($p < 0{,}05$).

3.3.2 Ocena właściwości antybakteryjnych

Analiza morfometryczna

W celu przygotowanie próbek do obrazowania, materiały utrwalano 3% aldehydem glutarowym (Fisher BioReagents) przez 24 h, następnie odwadniano zanurzając próbki w roztworach etanolu (Acros Organics) o wzrastających stężeniach (30%, 50%, 70% 80%, 90%, 95%, 99,8%) każdorazowo przez 10 min. Tak przygotowane próbki suszono w suszarce laboratoryjnej (24 godz., 50 °C), a następnie pokryto warstwą złota (20 min, 20 mA; Q150R Quorum Technologies). Rozmieszczenie i morfologię bakterii na przygotowanych powierzchniach oceniano na podstawie mikrofotografii SEM wykonanych przy napięciu przyspieszającym 15 kV oraz powiększeniach 1000×, 5000× i 10000×. Średnią długość i szerokość komórek bakteryjnych oraz ich gęstość (liczbę bakterii na 200 μm^2) obliczono z wykorzystaniem oprogramowania ImageJ (NIH) **[A2,A3,A4]**.

Analiza żywotności komórek

Analizę żywotności komórek bakteryjnych przeprowadzono z wykorzystaniem testu LIVE/DEAD® BacLight Bacterial Viability Kit (Life Technologies, Thermo Fisher Scientific) oraz fluorescencyjnego mikroskopu konfokalnego (Olympus FluoView FV1000). Żywe komórki bakteryjne oznaczono zielonym barwnikiem SYTO9, natomiast martwe komórki bakteryjne oznaczono na czerwono jodkiem propidyny (PI). Analizę procentową żywych i martwych komórek przeprowadzono przy użyciu oprogramowania ImageJ (Fiji, NIH) **[A2,A3,A4]**.

3.4. Badania biologiczne z wykorzystaniem linii komórkowej

3.4.1 Hodowla komórkowa

Linię komórkową szczurzego nerwiaka zarodkowego B35 (ATCC® CRL-2754™) hodowano w 15 ml pożywki Eagle/Dulbecco F-12 (DMEM/F12, Sigma-Aldrich) uzupełnionej 10% płodową surowicą bydlęcą (FBS, Gibco) i gentamycyną (40 mg/ ml, Krka) w atmosferze o stałej wilgotności (80%) i stężeniu dwutlenku węgla (5%) w 37°C (Heracell™ 150i, Thermo Scientific). Komórki do eksperymentów przygotowano przez trypsynizację 0,25% roztworem trypsyna-EDTA (Sigma-Aldrich) w PBS. Następnie trypsynę zobojętniano przez dodanie równej ilości pożywki hodowlanej, a komórki zliczano w komorze Bürkera. Na każdą próbkę wysiano po $2 \cdot 10^5$ komórek w 2 ml pożywki i hodowano przez 48 godzin. Po tym czasie do każdego dołka dodano 1 ml 0,25% roztworu trypsyna-EDTA (Sigma-Aldrich). Otrzymane zawiesiny komórek wirowano przy 1500 obr./min przez 3 min **[A4]**.

3.4.2. Ocena biokompatybilności

Ocena cytotoksyczności

Do analizy cytotoksyczności badanych materiałów wykorzystano test MTT (bromek 3-[4,5-dimetylotiazol-2-ilo]-2,5-difenylotetrazoliowy). 50 µl roztworu MTT (0,05 mg/ml w czerwieni fenolowej i wolnym od FBS DMEM-F12; PAA) dodano do odwirowanych wcześniej komórek. Po 1-2 godzinach w inkubatorze CO_2 roztwór MTT usunięto, a powstałe kryształy formazanu rozpuszczono w 400 µl izopropanolu. Absorbancję roztworów mierzono spektrofotometrycznie przy długości fali równej 570 nm, stosując wielodołkowy czytnik płytek SYNERGY4 (BioTek Instruments) **[A4]**.

Analiza cyklu komórkowego

Do przeprowadzenia analizy cyklu komórkowego zastosowano cytometr przepływowy (Becton Dickinson Aria III). Komórki wybarwiono za pomocą 250 µl buforu hipotonicznego (składającego się z 100 µg/mL PI w PBS; 5 mg/L kwasu cytrynowego; roztworu 1:9 Triton-X; 100 µg/mL RNaza w PBS firmy Sigma), poziomy DNA oceniano poprzez pomiary fluorescencji przy użyciu sortera BD FACSAriaTM III (Becton, Dickinson and Company) w konfiguracji PE (linia lasera wzbudzającego 547 nm; emisja: 585 nm) **[A4]**.

Ocena zjawiska apoptozy

Do oceny liczby komórek martwych i apoptotycznych hodowanych na badanych próbkach wykorzystano zestaw FITC Annexin-V Apoptosis Detection Kit z PI (Bio Legend). Do komórek zebranych po 48 godzinach hodowli dodano 50 µl buforu wiążącego aneksynę V, 2,5 µl aneksyny V FITC i 10 µl PI (100 µg/ml). Następnie próbki odwirowano i inkubowano w ciemności przez 20 min w temperaturze pokojowej (25°C). Przed pomiarem do każdej probówki dodano 250 µl buforu wiążącego aneksynę-V. Fluorescencję PI (komórek nekrotycznych) analizowano w konfiguracji kanału PE, a fluorescencję przeciwciał sprzężonych z Aneksyną-V z FITC (komórek apoptotycznych) w konfiguracji kanału FITC (linia lasera wzbudzającego 488 nm; emisja: lustro LP 503, filtr BP 530 /30) **[A4]**.

Analiza morfometryczna

W celu zobrazowania morfologii hodowanych komórek zastosowano mikroskopię SEM. Komórki nerwiaka zarodkowego utrwalano przy użyciu 3% aldehydu glutarowego (Fisher BioReagents) przez 24 godziny. Następnie komórki przemywano trzykrotnie wodą dejonizowaną i odwadniano poprzez zanurzenie próbek w roztworach etanolu (Acros Organics) o rosnących stężeniach (30%, 50%, 70%, 80%, 90%, 95%, 99,8%) przez 10 min. Próbki suszono przez 24 h w 50 °C, a następnie napylano warstwą złota (20 min, 20 mA; Q150R Quorum Technologies). Obrazowanie prowadzono przy napięciu przyspieszającym 10 kV i powiększeniach 3000x **[A4]**.

3.5. Analiza statystyczna

Analizę statystyczną oparto na teście t, a wartość p poniżej 0,05 uznano za istotną statystycznie. Wszystkie testy przeprowadzono w trzech powtórzeniach dla wszystkich materiałów we wszystkich punktach czasowych w tych samych warunkach.

4. Wyniki badań

*Tabela 1 Porównanie właściwości powierzchni szkła i platyny i ich wpływu na rozwój biofilmu bakteryjnego **[A2]***

Parametr	**Szkło**	**Platyna**
Właściwości powierzchni		
S_a [µm]	0,26 ± 0,01	0,21 ± 0,01
CA [°]	60,4 ± 7,5	35,2 ± 10,5
Ocena skuteczności antybakteryjnej		
Analiza morfometryczna		
Średnia długość bakterii po 3 h [µm]	2,00 ± 0,04	1,79 ± 0,03
Średnia długość bakterii po 24 h [µm]	1,94 ± 0,03	1,95 ± 0,03
Średnia długość bakterii po 48 h [µm]	2,04 ± 0,04	1,90 ± 0,03
Średnia szerokość bakterii po 3 h [µm]	0,77 ± 0,01	0,75 ± 0,01
Średnia szerokość bakterii po 24 h [µm]	0,70 ± 0,01	0,66 ± 0,01
Średnia szerokość bakterii po 48 h [µm]	0,71 ± 0,01	0,71 ± 0,01
Średnia gęstość bakterii/200 μm^2 po 3 h	15,3 ± 1,6	12,9 ± 2,1
Średnia gęstość bakterii/200 μm^2 po 24 h	28,9 ± 2,5	29,5 ± 3,0
Średnia gęstość bakterii/200 μm^2 po 48 h	11,3 ± 1,6	11,4 ± 2,3
Analiza LIVE/DEAD		
% komórek żywych po 3 h	20,5 ± 1,7	38,9 ± 2,0
% komórek żywych po 24 h	56,8 ± 0,6	61,8 ± 1,3
% komórek żywych po 48 h	62,5 ± 1,1	62,1 ± 0,7

*Tabela 2 Wartość CSC oraz stężenie uwolnionej Tc w zależności od zastosowanego stężenia Tc w trakcie polimeryzacji elektrochemicznej **[A3, A4]***

Materiał	**Stężenie Tc [mM]**								
	0	0,5	1	5	10	20	30	40	50
CSC [mC/cm^2]									
PEDOT/Tc	29,5 ± 5,8	26.8 ± 1.1	19,2 ± 6,1	18.5 ± 1.3	16,5 ± 2,6	9,2 ± 0,5	18,3 ± 0,6	13,1 ± 1,0	18,2 ± 2,0
PEDOP/Tc	54,2 ± 1,0	n/a	38,8 ± 5,3	63,6 ± 6,0	48,4 ± 7,9	28,5 ± 3,8	n/a	n/a	n/a
Stężenie Tc uwolnionej z matrycy polimerowej [µM]									
PEDOT/Tc	0	3.7± 1,0	38,2 ± 11,0	45,5 ± 12,2	22,5± 15,2	17,4 ± 0,1	18,0 ± 5,9	7,6 ± 3,0	6,2 ± 5,3
PEDOP/Tc	0	n/a	10,0 ± 2,9	123,5 ± 12,3	77,9 ± 12,8	111,9 ± 6.0	n/a	n/a	n/a

n/a – nie dotyczy

*Tabela 3 Wartość CSC oraz stężenie uwolnionej Tc w zależności od zastosowanej liczby cykli CV w trakcie polimeryzacji elektrochemicznej **[A3, A4]***

Materiał	**Liczba cykli CV**				
	15	25	50	75	100
CSC [mC/cm^2]					
PEDOT/Tc	11,0 ± 1,0	19,2 ± 6,1	17,6 ± 5,2	28,3 ± 4,8	37,2 ± 20,0
PEDOP/Tc	30,3 ± 2,1	63,7 ± 6,0	60,3 ± 6,7	119,0 ± 14,4	149,5 ± 21,0
Stężenie uwolnionej Tc z matrycy polimerowej [µM]					
PEDOT/Tc	0,4 ± 0,3	38,2 ± 11,0	11,8 ± 2,6	14,6 ± 11,7	19,8 ± 5,8
PEDOP/Tc	7,8 ± 2,3	123,5 ± 12,3	14,6 ± 3,6	22,6 ± 11,8	46,5 ± 12,7

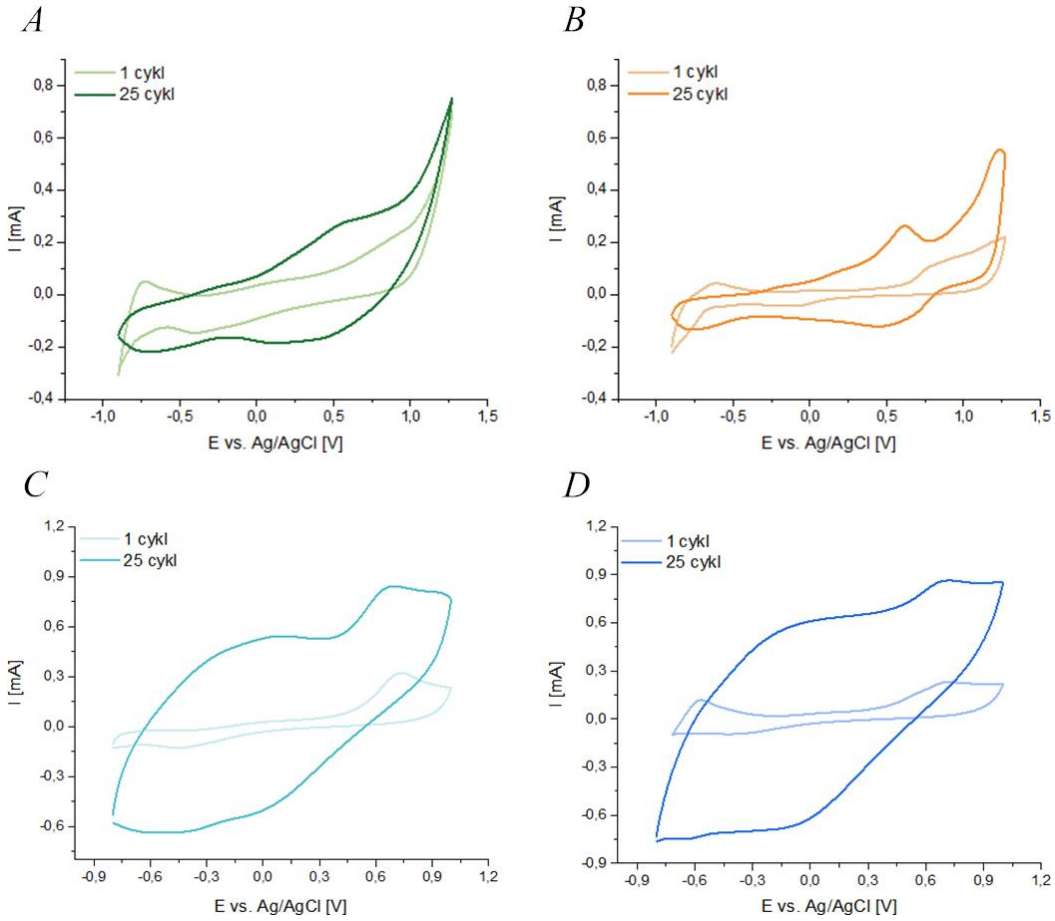

Rys. 5. Porównanie krzywych CV polimeryzacji EDOT (A), EDOT/Tc (B), EDOP (C) i EDOP/Tc (D) ***[A3,A4]***

Źródło: „Rys. 5. został opublikowany w a) Materials Science and Engineering: C 123, Czerwińska-Główka D., Przystaś W., Zabłocka-Godlewska E., Student S., Cwalina B., Łapkowski M., Krukiewicz K., *Electrically-responsive antimicrobial coatings based on a tetracycline-loaded poly(3,4-ethylenedioxythiophene) matrix,* 1-11 (2021); b) Bioelectrochemistry 144, Czerwińska-Główka D., Skonieczna M., Barylski A, Golba S., Student S., Przystaś W., Zabłocka-Godlewska E., Cwalina B., Krukiewicz K., *Bifunctional conducting polymer matrices with antibacterial and neuroprotective effects,* 1-14 2021. Umieszczone za zgodą Elsevier".

Tabela 4 Porównanie procesu polimeryzacji elektrochemicznej EDOT, EDOT/Tc, EDOP i EDOP/Tc otrzymanych matryc ***[A3,A4]***

Parametr	**EDOT**	**EDOT/Tc**	**EDOP**	**EDOP/Tc**
Zakres potencjałów polimeryzacji [V vs. Ag/AgCl]	-0,9 ÷ 1,27	-0,9 ÷ 1,27	-0,8 ÷ 1,0	-0,8 ÷ 1,0
Potencjał utlenienia [V vs. Ag/AgCl]	~1,27	~1,27	~0,7	~0,7

*Tabela 5 Porównanie właściwości elektrycznych Pt, PEDOP i PEDOP/Tc **[A4]***

Parametr	**Pt**	**PEDOP**	**PEDOP/Tc**
Rezystancja roztworu R_S [Ω]	118 ± 3	132 ± 2	118 ± 3
Rezystancja przenoszenia ładunku R_{CT} [Ω]	24 760 ± 3 895	488 ± 11	2 416 ± 141
Element Warburga A_w	6411 ± 1691	165 ± 14	510 ± 139
$P \cdot 10^5$	4,96 ± 0,15	11,60 ± 0,35	7,20 ± 0,42
n	0,895 ± 0,007	0,745 ± 0,006	0,885 ± 0,009
χ^2	0,00426	0,00434	0,00098
Max. potencjał anodowy (dla gęstości ładunku 36 μC/cm^2) [V]	0,6	0,25	0,35

*Tabela 6 Porównanie adhezji Pt, PEDOP i PEDOP/Tc do podłoża **[A4]***

Parametr	**Pt**	**PEDOP**	**PEDOP/Tc**
Siła powodująca uszkodzenie warstwy Pt [N]	4,1 ± 0,5	4,9 ± 1,6	3,3 ± 0,5
Siła powodująca uszkodzenie warstwy polimeru [N]	n/a	1,5 ± 0,1	1,3 ± 0,2

n/a – nie dotyczy

*Tabela 7 Porównanie właściwości powierzchni Pt, PEDOT, PEDOT/Tc, PEDOP i PEDOP/Tc **[A3,A4]***

Parametr	**Pt**	**PEDOT**	**PEDOT/Tc**	**PEDOP**	**PEDOP/Tc**
S_a [μm]	0,21 ± 0,01	0,62 ± 0,03	0,63 ± 0,06	4,36 ± 0,52	4,13 ± 0,90
CA [°]	35,2 ± 10,5	31,5 ± 2,6	26,2 ± 3,5	38,2 ± 4,3	45,8 ± 8,5

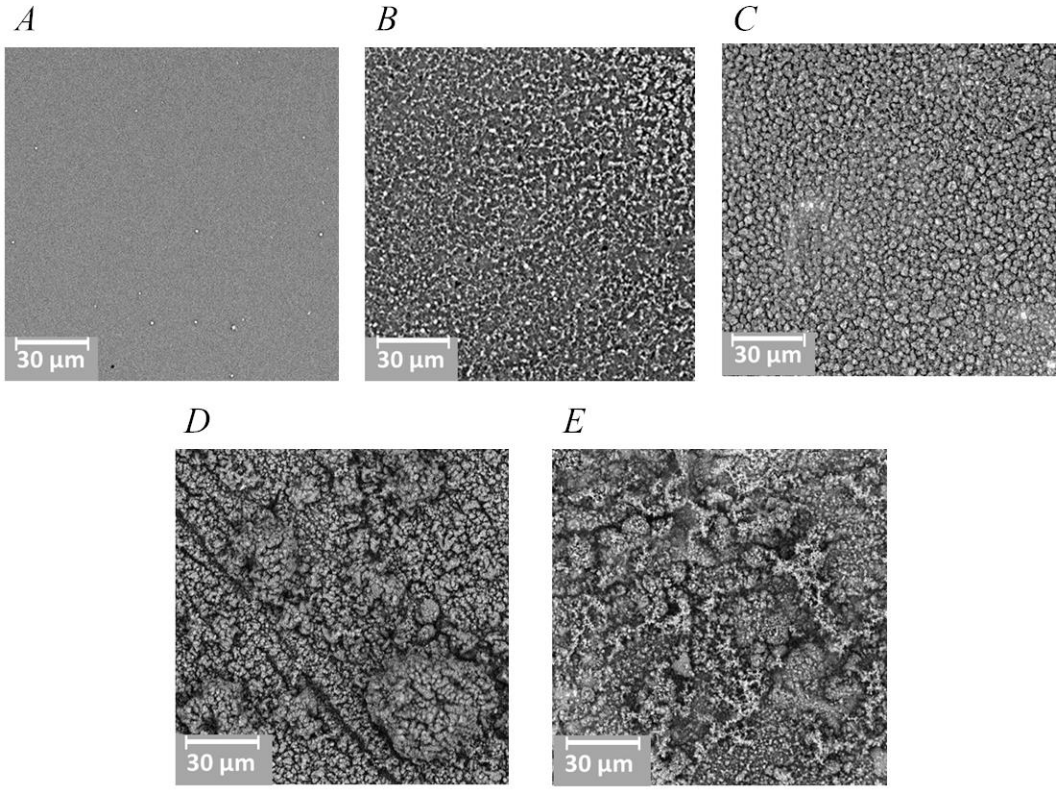

Rys. 6. Obrazy SEM powierzchni Pt (A), PEDOT (B), PEDOT/Tc (C), PEDOP (D) i PEDOP/Tc (E) ***[A3,A4]***

Źródło: „Rys. 6. został opublikowany w a) Materials Science and Engineering: C 123, Czerwińska-Główka D., Przystaś W., Zabłocka-Godlewska E., Student S., Cwalina B., Łapkowski M., Krukiewicz K., *Electrically-responsive antimicrobial coatings based on a tetracycline-loaded poly(3,4-ethylenedioxythiophene) matrix,* 1-11 (2021); b) Bioelectrochemistry 144, Czerwińska-Główka D., Skonieczna M., Barylski A, Golba S., Student S., Przystaś W., Zabłocka-Godlewska E., Cwalina B., Krukiewicz K., *Bifunctional conducting polymer matrices with antibacterial and neuroprotective effects,* 1-14 2021. Umieszczone za zgodą Elsevier".

Tabela 8 Porównanie efektywności uwalniania Tc z PEDOT/Tc i PEDOP/Tc ***[A3,A4]***

Parametr	**PEDOT/Tc**	**PEDOP/Tc**
Stężenie Tc osiągnięte podczas spontanicznego uwalniania [mg/l]	5,7	9,4
Stężenie Tc osiągnięte podczas wymuszonego uwalniania [mg/l]	18,1	59,4

*Tabela 9 Porównanie właściwości antybakteryjnych Pt, PEDOT, PEDOT/Tc, PEDOP oraz PEDOP/Tc **[A3,A4]***

Parametr	**Pt [A3]**	**PEDOT [A3]**	**PEDOT/Tc [A3]**	**Pt [A4]**	**PEDOP [A4]**	**PEDOP/Tc [A4]**
Analiza morfometryczna						
Średnia długość bakterii po 3 h [µm]	1,77 ± 0,04	1,64 ± 0,03	1,73 ± 0,03	1,70 ± 0,03	1,35 ± 0,03	1,40 ± 0,04
Średnia długość bakterii po 24 h [µm]	2,02 ± 0,03	1,80 ± 0,03	1,91 ± 0,03	1,90 ± 0,04	1,54 ± 0,03	1,28 ± 0,04
Średnia długość bakterii po 48 h [µm]	2,17 ± 0,06	1,84 ± 0,04	1,97 ± 0,03	1,87 ± 0,04	1,50 ± 0,03	4,89 ± 0,39
Średnia szerokość bakterii po 3 h [µm]	0,70 ± 0,01	0,62 ± 0,01	0,64 ± 0,01	0,62 ± 0,01	0,47± 0,01	0,55 ± 0,01
Średnia szerokość bakterii po 24 h [µm]	0,66 ± 0,01	0,60 ± 0,01	0,60 ± 0,01	0,61 ± 0,01	0,50 ± 0,01	0,44 ± 0,01
Średnia szerokość bakterii po 48 h [µm]	0,63 ± 0,01	0,51 ± 0,01	0,52 ± 0,01	0,59 ± 0,01	0,49 ± 0,01	0,64 ± 0,02
Średnia gęstość bakterii/200 μm^2 po 3 h	27,9 ± 3,8	21,5 ± 1,4	13,2 ± 2,8	11,5 ± 1,0	10,7 ± 0,9	0,7 ± 0,1
Średnia gęstość bakterii/200 μm^2 po 24 h	25,1 ± 5,2	22,7 ± 4,8	15,0 ± 2,0	9,7 ± 1,4	17,4 ± 2,0	0,9 ± 0,3
Średnia gęstość bakterii/200 μm^2 po 48 h	28,0 ± 4,0	12,7 ± 1,8	10,1 ± 1,5	3,8 ± 0,5	4,9 ± 0,7	1,9 ± 0,5
Analiza LIVE/DEAD						
% komórek	74,8 ± 2,2	44,7 ± 2,3	42,7 ± 0,7	61,8 ± 6,4	25,8 ± 4,0	45,6 ± 2,4

żywych po 3 h						
% komórek żywych po 24 h	59,2 ± 1,2	59,6 ± 1,0	48,2 ± 1,7	43,8 ± 5,8	36,7 ± 2,6	53,4 ± 1,2
% komórek żywych po 48 h	60,6 ± 1,1	63,7 ± 0,5	70,0 ± 1,0	47,4 ± 0,8	48,8 ± 0,5	21,4 ± 2,4

Tabela 10 Porównanie właściwości neuroprotekcyjnych Pt, PEDOP i PEDOP/Tc ***[A4]***

Parametr	**Pt**	**PEDOP**	**PEDOP/Tc**
Analiza cytotoksyczności po 48 h			
% komórek żywych	86,2 ± 4,4	59,3 ± 3,6	83,7 ± 4,3
Analiza cyklu komórkowego po 48 h			
% komórek w fazie sub-G1	3,6 ± 1,5	3,7 ± 0,7	6,6 ± 0,6
% komórek w fazie G0/G1	68,2 ± 0,7	66,2 ± 3,0	68,3 ± 1,2
% komórek w fazie S	9,4 ± 0,2	10,4 ± 1,3	9,6 ± 0,4
% komórek w fazie G2/M	18,2 ± 1,5	18,6 ± 0,7	15,0 ± 1,0
Ocena zjawiska apoptozy			
% komórek normalnych	74,0 ± 0,7	61,4 ± 1,7	68,8 ± 0,5
% komórek wczesno apoptotycznych	2,9 ± 0,6	6,7 ± 1,8	1,9 ± 0,1
% komórek późno apoptotycznych	19,8 ± 1,3	30,8 ± 0,4	23,9 ± 1,8
% komórek nekrotycznych	3,3 ± 0,2	1,1 ± 0,4	5,3 ± 1,7
Analiza morfometryczna			
Średnia długość neurytów/µm	28,6 ± 3,0	21,4 ± 2,4	35,5 ± 4,3
Liczba neurytów/ komórkę	3,6 ± 0,3	3,2 ± 0,3	4,1 ± 0,3

5. Dyskusja

5.1. Określenie możliwości regulowania wzrostu biofilmu poprzez stymulację elektryczną oraz obecność materiałów elektroaktywnych **[A1]**

Pierwszym etapem moich prac było określenie możliwości regulowania wzrostu biofilmu poprzez stymulację elektryczną oraz obecność materiałów elektroaktywnych. Przegląd literatury [**A1**] stanowi wprowadzenie do tematu prac oryginalnych pokazując związek pomiędzy elektrochemią a mikrobiologią. Praca podkreśla znacznie technik elektrochemicznych w monitorowaniu i modulacji wzrostu biofilmu bakteryjnego, a także wpływ elektrostymulacji na zachowanie bakterii. W publikacji skupiłam się na opisie roli prądów elektrycznych w funkcjonowaniu biofilmu bakteryjnego. Warto podkreślić, że nawet pojedyncze bakterie w postaci planktonu mogą odbierać sygnały elektryczne, natomiast dopiero w większych skupiskach stają się elektroaktywne i podatne na stymulację elektryczną. Ponadto, komórki bakteryjne w biofilmie różnicują się do pełnienia konkretnych funkcji poprzez komunikację chemiczną oraz elektryczną. Taki sposób organizacji umożliwia efektywny dostęp do substancji odżywczych, a przez to wzrost biofilmu i jego uodpornienie na działanie czynników zewnętrznych, w tym związków antybakteryjnych.

5.2. Badanie podatności powierzchni platyny na rozwój biofilmu bakteryjnego **[A2]**

Kolejnym etapem pracy było określenie podatności powierzchni platyny na rozwój biofilmu bakteryjnego **[A2]**. W literaturze istnieją doniesienia na temat antybakteryjnego charakteru metali szlachetnych w postaci jonów, nanocząstek lub napylonych warstw [80–82]. Metody napylania metali pozwalają na dokładne pokrycie dowolnych powierzchni równą warstwą metalu, co nadaje im znaczny potencjał aplikacyjny. Platyna jest powszechnie stosowana w urządzeniach biomedycznych, ponieważ charakteryzuje się wykazaną biokompatybilnością i przewodnością elektryczną, co jest szczególnie istotne w funkcjonowaniu implantów neurologicznych czy rozruszników serca. Z tego względu zdecydowałam o napyleniu cienkiej warstwy platyny na powierzchnię czystego szkiełka mikroskopowego stosując napylarkę próżniową. Aby ocenić, czy taka warstwa może stanowić materiał antybakteryjny, przeprowadziłam badania mikrobiologiczne z wykorzystaniem modelowego szczepu bakterii Gram-ujemnych – *Escherichia coli*.

Zarówno chropowatość jak i hydrofilowość materiałów mają wpływ na skuteczną adhezję bakterii do powierzchni [83,84]. Ocena fizykochemiczna pozwoliła ustalić, że powierzchnia szkła z napyloną warstwą Pt była nieznacznie mniej chropowata oraz bardziej

hydrofilowa w odniesieniu do szkła (Tabela 1). Przyjmuje się, że chropowatość powierzchni sprzyja przyczepności bakterii, a bakterie o właściwościach hydrofilowych (w tym *E.coli*) preferują osadzanie się na powierzchniach hydrofilowych. Tym samym otrzymane wyniki nie dały jednoznacznej odpowiedzi co do sugerowanych właściwości antybakteryjnych podłoży. W celu weryfikacji hipotezy badawczej przeprowadziłam hodowlę bakteryjną w układzie zamkniętym, analizując próbki po 3h, 24h i 48h. Analiza morfometryczna przeprowadzona na podstawie mikrofotografii SEM umożliwiła wyliczenie gęstości bakterii, ich długości i szerokości. Różnice między gęstościami zaobserwowano po 3h hodowli, gdzie na warstwie Pt było ich o 15,7% mniej niż na czystym szkle. Był to jednak efekt krótkotrwały, gdyż w kolejnych punktach czasowych różnice w gęstości bakterii na porównywanych materiałach były niewielkie. Ponadto, badane bakterie posiadały przeciętne wymiary komórek w kształcie pałeczki, przy czym na powierzchni szkła były dłuższe i szersze niż na powierzchni szkła z napyloną warstwą Pt. Po 24h hodowli odnotowałam wzrost długości wszystkich bakterii, weszły one w fazę podziału i znacząco zwiększyły swoją populację. Ostatni punkt czasowy przedstawia fazę śmierci komórek spowodowaną brakiem dostępności do świeżej pożywki oraz nagromadzeniem metabolitów, co przejawia się zmniejszeniem gęstości bakterii na obydwu badanych powierzchniach.

Analiza LIVE/DEAD z wykorzystaniem mikroskopii konfokalnej umożliwiła ocenę stosunku liczby komórek żywych i martwych. Wyniki wskazały, że procent żywych komórek na powierzchni napylonej Pt był znacznie wyższy niż na powierzchni szkła zarówno w pierwszej jak i drugiej fazie wzrostu i namnażania bakterii (3h, 24h). Po 48h, mimo spadku gęstości bakterii, większość z nich wciąż była żywa zarówno na powierzchni czystego szkła jak i warstwy Pt. Na podstawie zebranych danych ustaliłam, że napylona warstwa Pt nie wpływała hamująco na rozwój bakterii. Wręcz przeciwnie, ich żywotność była zwiększona w odniesieniu do bakterii hodowanych na powierzchni kontrolnej.

W konsekwencji uzyskane wyniki nie potwierdziły antybakteryjnego charakteru napylonej warstwy metalu, a wręcz wskazały ryzyko możliwości zwiększonego namnażania się bakterii na jej powierzchni. Może to być związane ze znaczną stabilnością fizykochemiczną osadzonej warstwy, co wpływa na brak możliwości uwalniania jonów i nanocząstek Pt. Ponieważ platyna jest materiałem często stosowanym w biomedycynie, w kolejnych badaniach skupiłam się na opracowaniu metod modyfikacji jej powierzchni tak, aby zminimalizować możliwość jej kolonizacji przez bakterie.

5.3. Otrzymanie i charakterystyka matryc polimerowych **[A3,A4]**

Jedną z metod ograniczenia tworzenia się biofilmu bakteryjnego jest zastosowanie impulsów elektrycznych. W związku z tym postanowiłam zmodyfikować powierzchnię Pt organiczną warstwą elektroaktywną zbudowaną z polimerów przewodzących **[A3,A4]**. Wykorzystałam polimeryzację elektrochemiczną do otrzymania powłoki PEDOT powszechnie wykorzystywanej w bioinżynierii [85] oraz PEDOP o znacznym potencjale biomedycznym [74] (Rys. 5). Ponadto, wykorzystałam możliwość zastosowania polimerów przewodzących jako nośników związków biologicznych unieruchamiając w ich strukturze antybiotyk o szerokim spektrum działań bakteriobójczych, tetracyklinę (Tc). Działanie tetracykliny opiera się na wiązaniu leku z podjednostką rybosomalną 30S bakterii oraz zakłóceniu biosyntezy białek [86].

Proces elektrochemicznej polimeryzacji EDOT i EDOT/Tc przeprowadziłam z wykorzystaniem woltamperometrii cyklicznej w szerokim zakresie potencjałów, a nieodwracalny pik świadczący o utlenieniu monomeru zaobserwowałam przy potencjale 1,27 V. Natomiast polimeryzację EDOP przeprowadziłam w węższym zakresie potencjałów obserwując nieodwracalny pik utlenienia monomeru przy potencjale 0,7 V. Zawężenie zakresu potencjałów polimeryzacji korzystnie wpływa na proces immobilizacji biocząsteczek w strukturze matrycy polimerowej minimalizując ryzyko ich przypadkowego utlenienia, które mogłoby zmniejszyć skuteczność ich działania biologicznego.

Zauważyłam, że dla każdego układu po 25 cyklach polimeryzacji otrzymałam krzywe CV o różnej powierzchni (Rys. 5), co świadczy o różnicy w pojemności elektrycznej otrzymanych materiałów. Prądy płynące przez matryce polimerowe były wyższe w przypadku PEDOP i PEDOP/Tc w porównaniu z PEDOT i PEDOT/Tc, co wskazuje na bardziej rozwiniętą powierzchnię zdolną do gromadzenia większej ilości ładunku. Mimo że każdy układ polimerowy charakteryzował się wyższym CSC w odniesieniu do czystej Pt czy Au [57,87], wyższe wartości odnotowałam dla układów opartych na PEDOP niż na PEDOT (Tabela 2). Najwyższy wynik uzyskałam dla matrycy PEDOP/Tc ($63,6 \pm 6,0$ mC/cm^2), który znacznie przewyższał wartość uzyskaną dla matrycy PEDOT/Tc ($19,2 \pm 6,1$ mC/cm^2). Ponadto, okazał się również wysoki w odniesieniu do innych matryc polimerowych z immobilizowanymi biocząsteczkami m.in. PEDOP/kwercetyna ($41,9 \pm 3,5$ mC/cm^2) [75], PEDOP/ibuprofen (30 ± 1 mC/cm^2) [88], PEDOT/heparyna (20,9 mC/cm^2) [89] czy PEDOT/deksametazon ($2,6 \pm 0,2$ mC/cm^2) [90].

Kolejne badania miały na celu ustalenie mechanizmu przewodzenia ładunku dla układów PEDOP i PEDOP/Tc. Wyniki uzyskane z wykorzystaniem EIS (Tabela 5) wykazały, że obecność PEDOP i PEDOP/Tc znacząco wpłynęła na obniżenie impedancji elektrody Pt o jeden rząd wielkości, szczególnie w zakresie niskich częstotliwości (<100 Hz). Co więcej, stosując symulację za pomocą układu zastępczego (obwód Randlesa) zaobserwowałam znaczny spadek oporu przenoszenia ładunku zarówno dla PEDOP/Tc (2 416 ± 141 Ω) jak i dla PEDOP (488 ± 11 Ω) w porównaniu z napyloną warstwą Pt (24,8 ± 3,9 kΩ). Wartości te są porównywalne z danymi przedstawionymi dla innych polimerów, m.in. poli(ε-dekalakton)/CNT (2 450 Ω), poli(ε-dekalakton)/AgNW (643 Ω) [91] PEDOP-Ag (500 Ω) [92] czy rGO/PEDOT (444,2 Ω) [93]. Niski opór przenoszenia ładunku jest niezwykle istotny przy projektowaniu neuroelekrod wykorzystywanych do badania funkcjonowania tkanki nerwowej, ponieważ wpływa na zwiększenie czułości urządzeń [20].

Badanie adhezji powłok polimerowych jest istotne przy projektowaniu interfejsów neuronowych, w związku z tym, w celu sprawdzenia wytrzymałości adhezji powłoki PEDOP do podłoża wykonałam test zarysowania (tzw. *scratch test*). Zmierzyłam zarówno obciążenie przy którym całkowicie uszkodzona została warstwa Pt oraz obciążenie, przy którym uszkodzeniu uległa warstwa polimeru (Tabela 6). Uzyskane wyniki pozwoliły stwierdzić, że siła adhezji polimerów jest podobna, natomiast siła połączenia między napyloną warstwą Pt a szkłem trzykrotnie większa. Projektując interfejsy neuronowe, należy wziąć pod uwagę mechaniczne interakcje między implantem a mózgiem. Siła działająca na neuroelektrodę podczas jej implantacji zależy od kilku parametrów, w tym geometrii elektrody, jej właściwości mechanicznych i szybkości implantacji. Typowe siły stosowane podczas implantacji są rzędu mN [94]. Po implantacji, elektroda poddawana jest siłom związanym z normalną pracą mózgu, ruchami głowy, itp., które ocenia się na kilka pN [95]. Siła adhezji rzędu 1,5 N, potwierdzona zarówno dla PEDOP jak i PEDOP/Tc, sugeruje, że powłoki te nie powinny ulec uszkodzeniu ani podczas procesu implantacji ani podczas dalszej obecności w organizmie. W celu określenia podatności powierzchni polimerów na adhezję bakterii i komórek nerwowych zbadałam morfologię i hydrofilowość otrzymanych matryc (Tabela 7). Przeanalizowałam chropowatość powierzchni, która determinuje łatwość adhezji drobnoustrojów jak i możliwość zakotwiczenia się komórek nerwowych. Powierzchnie PEDOT i PEDOT/Tc wydają się zdecydowanie bardziej jednorodne, o podobnej ziarnistości w porównaniu do przestrzennie pofałdowanej, gąbczastej warstwy PEDOP i PEDOP/Tc (Rys.6). Obserwacje te potwierdziłam analizując parametr chropowatości wyrażony jako średnie arytmetyczne odchylenie wysokości nierówności powierzchni od płaszczyzny

odniesienia (S_a), który był średnio ponad 6-krotnie wyższy dla matryc PEDOP w porównaniu z matrycami PEDOT. Sugerując się analizą morfologii założyłam, że przyczepność bakterii na obu powierzchniach polimerowych będzie preferencyjna w porównaniu z napyloną warstwą Pt. Jednocześnie polimery PEDOP oraz PEDOP/Tc, jako te o wyższej chropowatości, powinny sprzyjać adhezji komórek nerwowych. Oceniłam również hydrofilowość polimerów na podstawie analizy kąta zwilżania. Stwierdziłam, że wszystkie proponowane powierzchnie są hydrofilowe, w związku z czym nie stanowią bariery dla adhezji hydrofilowych bakterii *E.coli*.

Aby ocenić potencjał antybakteryjny powłok, zbadałam ilość Tc, jaka uwolniła się z matryc PEDOT/Tc oraz PEDOP/Tc spontanicznie oraz na skutek stymulacji elektrycznej. Ze względu na obecność chromoforów w strukturze Tc, uwalnianie leku monitorowałam z wykorzystaniem spektrofotometrii UV-Vis. Ilość Tc uwalnianej z matryc polimerowych PEDOT/Tc i PEDOP/Tc była zależna od początkowego stężenia leku wykorzystanego w trakcie procesu polimeryzacji. Przeprowadzone badania pozwoliły mi wnioskować, że przy stężeniu 1 mM (PEDOT/Tc) oraz 5 mM (PEDOP/Tc) matryce osiągnęły stan nasycenia lekiem, a jego wyższe stężenie nie skutkowało zwiększeniem ilości unieruchomionej Tc (Tabela 2). Przeanalizowałam również wpływ wzrostu liczby cykli CV w procesie elektropolimeryzacji na ilość uwolnionego leku (Tabela 3). W trakcie procesu polimeryzacji elektrochemicznej w każdym cyklu CV na powierzchni tworzy się nowa warstwa polimeru, a lek jest unieruchamiany pomiędzy nimi. Wytworzenie zbyt cienkich warstw może znacznie ograniczyć możliwą pojemność matrycy polimerowej, a tym samym ilość uwalnianego leku. Natomiast wytworzenie zbyt grubej warstwy polimerowej uniemożliwia uwolnienie części leku znajdującej się przy powierzchni elektrody, stąd dalszy wzrost liczby cykli CV nie wiązał się ze wzrostem wydajności uwalniania Tc.

Porównując ilości Tc uwolnione z matryc PEDOT/Tc i PEDOP/Tc (Tabela 8) odnotowałam, że matryca na bazie PEDOP umożliwiła uwolnienie większych ilości Tc, zarówno w wyniku spontanicznego jak i wymuszonego uwalniania. Gąbczasta struktura PEDOP/Tc okazała się bardziej wydajna pozwalając na immobilizację większej ilości Tc, a tym samym uzyskanie wyższych stężeń uwolnionej Tc. Procent uwolnionego leku w odniesieniu do ilości leku w roztworze w trakcie procesu polimeryzacji wynosił ~3% dla obydwu matryc polimerowych.

Metoda chronoamperometryczna (wymuszone uwalnianie) pozwoliła na uwolnienie ponad trzy razy więcej leku z matrycy PEDOT/Tc oraz ponad sześć razy więcej w przypadku matrycy PEDOP/Tc w porównaniu z uwalnianiem spontanicznym. Jest to związane z faktem

zastosowania stymulacji elektrycznej, która umożliwiła uwolnienie leku z głębszych warstw matrycy polimerowej. Dla matrycy PEDOT/Tc podczas uwalniania spontanicznego zaobserwowałam w ciągu pierwszych 15 minut eksperymentu wzmożone uwalnianie Tc, którego stężenie następnie osiągnęło stały poziom. Natomiast w przypadku PEDOP/Tc, zaobserwowałam szybki wzrost stężenia Tc w ciągu pierwszych 4 godzin uwalniania, a stopniowy wzrost trwał aż do 4 dnia eksperymentu, gdy odnotowałam maksymalne stężenie Tc. W każdym z analizowanych przypadków osiągnięto stężenia znacznie większe niż minimalne skuteczne stężenie Tc (16 µg/l) [96]. Na podstawie wyników uzyskanych z eksperymentu spontanicznego uwalniania Tc można wnioskować, że mimo, że matryca PEDOP/Tc pozwoliła na końcowe uwolnienie większej ilości leku, to matryca PEDOT/Tc uwalniała lek szybciej. Oczekuje się, że początkowe gwałtowne uwalnianie Tc z matrycy PEDOP/Tc będzie skutecznie eliminować bakterie obecne na powierzchni, natomiast dalsze stopniowe uwalnianie wydłuży efekt terapeutyczny.

5.4. Ocena właściwości antybakteryjnych Pt, PEDOT, PEDOT/Tc, PEDOP oraz PEDOP/Tc **[A3,A4]**

W celu oceny wpływu powierzchni polimerowych PEDOT, PEDOT/Tc, PEDOP oraz PEDOP/Tc na kontrolę wzrostu bakterii przeprowadziłam hodowlę komórkową modelowego szczepu bakterii (*Escherichia coli)* w systemie zamkniętym. Próbki pobierałam w 3 punktach czasowych (3h, 24h i 48h) i na podstawie metod mikroskopowych przeprowadziłam analizę morfometryczną oraz analizę żywotności bakterii (Tabela 9).

Badając matryce polimerowe zaobserwowałam mniejsze gęstości komórek bakteryjnych w odniesieniu do napylonej warstwy Pt zarówno dla matrycy PEDOT (22,9%) jak i dla PEDOT/Tc (52,7%). Efekt ten był długotrwały i obserwowany zarówno po 24h i 48h, co wskazuje na skuteczność antybakteryjną zarówno uwalnianego leku jak i samej matrycy PEDOT. Podobne wnioski można wysnuć na podstawie analizy morfometrycznej, gdzie najdłuższe i najszersze komórki bakteryjne zaobserwowałam na powierzchni Pt. Można przypuszczać, że powierzchnie polimerów miały hamujący wpływ na wzrost komórek i dostępność niezbędnych składników odżywczych. Analiza LIVE/DEAD potwierdziła, że procent żywych komórek bakteryjnych na powierzchni PEDOT/Tc był istotnie niższy w porównaniu z powierzchniami Pt oraz PEDOT. Matryca PEDOT/Tc okazała się skutecznym nośnikiem antybiotyku wykazując aktywność antybakteryjną nawet bez stymulacji elektrycznej, chociaż mogłaby ona dodatkowo wzmocnić działanie biologiczne tego materiału.

Badania mikrobiologiczne przeprowadzone z wykorzystaniem matryc PEDOP oraz PEDOP/Tc wykazały ich silny wpływ na bakterie. Matryca PEDOP/Tc wykazała znaczne działanie antybakteryjne wyrażone poprzez znikomą adhezję we wszystkich punktach czasowych, zmniejszenie żywotności, a także charakterystyczne wydłużenie komórek bakteryjnych obserwowane po 48 h hodowli. Z kolei matryca PEDOP okazała się warstwą silnie promującą adhezję komórek bakteryjnych, na której zaobserwowałam znaczną proliferację bakterii w odniesieniu do próbki kontrolnej Pt.

Na podstawie zebranych danych stwierdziłam, że obie matryce z immobilizowanym lekiem (PEDOT/Tc, PEDOP/Tc) wykazują charakter antybakteryjny względem bakterii *E. coli*. Jednak matryca PEDOP/Tc okazała się pod tym względem bardziej skuteczna od matrycy PEDOT/Tc, dlatego została wytypowana do badań na linii komórkowej B35 w celu oceny jej potencjału jako materiału dla inżynierii tkanki nerwowej.

5.5. Właściwości neuroprotekcyjne **[A4]**

Do przeprowadzenia badań na linii komórkowej wybrałam matrycę PEDOP/Tc ze względu na obserwowane silne działanie hamujące rozwój bakterii, a także warstwę PEDOP oraz napyloną Pt jako próbki odniesienia. Co więcej, wybrany antybiotyk należy do grupy tetracyklin, która według doniesień literaturowych może wykazywać działanie protekcyjne względem komórek nerwowych [79,97]. W celu weryfikacji tej hipotezy przeprowadziłam badania przy użyciu szczurzej linii komórkowej nerwiaka niedojrzałego B35, których żywotność i morfologię po 48h hodowli analizowałam przy użyciu testów MTT, cyklu komórkowego, apoptozy oraz mikrofotografii SEM (Tabela 10).

Żywotność komórek B35 na powierzchni PEDOP/Tc (83,7%) była porównywalna z kontrolną warstwą Pt (86,2%) wskazując, że powłoka PEDOP/Tc spełnia kryteria biozgodności określone w normie ISO 10993. Warstwa PEDOP natomiast nie spełniała opisanych kryteriów, ponieważ żywotność hodowanych na niej komórek wyniosła jedynie 59,3%. Otrzymane wyniki wskazują, że dodatek Tc wpłynął na poprawę biokompatybilności polimeru przewodzącego. Analiza cyklu komórkowego wykazała większą liczbę komórek znajdującą się we frakcji sub-G1 dla matrycy PEDOP/Tc, w związku z tym w kolejnych badaniach oceniłam rodzaj śmierci komórkowej przeprowadzając test apoptozy. Uzyskane wyniki wskazały, że komórki obumierały na skutek zaprogramowanej, fizjologicznej śmierci. Co więcej, mikroskopia SEM umożliwiła mi zaobserwowanie bardzo dobrej integracji neuronów z warstwami PEDOP i PEDOP/Tc. Zaobserwowałam różnice w rozgałęzieniu

i liczbie neurytów w przeliczeniu na komórkę w zależności od stosowanego materiału (Tabela 10). Wykorzystanie matrycy PEDOP/Tc pozwoliło na równomierne rozmieszczenie neurytów oraz ich usieciowanie, natomiast komórki hodowane na warstwie PEDOP ulegały agregacji nie tworząc tak rozległych sieci. Ścisła integracja między wytworzoną matrycą PEDOP/Tc a neuronami sprawia, że polimer wykazuje się znacznym potencjałem aplikacyjnym jako powłoka dla urządzeń biomedycznych, przede wszystkim interfejsów neuronowych. Z racji tak obiecujących wyników, sposób otrzymania przedstawionej matrycy PEDOP/Tc zgłoszono do ochrony własności intelektualnej.

5.6. Analiza morfometryczna komórek bakteryjnych i komórek nerwowych **[A5]**

Istotnym elementem badań przedstawionych w mojej pracy była analiza morfometryczna bakterii i komórek nerwowych. Skaningowy mikroskop elektronowy stanowi wartościowy instrument badawczy wykorzystywany do określenia cech morfologicznych izolowanych mikroorganizmów i komórek. Szeroki zakres deskryptorów morfologicznych umożliwia przełożenie otrzymanych obrazów mikroskopowych na dane ilościowe, co może pomóc w ocenie charakteru antybakteryjnego, cytotoksyczności czy biokompatybilności badanych materiałów. W artykule **[A5]** omówiłam konieczność odpowiedniego przygotowanie próbek biologicznych, które wymagają utrwalenia i odwodnienia w celu uzyskania najlepszych rezultatów obrazowania SEM. Nieodpowiednia preparatyka może spowodować wysuszenie materiału biologicznego, skutkującego obkurczeniem oraz odkształceniem się komórek, a przez to prowadzić do błędnych wniosków.

Analiza biologiczna z wykorzystaniem SEM może służyć zarówno do obrazowania morfologii komórek prokariotycznych i eukariotycznych, jak i określenia ich przyczepności do powierzchni. Dokładna charakterystyka morfometryczna umożliwia również określenie liczby i rozmieszczenia hodowanych komórek na badanych materiałach, ocenę budowy błony komórkowej, długości i szerokości komórek, objętości, która związana jest z ich kondycją, stopnia rozgałęzienia neurytów, ocenę ich długości, liczby jąder komórkowych i wiele innych cech, które są istotnie skorelowane ze stosowanymi lekami, dostępnością składników odżywczych czy warunkami środowiskowymi.

W publikacji podkreśliłam fakt, że morfologia komórek prokariotycznych i eukariotycznych to krytyczny element umożliwiający ocenę przebiegu cyklu komórkowego, sprawności czy proliferacji w badaniach biologicznych. Precyzyjne i obiektywne pomiary kształtu umożliwiają określenie użyteczności stosowanego biomateriału.

6. Podsumowanie

Rozprawa doktorska obejmuje pięć publikacji, w tym dwie prace przeglądowe, trzy prace oryginalne oraz zgłoszenie patentowe. W moich badaniach skupiłam się na opracowaniu bifunkcjonalnych materiałów bioinżynieryjnych wykazujących działanie antybakteryjne i neuroprotekcyjne na bazie polimerów przewodzących, PEDOT i PEDOP, będących nośnikami modelowego antybiotyku, tetracykliny. Uzyskałam powłoki o dobrych właściwościach elektrycznych i wysokiej pojemności na lek, spośród których najlepsze właściwości posiadały matryce PEDOP i PEDOP/Tc. Ponadto, matryca PEDOP/Tc dała się poznać jako niezwykle skuteczna pod kątem działania antybakteryjnego w odniesieniu do innych przebadanych materiałów. Wyniki badań komórkowych potwierdziły, że warstwa PEDOP/Tc może służyć jako neuroelektroda o bifunkcyjnych właściwościach biologicznych, odmiennych dla komórek eukariotycznych i prokariotycznych, stanowiąc tym samym obiecującą alternatywę dla powszechnie stosowanych elektrod. Ponieważ moje osiągnięcie ma potencjalne zastosowanie w przemyśle, zostało zgłoszone do ochrony patentowej. Elementem dopełniającym moją pracę doktorską była publikacja dotycząca analizy morfometrycznej bakterii oraz komórek nerwowych na podstawie obrazów otrzymanych za pomocą skaningowego mikroskopu elektronowego. W trakcie pracy zoptymalizowałam procedurę przygotowania próbek biologicznych do pomiarów SEM, a także wyselekcjonowałam deskryptory morfometryczne, które mogą posłużyć do przeprowadzenia rozszerzonej analizy stanu komórek. W ten sposób usystematyzowałam aktualny stan wiedzy oraz zaproponowałam procedurę przygotowania próbek i analizy obrazów, która cechuje się prostotą, zmniejszonym wykorzystaniem niebezpiecznych odczynników i dostarcza szeregu informacji zarówno o komórkach eukariotycznych jak i prokariotycznych.

7. Dorobek naukowy

7.1. Liczbowe zestawienie dorobku (31.05.2022, Scopus):

Liczba publikacji: 8

Liczba cytowań: 29

Sumaryczny IF: 42.464

Sumaryczna liczba punktów MEiN: 960

Indeks H: 3

7.2. Staże naukowe

2017 – 3,5 miesięczny staż w National University of Ireland (Galway) (Centre for Research in Medical Devices).

7.3. Udział w projektach naukowych

- Naukowy opiekun pomocniczy w projekcie PBL VII edycja pt. Bakteriostatyczne i elektroaktywne powłoki poprawiające adhezję komórek dla celów inżynierii biomedycznej (2022).
- Grant na dofinansowanie rozpoczęcia działalności naukowej w nowej dziedzinie badawczej pt:" Zastosowanie poliestrów alifatycznych opartych na izosorbidzie do otrzymywania nanowłókien metodą elektroprzędzenia i ocena ich przydatności jako rusztowania (scaffolds) i wszczepy" w ramach priorytetowego obszaru badawczego POB3. 30 IV 2021-30 X 2022. (04/040/SDU/10-22-03). Kierownik projektu.
- Udział w projekcie badawczym NCN *Elektroaktywne polimery jako powłoki odpowiednie do sterowania wzrostem biofilmu bakteryjnego*, realizowanego na Katedrze Fizykochemii i Technologii Polimerów, Wydziale Chemicznym Politechniki Śląskiej (19 VII 2017 – 18 VII 2021), Sonata NCN- 2016/23/D/ST5/01306.
- Realizacja projektu *Zastosowanie analizy morfometrycznej do oceny wpływu przewodzących matryc polimerowych na bakterie i komórki nerwowe*, w ramach dotacji SBM, 5.05.2021-31.12.2021,(04/040/BKM21/0178).
- Realizacja projektu *Wpływ właściwości powierzchni PEDOP/Tc na wzrost komórek nerwowych*, w ramach dotacji SBM, 2020, Wykonawca w projekcie.
- Badania mikrobiologiczne w projekcie *New approach in the photogeneration of singlet oxygen: carbon-based nanomaterials* finansowanym przez Narodowe Centrum

Nauki (UMO-2016/21/D/ST5/01641) trwającym od 27 I 2017 – 26 I 2020.

- Badania mikrobiologiczne w projekcie PBL III Edycja *Organiczne powłoki antybakteryjne aktywowane światłem widzialnym* realizowane w ramach projektu POWER POWR-03.05.00-00-Z098/17-00.
- Realizacja projektu *Badanie wzrostu komórek nerwowych na przewodzących matrycach polimerowych z immobilizowanym lekiem*, w ramach dotacji BKM, 2019.

7.4. Udział w konferencjach

- National Scientific Conference "Understand the Science" V Edition, online, 25 IX 2021, **Czerwińska-Główka D**., Skonieczna M., Student S., Przystaś W., Zabłocka-Godlewska E., Cwalina B., Krukiewicz K.,: *Bifunctional conducting polymer matrices with antibacterial and neuroprotective effects* (komunikat ustny, autor prezentujący)
- 72nd Annual Meeting of the International Society of Electrochemistry held in Jeju Island Korea, online, 29.08-2 IX 2021, **Czerwińska-Główka D**., Skonieczna M., Student S., Przystaś W., Zabłocka-Godlewska E., Cwalina B., Krukiewicz K.,: *The influence of surface morphology of poly(3,4-ethelenedioxypyrrole) on the adhesion and development of bacteria and neural cells* (prezentacja posterowa, autor prezentujący)
- XXVI International Symposium on Bioelectrochemistry and Bioenergetics, Cluj Napoca, online 9-13 V 2021, **Czerwińska-Główka D**., Skonieczna M., Przystaś W., Zabłocka-Godlewska E., Student S., Cwalina B., Krukiewicz K.: *Antimicrobial and neuroprotective tetracycline-loaded poly(3,4-ethylenedioxypyrrole) for biomedical applications* (prezentacja posterowa, autor prezentujący)
- 9th European Young Engineers Conference, Warszawa, online, 19-21 IV 2021, **Czerwińska-Główka D**., Skonieczna M., Krukiewicz K., Przystaś W., Zabłocka-Godlewska E., Student S., Cwalina B,, Łapkowski M.: *Antibacterial and neuroprotective conducting polymers for biomedical applications* (prezentacja posterowa, autor prezentujący)
- UK-Poland Conference on Bioinspired Materials, online, 23-24 XI 2020, **Czerwińska-Główka D**., Skonieczna M., Łapkowski M., Krukiewicz K.,: *Electroactive polymer surfaces for biomedical applications* (prezentacja posterowa, autor prezentujący)
- UK-Poland Bioinspired Materials Conference, online, 23-24 XI 2020, Skorupa M.,

Więcławska D., **Czerwińska-Główka D**., Krukiewicz K., *Influence of doping ions on the properties of PEDOT and its potential biomedical applications* (prezentacja posterowa)

- 1st Scientific Summer School on-line, 8 VIII 2020, **Czerwińska-Główka D**., Krukiewicz K., Przystaś W., Zabłocka-Godlewska E., Student S., Cwalina B, Łapkowski M.,: *Conductive polymers as antibacterial surfaces* (prezentacja posterowa, autor prezentujący)
- 5th International Conference on Composite Materials and Material Engineering (ICCMME 2020), Seul, 13-16 I 2020, Skorupa M., Więcławska D., **Czerwińska-Główka D**., Krukiewicz K., *PEDOT/AgNW as a composite electroactive coating for the control of biofilm growth* (komunikat ustny)
- III Konferencja Naukowo-Techniczna 'Innowacje w Przemyśle Chemicznym', Gliwice, 29-30 X 2019, **Czerwińska-Główka D**., Krukiewicz K., Przystaś W., Zabłocka-Godlewska E., Student S., Cwalina B., Łapkowski M.,: *Badanie właściwości antybakteryjnych cienkiej warstwy platynowej* (prezentacja posterowa, autor prezentujący)
- 8th European Young Engineers Conference, Warszawa, 8-10 IV 2019, **Czerwińska-Główka D**., *Controlling the growth of bacterial biofilm on electroactive surfaces* (komunikat ustny, autor prezentujący)
- XX. Linz Winter Workshop 2018, Austria, 2-5 II 2018, Advances in Single-Molecule Research for Biology & Nanoscience, **Czerwińska-Główka D**., Krukiewicz K., Cwalina B., *Control of biofilm formation on the surface of conductive polymers* (prezentacja posterowa, autor prezentujący)
- XVI International Congress of Young Chemists, Bydgoszcz, 10-14 X 2018, **Czerwińska-Główka D**., *Controlling the formation of biofilm on electroactive surface* (komunikat ustny, autor prezentujący)
- Pomiędzy naukami, VII Edycja Konferencji dla Młodych Naukowców, 14 IX 2018, Chorzów, **Czerwińska D**., Krukiewicz K., Cwalina B.,: *Kontrola wzrostu biofilmu na powierzchniach elektroaktywnych* (komunikat ustny, autor prezentujący)
- 23rd Topical Meeting of the International Society of Electrochemistry, Vilnius (Lithuania), 8-11 V 2018, Krukiewicz K., **Czerwinska D**., Cwalina B.: *Electrochemical impedance analysis on drug-loaded conducting polymer matrices* (presentacja posterowa)

- Gliwice Scientific Meetings, Gliwice, 17-18 XI 2017, **Czerwińska D**., Krukiewicz K., Erfurt K., Chrobok A., Biggs M.,: *The influence of electrochemical modyfication on surface properties of ITO* (prezentacja posterowa, autor prezentujący)
- 2nd International Summer School "Multifunctional Smart Coatings and Surfaces, Aveiro,
  Portugal, 24 – 28 VII 2017, Krukiewicz K., **Czerwinska D.**, Vallejo-Giraldo C., Erfurt K., Chrobok A., Biggs M.: *The influence of electrochemical modification on surface properties of ITO* (prezentacja posterowa)

7.5. Inne osiągnięcia

- Grant rektorski w ramach programu projakościowego na granty za publikacje wydane w czasopismach TOP1, TOP10, czasopismach Nature lub Science oraz za monografie w wysoko punktowanych wydawnictwach, w ramach programu Inicjatywa Doskonałości – Uczelnia Badawcza za publikację „Bifunctional conducting polymer matrices with antibacterial and neuroprotective effects" w czasopiśmie Bioelectrochemistry – TOP10.
- Grant rektorski projakościowy II stopnia w ramach konkursu projakościowego na rektorskie granty za wysoko punktowane publikacje lub udzielone patenty.
- Grant rektorski w ramach programu projakościowego na granty za publikacje wydane w czasopismach TOP1, TOP10, czasopismach Nature lub Science oraz za monografie w wysoko punktowanych wydawnictwach, w ramach programu Inicjatywa Doskonałości – Uczelnia Badawcza za publikację „Electrically-responsive antimicrobial coatings based on a tetracycline-loaded poly(3,4-ethylenedioxythiophene) matrix" w czasopiśmie Materials Science and Engineering: C – TOP10.
- Grant rektorski w ramach programu projakościowego na granty za publikacje wydane w czasopismach TOP1, TOP10, czasopismach Nature lub Science oraz za monografie w wysoko punktowanych wydawnictwach, w ramach programu Inicjatywa Doskonałości – Uczelnia Badawcza za publikację „A journey in the complex interactions between electrochemistry and bacteriology: From electroactivity to electromodulation of bacterial biofilms" w czasopiśmie Bioelectrochemistry – TOP10.

8. Bibliografia

[1] World Health Organisation, Neurological Disorders: Public Health Challenges., Geneva, Switzerland, 2006.

[2] World Health Organisation, Dementia a public health priority, 2012.

[3] F. He, R. Lycke, M. Ganji, C. Xie, L. Luan, Ultraflexible Neural Electrodes for Long-Lasting Intracortical Recording, IScience. 23 (2020) 101387. https://doi.org/10.1016/j.isci.2020.101387.

[4] G. Hong, C.M. Lieber, Novel electrode technologies for neural recordings, Nat. Rev. Neurosci. 20 (2019) 330–345. https://doi.org/10.1038/s41583-019-0140-6.

[5] M. Kazamel, P.P. Warren, History of electromyography and nerve conduction studies: A tribute to the founding fathers, J. Clin. Neurosci. 43 (2017) 54–60. https://doi.org/10.1016/j.jocn.2017.05.018.

[6] I. Vėbraitė, Y. Hanein, Soft Devices for High-Resolution Neuro-Stimulation: The Interplay Between Low-Rigidity and Resolution, Front. Med. Technol. 3 (2021) 1–23. https://doi.org/10.3389/fmedt.2021.675744.

[7] T.A. Thrasher, H.M. Flett, M.R. Popovic, Gait training regimen for incomplete spinal cord injury using functional electrical stimulation, Spinal Cord. 44 (2006) 357–361. https://doi.org/10.1038/sj.sc.3101864.

[8] D.M. Thompson, A.N. Koppes, J.G. Hardy, C.E. Schmidt, Electrical Stimuli in the Central Nervous System Microenvironment, Annu. Rev. Biomed. Eng. 16 (2014) 397–430. https://doi.org/10.1146/annurev-bioeng-121813-120655.

[9] A.P. Salazar, A.S. Pagnussat, G.A. Pereira, G. Scopel, J.L. Lukrafka, Neuromuscular electrical stimulation to improve gross motor function in children with cerebral palsy: a meta-analysis, Brazilian J. Phys. Ther. 23 (2019) 378–386. https://doi.org/10.1016/j.bjpt.2019.01.006.

[10] B.L. Shideler, T.C. Bulea, J. Chen, C.J. Stanley, A.J. Gravunder, D.L. Damiano, Toward a hybrid exoskeleton for crouch gait in children with cerebral palsy: neuromuscular electrical stimulation for improved knee extension, J. Neuroeng. Rehabil. 17 (2020) 121. https://doi.org/10.1186/s12984-020-00738-7.

[11] N.C. Swann, C. de Hemptinne, M.C. Thompson, S. Miocinovic, A.M. Miller, R. Gilron, J.L. Ostrem, H.J. Chizeck, P.A. Starr, Adaptive deep brain stimulation for Parkinson's disease using motor cortex sensing, J. Neural Eng. 15 (2018) 046006. https://doi.org/10.1088/1741-2552/aabc9b.

[12] N. Zangiabadi, L.Di. Ladino, F. Sina, J.P. Orozco-Hernández, A. Carter, J.F. Téllez-Zenteno, Deep brain stimulation and drug-resistant epilepsy: A review of the literature, Front. Neurol. 10 (2019) 1–18. https://doi.org/10.3389/fneur.2019.00601.

[13] A.A. Saoji, W.J. Adkins, A.P. Olund, E.R. Nelson-Bakkum, K. Koka, Effect of exceeding compliance voltage on speech perception in cochlear implants, Hear. Res. 400 (2021) 108112. https://doi.org/10.1016/j.heares.2020.108112.

[14] A. Barriga-Rivera, T. Guo, C.-Y. Yang, A. Al Abed, S. Dokos, N.H. Lovell, J.W. Morley, G.J. Suaning, High-amplitude electrical stimulation can reduce elicited

neuronal activity in visual prosthesis, Sci. Rep. 7 (2017) 42682. https://doi.org/10.1038/srep42682.

[15] J.-W. Jeong, G. Shin, S. Il Park, K.J. Yu, L. Xu, J.A. Rogers, Soft Materials in Neuroengineering for Hard Problems in Neuroscience, Neuron. 86 (2015) 175–186. https://doi.org/10.1016/j.neuron.2014.12.035.

[16] Ocena biologiczna (biozgodności) Urząd Rejestracji Produktów Leczniczych Wyrobów Medycznych i Produktów Biobójczych, (2019) 2014–2016. http://www.urpl.gov.pl/en/printpdf/267.

[17] S.P. Lacour, G. Courtine, J. Guck, Materials and technologies for soft implantable neuroprostheses, Nat. Rev. Mater. 1 (2016) 16063. https://doi.org/10.1038/natrevmats.2016.63.

[18] H.-Y. Lai, L.-D. Liao, C.-T. Lin, J.-H. Hsu, X. He, Y.-Y. Chen, J.-Y. Chang, H.-F. Chen, S. Tsang, Y.-Y.I. Shih, Design, simulation and experimental validation of a novel flexible neural probe for deep brain stimulation and multichannel recording, J. Neural Eng. 9 (2012) 036001. https://doi.org/10.1088/1741-2560/9/3/036001.

[19] E. Castagnola, A. Ansaldo, E. Maggiolini, T. Ius, M. Skrap, D. Ricci, L. Fadiga, Smaller, softer, lower-impedance electrodes for human neuroprosthesis: a pragmatic approach, Front. Neuroeng. 7 (2014) 1–17. https://doi.org/10.3389/fneng.2014.00008.

[20] M.R. Abidian, D.C. Martin, Experimental and theoretical characterization of implantable neural microelectrodes modified with conducting polymer nanotubes, Biomaterials. 29 (2008) 1273–1283. https://doi.org/10.1016/j.biomaterials.2007.11.022.

[21] D.R. Merrill, M. Bikson, J.G.R. Jefferys, Electrical stimulation of excitable tissue: design of efficacious and safe protocols, J. Neurosci. Methods. 141 (2005) 171–198. https://doi.org/10.1016/j.jneumeth.2004.10.020.

[22] M. Rai, A.P. Ingle, S. Medici, Biomedical applications of metals, 2018. https://doi.org/10.1007/978-3-319-74814-6.

[23] Z.J. Du, C.L. Kolarcik, T.D.Y. Kozai, S.D. Luebben, S.A. Sapp, X.S. Zheng, J.A. Nabity, X.T. Cui, Ultrasoft microwire neural electrodes improve chronic tissue integration, Acta Biomater. 53 (2017) 46–58. https://doi.org/10.1016/j.actbio.2017.02.010.

[24] S. Mohapatra, Sterilization and Disinfection, in: Essentials of Neuroanesthesia, Elsevier, 2017: pp. 929–944. https://doi.org/10.1016/B978-0-12-805299-0.00059-2.

[25] S. Voidazan, S. Albu, R. Toth, B. Grigorescu, A. Rachita, I. Moldovan, Healthcare Associated Infections—A New Pathology in Medical Practice?, Int. J. Environ. Res. Public Health. 17 (2020) 760. https://doi.org/10.3390/ijerph17030760.

[26] S. Glage, S. Paret, A. Winkel, M. Stiesch, A. Bleich, J.K. Krauss, K. Schwabe, A new model for biofilm formation and inflammatory tissue reaction: intraoperative infection of a cranial implant with Staphylococcus aureus in rats, Acta Neurochir. (Wien). 159 (2017) 1747–1756. https://doi.org/10.1007/s00701-017-3244-7.

[27] J.L. Del Pozo, M.S. Rouse, J.N. Mandrekar, J.M. Steckelberg, R. Patel, The electricidal effect: Reduction of Staphylococcus and Pseudomonas biofilms by prolonged exposure to low-intensity electrical current, Antimicrob. Agents Chemother. 53 (2009) 41–45.

https://doi.org/10.1128/AAC.00680-08.

[28] B.L. Bassler, How bacteria talk to each other: regulation of gene expression by quorum sensing, Curr. Opin. Microbiol. 2 (1999) 582–587. https://doi.org/10.1016/S1369-5274(99)00025-9.

[29] M.R. Parsek, E.P. Greenberg, Sociomicrobiology: the connections between quorum sensing and biofilms, Trends Microbiol. 13 (2005) 27–33. https://doi.org/10.1016/j.tim.2004.11.007.

[30] A. Prindle, J. Liu, M. Asally, S. Ly, J. Garcia-Ojalvo, G.M. Süel, Ion channels enable electrical communication in bacterial communities, Nature. 527 (2015) 59–63. https://doi.org/10.1038/nature15709.

[31] J. Humphries, L. Xiong, J. Liu, A. Prindle, F. Yuan, H.A. Arjes, L. Tsimring, G.M. Süel, Species-Independent Attraction to Biofilms through Electrical Signaling, Cell. 168 (2017) 200-209.e12. https://doi.org/10.1016/j.cell.2016.12.014.

[32] E. Ben Jacob, I. Becker, Y. Shapira, H. Levine, Bacterial linguistic communication and social intelligence, Trends Microbiol. 12 (2004) 366–372. https://doi.org/10.1016/j.tim.2004.06.006.

[33] S. Majumdar, S. Mondal, Conversation game: talking bacteria, J. Cell Commun. Signal. 10 (2016) 331–335. https://doi.org/10.1007/s12079-016-0333-y.

[34] J. Liu, A. Prindle, J. Humphries, M. Gabalda-Sagarra, M. Asally, D.D. Lee, S. Ly, J. Garcia-Ojalvo, G.M. Süel, Metabolic co-dependence gives rise to collective oscillations within biofilms, Nature. 523 (2015) 550–554. https://doi.org/10.1038/nature14660.

[35] H.-C. Flemming, J. Wingender, U. Szewzyk, P. Steinberg, S.A. Rice, S. Kjelleberg, Biofilms: an emergent form of bacterial life, Nat. Rev. Microbiol. 14 (2016) 563–575. https://doi.org/10.1038/nrmicro.2016.94.

[36] W. Michael Dunne Jr., Bacterial Adhesion : Seen Any Good Biofilms Lately ?, Clin. Microbiol. Rev. 15 (2002) 155–166. https://doi.org/10.1128/CMR.15.2.155.

[37] C.D. Owens, K. Stoessel, Surgical site infections: epidemiology, microbiology and prevention, J. Hosp. Infect. 70 (2008) 3–10. https://doi.org/10.1016/S0195-6701(08)60017-1.

[38] W. Bereket, K. Hemalatha, B. Getenet, T. Wondwossen, A. Solomon, A. Zeynudin, S. Kannan, Update on bacterial nosocomial infections., Eur. Rev. Med. Pharmacol. Sci. 16 (2012) 1039–44. https://doi.org/10.1155/2018/2127814.

[39] T. Ursell, T.K. Lee, D. Shiomi, H. Shi, C. Tropini, R.D. Monds, A. Colavin, G. Billings, I. Bhaya-Grossman, M. Broxton, B.E. Huang, H. Niki, K.C. Huang, Rapid, precise quantification of bacterial cellular dimensions across a genomic-scale knockout library, BMC Biol. 15 (2017) 17. https://doi.org/10.1186/s12915-017-0348-8.

[40] A. Amir, Cell Size Regulation in Bacteria, Phys. Rev. Lett. 112 (2014) 208102. https://doi.org/10.1103/PhysRevLett.112.208102.

[41] O. Ciofu, E. Rojo-Molinero, M.D. Macià, A. Oliver, Antibiotic treatment of biofilm infections, APMIS. 125 (2017) 304–319. https://doi.org/10.1111/apm.12673.

[42] N. Wellman, S.M. Fortun, B.R. McLeod, Bacterial biofilms and the bioelectric effect.,

Antimicrob. Agents Chemother. 40 (1996) 2012–4. papers://71b3262e-544c-4e65-bc57-5ad73365e40b/Paper/p1940.

[43] A. Zhuang, Q. Pan, Y. Qian, S. Fan, X. Yao, L. Song, B. Zhu, Y. Zhang, Transparent Conductive Silk Film with a PEDOT-OH Nano Layer as an Electroactive Cell Interface, ACS Biomater. Sci. Eng. 7 (2021) 1202–1215. https://doi.org/10.1021/acsbiomaterials.0c01665.

[44] M.R. Abidian, D.-H. Kim, D.C. Martin, Conducting-Polymer Nanotubes for Controlled Drug Release, Adv. Mater. 18 (2006) 405–409. https://doi.org/10.1002/adma.200501726.

[45] C.L. Kolarcik, K. Catt, E. Rost, I.N. Albrecht, D. Bourbeau, Z. Du, T.D.Y. Kozai, X. Luo, D.J. Weber, X. Tracy Cui, Evaluation of poly(3,4-ethylenedioxythiophene)/carbon nanotube neural electrode coatings for stimulation in the dorsal root ganglion, J. Neural Eng. 12 (2015) 016008. https://doi.org/10.1088/1741-2560/12/1/016008.

[46] D. Esrafilzadeh, J.M. Razal, S.E. Moulton, E.M. Stewart, G.G. Wallace, Multifunctional conducting fibres with electrically controlled release of ciprofloxacin, J. Control. Release. 169 (2013) 313–320. https://doi.org/10.1016/j.jconrel.2013.01.022.

[47] K. Krukiewicz, T. Jarosz, J.K. Zak, M. Lapkowski, P. Ruszkowski, T. Bobkiewicz-Kozlowska, B. Bednarczyk-Cwynar, Advancing the delivery of anticancer drugs: Conjugated polymer/triterpenoid composite, Acta Biomater. 19 (2015) 158–165. https://doi.org/10.1016/j.actbio.2015.03.006.

[48] K. Krukiewicz, M. Cichy, P. Ruszkowski, R. Turczyn, T. Jarosz, J.K. Zak, M. Lapkowski, B. Bednarczyk-Cwynar, Betulin-loaded PEDOT films for regional chemotherapy, Mater. Sci. Eng. C. 73 (2017) 611–615. https://doi.org/10.1016/j.msec.2016.12.115.

[49] N. Alizadeh, E. Shamaeli, Electrochemically controlled release of anticancer drug methotrexate using nanostructured polypyrrole modified with cetylpyridinium: Release kinetics investigation, Electrochim. Acta. 130 (2014) 488–496. https://doi.org/10.1016/j.electacta.2014.03.055.

[50] R. Wadhwa, C.F. Lagenaur, X.T. Cui, Electrochemically controlled release of dexamethasone from conducting polymer polypyrrole coated electrode, J. Control. Release. 110 (2006) 531–541. https://doi.org/10.1016/j.jconrel.2005.10.027.

[51] K. Krukiewicz, A. Kruk, R. Turczyn, Evaluation of drug loading capacity and release characteristics of PEDOT/naproxen system: Effect of doping ions, Electrochim. Acta. 289 (2018) 218–227. https://doi.org/10.1016/j.electacta.2018.09.011.

[52] C. Vallejo-Giraldo, A. Kelly, M.J.P. Biggs, Biofunctionalisation of electrically conducting polymers, Drug Discov. Today. 19 (2014) 88–94. https://doi.org/10.1016/j.drudis.2013.07.022.

[53] R.A. Green, C.M. Williams, N.H. Lovell, L.A. Poole-Warren, Novel neural interface for implant electrodes: improving electroactivity of polypyrrole through MWNT incorporation, J. Mater. Sci. Mater. Med. 19 (2008) 1625–1629. https://doi.org/10.1007/s10856-008-3376-7.

[54] Y. Zhao, Y. Liang, S. Ding, K. Zhang, H. Mao, Y. Yang, Application of conductive

PPy/SF composite scaffold and electrical stimulation for neural tissue engineering, Biomaterials. 255 (2020) 120164. https://doi.org/10.1016/j.biomaterials.2020.120164.

[55] M.R. Abidian, D.C. Martin, Multifunctional Nanobiomaterials for Neural Interfaces, Adv. Funct. Mater. 19 (2009) 573–585. https://doi.org/10.1002/adfm.200801473.

[56] R. Gerwig, K. Fuchsberger, B. Schroeppel, G.S. Link, G. Heusel, U. Kraushaar, W. Schuhmann, A. Stett, M. Stelzle, PEDOT–CNT Composite Microelectrodes for Recording and Electrostimulation Applications: Fabrication, Morphology, and Electrical Properties, Front. Neuroeng. 5 (2012) 1–11. https://doi.org/10.3389/fneng.2012.00008.

[57] K. Krukiewicz, M. Chudy, C. Vallejo-Giraldo, M. Skorupa, D. Więcławska, R. Turczyn, M. Biggs, Fractal form PEDOT/Au assemblies as thin-film neural interface materials, Biomed. Mater. 13 (2018) 054102. https://doi.org/10.1088/1748-605X/aabced.

[58] K.A. Ludwig, J.D. Uram, J. Yang, D.C. Martin, D.R. Kipke, Chronic neural recordings using silicon microelectrode arrays electrochemically deposited with a poly(3,4-ethylenedioxythiophene) (PEDOT) film, J. Neural Eng. 3 (2006) 59–70. https://doi.org/10.1088/1741-2560/3/1/007.

[59] S. Cui, J. Mao, M. Rouabhia, S. Elkoun, Z. Zhang, A biocompatible polypyrrole membrane for biomedical applications, RSC Adv. 11 (2021) 16996–17006. https://doi.org/10.1039/D1RA01338F.

[60] R. Balint, N.J. Cassidy, S.H. Cartmell, Electrical Stimulation: A Novel Tool for Tissue Engineering, Tissue Eng. Part B Rev. 19 (2013) 48–57. https://doi.org/10.1089/ten.teb.2012.0183.

[61] C.R. Broda, J.Y. Lee, S. Sirivisoot, C.E. Schmidt, B.S. Harrison, A chemically polymerized electrically conducting composite of polypyrrole nanoparticles and polyurethane for tissue engineering, J. Biomed. Mater. Res. Part A. 98A (2011) 509–516. https://doi.org/10.1002/jbm.a.33128.

[62] G. Shi, M. Rouabhia, Z. Wang, L.H. Dao, Z. Zhang, A novel electrically conductive and biodegradable composite made of polypyrrole nanoparticles and polylactide, Biomaterials. 25 (2004) 2477–2488. https://doi.org/10.1016/j.biomaterials.2003.09.032.

[63] S.C. Luo, E.M. Ali, N.C. Tansil, H.H. Yu, S. Gao, E.A.B. Kantchev, J.Y. Ying, Poly(3,4-ethylenedioxythiophene) (PEDOT) nanobiointerfaces: Thin, ultrasmooth, and functionalized PEDOT films with in vitro and in vivo biocompatibility, Langmuir. 24 (2008) 8071–8077. https://doi.org/10.1021/la800333g.

[64] A. Madhan Kumar, A.Y. Adesina, M.A. Hussein, S. Ramakrishna, N. Al-Aqeeli, S. Akhtar, S. Saravanan, PEDOT/FHA nanocomposite coatings on newly developed Ti-Nb-Zr implants: Biocompatibility and surface protection against corrosion and bacterial infections, Mater. Sci. Eng. C. 98 (2019) 482–495. https://doi.org/10.1016/j.msec.2019.01.012.

[65] C. Bodart, N. Rossetti, J. Hagler, P. Chevreau, D. Chhin, F. Soavi, S.B. Schougaard, F. Amzica, F. Cicoira, Electropolymerized Poly(3,4-ethylenedioxythiophene) (PEDOT) Coatings for Implantable Deep-Brain-Stimulating Microelectrodes, ACS Appl. Mater. Interfaces. 11 (2019) 17226–17233. https://doi.org/10.1021/acsami.9b03088.

[66] C. Kleber, K. Lienkamp, J. Rühe, M. Asplund, Electrochemically Controlled Drug Release from a Conducting Polymer Hydrogel (PDMAAp/PEDOT) for Local Therapy and Bioelectronics, Adv. Healthc. Mater. 8 (2019) 1801488. https://doi.org/10.1002/adhm.201801488.

[67] S. Carli, G. Fioravanti, A. Armirotti, F. Ciarpella, M. Prato, G. Ottonello, M. Salerno, A. Scarpellini, D. Perrone, E. Marchesi, D. Ricci, L. Fadiga, A New Drug Delivery System based on Tauroursodeoxycholic Acid and PEDOT, Chem. – A Eur. J. 25 (2018) chem.201805285. https://doi.org/10.1002/chem.201805285.

[68] A.K. Jayaram, C. Pitsalidis, E. Tan, C.-M. Moysidou, M.F.L. De Volder, J.-S. Kim, R.M. Owens, 3D Hybrid Scaffolds Based on PEDOT:PSS/MWCNT Composites, Front. Chem. 7 (2019) 1–9. https://doi.org/10.3389/fchem.2019.00363.

[69] S. Wang, S. Guan, Z. Zhu, W. Li, T. Liu, X. Ma, Hyaluronic acid doped-poly(3,4-ethylenedioxythiophene)/chitosan/gelatin (PEDOT-HA/Cs/Gel) porous conductive scaffold for nerve regeneration, Mater. Sci. Eng. C. 71 (2017) 308–316. https://doi.org/10.1016/j.msec.2016.10.029.

[70] S. Gomez-Carretero, B. Libberton, M. Rhen, A. Richter-Dahlfors, Redox-active conducting polymers modulate Salmonella biofilm formation by controlling availability of electron acceptors, Npj Biofilms Microbiomes. 3 (2017). https://doi.org/10.1038/s41522-017-0027-0.

[71] K. Butina, S. Löffler, M. Rhen, A. Richter-Dahlfors, Electrochemical sensing of bacteria via secreted redox active compounds using conducting polymers, Sensors Actuators, B Chem. 297 (2019) 126703. https://doi.org/10.1016/j.snb.2019.126703.

[72] S. Gomez-Carretero, R. Nybom, A. Richter-Dahlfors, Electroenhanced Antimicrobial Coating Based on Conjugated Polymers with Covalently Coupled Silver Nanoparticles Prevents Staphylococcus aureus Biofilm Formation, Adv. Healthc. Mater. 6 (2017) 1–10. https://doi.org/10.1002/adhm.201700435.

[73] P. Schottland, K. Zong, C.L. Gaupp, B.C. Thompson, C.A. Thomas, I. Giurgiu, R. Hickman, K.A. Abboud, J.R. Reynolds, Poly(3,4-alkylenedioxypyrrole)s: Highly Stable Electronically Conducting and Electrochromic Polymers, Macromolecules. 33 (2000) 7051–7061. https://doi.org/10.1021/ma000490f.

[74] K. Krukiewicz, A. Kowalik, D. Czerwinska-Glowka, M.J.P. Biggs, Electrodeposited poly(3,4-ethylenedioxypyrrole) films as neural interfaces: Cytocompatibility and electrochemical studies, Electrochim. Acta. 302 (2019) 21–30. https://doi.org/10.1016/j.electacta.2019.02.023.

[75] K. Krukiewicz, B. Gniazdowska, T. Jarosz, A.P. Herman, S. Boncel, R. Turczyn, Effect of immobilization and release of ciprofloxacin and quercetin on electrochemical properties of poly(3,4-ethylenedioxypyrrole) matrix, Synth. Met. 249 (2019) 52–62. https://doi.org/10.1016/j.synthmet.2019.02.001.

[76] K. Krukiewicz, P. Zawisza, A.P. Herman, R. Turczyn, S. Boncel, J.K. Zak, An electrically controlled drug delivery system based on conducting poly(3,4-ethylenedioxypyrrole) matrix, Bioelectrochemistry. 108 (2016) 13–20. https://doi.org/10.1016/j.bioelechem.2015.11.002.

[77] T. Tikka, B.L. Fiebich, G. Goldsteins, R. Keinänen, J. Koistinaho, Minocycline, a tetracycline derivative, is neuroprotective against excitotoxicity by inhibiting activation

and proliferation of microglia, J. Neurosci. (2001). https://doi.org/10.1523/jneurosci.21-08-02580.2001.

[78] D. Orsucci, V. Calsolaro, M. Mancuso, G. Siciliano, Neuroprotective Effects of Tetracyclines: Molecular Targets, Animal Models and Human Disease, CNS Neurol. Disord. - Drug Targets. (2012). https://doi.org/10.2174/187152709788680689.

[79] D.C. Baptiste, K.J. Powell, C.A.B. Jollimore, C. Hamilton, T.L. Levatte, M.L. Archibald, B.C. Chauhan, G.S. Robertson, M.E.M. Kelly, Effects of minocycline and tetracycline on retinal ganglion cell survival after axotomy, Neuroscience. 134 (2005) 575–582. https://doi.org/10.1016/j.neuroscience.2005.04.011.

[80] M.Y. Vaidya, A.J. McBain, J.A. Butler, C.E. Banks, K.A. Whitehead, Antimicrobial Efficacy and Synergy of Metal Ions against Enterococcus faecium, Klebsiella pneumoniae and Acinetobacter baumannii in Planktonic and Biofilm Phenotypes, Sci. Rep. 7 (2017) 5911. https://doi.org/10.1038/s41598-017-05976-9.

[81] M. Hashimoto, H. Yanagiuchi, H. Kitagawa, Y. Honda, Inhibitory effect of platinum nanoparticles on biofilm formation of oral bacteria, Nano Biomed. 9 (2017) 77–82. https://doi.org/10.11344/nano.9.77.

[82] H.B. Wang, Q.F. Wei, J.Y. Wang, J.H. Hong, X.Y. Zhao, Sputter deposition of nanostructured antibacterial silver on polypropylene non-wovens, Surf. Eng. 24 (2008) 70–74. https://doi.org/10.1179/174329408X277493.

[83] S. Wu, B. Zhang, Y. Liu, X. Suo, H. Li, Influence of surface topography on bacterial adhesion: A review (Review), Biointerphases. 13 (2018) 060801. https://doi.org/10.1116/1.5054057.

[84] Y. Yuan, M.P. Hays, P.R. Hardwidge, J. Kim, Surface characteristics influencing bacterial adhesion to polymeric substrates, RSC Adv. 7 (2017) 14254–14261. https://doi.org/10.1039/C7RA01571B.

[85] C. Boehler, Z. Aqrawe, M. Asplund, Applications of PEDOT in bioelectronic medicine, Bioelectron. Med. 2 (2019) 89–99. https://doi.org/10.2217/bem-2019-0014.

[86] I. Chopra, M. Roberts, Tetracycline Antibiotics: Mode of Action, Applications, Molecular Biology, and Epidemiology of Bacterial Resistance, Microbiol. Mol. Biol. Rev. 65 (2001) 232–260. https://doi.org/10.1128/MMBR.65.2.232-260.2001.

[87] U.A. Aregueta-Robles, A.J. Woolley, L.A. Poole-Warren, N.H. Lovell, R.A. Green, Organic electrode coatings for next-generation neural interfaces, Front. Neuroeng. 7 (2014) 1–18. https://doi.org/10.3389/fneng.2014.00015.

[88] K. Krukiewicz, A. Kowalik, R. Turczyn, M.J.P. Biggs, In vitro attenuation of astrocyte activation and neuroinflammation through ibuprofen-doping of poly(3,4-ethylenedioxypyrrole) formulations, Bioelectrochemistry. 134 (2020) 107528. https://doi.org/10.1016/j.bioelechem.2020.107528.

[89] Z.A. King, C.M. Shaw, S.A. Spanninga, D.C. Martin, Structural, chemical and electrochemical characterization of poly(3,4-Ethylenedioxythiophene) (PEDOT) prepared with various counter-ions and heat treatments, Polymer (Guildf). 52 (2011) 1302–1308. https://doi.org/10.1016/j.polymer.2011.01.042.

[90] S. Carli, G. Fioravanti, A. Armirotti, F. Ciarpella, M. Prato, G. Ottonello, M. Salerno, A. Scarpellini, D. Perrone, E. Marchesi, D. Ricci, L. Fadiga, A New Drug Delivery

System based on Tauroursodeoxycholic Acid and PEDOT, Chem. – A Eur. J. 25 (2018) chem.201805285. https://doi.org/10.1002/chem.201805285.

[91] K. Krukiewicz, J. Britton, D. Więcławska, M. Skorupa, J. Fernandez, J.R. Sarasua, M.J.P. Biggs, Electrical percolation in extrinsically conducting, poly(ε-decalactone) composite neural interface materials, Sci. Rep. 11 (2021) 1–10. https://doi.org/10.1038/s41598-020-80361-7.

[92] A. Kharkwal, D. Melepurath, A.G. Joshi, A.K. Srivastava, Red to blue high electrochromic contrast and rapid switching poly(3,4-ethylenedioxypyrrole)-Au/Ag nanocomposite devices for smart windows, ChemPhysChem. 12 (2011) 1176–1188. https://doi.org/10.1002/cphc.201000973.

[93] M. Ates, Y. Bayrak, H. Ozkan, O. Yoruk, M. Yildirim, O. Kuzgun, Synthesis of rGO/TiO 2 /PEDOT nanocomposites, supercapacitor device performances and equivalent electrical circuit models, J. Polym. Res. 26 (2019) 1–16. https://doi.org/10.1007/s10965-018-1692-2.

[94] D. Prodanov, J. Delbeke, Mechanical and Biological Interactions of Implants with the Brain and Their Impact on Implant Design, Front. Neurosci. 10 (2016). https://doi.org/10.3389/fnins.2016.00011.

[95] W.J. Tyler, The mechanobiology of brain function, Nat. Rev. Neurosci. 13 (2012) 867–878. https://doi.org/10.1038/nrn3383.

[96] J. Bengtsson-Palme, D.G.J. Larsson, Concentrations of antibiotics predicted to select for resistant bacteria: Proposed limits for environmental regulation, Environ. Int. 86 (2016) 140–149. https://doi.org/10.1016/j.envint.2015.10.015.

[97] M. Domercq, C. Matute, Neuroprotection by tetracyclines, Trends Pharmacol. Sci. 25 (2004) 609–612. https://doi.org/10.1016/j.tips.2004.10.001.

Publikacje

Bioelectrochemistry 131 (2020) 107401

Contents lists available at ScienceDirect

Bioelectrochemistry

journal homepage: www.elsevier.com/locate/bioelechem

A journey in the complex interactions between electrochemistry and bacteriology: From electroactivity to electromodulation of bacterial biofilms

Dominika Czerwińska-Główka [a], Katarzyna Krukiewicz [a,*]

[a] Department of Physical Chemistry and Technology of Polymers, Silesian University of Technology, M. Strzody 9, 44-100 Gliwice, Poland

ARTICLE INFO

Article history:
Received 17 July 2019
Received in revised form 1 October 2019
Accepted 1 October 2019
Available online 14 October 2019

Keywords:
Antimicrobial activity
Bacterial biofilm
Bacteriology
Electrical stimulation
Electroanalysis
Microbial fuel cells

ABSTRACT

Although the term bioelectrochemistry tends to be associated with animal and human tissues, bioelectric currents exist also in plants and bacteria. Especially the latter, when agglomerated in the form of biofilms, can exhibit electroactivity and susceptibility to electrical stimulation. Therefore, electrochemical methods appear to become powerful techniques to expand the conventional strategies of biofilm characterization and modification. In this review, we aim to provide the insight into the electrochemical behaviour of bacteria and present the variety of electrochemical techniques that can be used either for the non-destructive monitoring of bacterial communities or modulation of their growth. The most common applications of electrical stimulation on biofilms are presented, including the prevention of bacterial growth by charging the surface of the materials, changing the direction of bacterial movement under the influence of the electric field and increasing of the potency of antibiotics when bactericides are coupled with the electric field. Also, the industrial applications of microbial electrotechnologies are described, such as bioremediation, wastewater treatment, and microbial fuel cells. Consequently, we are showing the complexity of interactions that exist between electrochemistry and bacteriology that can be used for the benefit of these two disciplines.

Contents

1. Introduction

Despite the electrochemical aspects of bacteriology has been known in the literature for more than 100 years [1], in the beginning this field of bioelectrochemistry was considered as a scientific curiosity rather than applied science. The advances in the fundamental research have finally

* Corresponding author.
E-mail address: katarzyna.krukiewicz@polsl.pl (K. Krukiewicz).

https://doi.org/10.1016/j.bioelechem.2019.107401

led to the development of so-called microbial electrochemical technologies, in which bacteria started to be applied to solve industrial problems in terms of bioproduction, bioremediation, wastewater treatment, biosensing and many more [2].

In this review, we aim to present a storyline of the progress in the research focused on the interactions between electrochemistry and bacteriology. In the belief that no scientific breakthrough is possible without previous theoretical considerations and basic research, we start our discussion from providing the basic aspects of bacterial bioelectrochemistry, namely the description of the process of electrical signalling among bacteria and biofilms. The confirmation of the existence of bioelectric currents in bacterial biofilms led to the concept of applying electrochemical methods for biofilm characterization. Consequently, we present a summary of numerous electrochemical techniques that can be used for the non-destructive monitoring of bacterial communities and evaluating their electrical properties. Knowing that bacterial biofilms can express electroactivity allowed to take an important step forward, namely to develop a concept of using electric current to affect bacteria. Indeed, this idea was a spark of inspiration to the development of microbial electrochemical technologies, such as bioremediation, wastewater treatment and microbial fuel cells, as well as specific biomedical applications involving the prevention of bacterial growth, changing the direction of bacterial movement or increasing the potency of antibiotics through electrical stimulation. Due to its consecutive structure, this review provides an overview of the complexity of interactions existing between electrochemistry and bacteriology that can be used for the benefit of both of these disciplines.

2. Bioelectrical currents in animals, plants and bacteria

The electric current is commonly understood as the ordered movement of electrons. However, when referring to living organisms, the most common charge carriers appear to be ions, such as K^+, Na^+, Ca^{2+}, Cl^-, giving rise to the bioelectrical currents (Scheme 1). Since the cell membranes are semipermeable, they exhibit selectivity for one type of ions, resulting in the regulation of extracellular and intracellular ion concentrations. These small, charged particles can travel across the membrane by means of diffusion through the ion channels by the ion pump mechanism, at which it is necessary to provide energy for the transport of ions [3–5]. The local potential changes generated by moving ions allow targeting the metabolism, electrical impulses or cell membrane permeability depending on the external signal. The electric signals can be also used to allow both plant or animal cells and bacteria in biofilms to communicate with each other, with the complexity of the messages varying from simple signals to complex long-distance electrical signalling, which is faster than any chemical signalling [6–8].

In 1791, Luigi Galvani was the first scientist to describe the existence of bioelectrical current in animals on the example of a frog [9]. He showed that touching the muscle of the frog's limb simultaneously with two different, interconnected metals, caused its contraction. Admittedly, it did not refer to the electricity of tissues but to the current caused by the contact of metals with moisture. However, these studies started an interest in the field of bioelectrochemistry [10] and led to the formation of widely accepted principles. Generally, the organisms are made up of cells that regulate the exchange of chemicals through the cell membrane. Intracellular signalling uses readily available particles such as ions. The flow of ions is regulated through the ion channels made from proteins that allow for the passage of some ions and are able to block others. The mechanism depends on the inward movement of sodium ions when depolarization takes place, followed by potassium ions flowing outside causing repolarization [7]. The action potential formed as the result of these activities is responsible for the rapid transport of information, which are transmitted along the axons in the nervous system and over the surface of some muscle or glandular cells. These signals are transmitted to the whole organism; they have a constant speed and amplitude, and are used to control metabolic processes and physiological functions. Electrical signals allow to see, feel and control the main physiological processes, including development and regeneration of the cells. Relevant environmental signals, such as light or temperature, can affect ionic conductivity altering membrane potential [11–13]. Currently, bioelectricity is also used in various diagnostic tests. Such studies include measurements of electrical effects from heart or brain cells [14].

Electrical signalling, however, does not apply only to the animal world, but also to the kingdom of plants. In 1873, Burdon-Sanderson discovered the presence of action potentials in plants by stimulating the leaf of *Dionaea* [15]. Since then, the detailed examination of the plants for their electroactivity has begun. In the case of plants, the transmission of signal plays an important role in inter- and intra-cellular communication. The electrical signals include action potentials, variation potentials and local electrical potential [6,16,17], all of them resulting in numerous changes in the membrane potential. The action

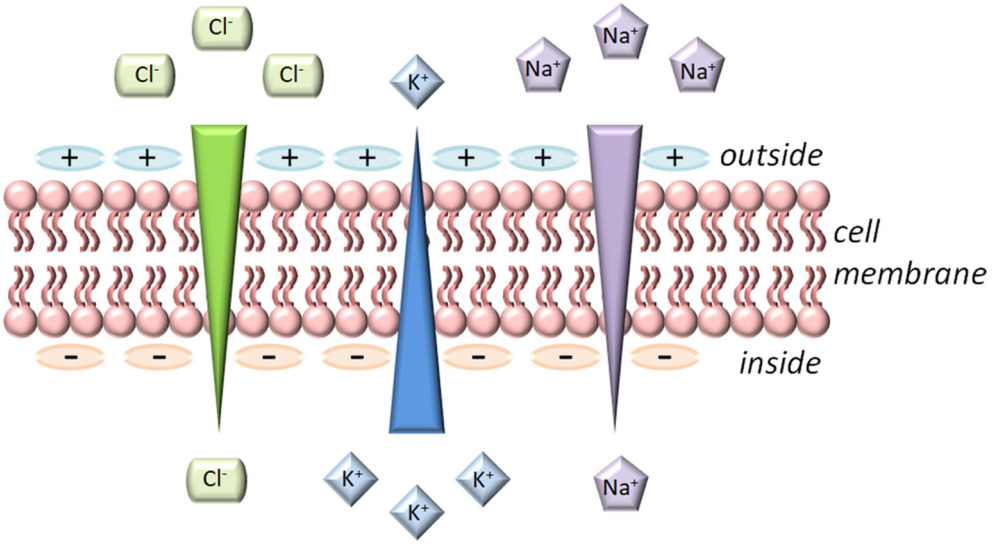

Scheme 1. Amino acid sequence of the peptide Pc_312–324.

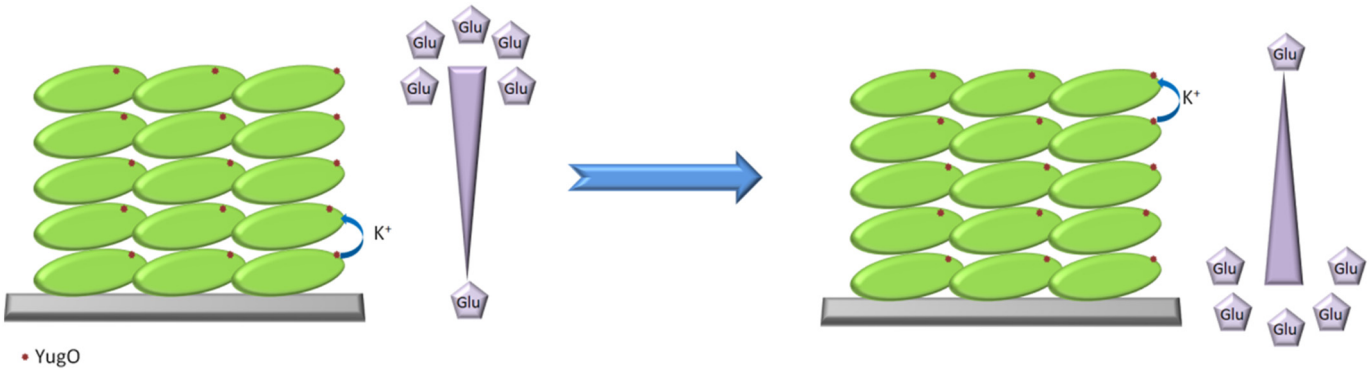

Scheme 2. Combination of the electrical signalling with the metabolism of bacteria: the limitation of glutamate inside the biofilm leading to the release of potassium ions through the YugO potassium channel, followed by the change in glutamate concentration gradient.

potential is a typical long-range signalling, which is a self-perpetuating electrical signal based on the activity of ionic potential. The variation potential, although also occurs due to transient changes in electrical potential, yet cannot be electrically induced but changes with the intensity of the stimulus. The last one, namely local electrical potential, is produced only regionally and cannot be transported to other parts of the plant. The transmission of long-distance electrical signals with constant speed and amplitude is mainly associated with action potential depending on two K^+ channels, Cl^- and changes in Ca^{2+} concentration, and is also associated with signalling in plants [6,13]. The environmental stimulus causing the action potential in plants may be derived from a change in temperature, light, or electrical stimulation as well as the presence of pathogens [7,16]. It affects the possibility of nutrition, gas exchange, water uptake, leaf movement or energy production.

Another group of organisms constituting a separate kingdom are bacteria, the microorganisms characterized by various dimensions and shapes. As the only ones, they do not possess cellular organelles surrounded by a membrane. Contrastingly, bacterial cells are embedded in extracellular polymeric substances (EPS), forming tightly packed bacterial clusters, biofilms, which seem to be preferred form of bacterial communities. Under such conditions, bacteria can share their functions and exchange information [18,19]. In order to coordinate their behaviour, bacteria use chemical and electrical signalling. Bacteria produce, secrete and may sense certain molecules, thanks to which they are able to recognize the surrounding, the presence of other bacteria and various species. Such a chemical process is called *quorum sensing* [20–22]. Another way of communication is possible by transmitting electrical impulses. It is long-distance signalling by potassium ion channels in which the propagation of spatially ordered potassium waves takes place. The exact mechanism of this phenomenon in the viscous structure of the extracellular polymer matrix has not been thoroughly studied yet, emerging as a potential field of investigations in the scientific community. According to Masi et al. [23], the electrical activity depends strictly on the ability of bacteria to form the biofilm, and not necessarily only on the density of the bacterial population. Consequently, a single bacterium can receive an electrical signal, but only in a larger cluster bacteria can cooperate.

Priendle et al. [24] found that electrical signalling is combined with the metabolism of bacteria. Bacterial biofilms grow in certain cycles depending on the concentration levels of glutamate. When bacteria in the interior of the biofilm sense its depletion, the amount of produced ammonium ions decreases. As a result, when microorganisms on the circumference of the colony notice this change, they stop growing. When the amount of glutamate is topped up in the internal cells, the amount of ammonium increases and the bacteria on the perimeter of the biofilm begin to grow again. What is crucial, suitable glutamate and ammonium concentrations are affected by the membrane potential, which is synchronized by the biofilm thanks to the signalling process using potassium ions. Correspondingly, the depletion of glutamate inside the biofilm leads to the release of potassium ion through the YugO potassium channel (Scheme 2) [25–27]. Similar process is also responsible for the long-term effects of the bacteria on the behaviour of other bacterial cells that do not belong to the biofilm. Potassium ions emitted from biofilm affect the change in the membrane potential of distant cells changing their mobility [28]. It is a common case that two adjacent bacterial colonies compete for nutrients, which is why their average growth rate is slower than for a single biofilm. These two biofilms can synchronize oscillations of growth rate and electrical signalling. At lower glutamate concentrations, biofilms benefit from the strategy of sharing resources over time to avoid competition [29,30].

3. Electrochemical analysis of bacterial biofilms

The development of biofilm begins with the settlement of bacteria on the surface of the material, which occurs through the action of Van der Waals forces, acid-base interactions and electrostatic forces [31]. Generally, bacteria attach themselves to the surface, start to produce extracellular polymeric substances and begin to multiply. The three-dimensional structure obtained in this way is more difficult to remove than a single bacterium, because it greatly hinders the diffusion of molecules, including antibiotics [32,33]. Yet, it can be electroactive and susceptible to electrical stimulation. The electrical activity of biofilm was clearly demonstrated by Masi et al. [23] in a multi-electrode array (MEA) system equipped with 59 microelectrodes, which enabled high spatio-temporal resolution. Action potentials produced during the development of biofilm were examined continuously for at least 72 h. The research was carried out on two strains of bacteria: able to create biofilms (*Bacillus licheniformis* and *Pseudomonas alcaliphila*) and non-biofilm forming (*Escherichia coli HEC30*). In the case of bacteria forming a biofilm, as the amount of biofilm increased, a jump in the action potential was observed on the MEA device. This dependence was not observed in the case of non-biofilm forming bacteria. Therefore, it was concluded that electrical activity does not depend on the density of bacteria, but on the possibility of creating a biofilm. The experiments once again proved that even though single bacteria can receive an electrical signal, the formation of a biofilm is necessary to observe their cooperation.

For the description of the electrical activity of biofilms, it is necessary to be able to assess the rate of electron transfer between the bacteria and conductive surface. Biofilms exhibiting this kind of behaviour are called electrochemically active biofilms and are used e.g. in microbial fuel cells (MFCs). In the pursuit of maximizing electrical power production from these devices, researchers are looking for the bacteria possessing a strictly defined mechanism of electron transfer between their surface and the surface of the electrode. The evaluation of electron transfer, however, depends on many factors like electrode material, reactor configuration and culture conditions [34], which greatly affect the measured current. Even though the most popular electrode materials

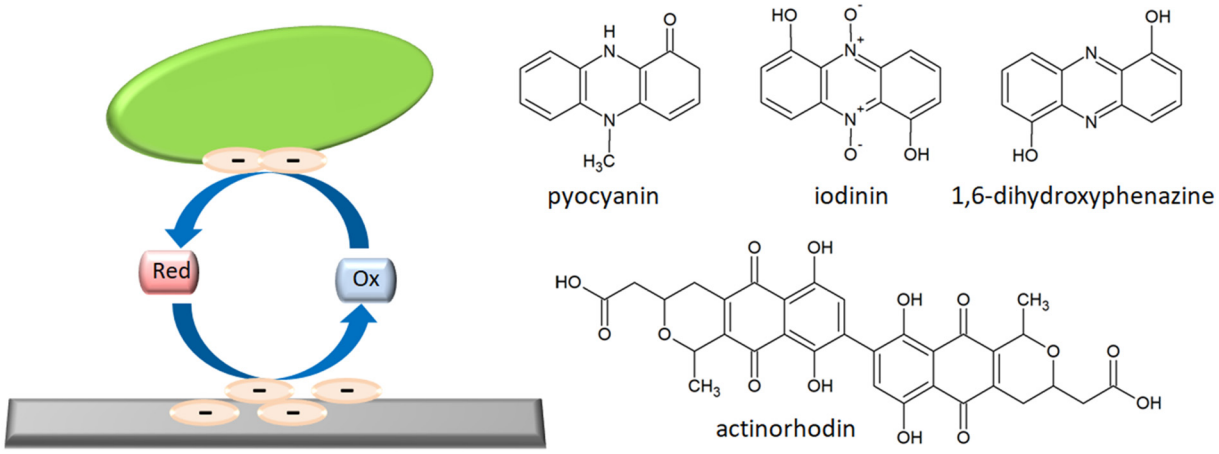

Scheme 3. The schematic representation of electron transfer between electrode and bacteria through EAMs, and the examples of EAMs: pyocyanin, iodinin, 1,6-dihydroxyphenazine and actinorhodin [39–41].

are of similar carbon-based type, especially glassy carbon due to its nonporosity and low background currents, still it is crucial to be able to compare between the performance of different systems. Therefore, there is an urgent need to develop non-destructive methods allowing to evaluate both thermodynamic and kinetic parameters of electron transfer process. In response to this need, a powerful set of electrochemical techniques was described by Marsili et al. [35] who cultivated the biofilm of bacteria that reduce metal, *Geobacter sulfurreducens,* on the surface of polished glassy carbon electrodes in a three-electrode anaerobic reactor. Consecutively, the biofilm was evaluated using cyclic voltammetry, differential pulse voltammetry and electrochemical impedance spectroscopy, in order to assess the electron transfer efficiency. During the measurements, a narrow range of potentials (−0.55 V to 0.24 V vs. SHE) was used so as not to inhibit the formation of a biofilm. After 72 h, the electrodes were completely covered with biofilm and showed a stable rate of electron transfer. Due to the high repeatability of acquired results, *Geobacter sulfurreducens* current density was estimated at approximately 2 A/m^2. In this way, electrochemical techniques were shown to allow to define electron transfer from cells to electrodes. Since these methods are not destructive, it is possible to apply them to compare the performance of many bacterial strains, as already shown in some literature proceedings [36,37]. Therefore, it has been proven that the electroanalytical techniques may be applied as efficient screening methods for the identification of microorganisms and MFCs design leading to the highest efficiency in the power production.

The most traditional methods of monitoring microbial colonization, macroscopic approaches, are found to fail in providing the information of the effect of colony size, which is caused by the variations in biofilm thickness reaching from 1 to 2 μm (single bacteria) to ≥50 μm [38]. Therefore, Bressel et al. [38] used a sophisticated combination of gravimetric, optical and electrochemical techniques to monitor the growth of 5 μm-thick mixed biofilms on the surface of platinum and gold electrodes. These methods allowed to assess with high local resolution how the development of biofilm affects its electrochemical properties. In short, the formation of biofilm on metallic surfaces, simultaneously with the monitoring of open circuit potentials, was observed with electrochemical quartz crystal microbalance. Confocal scanning laser microscopy enabled three-dimensional imaging of bacterial layers. Together with the use of fluorescent dyes, it allowed the assessment of the viability of growing bacteria. Cyclic voltammetry was also used, showing that biofilm formation on the surface of Pt electrode inhibited hydrogen adsorption and oxide formation, as well as catalyzed oxygen reduction. The combination of these techniques provided unprecedented set of data allowing to correlate biofilm morphology with its electrochemical behaviour in terms of the potential shift phenomena. Moreover, it offered a non-destructive and continuous evaluation of biofilm properties, which was not achievable through the application of classical microscopic techniques.

Becerro et al. [42], on the other hand, used cyclic voltammetry (CV) and differential pulse voltammetry (DPV) to assess the growth of *Staphylococcus epidermidis* biofilm and the adhesion of the bacteria to the surface. In particular, electrochemical methods were chosen to investigate the redox behaviour of electrochemically active molecules (EAM) secreted by the bacteria (Scheme 3). Consequently, EAMs reacting with free electrons from the electrode were monitored using thin-layer microelectrodes, and their redox signals were easily detected on both CV and DPV curves. The results were collected every 30 min and the culture was maintained for 65 h. The authors noticed an increase in the total amount of current which was proportional to the state of growth of biofilm, namely initial media adaptation, lag phase, exponential phase, stationary phase as well as final decline phase. At the end of the analysis, the measured current decreased due to the reduced metabolic activity of the bacteria and their death. Even though both CV and DPV were found to be useful in the analysis, it was DPV which allowed to precisely determine the number of redox centers, as well as it was more prone to the changes in EAM concentrations. The results clearly showed that electrochemical analysis of biofilms allows the monitoring of bacterial activity already in the initial stage of biofilm development, which is not so easy to accomplish with other experimental techniques, Consequently, early detection of bacterial presence on the surface makes it possible to eliminate bacterial biofilms with antibacterial agents even before the extracellular matrix is generated.

Electrochemical methods have been found to provide numerous information describing the state of the biofilm and its properties, including the kinetics of growth, interfacial/extracellular electron transfer, redox behaviour of EAMs, as well as biofilm resistance, capacitance and impedance, etc. Consequently, the detailed list of electrochemical methods suitable for the characterization of biofilm has been presented in Table 1. This summary shows the electrochemical aspects of biofilms by linking the electrochemical properties of the bacteria with the experimental techniques used for their quantification. For each case, the detailed experimental conditions are provided in order to indicate the range of parameters allowing for the non-destructive testing of living bacteria.

4. The effect of electrical stimulation on bacteria

The interest in electrical stimulation is increasing due to the more available knowledge about the electrical properties of tissues and cells. Electrical signals are processed and conducted by electrically excitable cells, in which cell membrane contains ion channels that allow the propagation of an electrical signal. Due to the appropriate stimulus, the ion

Table 1
Electrochemical methods and experimental conditions applied for the characterization of electrochemical properties of specific bacterial biofilms.

Method	Experimental conditions	Measured property	Bacterial strain	Reference
Cyclic voltammetry (CV)	Equilibrium time: 5 s Scan rate: 1 mV/s Potential range: −0.558 V to 0.242 V (vs. SHE)	The kinetics of interfacial electron transfer between bacteria and electrodes	*Geobacter sulfurreducens*	[35]
	Potential range: −0.45 V to 1.2 V (vs. SHE) Scan rate: 50 mV/s	Rate of hydrogen adsorption, oxygen reduction	Mixed culture biofilm	[38]
	Potential range: −1 V to 1 V Scan rate: 100 mV/s Sampling interval: 1 mV	Redox behaviour of EAMs	*Staphylococcus epidermidis*	[42]
	Scan rate: 10 mV/s Potential range: 0.24 V to −0.56 V (vs. SHE)	Electron transfer	*Geobacter sulfurreducens*	[36]
	Scan rate: 2 mV/s Potential range: −0.49 V to 0.71 V (vs. SHE)	Extracellular electron transfer	*Shewanella oneidensis*	[43]
	Scan rate: 10 mV/s Potential range: −0.7 V to 0 V (vs. SCE)	Extracellular electron transfer	*Pseudomonas aeruginosa*	[44]
	Scan rate: 5–100 mV/s Potential range: −0.6 V to 0.6 V (vs. SCE)	Electroactivity of bioanodes	*Lactobacillus rhamnosus GG*	[45]
	Scan rate: 1 mV/s Potential range: 0.1 V to 1.2 V (vs. NHE)	Redox behaviour of biofilm	*Acidithiobacillus thiooxidans*	[46]
	Scan rate: 10 mV/s Potential range: −0.7 V to 0 V (vs. Ag/AgCl)	Determination of a pseudo-linear response for the catalytic behavior of biofilms	*Geobacter sulfurreducens*	[47]
Differential pulse voltammetry (DPV)	Potential range: −0.558 V to 0.242 V (vs. SHE) Pulse height: 50 mV Pulse width: 300 ms Step height: 2 mV Step time: 500 ms Scan rate: 4 mV/s Accumulation time: 5 s	The kinetics of interfacial electron transfer between bacteria and electrodes	*Geobacter sulfurreducens*	[35]
	Potential range: −1 V to 1 V Signal amplitude: 0.1 V Increment: 2 mV Pulse width: 0.25 s Sampling width: 0.0167 s Pulse period: 0.55 s	Redox behaviour of EAMs	*Staphylococcus epidermidis*	[42]
Square wave voltammetry (SWV)	Potential range: −0.7 V to 0 V (vs. Ag/AgCl) Scan rate: 20 mV/s Sweep time: 45 s Pulse height: 25 mV Frequency: 10 Hz Step size: 2 mV	Determination of a pseudo-linear response for the catalytic behaviour of biofilms	*Geobacter sulfurreducens*	[47]
	Potential range: 0.5 V to − 0.2 V (vs. SCE) Step increment: 4 mV Amplitude: 25 mV Frequency: 15 Hz Quiet time: 2 s	Redox behaviour of EAMs	*Pseudomonas aeruginosa*	[48]
Chronoamperometry (CA)	Potential: 0.242 V (vs. SHE)	The kinetics of interfacial electron transfer between bacteria and electrodes	*Geobacter sulfurreducens*	[35]
	Potentials: 0.71 V, 0.21 V, −0.19 V (vs. SHE)	Bioelectrocatalytic current production	*Shewanella oneidensis*	[43]
	Potential: 0 V (vs. SCE)	Electroactivity of bioanodes	*Lactobacillus rhamnosus GG*	[45]
Electrochemical impedance spectroscopy (EIS)	Perturbation amplitude: 10 mV Frequency range: 100 kHz to 0.01 Hz	Double-layer capacitance (correlated with cell density)	Indigenous microorganisms in the raw dam water	[49]
	Perturbation amplitude: 10 mV Frequency range: 1 kHz to 1 mHz	Electrical properties of biofilms interface: biofilm resistance, biofilm capacitance, charge transfer resistance	*Acidithiobacillus thiooxidans*	[46]
	Perturbation amplitude: 5 mV Frequency range: 100 kHz to 0.1 Hz	Biofilm impedance, conductance	*Geobacter sulfurreducens*	[47]
Potentiostatic EIS (pEIS)	Potentials of interest: 0.04 V, −0.06 V, −0.16 V, −0.26 V (vs. SHE) Perturbation amplitude: 10 mV Frequency range: 100 kHz to 0.01 Hz	Electron transfer characteristics of active cells attached to electrodes	*Geobacter sulfurreducens*	[35]

(continued on next page)

Table 1 (*continued*)

Method	Experimental conditions	Measured property	Bacterial strain	Reference
	Potential of interest: OCP Perturbation amplitude: 10 mV Frequency range: 100 kHz to 0.01 Hz	Electron transfer	*Geobacter sulfurreducens*	[36]
Electrochemical quartz crystal microbalance (EQCM)	Resonance frequency: 5 MHz Polarization potential: 0 V (vs. Ag/AgCl)	Potential shift Biofilm frequency shift and current	Mixed culture biofilm *Geobacter sulfurreducens*	[38] [47]

permeability through the membrane is changes and action potential is achieved, allowing to pass the information throughout the body. The action potential can be triggered by external electrical stimulation, which is increasingly used in many fields of medicine. Currently, electrical stimulation is used in treating the damages to the brain and nervous system, in spinal cord injuries or cerebral palsy [50–52]. Also, in the case of muscle stimulation in their weakness or paralysis [53–55] or in orthopaedics after injuries or surgery [56,57]. It is also applicable in cardiology [57,58] and various types of implants [50]. Electrical stimulation can be used in the system of administration of anti-inflammatory drugs, in the treatment of wounds and rehabilitation [57]. Therefore, it is highly expected that the electrical stimulation should have a significant influence on the behaviour of bacteria and biofilms.

As shown in the previous sections, electrochemical methods are highly useful in the monitoring of the biofilm development by observing the changes in the electrical properties of the electrodes. Similarly as in the case of excitable animal cells, it is also possible to affect bacteria deposited on conductive materials by applying electric current. Using electrochemical methods for the control of biofilm development usually brings the difficulty of connecting bacteria to selected surfaces or removing already embedded layers from the electrodes [59]. The mechanism of inhibition of bacterial growth under the influence of the electric field is not yet fully understood. There are some assumptions indicating possible mechanisms, including direct and indirect approaches (Scheme 4). Direct approach indicates that the electric current directly leads to cell death through the damage to the bacterial membrane or through blocking the multiplication of bacterial cells. As an indirect influence, temperature and pH are given, among others. However, now it is known that the temperature does not change much during the current flow. Contrarily, the pH does change at the electrodes, reaching more alkaline pH at the cathode and more acidic pH at the anode. Another indirect action is the production of toxic products of electrolysis, such as H_2O_2 [60,61]. During the electrochemical reaction biocides are generated, which cause unfavourable changes in the composition of microorganisms leading to their death [59]. The bacterial mortality can be also explained by galvanotaxy, which is the movement of particles to a cathode or anode under the influence of an electric field. The proposed reasons are likely, but the main mechanism of action of electric field on bacteria is still not fully understood and requires additional research in this direction [60].

5. Specific applications of electro-bacteriology

5.1. Electrically-induced antimicrobial activity

Individual bacteria living in the organism can be removed relatively easily using antibacterial agents. However, when bacteria accumulate and form a society, they start to cooperate with each other, communicate and take common actions, which makes them much more dangerous and harder to remove. Many serious bacterial diseases are associated with the infection of medical equipment with bacterial biofilms [62]. Bacteria can group on implants, valves and pacemakers, catheters and other biomedical devices. After implantation, they break healthy cell membranes what prevents wound healing and leads to serious infections. Due to the increasing resistance of biofilms to germicides, dealing with the infections often ends up with the removal of the implant and carries a risk to the health and life of patients [22,60]. Increasingly frequent use of antibiotics makes the bacteria efficiently immunized to their effects, and administered drugs are becoming less and less effective. Consequently, the inability to inhibit bacterial growth through the use of drugs prevents efficient treatment [32].

Since the bacterial membrane is charged, the presence of opposed charge on the surface of biomaterial can lead to the situation when biomaterial and bacteria repel one another. To use and strengthen this phenomenon, electricity may be applied, so that bacteria can be more easily separated from the surface [31,61]. Consequently, it has been shown that the electric field can affect the potential, shape and the behaviour of bacterial membrane, leading to the inactivation of bacterial growth and increased mortality (see Table 2). When investigating this effect also in relation to biofilms on implants, bactericidal and bacteriostatic character caused by electrical stimulation was confirmed and was called the electric effect [31,63]. To provide specific examples, stainless steel

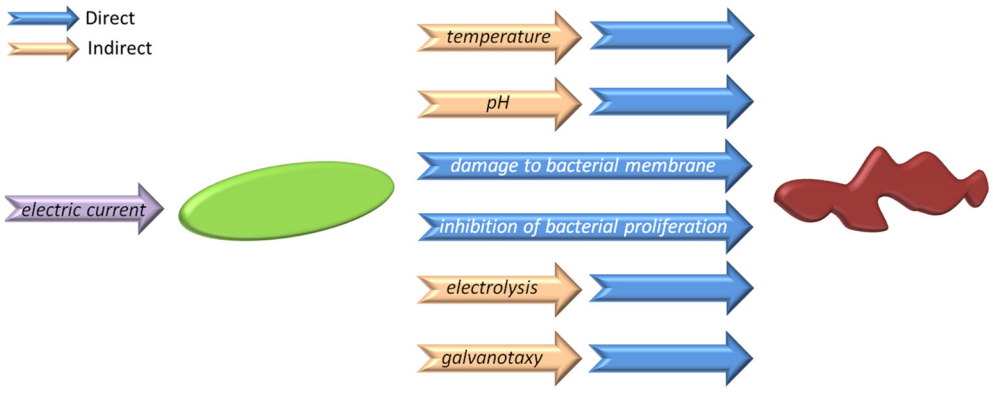

Scheme 4. Proposed direct and indirect mechanisms of inhibition of bacterial growth under the influence of electric current.

Table 2
Specific application of bacteria-based electro-technologies.

Application	Stimulus	Working conditions	Effect	Bacterial strain	Reference
Antibacterial neural electrodes	Electric field	Electric field strength: 0–10 V/cm Time: 0.25–4 h	Inactivation of bacterial growth	*Staphylococcus aureus, Escherichia coli*	[65]
Preventing infections by galvanotaxis	Direct current	Current intensity: 0.07–0.70 mA Time: 4 days	Reduced motility of bacteria	*Escherichia coli, Pseudomonas aeruginosa*	[67]
Sterilization	Direct current	Current intensity: 1 mA Time: 24 h	Increased mortality of bacteria	*Pseudomonas Aeruginosa, Klebsiella pneumoniae*	[68]
Bactericidal effect	Alternative (AC), direct (DC) and superimposed (SP) currents	DC field intensity: 1.25 V/cm, 2 V/cm AC field component: 1.25 V/cm AC frequency: 10 MHz SP electric field: 0.5 V DC field +0.5 V AC field at 10 MHz Time: 24 h Additional treatment: 10 μg/ml gentamycin	Reduced viability of the bacteria	*Escherichia coli*	[33]
Preventing orthopaedic infections	Direct current	Current intensity: 100 μA Time: 21 days	Bacterial detachment and decreased viability	*Staphylococcus epidermidis*	[64]
	Direct current	Current intensity: 50–250 μA Time: 4 h Additional treatment: gentamycin	Enhanced susceptibility of biofilm to antibiotic	*Staphylococcus aureus*	[69]
	Direct current	Current intensity: 200 μA Time: 21 days	Significantly reduced bacterial growth	*Staphylococcus epidermidis*	[71]
	Block current	Current intensity: 15–100 μA Frequency: 0.1–2 Hz Duty cycle: 5–50% Time: 8000 s	Bacterial detachment and decreased viability	*Staphylococcus epidermidis*	[72]
	Electrical stimulation	Potentials: 15–30 V Pulse duration: 0.4 ms Frequency: 20 Hz Time: 2 days	Decrease in biofilm formation	*Straphylococcus aureus*	[63]
Biological wastewater treatment	Direct current	Current intensity: 13 and 70 mA Electric field strength: 0, 0.28, 0.57, 1.14 V/cm Time: 50 h	Stimulation of aerobic activity	Aerobic bacteria	[90]
	Direct current	Current intensity: 6.2–24.7 A/m^2 Time: 4 h	Avoiding bacteria inactivation	Heterotropic bacterial mass	[83]
Soil bioremediation	Direct current	Electric field strength: 5 V/m Current density: 6 $\mu A/cm^2$ Time: 90 days	Increased efficiency of biodegradation	*Pseudomonas putida, Bacillus subtilis, Klebsiella pneumoniae*	[85]
	Direct current	Electric field strength: 2 V/cm Time: 72 h	Controlling the direction of bacterial migration	*Pseudomonas fluorescens*	[86]
	Direct current	Electric field strength: 1.4 V/cm Time: 34 days	Stimulating bioremediation without harmful effects on bacteria	Soil bacteria	[91]
	Direct current	Electric field strength: 1.3 V/cm Time: 42 days	Increased efficiency of biodegradation	Mixed culture of petroleum-utilizing bacteria	[92]

pin implants were tested to prevent spinal infections [64]. *Staphylococcus epidermidis* was inoculated in the tibia bone of the goats and their behaviour was observed under the influence of the constant electric current of 100 μA. After 21 days, the implants were removed and the development of biofilms was assessed. It has been shown that bacteria detached from the implant surface and their viability decreased. The results suggested that the use of electric currents under real conditions could be effective.

In neural applications, the effectiveness of vertical electrical stimulation on amorphous carbon was also shown to increase bacterial mortality [65]. The applied electric field intensity of 2.5 V/cm exhibited bactericidal properties with no negative effects on neural cells. Two types of bacteria were tested: gram-positive (*Staphylococcus aureus*) and gram-negative (*Escherichia coli*). The mortality of both types of bacteria increases with a higher field intensity (10 V/cm) for a shorter period of time, or lower field intensity (2.5 V/cm) of current for a long time. However, in such conditions, *Escherichia coli* with a thinner cell wall reacted faster than *Staphylococcus aureus* possessing a thicker wall. After discontinuing the field, the bacteria were incubated to check their regeneration. *Escherichia coli* turned out to recover faster and were more active than *Staphylococcus aureus*, for which no recovery was observed.

The ability to change the direction of bacterial movement under the influence of the electric field was also noted. The works of Shi et al. [66] and Berthelot et al. [67] demonstrated that electrical stimulation can be a valuable method of preventing infections by directing bacterial cells away from the site of injured tissues. Forced direction of bacterial migration would allow the control and the ability to protect tissue against the development of bacteria in the exposed area. This phenomenon could also help to reduce the use of antimicrobial agents. However, it was observed that different bacteria react in a different manner in response to the electric field [32]. The relevant tests were carried out in a microfluidic channel where the electric currents of 0, 0.07 and 0.125 mA were applied for 60 s. On the examples of *Escherichia coli*

and *Pseudomonas aeruginosa*, it was shown that these bacteria migrate towards different electrodes. *Escherichia coli* moved towards the anode and *Pseudomonas aeruginosa* migrated towards the cathode. It was also shown that the electric field reduced the speed of bacteria, but at the same time increased their directionality.

The combination of bactericides and electric field can be used to increase the potency of antibiotics on bacteria living in the biofilms. This bioelectric effect turned out to be a very good method in which an antibiotic with poor performance becomes very effective after applying electric current [68]. It was also shown that the reduced viability of the bacteria due to the combination of the drug and the electric field is mainly caused by the supply of additional energy and not to the type of electrochemical signal used. Consequently, *Escherichia coli* biofilm was tested using alternating, direct and superimposed potentials for 24 h in combination with gentamycin treatment (10 μg/ml) [33]. The results showed that the applied potentials of equivalent energies gave similar results in the antibacterial action of the drug. Generally, in most studies related to the bioelectric effect, two electrodes are used in the electrolyte, between which the current is passed. As a result of the currents in the range of mA, reactive oxygen species and metal ions are generated in the course of electrochemical reactions from metal electrode surfaces. Therefore, the use of such a system would not be recommended in medicine due to its harmful effects on the body. The alternative approach may consider the application of conductive polypyrrole/chitosan films through which the electric current could pass [69]. This system was characterized by high flexibility, non-cytotoxicity and biodegradability. The efficacy of the drug (gentamycin) in combination with direct current flowing through conductive film was examined on the example of *Staphylococcus aureus* biofilm. The results were promising, indicating that the application of the bioelectric effect is a favourable way to limit the occurrence of bacterial infections related to medical equipment [61].

Infection associated with implantation is another major problem in biomedicine. It may result from the lack of strict compliance with hygiene rules by hospital staff or may be caused by bacteria coming from the patient's own skin [63]. One type of the biomaterials particularly susceptible to infection associated with the formation of biofilms are percutaneous pins used in orthopaedic anchoring frames. These infections can lead to inflammation of bones or surrounding tissues. Due to the fact that the bacteria are present on the implanted biomaterial, the patient's immune system protects them against antibacterial substances. Because in any treatment special care should be taken not to damage the surrounding tissues, bacteria and bacterial biofilms are so difficult to remove. Since the use of electric currents can affect bacteria and inhibit their growth [70], Del Pozo et al. [71] decided to test the electrical effect *in vivo* on rabbits with osteomyelitis in the presence of *Staphylococcus epidermidis*. A stainless steel implant was infected with bacteria and implanted into the medullary cavity of the tibia. The effect of treatment with low amperage continuous current (200 μA) was compared with the effect of intravenous doxycycline treatment and with a control group not subjected to any treatment. It was shown that the amount of bacteria was significantly decreased in the groups subjected to treatment, both electrical and based on antibiotics, than in a control group. In addition, using the electrical current turned out to be statistically more significant, as well as more efficient, than doxocycline treatment. Other work [72] showed that block current (15–100 μA, 0.1–2 Hz, 5–50% duty cycle) in addition to direct current (25–125 μA) was also suitable to inhibit bacterial growth. Consequently, using a block current in a parallel plate flow chamber allowed to stimulate 76% of *Staphylococcus epidermidis* to detach from surgical stainless steel and reduce the lifespan of remaining bacteria.

Literature reports have also shown that numerous materials used in orthopaedics can be easily modified by the electrochemical anodization technique giving the surface nanostructured features improving their antifouling properties [73,74]. Moreover, the materials obtained in such a way usually show an increase in osteoblast adhesion and provide a developed bone-implant interface [75]. By coupling anodized surfaces with additional electrical stimulation, it is possible to further enhance the antibacterial effect of the surface [63]. Consequently, electric stimulation by a multi-channel electrical stimulator was used to limit the growth of *Straphylococcus aureus* on anodized titanium. The results showed that the electrical stimulation (15–30 V) on the anodized metal surface was able to limit the formation of biofilm to a higher extend than on both the surface of unmodified and non-electrically stimulated titanium. Therefore, it was concluded that there exists a synergistic interaction between the electrochemically-tailored surface of the material and additional electrical stimulation that leads to the prevention in the biofilm formation and the increase in the osteoblast function. For that reason, a proposed mixed approach seems to act as a promising way to treat orthopaedic device-related infections.

5.2. Bacteria-based electro-technologies

Bacterial biofilms are extremely widespread systems on Earth. They perform many important functions that we are able to use for our own sake. Microorganisms are responsible for the biogeochemical processes of elements in soil and water, therefore they can be used in drinking water purification systems [76], sewage degradation [77] or biocatalysis, which applies enzymes synthesized by selected microorganism in catalyzing the reactions mainly for pharmaceutical or food industry [78] (see Table 2). Biological water treatment processes enable the removal of many pollutants, are cheap and do not exhibit high energy consumption. Surface and underground water can be used as drinking water after proper treatment and purification. In microbiological filtration processes, bacteria growing on the membrane are involved in the removal of biological hazards, such as worms or pathogenic bacteria, but also chemical hazards in the form of metals, ammonium or synthetic compounds, for example derived from agriculture [79–81]. Biological systems can be also used in wastewater treatment, enabling the removal of environmental contaminants through microbial degradation. In this process, bacteria use oxygen metabolism to degrade biological compounds in wastewater, so that they are able to grow and multiply. In the next stage, anaerobic degradation takes place, where anaerobic bacteria are used for the removal of organic waste, mainly proteins, cellulose, lipids, starch and nucleic acids. Their main role is to reduce the volume of sludge and to produce methane [82]. Since the formation of biofilm is required in the aforementioned applications, researchers are focused on designing the techniques allowing to control the adhesion and growth of bacteria, as well as their organization in three-dimensional communities. In this section, we aim to show that the control of bacterial growth can be easily carried out using electrical stimulation, without having harmful effects on the microorganisms.

The example of combining electrochemistry and bacteriology is the application of electro-technologies, such as electrocoagulation or electrophoresis, for wastewater treatment. Even though exhibiting high efficiency, decreasing the amount of added chemicals and being easy to control automatically, these electro-technologies can be further improved by the addition of a biological process unit based on the action of the microorganisms. Therefore, the presence of bacteria is here crucial, and their growth and development are promoted. As the electric current may have negative effect on the viability of bacteria and their adhesion to the surface, minimizing the effect of electricity on bacteria is essential in electric wastewater treatment systems. Consequently, Wei et al. [83] studied the behaviour of heterotrophic bacterial mass from the membrane bioreactor by subjecting it to the constant current of different magnitude and duration. The results showed that the safe regime of the electric stimulation is the current density of 6.2 A/m^2 and time of 4 h. Below this threshold the bacterial viability was not significantly affected by the electric current, exhibiting less than 10% of death percentage. When using higher currents, the viability of the bacteria was decreased (15–29% of death percentage), which was, however, related more to the increase in the pH of the biomass fluid than

to the electricity itself. Extending the time of the process was also shown to have adverse effects on the bacteria by the increase in their mortality. Because the state of the bacteria was found to be dependent on their position in the bioreactor, whether they grow on the electrodes, between the electrodes or outside the space between the electrodes, sufficient mixing was indicated as the crucial factor to enhance the efficiency of the process by preventing local inactivation of microorganisms.

An important technology for removing contaminants from groundwater and soils is bioremediation, which uses live microorganisms to catalyze and biodegrade pollutants. One approach to maximize the efficiency of this process includes the application of electric field in order to force the transport of the contaminants in the soil [84]. Undoubtedly, the use of this method, called electrokinetics, is supposed to have a strong effect on the behaviour of the bacteria. For this reason, Olszanowski et al. [85] studied the migration of bacteria during the bioremediation process using a weak electric field. The bacterial activity of *Pseudomonas putida, Bacillus subtilis* and *Klebsiella pneumoniae* were analyzed after application of electric fields with the intensity of 5 V/m and the current density of 6 μA/cm^2. It was shown that the weak field had a significant impact on the speed and direction of bacterial migration. Bacteria were found to move towards the anode through the phenomenon of electrophoresis. The weak electric field contributed to the increase in the amount of bacteria in the sampling points comparing with the control soil not subjected to electrical stimulation. Moreover, these studies also showed that the application of electric field increased the efficiency of biodegradation of a model contaminant, crude oil, by almost 20%.

In the case when there is not enough bacteria in the soil to successfully carry out the bioremediation process, it is necessary to spread them further. This possibility was examined by Suni et al. [86] who performed the electroosmotic test in three types of soils, namely garden soil, sand and clay. Green fluorescent protein-marked *Pseudomonas fluorescens*, which is a phenol-degrading bacterial strain, was used and phenol was added as a bacterial growth medium in the soils. The research was carried out in a specially designed system resembling field conditions, which was based on a horizontal gel electrophoresis setup combined with microcosms. Currents with a constant voltage of 2 V/cm were used and the migration of bacteria with water towards the cathode was observed. Phosphate buffers were added to maintain the constant pH during the experiment. Analysis of the results indicated that migration using electroosmosis is an effective way to transport bacteria even in dense soils such as clay. In an easily permeable sand, the migration velocity achieved approx 1 cm/h, while in garden soil and clay the velocities were lower, but still substantial, i.e. 0.6 cm/h and 0.1 cm/h, respectively. Although this and further works [87–89] pointed out the potential of electroosmosis and electrokinetics in bioremediation, there are still very few studies expanding the scope of this process from the laboratory scale into field applications. One of these was performed in 2012 in Denmark, and showed the efficiency of electrokinetics in disseminating microorganisms used to degrade perchloroethylene [84]. An additional advantage of using electricity was heating the soil, so that in colder regions the bioremediation process can take place throughout the whole year [86].

6. Microbial fuel cells

The idea of employing bacteria to generate electricity dates back to 1911 and M.C. Potter, who was later supported by the works of Cohen, Karube and Bennetto [93]. Currently, after the significant progress in this area has been achieved, the fact that bacteria are able to generate electricity is crucial considering the urgent need for new energy sources. Microbial fuel cells (MFCs) are the devices that convert chemical energy into electricity employing microorganisms as biocatalysts [94]. In general, MFCs consist of an anaerobic anode and a cathodic chamber which are usually separated by an ion exchange membrane [95]. Organic matter is oxidized by bacteria on the anode to produce CO_2, protons and electrons. Protons are then passed through a membrane to a cathode and electrons are transferred through the outer perimeter, where they react with oxygen to form water. As anode materials, carbon materials such as carbon cloth, carbon paper or graphite brushes are most often used because of their large surface area and conductivity, whereas platinum is usually used as a cathode. MFCs have many advantages, such as mild working conditions, using organic substrates as a fuel, providing renewable sources of hydrogen, and the possibility to be used in sewage treatment systems or biosensors. Despite so many advantages, the low power density is still a major problem limiting the industrial application of MFCs [93,95]. Since the power that can be obtained in such a cell depends on many factors, including the substrate conversion factor, amount of bacteria, mass transfer within the device and, last but not least, the internal resistance of the whole MFC, the current research on microbial cells, focused on controlling and adapting various parameters, is a rapidly evolving field [96].

The power production by MFCs has increased greatly in the last decades. The first devices based on the oxygen reduction process could not reach the power of 1 mW/m^2 [97], what was obviously not efficient enough for any industrial application. One way to increase the efficiency of MFC was described by Logan et al. [98] who used two-chamber MFC with carbon paper as the anode, carbon paper covered with catalyst as the cathode and a proton exchange membrane inoculated with an anaerobic marine sediment. In this design, cysteine was chosen to serve as both oxygen scavenger and a substrate for the bacteria growth. Due to the presence of this amino acid, the substantial increase in electric energy was observed reaching a maximum power of 19 mW/m^2 (385 mg/l cysteine) and 39 mW/m^2 (770 mg/l cysteine). Additionally, it was shown that the cathode material can significantly affect the obtained power. By using a cathode made of platinum or platinum-ruthenium instead of carbon paper, the initial power of 19 mW/m^2 increased to 33 mW/m^2. Also, after analysis of the bacterial biofilm formed on the anode, it was found that the main bacteria involved in the oxidation of cysteine was *Shewanella* spp, closely related to *Shewanella affinis*.

Rodrigo et al. [99] in their research tested the possibility of generating energy from urban wastewater as a fuel. In their design, the activated sludge obtained from the sewage treatment was used for the development of aerobic and anaerobic bacteria. The maximum power density that was achieved was equal to 25 mW/m^2 (at the cell potential of 0.23 V), which showed the potential of urban wastewater as a fuel and was an inspiration for further research aiming to increase the efficiency of MFCs. For instance, Wu et al. [100] reached the maximum power density of 471 $\pm$ 13 mW/m^2 through the use of a composite anode combining a flat mesh to block oxygen crossover and graphite fiber brushes to stabilize the potential. This unique architecture allowed to increase the efficiency of power generation by 20% and 150% when compared with only brush anodes or only mesh anodes, respectively. Another advantage of this type of design was the limitation of the biofouling of the electrodes and increased coulombic efficiency of MFC. An interesting study was published by Chouler et al. [101] who used urine as an energy source for MFCs. The purpose of the study was to develop an effective, small scale MFC for energy generation in remote or impoverished regions of the world. Through the use of an air cathode configuration and two different types of biomass-derived oxygen reduction catalysts, it was possible to achieve the power density of 1.95 W/m^3. Moreover, the devices could be easily connected in parallel, which led to the substantial increase in the power output.

Apart from the generation of electricity, the use of wastewater in MFCs has an additional advantage, which is achieving biological wastewater treatment by removing organic matter in the form of chemical oxygen demand or biochemical oxygen demand. The studies performed by Liu et al. [102], who used a single-chamber MFC containing eight graphite anodes and one air cathode inoculated with a pure culture of *Geobacter metallireducens* or the bacteria present in the sewage, showed that it was possible to achieve the power density of 26 mW/m^2 while,

Table 3
Recent achievements in MFCs technology.

Anode material	Cathode material	Feedstock	Maximum power density	Additional benefit	Reference
Graphite	Graphite	Kitchen wastewater	250 mW/m^2	Substantial removal of chemical oxygen demand	[115]
Carbon felt	Carbon cloth/Pt/C	Pyroligneous liquor	383 mW/m^2	High current density, coulombic efficiency and phenol removal rate	[116]
Graphite brush/carbon mesh	Polyvinylidene fluoride binder/activated carbon/carbon black	Domestic wastewater	471 mW/m^2	Reduced oxygen contamination of the anode and the bio-fouling of cathode	[100]
Graphite	Cu–MnO_2 or Co–MnO_2/polytetrafluoroethylene/carbon cloth	Domestic wastewater	465–500 mW/m^2	Low cost of the cathode	[103]
TiO_2/Fe_2O_3 photoanode coupled with conventional bioanode (graphite felt)	Graphite	Culture medium	638 mW/m^2	Efficient removal of hexavalent chromium Cr(VI), efficient microbial oxidation and photoelectrocatalysis	[117]
Nitinols	Pt-coated Ti mesh	Synthetic wastewater	811 mW/m^2	Biocompatibility with human tissue and bacteria	[118]
Carbon cloth/carbon felt/granular activated carbon	Activated carbon/carbon black/polytetrafluoroethylene /stainless-steel mesh	Synthetic wastewater	1300 mW/m^2	Promoted mass transfer, reduced internal resistance, increased bioburden	[119]
MnO_2/carbon black/ polytetrafluoroethylene/stainless steel mesh	Carbon felt	Phosphate buffered saline, acetate, trace minerals, vitamins	1671 mW/m^2	High electrical conductivity, efficient electron transport, low overpotential	[120]
Carbon felt	$Co_3O_4/NiCo_2O_4$/activated carbon	Domestic wastewater, phosphate buffered saline, trace minerals, vitamins	1810 mW/m^2	Acceleration of the overall oxygen reduction reaction rate	[121]
Polypyrrole/$SrFe_{12}O_{19}$/poly (ethylene terephthalate)	Carbon cloth	Phosphate buffered saline mineral, vitamin solution, glucose	3317 mW/m^2	Magnetic field promoting bioelectrochemical reaction rates and decreasing anode charge transfer resistance	[104]
Poly(bisphenol A-co-epichorohydrin)/carbon nanotubes	Pt/C/carbon paper	Phosphate-buffered basal medium	3800 mW/m^2	Strong interaction between anode with bacteria, significant power output improvement	[105]

simultaneously, removing up to 80% of the chemical oxygen demand. Similar percentage of contaminant removal was reached by the 12 anodes/cathodes MFC described by Jiang et al. [103], but this design was found to produce the energy of 465–500 mW/m^2. Moreover, this substantially high power density was achieved by using copper- or cobalt-doped cathodes instead of the costly platinum electrodes.

Although the current MFC technologies (see Table 3) exhibit much better performance, being able to generate power densities in the range of several W/m^2 [104,105], the unsolved problem is the biofouling of the electrodes, leading to an increase in internal resistance and a decrease in the power density that occurs in time [103]. Still, MFCs focused on energy production can provide an interesting approach also to wastewater treatment. By increasing energy production, it may be possible to balance the costs associated with wastewater treatment, thanks to which this method can become available also in impoverished countries. Nevertheless, further research is still required to face the major problems associated with this technology, including the prevention of (bio)fouling and scaling up to meet the real-life needs.

The subject of microbial fuel cells is of a great interest to researchers, therefore, the number of publications on this topic increases steadily every year (Fig. 1). Due to the large number of research studies on MFCs, review works are being continuously published to systematize research achievements, focusing on various aspects of this technology. For instance, the classification of technologies based on interfacing microbiology and electrochemistry can be found in the paper of Schröder et al. [2]. Zhao et al. [106] focused on presenting electrochemical and electroanalytical techniques used in MFC studies, discussing in details the principles and possibilities of given techniques. On the other hand, Rimbound et al. [107] presented electroanalytical techniques regarding the formation and characterization of microbial anodes. The most current literature reports are discussing the concepts of using electrochemical techniques to study the interfacial kinetics of bacteria and characterize the biofilm [108], the strategies to improve the performance of MFCs [109–112], their scalability [113] and mathematical simulations allowing the formation of various MFC models for specific applications [114]. The Readers interested in the detailed aspects of MFC technology are encouraged to follow the aforementioned literature reports.

7. Conclusions and perspectives

Apart from animal tissues and plants, bioelectric currents exist also among bacteria. Even single bacterium can receive an electrical signal, but only in larger clusters, biofilms, they are able to cooperate making bacterial biofilms electroactive and susceptible to electrical stimulation. Consequently, electrochemical methods have been found to serve as efficient ways to provide numerous information describing the state of the biofilm and its properties. Cyclic voltammetry, differential pulse voltammetry, square wave voltammetry, chronoamperometry, electrochemical impedance spectroscopy, electrochemical quartz crystal microbalance, among others, have been successfully applied to assess the kinetics of growth, interfacial/extracellular electron transfer, redox behaviour of electrochemically active molecules, as well as biofilm resistance, capacitance and impedance. Also, the analysis of the redox behaviour of electrochemically active molecules secreted by the bacteria has been shown as a way to correlate the electrochemical investigations with the state of growth of biofilm, allowing early detection of bacterial presence. Besides, coupling electrochemical techniques with typical optical and gravimetric techniques has allowed providing an unprecedented set of data used to correlate biofilm morphology with its electrochemical behaviour.

Not only electrochemical methods are highly useful for the non-destructive monitoring of the biofilm development, but they can be also used to affect the bacteria. The most common application of electrical stimulation is the prevention of bacterial growth that is usually achieved by charging the surface to induce repulsive interactions

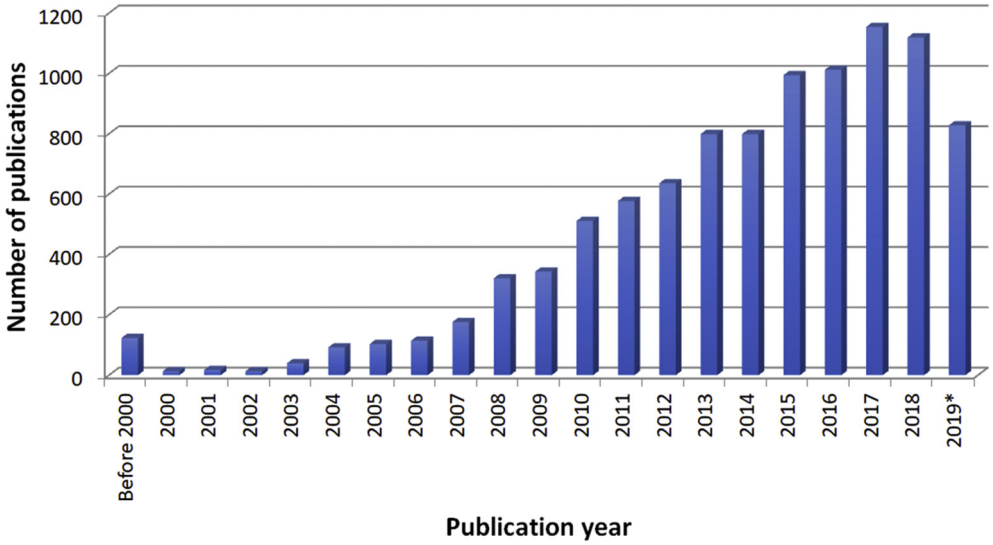

Fig. 1. Number of publications containing the phrase "microbial fuel cells" published in the literature between 1962 and 2019 (*until 30th August 2019) according to the Web of Science database.

between microorganisms and substrate. The ability to change the direction of bacterial movement under the influence of the electric field has been also noted, such as the increase of the potency of antibiotics when bactericides are coupled with the electric field. Even though the effectiveness of bioelectric effect has been confirmed by some biological studies under both *in vitro* and *in vivo* conditions, still there is a serious risk to the health and life of patients coming from reactive oxygen species and metal ions that are generated through electrochemical reactions from metal electrode. This makes it urgent to develop new types of electrodes or electrode coatings that will exhibit excellent electrochemical behaviour together with high biocompatibility and, as additional benefit, biodegradability.

Being responsible for the biogeochemical processes of elements in soil and water, microorganisms can be successfully used for bioremediation and wastewater treatment. Since the current approaches involve the use of advanced electro-technologies, such as electrocoagulation or electrophoresis, several researchers have put an effort to optimize the electrical signal to allow the adhesion and growth of bacteria without having harmful effects on the microorganisms. Consequently, by combining the effect of electric field and the presence of bacteria, it was possible to force the bacteria to migrate, as well as to increase the efficiency of biodegradation. An additional advantage of using electricity was heating the soil, allowing to employ the bioremediation strategy also in colder regions throughout the whole year. Nevertheless, basing on the number of literature reports these are microbial fuel cells that seem to be one of the most promising industrial application of bacteria and biofilms. Even though the concept of using bacteria to generate electricity is more than 100 years old, the last couple of years have brought a significant increase in power density reaching several W/m^2. This was possible mainly thanks to the modification of the materials used as the electrodes and the optimization of the composition of the feedstock. Aiming to face the environmental problems, current MFC technologies allow to produce energy from urban wastewater or urine as the feedstock. Still, further research is required to face the major problem associated with this technology, i.e. biofouling of the electrodes, leading to an increase in internal resistance and a decrease in the power density that occurs in time.

Acknowledgements

This work has been supported by the National Science Centre in Poland in the framework of Sonata 2016/23/D/ST5/01306 and Rector's grant in the area of scientific and development research, sponsorid="https://doi.org/10.13039/501100007835" xlink:role="http://www.elsevier.com/xml/linking-roles/grant-sponsor" xlink:type="simple">Silesian University of Technology, Poland (04/040/RGJ19/0096).

Declaration of Competing Interest

The authors declare that they have no known competing financial interests or personal relationships that could have appeared to influence the work reported in this paper.

Contributors

DCG reviewed the literature and drafted the manuscript. KK was in charge of the overall direction of the paper, planned its content, designed the figures and revised the manuscript. All authors have approved the final article.

References

[1] F. Aulenta, S. Puig, F. Harnisch, Microbial electrochemical technologies: maturing but not mature, Microb. Biotechnol. 11 (2018) 18–19, https://doi.org/10.1111/1751-7915.13045.
[2] U. Schröder, F. Harnisch, L.T. Angenent, Microbial electrochemistry and technology: terminology and classification, Energy Environ. Sci. 8 (2015) 513–519, https://doi.org/10.1039/c4ee03359k.
[3] M. Zhao, L. Chalmers, L. Cao, A.C. Vieira, M. Mannis, B. Reid, Electrical signaling in control of ocular cell behaviors, Prog. Retin. Eye Res. 31 (2012) 65–88, https://doi.org/10.1016/j.preteyeres.2011.10.001.
[4] H. Watson, Biological membranes, Essays Biochem. 15 (2015) 43–69, https://doi.org/10.1042/BSE0590043.
[5] D.J. Blackiston, K.A. McLaughlin, M. Levin, Bioelectric controls of cell proliferation: ion channels, membrane voltage and the cell cycle, Cell Cycle. 8 (2009) 3527–3536, https://doi.org/10.4161/cc.8.21.9888.
[6] E.D. Brenner, R. Stahlberg, S. Mancuso, J. Vivanco, F. Baluška, E. Van Volkenburgh, Plant neurobiology: an integrated view of plant signaling, Trends Plant Sci. 11 (2006) 413–419, https://doi.org/10.1016/j.tplants.2006.06.009.
[7] J. Fromm, S. Lautner, Electrical signals and their physiological significance in plants, Plant, Cell Environ. 30 (2007) 249–257, https://doi.org/10.1111/j.1365-3040.2006.01614.x.
[8] S.E.B. Tyler, Nature's electric potential: a systematic review of the role of bioelectricity in wound healing and regenerative processes in animals, humans, and plants, Front. Physiol. 8 (2017) https://doi.org/10.3389/fphys.2017.00627.
[9] L.A. Geddes, H.E. Hoff, The discovery of bioelectricity and current electricity The Galvani-Volta controversy, IEEE Spectr. 8 (1971) 38–46, https://doi.org/10.1109/MSPEC.1971.5217888.
[10] C.D. McCaig, A.M. Rajnicek, B. Song, M. Zhao, Controlling cell behavior electrically: current views and future potential, Physiol. Rev. 85 (2005) 943–978, https://doi.org/10.1152/physrev.00020.2004.

[11] J. Canales, C. Henriquez-Valencia, S. Brauchi, The integration of electrical signals originating in the root of vascular plants, Front. Plant Sci. 8 (2018) https://doi.org/10.3389/fpls.2017.02173.

[12] X. Yan, Z. Wang, L. Huang, C. Wang, R. Hou, Z. Xu, X. Qiao, Research progress on electrical signals in higher plants, Prog. Nat. Sci. 19 (2009) 531–541, https://doi.org/10.1016/j.pnsc.2008.08.009.

[13] K. Trebacz, H. Dziubinska, E. Krol, Electrical signals in long-distance communication in plants, in: F. Baluška, S. Mancuso, D. Volkmann (Eds.), Commun. Plants, Springer, Berlin, Heidelberg, 2006: pp. 277–290. doi:https://doi.org/10.1007/978-3-540-28516-8_19.

[14] Y. Jeong, Bio-Medical CMOS ICs (2011) https://doi.org/10.1007/978-1-4419-6597-4.

[15] J.S.I. Burdon-Sanderson, Note on the electrical phenomena which accompany irritation of the leaf of Dionæa muscipula, Proc. R. Soc. London. 21 (1873) 495–496, https://doi.org/10.1098/rspl.1872.0092.

[16] Z.Y. Wang, Q. Leng, L. Huang, L.L. Zhao, Z.L. Xu, R.F. Hou, C. Wang, Monitoring system for electrical signals in plants in the greenhouse and its applications, Biosyst. Eng. 103 (2009) 1–11, https://doi.org/10.1016/j.biosystemseng.2009.01.013.

[17] F. Baluška, S. Mancuso, Ion channels in plants, Plant Signal. Behav. 8 (2013), e23009. https://doi.org/10.4161/psb.23009.

[18] P. Mathema, D. Evans, I.S. Moore, C. Ranson, R. Martin, Concussed or not? An assessment of concussion experience and knowledge within elite and semiprofessional Rugby Union, Clin. J. Sport Med. 26 (2016) 320–325, https://doi.org/10.1097/JSM.0000000000000256.

[19] D. Dufour, V. Leung, C.M. Lévesque, Bacterial biofilm: structure, function, and antimicrobial resistance, Endod. Top. 22 (2010) 2–16, https://doi.org/10.1111/j.1601-1546.2012.00277.x.

[20] B.L. Bassler, How bacteria talk to each other: regulation of gene expression by quorum sensing, Curr. Opin. Microbiol. 2 (1999) 582–587, https://doi.org/10.1016/S1369-5274(99)00025-9.

[21] N.A. Whitehead, A.M. Barnard, H. Slater, N.J. Simpson, G.P. Salmond, Quorum-sensing in Gram-negative bacteria, FEMS Microbiol. Rev. 25 (2001) 365–404, https://doi.org/10.1111/j.1574-6976.2001.tb00583.x.

[22] M.R. Parsek, E.P. Greenberg, Sociomicrobiology: the connections between quorum sensing and biofilms, Trends Microbiol. 13 (2005) 27–33, https://doi.org/10.1016/j.tim.2004.11.007.

[23] E. Masi, M. Ciszak, L. Santopolo, A. Frascella, L. Giovannetti, E. Marchi, C. Viti, S. Mancuso, Electrical spiking in bacterial biofilms, J. R. Soc. Interface. (2015) https://doi.org/10.1098/rsif.2014.1036.

[24] A. Prindle, J. Liu, M. Asally, S. Ly, J. Garcia-Ojalvo, G.M. Süel, Ion channels enable electrical communication in bacterial communities, Nature (2015) https://doi.org/10.1038/nature15709.

[25] S.D. Beagle, S.W. Lockless, Microbiology: electrical signalling goes bacterial, Nature 527 (2015) 44–45, https://doi.org/10.1038/nature15641.

[26] J. Liu, A. Prindle, J. Humphries, M. Gabalda-Sagarra, M. Asally, D.D. Lee, S. Ly, J. Garcia-Ojalvo, G.M. Süel, Metabolic co-dependence gives rise to collective oscillations within biofilms, Nature 523 (2015) 550–554, https://doi.org/10.1038/nature14660.

[27] E.A. Libby, J. Dworkin, Habits of highly effective biofilms: ion signaling, Mol. Cell. 66 (2017) 733–734, https://doi.org/10.1016/j.molcel.2017.05.036.

[28] J. Humphries, L. Xiong, J. Liu, A. Prindle, F. Yuan, H.A. Arjes, L. Tsimring, G.M. Süel, Species-independent attraction to biofilms through electrical signaling, Cell 168 (2017) 200–209.e12, https://doi.org/10.1016/j.cell.2016.12.014.

[29] J. Liu, R. Martinez-Corral, A. Prindle, D.-y.D. Lee, J. Larkin, M. Gabalda-Sagarra, J. Garcia-Ojalvo, G.M. Süel, Coupling between distant biofilms and emergence of nutrient time-sharing, Science 356 (6338) (2017) 638–642, https://doi.org/10.1126/science:aah4204.

[30] S. Majumdar, S. Pal, Cross- species communication in bacterial world, J. Cell Commun. Signal. 11 (2017) 187–190, https://doi.org/10.1007/s12079-017-0383-9.

[31] J.L. Del Pozo, M.S. Rouse, J.N. Mandrekar, J.M. Steckelberg, R. Patel, The electricidal effect: reduction of Staphylococcus and Pseudomonas biofilms by prolonged exposure to low-intensity electrical current, Antimicrob. Agents Chemother. 53 (2009) 41–45, https://doi.org/10.1128/AAC.00680-08.

[32] R. Berthelot, S. Neethirajan, Harnessing electrical energy for anti-biofilm therapies: effects of current on cell morphology and motility, J. Exp. Nanosci. 12 (2017) 197–207, https://doi.org/10.1080/17458080.2017.1296977.

[33] Y.W. Kim, S. Subramanian, K. Gerasopoulos, H. Ben-Yoav, H.C. Wu, D. Quan, K. Carter, M.T. Meyer, W.E. Bentley, R. Ghodssi, Effect of electrical energy on the efficacy of biofilm treatment using the bioelectric effect, Npj Biofilms Microbiomes 1 (2015) https://doi.org/10.1038/npjbiofilms.2015.16.

[34] J. Babauta, R. Renslow, Z. Lewandowski, H. Beyenal, Electrochemically active biofilms: facts and fiction. A review, Biofouling 28 (2012) 789–812, https://doi.org/10.1080/08927014.2012.710324.

[35] E. Marsili, J.B. Rollefson, D.B. Baron, R.M. Hozalski, D.R. Bond, Microbial biofilm voltammetry: direct electrochemical characterization of catalytic electrode-attached biofilms, Appl. Environ. Microbiol. 74 (2008) 7329–7337, https://doi.org/10.1128/AEM.00177-08.

[36] S. Srikanth, E. Marsili, M.C. Flickinger, D.R. Bond, Electrochemical characterization of Geobacter sulfurreducens cells immobilized on graphite paper electrodes, Biotechnol. Bioeng. 99 (2008) 1065–1073, https://doi.org/10.1002/bit.21671.

[37] D.R. Bond, D.R. Lovley, Evidence for involvement of an electron shuttle in electricity generation by Geothrix fermentans, Appl. Environ. Microbiol. 71 (2005) 2186–2189, https://doi.org/10.1128/AEM.71.4.2186-2189.2005.

[38] A. Bressel, J.W. Schultze, W. Khan, G.M. Wolfaardt, H.-P. Rohns, R. Irmscher, M.J. Schöning, High resolution gravimetric, optical and electrochemical investigations of microbial biofilm formation in aqueous systems, Electrochim. Acta 48 (2003) 3363–3372, https://doi.org/10.1016/S0013-4686(03)00406-7.

[39] S.E. Darch, D. Koley, Quantifying microbial chatter: Scanning electrochemical microscopy as a tool to study interactions in biofilms,, Proc. R. Soc. A Math. Phys. Eng. Sci. 474 (2018) 20180405, https://doi.org/10.1098/rspa.2018.0405.

[40] L.E.P. Dietrich, T.K. Teal, A. Price-Whelan, D.K. Newman, Redox-active antibiotics control gene expression and community behavior in divergent bacteria, Science 321 (5893) (2008) 1203–1206, https://doi.org/10.1126/science:1160619.

[41] F.A.A. Alatraktchi, H.K. Johansen, S. Molin, W.E. Svendsen, Electrochemical sensing of biomarker for diagnostics of bacteria-specific infections, Nanomedicine 11 (2016) 2185–2195, https://doi.org/10.2217/nnm-2016-0155.

[42] S. Becerro, J. Paredes, M. Mujika, E. Pérez Lorenzo, S. Arana, Electrochemical real-time analysis of bacterial biofilm adhesion and development by means of thin-film biosensors, IEEE Sens. J. 16 (2016) 1856–1864, https://doi.org/10.1109/JSEN.2015.2504495.

[43] C. Grobbler, B. Virdis, A. Nouwens, F. Harnisch, K. Rabaey, P.L. Bond, Effect of the anode potential on the physiology and proteome of Shewanella oneidensis MR-1, Bioelectrochemistry 119 (2018) 172–179, https://doi.org/10.1016/j.bioelechem.2017.10.001.

[44] Y.-J. Qiao, Y. Qiao, L. Zou, X.-S. Wu, J.-H. Liu, Biofilm promoted current generation of Pseudomonas aeruginosa microbial fuel cell via improving the interfacial redox reaction of phenazines, Bioelectrochemistry 117 (2017) 34–39, https://doi.org/10.1016/j.bioelechem.2017.04.003.

[45] M. Jarosz, J. Grudzień, K. Kamiński, K. Gawlak, K. Wolski, M. Nowakowska, G.D. Sulka, Novel bioelectrodes based on polysaccharide modified gold surfaces and electrochemically active Lactobacillus rhamnosus GG biofilms, Electrochim. Acta 296 (2019) 999–1008, https://doi.org/10.1016/j.electacta.2018.11.154.

[46] M. Méndez-Tovar, J.V. García-Meza, I. González, Electrochemical monitoring of Acidithiobacillus thiooxidans biofilm formation on graphite surface with elemental sulfur, Bioelectrochemistry 128 (2019) 30–38, https://doi.org/10.1016/j.bioelechem.2019.03.004.

[47] J.T. Babauta, H. Beyenal, Use of a small overpotential approximation to analyze Geobacter sulfurreducens biofilm impedance, J. Power Sources 356 (2017) 549–555, https://doi.org/10.1016/j.jpowsour.2017.03.021.

[48] A.J. Robb, S. Vinogradov, A.S. Danell, E. Anderson, M.S. Blackledge, C. Melander, E.G. Hvastkovs, Electrochemical detection of small molecule induced Pseudomonas aeruginosa biofilm dispersion, Electrochim. Acta 268 (2018) 276–282, https://doi.org/10.1016/j.electacta.2018.02.113.

[49] F. Bimakr, M.P. Ginige, A.H. Kaksonen, D.C. Sutton, G.J. Puzon, K.Y. Cheng, Assessing graphite and stainless-steel for electrochemical sensing of biofilm growth in chlorinated drinking water systems, Sens. Actuat. B Chem. 277 (2018) 526–534, https://doi.org/10.1016/j.snb.2018.09.005.

[50] D.M. Thompson, A.N. Koppes, J.G. Hardy, C.E. Schmidt, Electrical stimuli in the central nervous system microenvironment, Annu. Rev. Biomed. Eng. 16 (2014) 397–430, https://doi.org/10.1146/annurev-bioeng-121813-120655.

[51] M.T. Fitch, J. Silver, CNS injury, glial scars, and inflammation: Inhibitory extracellular matrices and regeneration failure, Exp. Neurol. 209 (2008) 294–301, https://doi.org/10.1016/j.expneurol.2007.05.014.

[52] L. Ghasemi-Mobarakeh, M.P. Prabhakaran, M. Morshed, M.H. Nasr-Esfahani, H. Baharvand, S. Kiani, S.S. Al-Deyab, S. Ramakrishna, Application of conductive polymers, scaffolds and electrical stimulation for nerve tissue engineering, J. Tissue Eng. Regen. Med. 5 (2011) e17–e35, https://doi.org/10.1002/term.383.

[53] T.A. Thrasher, H.M. Flett, M.R. Popovic, Gait training regimen for incomplete spinal cord injury using functional electrical stimulation, Spinal Cord. 44 (2006) 357–361, https://doi.org/10.1038/sj.sc.3101864.

[54] N.A. Maffiuletti, M.A. Minetto, D. Farina, R. Bottinelli, Electrical stimulation for neuromuscular testing and training: state-of-the art and unresolved issues, Eur. J. Appl. Physiol. 111 (2011) 2391–2397, https://doi.org/10.1007/s00421-011-2133-7.

[55] M. Lawrence, M. Morari, Restoration of sensory-motor function by transcutaneous electrical stimulation, IEEE Eng. Med. Biol. Mag. 64–69 (2010).

[56] J.M. Khalifeh, Z. Zohny, M. MacEwan, M. Stephen, W. Johnston, P. Gamble, Y. Zeng, Y. Yan, W.Z. Ray, Electrical stimulation and bone healing: a review of current technology and clinical applications, IEEE Rev. Biomed. Eng. 11 (2018) 217–232, https://doi.org/10.1109/RBME.2018.2799189.

[57] S. Meng, M. Rouabhia, Z. Zhang, Electrical stimulation in tissue regeneration, Appl. Biomed. Eng., InTech (2011) 64, https://doi.org/10.5772/18874.

[58] P. Rl, N. Ac, D. Turcu, M. Bn, S. Sc, M. Berteanu, Effects of neuromuscular electrical stimulation in patients with heart failure - review heart failure and oxidative stress, J. Med. Life 11 (2018) 107–118.

[59] S.T. Sultana, J.T. Babauta, H. Beyenal, Electrochemical biofilm control: a review, Biofouling 31 (2015) 745–758, https://doi.org/10.1080/08927014.2015.1105222.

[60] M.R. Asadi, G. Torkaman, Bacterial inhibition by electrical stimulation, Adv. Wound Care (2014) https://doi.org/10.1089/wound.2012.0410.

[61] J.L. del Pozo, M.S. Rouse, R. Patel, Bioelectric effect and bacterial biofilms. A systematic review, Int. J. Artif. Organs 31 (2008) 786–795, https://doi.org/10.1177/039139880803100906.

[62] M. Jamal, W. Ahmad, S. Andleeb, F. Jalil, M. Imran, M.A. Nawaz, T. Hussain, M. Ali, M. Rafiq, M.A. Kamil, Bacterial biofilm and associated infections, J. Chin. Med. Assoc. 81 (2018) 7–11, https://doi.org/10.1016/j.jcma.2017.07.012.

[63] B. Ercan, K.M. Kummer, K.M. Tarquinio, T.J. Webster, Decreased Staphylococcus aureus biofilm growth on anodized nanotubular titanium and the effect of electrical stimulation, Acta Biomater. 7 (2011) 3003–3012, https://doi.org/10.1016/j.actbio.2011.04.002.

[64] A.J. van der Borden, P.G.M. Maathuis, E. Engels, G. Rakhorst, H.C. van der Mei, H.J. Busscher, P.K. Sharma, Prevention of pin tract infection in external stainless steel

fixator frames using electric current in a goat model, Biomaterials 28 (2007) 2122–2126, https://doi.org/10.1016/j.biomaterials.2007.01.001.
[65] S. Jain, A. Sharma, B. Basu, Vertical electric field induced bacterial growth inactivation on amorphous carbon electrodes, Carbon N. Y. 81 (2015) 193–202, https://doi.org/10.1016/j.carbon.2014.09.048.
[66] W. Shi, B.A.D. Stocker, J. Adler, Effect of the surface composition of motile Escherichia coli and motile Salmonella species on the direction of galvanotaxis, J. Bacteriol. 178 (1996) 1113–1119, https://doi.org/10.1128/jb.178.4.1113-1119.1996.
[67] R. Berthelot, K. Doxsee, S. Neethirajan, Electroceutical approach for impairing the motility of pathogenic bacterium using a microfluidic platform, Micromachines 8 (2017) 207, https://doi.org/10.3390/mi8070207.
[68] N. Wellman, S.M. Fortun, B.R. McLeod, Bacterial biofilms and the bioelectric effect, Antimicrob. Agents Chemother. 40 (1996) 2012–2014.
[69] J. Zhang, K.G. Neoh, X. Hu, E.T. Kang, Mechanistic insights into response of Staphylococcus aureus to bioelectric effect on polypyrrole/chitosan film, Biomaterials 35 (2014) 7690–7698, https://doi.org/10.1016/j.biomaterials.2014.05.069.
[70] H.J.B. Arnout, J. van der Borden, Hester van der Werf, Henny C. van der Mei, Electric current-induced detachment of Staphylococcus epidermidis Biofilms from Surg. Stainless Steel 70 (2004) 6871–6874. doi:10.1128/AEM.70.11.6871.
[71] J.L. Del Pozo, M.S. Rouse, G. Euba, C.-I. Kang, J.N. Mandrekar, J.M. Steckelberg, R. Patel, The electricidal effect is active in an experimental model of Staphylococcus epidermidis Chronic Foreign Body Osteomyelitis, Antimicrob. Agents Chemother. 53 (2009) 4064–4068, https://doi.org/10.1128/AAC.00432-09.
[72] A.J. van der Borden, H.C. van der Mei, H.J. Busscher, Electric block current induced detachment from surgical stainless steel and decreased viability of Staphylococcus epidermidis, Biomaterials 26 (2005) 6731–6735, https://doi.org/10.1016/j.biomaterials.2004.04.052.
[73] A. Kazek-Kęsik, A. Nosol, J. Płonka, M. Śmiga-Matuszowicz, M. Gołda-Cępa, M. Krok-Borkowicz, M. Brzychczy-Włoch, E. Pamuła, W. Simka, PLGA-amoxicillin-loaded layer formed on anodized Ti alloy as a hybrid material for dental implant applications, Mater. Sci. Eng. C. 94 (2019) 998–1008, https://doi.org/10.1016/j.msec.2018.10.049.
[74] H. Chouirfa, H. Bouloussa, V. Migonney, C. Falentin-Daudré, Review of titanium surface modification techniques and coatings for antibacterial applications, Acta Biomater. 83 (2019) 37–54, https://doi.org/10.1016/j.actbio.2018.10.036.
[75] R. Rodriguez, K. Kim, J.L. Ong, In vitro osteoblast response to anodized titanium and anodized titanium followed by hydrothermal treatment, J. Biomed. Mater. Res. 65A (2003) 352–358, https://doi.org/10.1002/jbm.a.10490.
[76] S.J. Fowler, B.F. Smets, Microbial biotechnologies for potable water production, Microb. Biotechnol. 10 (2017) 1094–1097, https://doi.org/10.1111/1751-7915.12837.
[77] A.L. Nascimento, A.J. Souza, P.A.M. Andrade, F.D. Andreote, A.R. Coscione, F.C. Oliveira, J.B. Regitano, Sewage sludge microbial structures and relations to their sources, treatments, and chemical attributes, Front. Microbiol. 9 (2018) 1–11, https://doi.org/10.3389/fmicb.2018.01462.
[78] M.G. Kalyuzhnaya, S. Yang, O.N. Rozova, N.E. Smalley, J. Clubb, A. Lamb, G.A.N. Gowda, D. Raftery, Y. Fu, F. Bringel, S. Vuilleumier, D.A.C. Beck, Y.A. Trotsenko, V.N. Khmelenina, M.E. Lidstrom, Highly efficient methane biocatalysis revealed in a methanotrophic bacterium, Nat. Commun. 4 (2013) 2785, https://doi.org/10.1038/ncomms3785.
[79] A. Gülay, K. Tatari, S. Musovic, R.V. Mateiu, H.-J. Albrechtsen, B.F. Smets, Internal porosity of mineral coating supports microbial activity in rapid sand filters for groundwater treatment, Appl. Environ. Microbiol. 80 (2014) 7010–7020, https://doi.org/10.1128/AEM.01959-14.
[80] M.J. Hedegaard, H.-J. Albrechtsen, Microbial pesticide removal in rapid sand filters for drinking water treatment – potential and kinetics, Water Res. 48 (2014) 71–81, https://doi.org/10.1016/j.watres.2013.09.024.
[81] C.O. Lee, R. Boe-Hansen, S. Musovic, B. Smets, H.-J. Albrechtsen, P. Binning, Effects of dynamic operating conditions on nitrification in biological rapid sand filters for drinking water treatment, Water Res. 64 (2014) 226–236, https://doi.org/10.1016/j.watres.2014.07.001.
[82] K.V. Ramana, L. Singh, Microbial degradation of organic wastes at low temperatures, Def. Sci. J. 50 (2000) 371–382, https://doi.org/10.14429/dsj.50.3748.
[83] V. Wei, M. Elektorowicz, J.A. Oleszkiewicz, Influence of electric current on bacterial viability in wastewater treatment, Water Res. 45 (2011) 5058–5062, https://doi.org/10.1016/j.watres.2011.07.011.
[84] I. Hassan, E. Mohamedelhassan, E.K. Yanful, Z.-C. Yuan, A review article: electrokinetic bioremediation current knowledge and new prospects, Adv. Microbiol. 06 (2016) 57–72, https://doi.org/10.4236/aim.2016.61006.
[85] A. Olszanowski, K. Piechowiak, The use of an electric field to enhance bacterial movement and hydrocarbon biodegradation in soils, Polish J. Environ. Stud. 15 (2006) 303–309.
[86] S. Suni, M. Romantschuk, Mobilisation of bacteria in soils by electro-osmosis, FEMS Microbiol. Ecol. 49 (2004) 51–57, https://doi.org/10.1016/j.femsec.2004.01.016.
[87] E. Mena, J. Villaseñor, P. Cañizares, M.A. Rodrigo, Effect of electric field on the performance of soil electro-bioremediation with a periodic polarity reversal strategy, Chemosphere 146 (2016) 300–307, https://doi.org/10.1016/j.chemosphere.2015.12.053.
[88] T. Li, Y. Wang, S. Guo, X. Li, Y. Xu, Y. Wang, X. Li, Effect of polarity-reversal on electrokinetic enhanced bioremediation of Pyrene contaminated soil, Electrochim Acta 187 (2016) 567–575, https://doi.org/10.1016/j.electacta.2015.11.097.
[89] C. Cameselle, S. Gouveia, Electrokinetic remediation for the removal of organic contaminants in soils, Curr. Opin. Electrochem. 11 (2018) 41–47, https://doi.org/10.1016/j.coelec.2018.07.005.
[90] A.N. Alshawabkeh, Y. Shen, K.Y. Maillacheruvu, Effect of DC electric fields on COD in aerobic mixed sludge processes, Environ. Eng. Sci. 21 (2004) 321–329, https://doi.org/10.1089/109287504323066969.
[91] L.Y. Wick, F. Buchholz, I. Fetzer, S. Kleinsteuber, C. Härtig, L. Shi, A. Miltner, H. Harms, G.N. Pucci, Responses of soil microbial communities to weak electric fields, Sci. Total Environ. 408 (2010) 4886–4893, https://doi.org/10.1016/j.scitotenv.2010.06.048.
[92] Y. Yuan, S.-H. Guo, F.-M. Li, T.-T. Li, Effect of an electric field on n-hexadecane microbial degradation in contaminated soil, Int. Biodeterior. Biodegradation. 77 (2013) 78–84, https://doi.org/10.1016/j.ibiod.2012.10.012.
[93] C. Santoro, C. Arbizzani, B. Erable, I. Ieropoulos, Microbial fuel cells: From fundamentals to applications. A review, J. Power Sources. 356 (2017) 225–244, https://doi.org/10.1016/j.jpowsour.2017.03.109.
[94] B.E. Logan, J.M. Regan, Electricity-producing bacterial communities in microbial fuel cells, Trends Microbiol. 14 (2006) 512–518, https://doi.org/10.1016/j.tim.2006.10.003.
[95] M. Rahimnejad, A. Adhami, S. Darvari, A. Zirepour, S.E. Oh, Microbial fuel cell as new technology for bioelectricity generation: a review, Alexandr. Eng. J. 54 (2015) 745–756, https://doi.org/10.1016/j.aej.2015.03.031.
[96] K. Rabaey, W. Verstraete, Microbial fuel cells: novel biotechnology for energy generation, Trends Biotechnol. 23 (2005) 291–298, https://doi.org/10.1016/j.tibtech.2005.04.008.
[97] B.E. Logan, M.J. Wallack, K.-Y. Kim, W. He, Y. Feng, P.E. Saikaly, Assessment of microbial fuel cell configurations and power densities, Environ. Sci. Technol. Lett. 2 (2015) 206–214, https://doi.org/10.1021/acs.estlett.5b00180.
[98] B.E. Logan, C. Murano, K. Scott, N.D. Gray, I.M. Head, Electricity generation from cysteine in a microbial fuel cell, Water Res. 39 (2005) 942–952, https://doi.org/10.1016/j.watres.2004.11.019.
[99] M.A. Rodrigo, P. Cañizares, J. Lobato, R. Paz, C. Sáez, J.J. Linares, Production of electricity from the treatment of urban waste water using a microbial fuel cell, J. Power Sources 169 (2007) 198–204, https://doi.org/10.1016/j.jpowsour.2007.01.054.
[100] S. Wu, W. He, W. Yang, Y. Ye, X. Huang, B.E. Logan, Combined carbon mesh and small graphite fiber brush anodes to enhance and stabilize power generation in microbial fuel cells treating domestic wastewater, J. Power Sources 356 (2017) 348–355, https://doi.org/10.1016/j.jpowsour.2017.01.041.
[101] J. Chouler, G.A. Padgett, P.J. Cameron, K. Preuss, M.-M. Titirici, I. Ieropoulos, M. Di Lorenzo, Towards effective small scale microbial fuel cells for energy generation from urine, Electrochim. Acta 192 (2016) 89–98, https://doi.org/10.1016/j.electacta.2016.01.112.
[102] H. Liu, R. Ramnarayanan, B.E. Logan, Production of electricity during wastewater treatment using a single chamber microbial fuel cell, Environ. Sci. Technol. 38 (2004) 2281–2285, https://doi.org/10.1021/es034923g.
[103] D. Jiang, M. Curtis, E. Troop, K. Scheible, J. McGrath, B. Hu, S. Suib, D. Raymond, B. Li, A pilot-scale study on utilizing multi-anode/cathode microbial fuel cells (MAC MFCs) to enhance the power production in wastewater treatment, Int. J. Hydrogen Energy. 36 (2011) 876–884, https://doi.org/10.1016/j.ijhydene.2010.08.074.
[104] F. Li, D. Wang, Q. Liu, B. Wang, W. Zhong, M. Li, K. Liu, Z. Lu, H. Jiang, Q. Zhao, C. Xiong, The construction of rod-like polypyrrole network on hard magnetic porous textile anodes for microbial fuel cells with ultra-high output power density, J. Power Sources 412 (2019) 514–519, https://doi.org/10.1016/j.jpowsour.2018.11.090.
[105] H. Li, B. Liao, J. Xiong, X. Zhou, H. Zhi, X. Liu, X. Li, W. Li, Power output of microbial fuel cell emphasizing interaction of anodic binder with bacteria, J. Power Sources 379 (2018) 115–122, https://doi.org/10.1016/j.jpowsour.2018.01.040.
[106] F. Zhao, R.C.T. Slade, J.R. Varcoe, Techniques for the study and development of microbial fuel cells: an electrochemical perspective, Chem. Soc. Rev. 38 (2009) 1926–1939, https://doi.org/10.1039/b819866g.
[107] M. Rimboud, D. Pocaznoi, B. Erable, A. Bergel, Electroanalysis of microbial anodes for bioelectrochemical systems: basics, progress and perspectives, Phys. Chem. Chem. Phys. 16 (2014) 16349–16366, https://doi.org/10.1039/c4cp01698j.
[108] L. Yasri, E.P.L. Roberts, S. Gunasekaran, The electrochemical perspective of bioelectrocatalytic activities in microbial electrolysis and microbial fuel cells, Energy Rep. 5 (2019) 1116–1136.
[109] A.J. Slate, K.A. Whitehead, D.A.C. Brownson, C.E. Banks, Microbial fuel cells: an overview of current technology, Renew. Sustain. Energy Rev. 101 (2019) 60–81, https://doi.org/10.1016/j.rser.2018.09.044.
[110] M. Breheny, K. Bowman, N. Farahmand, O. Gomaa, T. Keshavarz, G. Kyazze, Biocatalytic electrode improvement strategies in microbial fuel cell systems, J. Chem. Technol. Biotechnol. 94 (2019) 2081–2091, https://doi.org/10.1002/jctb.5916.
[111] S. Chen, S.A. Patil, R.K. Brown, U. Schröder, Strategies for optimizing the power output of microbial fuel cells: transitioning from fundamental studies to practical implementation, Appl. Energy 233–234 (2019) 15–28, https://doi.org/10.1016/j.apenergy.2018.10.015.
[112] P. Choudhury, U.S. Prasad Uday, T.K. Bandyopadhyay, R.N. Ray, B. Bhunia, Performance improvement of microbial fuel cell (MFC) using suitable electrode and Bioengineered organisms. A review, Bioengineered 8 (2017) 471–487, https://doi.org/10.1080/21655979.2016.1267883.
[113] M. Abdallah, S. Feroz, S. Alani, E.T. Sayed, A. Shanableh, Continuous and scalable applications of microbial fuel cells: a critical review, Springer Netherlands, 2019. doi:10.1007/s11157-019-09508-x.
[114] C. Xia, D. Zhang, W. Pedrycz, Y. Zhu, Y. Guo, Models for microbial fuel cells: a critical review, J. Power Sources 373 (2018) 119–131, https://doi.org/10.1016/j.jpowsour.2017.11.001.
[115] H. Nagar, N. Badhrachalam, V.V.B. Rao, S. Sridhar, A novel microbial fuel cell incorporated with polyvinylchloride/4A zeolite composite membrane for kitchen

wastewater reclamation and power generation, Mater. Chem. Phys. 224 (2019) 175–185, https://doi.org/10.1016/j.matchemphys.2018.12.023.

[116] G. Sun, K. Kang, L. Qiu, X. Guo, M. Zhu, Electrochemical performance and microbial community analysis in air cathode microbial fuel cells fuelled with pyroligneous liquor, Bioelectrochemistry. 126 (2019) 12–19, https://doi.org/10.1016/j.bioelechem.2018.11.006.

[117] G. Ren, Y. Sun, A. Lu, Y. Li, H. Ding, Boosting electricity generation and Cr(VI) reduction based on a novel silicon solar cell coupled double-anode (photoanode/bioanode) microbial fuel cell, J. Power Sources 408 (2018) 46–50, https://doi.org/10.1016/j.jpowsour.2018.10.081.

[118] E. Taşkan, S. Bulak, B. Taşkan, M. Şaşmaz, S. El Abed, A. El Abed, Nitinol as a suitable anode material for electricity generation in microbial fuel cells, Bioelectrochemistry 128 (2019) 118–125, https://doi.org/10.1016/j.bioelechem.2019.03.008.

[119] B. Fu, T. Xu, X. Guo, P. Liang, X. Huang, X. Zhang, Optimization and simulation of a carbon-based flow-through composite anode configuration to enhance power generation and improve effluent quality simultaneously for microbial fuel cells, J. Clean. Prod. 229 (2019) 542–551, https://doi.org/10.1016/j.jclepro.2019.04.308.

[120] S. Zhang, W. Su, Y. Wei, J. Liu, K. Li, Mesoporous MnO2 structured by ultrathin nanosheet as electrocatalyst for oxygen reduction reaction in air-cathode microbial fuel cell, J. Power Sources 401 (2018) 158–164, https://doi.org/10.1016/j.jpowsour.2018.08.102.

[121] S. Zhang, W. Su, K. Li, D. Liu, J. Wang, P. Tian, Metal organic framework-derived Co3O4/NiCo2O4 double-shelled nanocage modified activated carbon air-cathode for improving power generation in microbial fuel cell, J. Power Sources 396 (2018) 355–362, https://doi.org/10.1016/j.jpowsour.2018.06.057.

materials

MDPI

Article

Bacterial Surface Colonization of Sputter-Coated Platinum Films

Dominika Czerwińska-Główka [1], Wioletta Przystaś [2,3], Ewa Zabłocka-Godlewska [2,3], Sebastian Student [3,4], Beata Cwalina [2,3], Mieczysław Łapkowski [1] and Katarzyna Krukiewicz [1,*]

[1] Department of Physical Chemistry and Technology of Polymers, Silesian University of Technology, 44-100 Gliwice, Poland; dominika.czerwinska-glowka@polsl.pl (D.C.-G.); mieczyslaw.lapkowski@polsl.pl (M.L.)
[2] Department of Environmental Biotechnology, Faculty of Energy and Environmental Engineering, Silesian University of Technology, 44-100 Gliwice, Poland; wioletta.przystas@polsl.pl (W.P.); ewa.zablocka-godlewska@polsl.pl (E.Z.-G.); beata.cwalina@polsl.pl (B.C.)
[3] Biotechnology Centre, Silesian University of Technology, 44-100 Gliwice, Poland; sebastian.student@polsl.pl
[4] Department of Systems Biology and Engineering, Faculty of Automatic Control, Electronics and Computer Science, Silesian University of Technology, 44-100 Gliwice, Poland
* Correspondence: katarzyna.krukiewicz@polsl.pl

Received: 5 May 2020; Accepted: 11 June 2020; Published: 12 June 2020

Abstract: Due to its biocompatibility and advantageous electrochemical properties, platinum is commonly used in the design of biomedical devices, e.g., surgical instruments, as well as electro-medical or orthopedic implants. This article verifies the hypothesis that a thin layer of sputter-coated platinum may possess antibacterial effects. The purpose of this research was to investigate the adhesion and growth ability of a model strain of Gram-negative bacteria, *Escherichia coli,* on a surface of a platinum-coated glass slide. Although some previous literature reports suggests that a thin layer of platinum would inhibit the formation of bacterial biofilm, the results of this study suggest otherwise. The decrease in the number of bacterial cells attached to the platinum-coated glass, which was observed within first three hours of culturing, was found to be a short-time effect, vanishing after 24 h. Consequently, it was shown that a thin layer of sputter-coated platinum did not exhibit any antibacterial effect. For this reason, this study indicates an urgent need for the development of new methods of surface modification that could reduce bacterial surface colonization of platinum-based biomedical devices.

Keywords: antimicrobial properties; bacterial attachment; bacterial growth; *Escherichia coli*; glass; platinum; sputter-coating

1. Introduction

The antimicrobial properties of metals have been known for centuries [1]. Noble metal ions, particularly, have been indicated as potential antibacterial agents. For instance, Vaidya et al. [2] tested various solutions of metal ions (silver, copper, platinum, gold and palladium) for their antimicrobial properties against *Enterococcus faecium, Acinetobacter baumannii* and *Klebsiella pneumoniae,* confirming the superiority of platinum, gold and palladium over non-noble metal ions. Apart from antibacterial activity, noble metals, especially platinum, offer high strength and stability in different conditions, as well as biocompatibility. Furthermore, high electrical conductivity of platinum is an excellent property qualifying this metal for the design of pacemakers, hearing aids and neurological implants [3–5].

Antimicrobial effects may be also achieved by the use of metal nanoparticles. Consequently, nanoparticles of gold, silver, zinc, silica or platinum have been successfully used in the design of biomedical devices [6,7], as bactericidal [8–11] or antibiofouling agents [12,13]. For instance, Gopal et

al. [14] studied the behavior of bacteria exposed to platinum nanoparticles with various sizes, showing the toxicity of small nanoparticles (1–3 nm) and bacterial tolerance of larger nanoparticles (4–21 nm). Small nanoparticles with a spherical morphology were supposed to pass through the pores of the bacterial membrane. In contrast, larger ones, possessing cuboid or flower shapes, were not able to penetrate the membrane. In other studies, Huang et al. [15] indicated a different mechanism of antibacterial action of silver nanoparticles coated with catechol-conjugated chitosan against Gram-negative (*Escherichia coli*) and Gram-positive (*Staphylococcus aureus*) bacteria. In the case of *Staphylococcus aureus*, nanoparticles induced damage to the cell wall and leakage of cytoplasmic proteins. In the case of *Escherichia coli,* nanoparticles were found to adsorb onto the surface of bacterial cells, leading to the change in permeability of a cell membrane, allowing the passage of silver ions into the cytoplasm and thus causing the damage to the bacterial cell. In the work of Kummala et al. [16], silver and titanium dioxide nanoparticles were deposited onto a glass surface by a liquid flame spray technique. This method allowed to distribute nanoparticles uniformly over the entire surface, with a layer thickness controlled through sputtering time. As-formed coatings exhibited antibacterial activity against Gram-positive (*Staphylococcus aureus*) and Gram-negative (*Escherichia coli*) bacteria, and were able to effectively reduce their growth.

Demonstration of antibacterial properties of noble metal ions, as well as their nanoparticles, suggested the desirability of investigating whether noble metals as coatings in a form of ultrathin layers would also exhibit antibacterial activity. Such a thin layer of metal (for example platinum) could be obtained by the use of sputtering techniques. Metal sputtering methods have been increasingly investigated as processes allowing to form a variety of unique materials. For instance, thin layers of copper and silver were sputtered alternately on glass and plastic surfaces, and their antibacterial activity was confirmed against *Staphylococcus epidermidis* and *Staphylococcus aureus* strains [17]. Similarly, Wang et al. [18] used radio frequency magnetron sputtering to deposit nanostructured silver films on the surface of polypropylene nonwovens. The antibacterial properties of as-formed layers were assessed against *Staphylococcus aureus* and *Escherichia coli*, demonstrating the enhancement of antibacterial effects with the thickness of silver layer. Furthermore, Musil [19] described flexible antibacterial coatings fabricated through a reactive magnetron sputtering method. Cr–Cu–O, Al–Cu–N and Zr–Cu–N coatings were given as examples, and their antibacterial properties were analyzed against *Escherichia coli*. It was shown that sputter-coating allowed to produce thick, durable and flexible coatings effective against model bacterial strain after just three hours of contact. Due to the fact that sputter-coating can be used to modify any type of surface, coatings obtained in this way have numerous potential industrial applications in a variety of fields, particularly in biomedical engineering.

In the light of previous research studies showing the antibacterial activity of surfaces modified through sputter-coating, it could be expected that also sputter-coated platinum films should possess similar biocidal characteristics. To verify whether a thin layer of platinum can serve as an efficient factor inhibiting the adhesion and multiplication of bacteria, we compared the behavior of *Escherichia coli* cultured on the surface of platinum-coated and noncoated (bare) glass slides. According to Gaynes et al. [20], *Escherichia coli* was the most commonly reported Gram-negative pathogen in 2013. In addition, *Escherichia coli* has been identified by Vihta et al. [21] as a major cause of bloodstream infection with a critical antimicrobial resistance. As bacterial culture was conducted in a closed system, *Escherichia coli* was expected to grow in a predictable way, giving a growth curve consisting of four different phases: the initial phase (lag phase) referring to metabolically active bacteria that may increase in cell mass, but not in the cell number; the logarithmic phase (log phase), in which a rapid exponential growth of bacteria population is observed; the stationary phase, in which the population of bacteria begins to decline as nutrients are consumed and inhibitory products are accumulated; and, finally, a death phase, in which bacterial cells die due to the lack of nutrients, the excess of toxic substances and also some harmful conditions [22–24]. Therefore, to extensively analyze the effect of surface modification on the attachment and growth of *Escherichia coli*, the bacterial cells were characterized in terms of their dimensions and vitality after 3 h, 24 h and 48 h, corresponding to the initial phase, logarithmic phase and death phase during the growth of

bacteria. The biologic features were discussed together with the physicochemical characteristics of platinum and glass (roughness and hydrophilicity), revealing the relationship between the surface morphology of the materials and their interactions with microorganisms.

2. Materials and Methods

2.1. Preparation and surface characterization of bare and Pt-coated glass slides

A glass support substrate (microscopic slide, Labglass, 75 mm × 25 mm × 1 mm) was used as the reference material. To fabricate Pt-coated films, glass slides were sputter-coated with a thin layer of Pt (4.8 nm) using a sputter-coater (automatic, rotary-pump coating system, Q150R Quorum Technologies, Lewes, UK) working at 30 mA for 120 s. According to the specifications of the manufacturer, the conditions of the sputter-coating process allowed to produce a continuous platinum film with the grain size in the order of 2 nm. To compare both materials, their roughness was examined using scanning electron microscopy (Phenom ProX, Thermo Fisher Scientific, Waltham, MA, USA) and the 3D Roughness Reconstruction software (Phenom ProSuits, Thermo Fisher Scientific, Waltham, MA, USA). The wettability of materials was determined by contact angle measurements, by means of a DataPhysics OCA15 goniometer (DataPhysics Instruments, Filderstadt, Germany) using deionized water. In all measurements, three sample sites were analyzed on three different sample surfaces, giving n = 9.

2.2. Culturing Bacteria and Examining Their Growth on Bare and Pt-Coated Glass Slides

The bacterial strain of Gram-negative *Escherichia coli* (DSM 30083, U5/41) was cultured in 23 g/L agar broth (BTL, Warsaw, Poland) at 35 °C for 48 h in an incubator. After this time, the agar slants were washed with physiological salt (0.85% water solution of NaCl; Acros Organics, Geel, Belgium). At such prepared suspension of bacteria, the turbidity was established between 3 and 4 according to McFarland scale, which corresponds to estimated bacteria number of $10.5 \cdot 10^8$ cells/mL. This suspension was used for the inoculation of bare and Pt-coated glass slides.

The sterilization of bare and Pt-coated glass slides—necessary before starting biologic examinations—was achieved through placing the substrates in 12-well plates and immersing them for 1 h in 70% ethanol (obtained by dilution of 99.8% ethanol, Acros Organics, Geel, Belgium). This method of sterilization did not change the surface properties of the materials. After this, ethanol was removed, and the samples were rinsed three times with distilled water. Next, they were left to dry.

Consecutively, 0.1 mL of bacterial saline suspension was applied on bare and Pt-coated glass slides. Then, 2 mL of culture nutrient-poor growth medium, containing 10-g/L tryptone (BTL, Warsaw, Poland), 5 g/L yeast extract (BTL, Warsaw, Poland) and 10 g/L physiological saline (Acros Organics, Geel, Belgium) at pH = 7, was added. Culturing of bacteria was carried out for 2 days in an incubator at 35 °C. Samples for analysis were taken after 3 h, 24 h and 48 h.

In order to obtain reliable results, the experiments were performed in triplicate for all materials under the same conditions. The results were presented as mean values ± standard deviation. A Student's *t*-test was performed to determine the statistical significance ($p < 0.05$).

2.3. Staining and Imaging Bacterial Cells Adhered to Glass Slides

The two-color fluorescence assay LIVE/DEAD® BacLight Bacterial Viability Kit (Life Technologies, Thermo Fisher Scientific, Waltham, MA, USA) was used to stain bacteria; live bacterial cells were labeled in green with SYTO9 stain, whereas dead bacterial cells were labeled in red with D-propidium iodide. Confocal fluorescent microscope (Olympus FluoView FV1000, Tokyo, Japan) was used to visualize bacteria on bare (noncoated) and Pt-coated glass slides, and then to analyze the number of live and dead cells. Image analysis was accomplished using ImageJ software (NIH, Bethesda, MD, USA).

Scanning electron microscopy was used to visualize and analyze the morphology of bacteria grown on bare and Pt-coated glass surfaces. Before the samples could be visualized, the materials underwent several stages of conditioning (dehydration). Consequently, the materials were fixed

using 3% glutaraldehyde (Fisher BioReagents, Waltham, MA, USA) for 24 h and dehydrated by immersing the samples in the solutions of ethanol (Acros Organics) with increasing concentrations (30%, 50%, 70%, 80%, 90%, 95%, 99.8%), and then dried in the dryer (24 h, 50 °C). Dehydrated samples were sputter-coated with a gold layer for better image quality (20 min, 20 mA; Q150R Quorum Technologies, Lewes, UK), and then their surface was examined by scanning electron microscopy (Phenom ProX, Thermo Fisher Scientific, Waltham, MA, USA). Images were taken with an accelerating voltage of 15 kV at the magnifications of 1000×, 5000× and higher. The average length and width of bacteria, as well as their density (number of bacteria per 200 μm^2) were calculated using the ImageJ software (NIH, Bethesda, MD, USA).

3. Results and Discussions

3.1. Materials Characterization

This article concerns the investigations of antibacterial properties of a thin layer of platinum sputter-coated on the surface of a glass slide in relation to a noncoated slide (bare glass). Sputter coating allows for a full surface coverage, resulting in the formation of a thin coating with a distinct metallic gloss. Imaging of the sputter-coated sample using SEM confirmed that platinum is present on the surface of a glass slide and forms a homogeneous layer (Figure 1). Surface properties, such as surface roughness, charge, wettability or surface energy, are among many material features that can influence the phenomenon of bacterial adherence [25,26]. Literature data indicate that higher roughness [27,28] and more hydrophobic nature of a surface [29–31] result in facilitated adhesion of bacteria. However, these effects are observed particularly in the first stages of surface colonization by bacterial cells, and they vanish as the biofilm becomes mature [28,32].

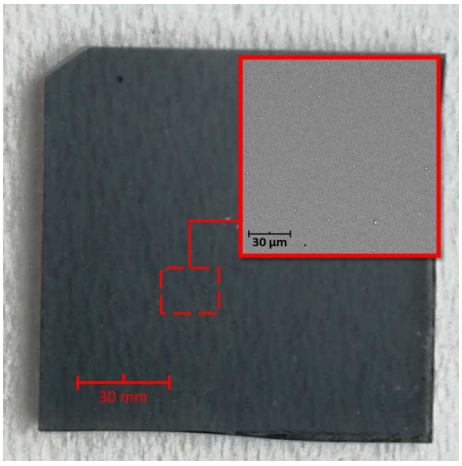

Figure 1. Homogeneity of a sputter-coated layer of platinum. Optical image of a Pt-coated glass slide and a SEM image as the inset.

The surface area roughness of bare and Pt-coated glass slides, expressed by the arithmetical mean height (S_a), varied slightly, retaining values of 0.26 ± 0.01 µm for a bare glass slide and 0.21 ± 0.01 µm for a Pt-coated glass slide, respectively. Even though the difference in S_a was slight, it was supposed to affect the adhesion of bacteria. The greater roughness promotes the adhesion, as shown by Han et al. [27], who analyzed the development of *Streptococcus mutans*, *Streptococcus sanguinis* and polymicrobial (Microcosm) biofilms on modified surfaces of titanium. A significantly higher number of bacteria of each strain was observed on the surface of titanium that was sandblasted with large grits and acid-etched (S_a of 1.4 µm), than on the surface of pickled titanium disk (S_a of 0.3 µm). However, during biofilm maturation, the effect of surface roughness decreased. Therefore, based on the surface roughness analysis, it was supposed that the attachment of bacteria to the surface of bare glass should be slightly enhanced as compared with Pt-coated glass.

Another important surface feature that can significantly affect the process of bacterial adhesion is surface hydrophilicity. It is accepted that bacteria with hydrophilic properties prefer hydrophilic

material surfaces, whereas the ones with hydrophobic characteristics prefer hydrophobic surfaces. Consequently, a difference in the wettability between bare glass slides and Pt-coated slides was investigated by determining the contact angle (θ) at room temperature (T ≈ 20 °C) using deionized water. The results (Figure 2) showed that the surface of Pt-coated glass was evidently more hydrophilic (θ = 35.2° ± 10.5°) than a surface of bare glass (θ = 60.4° ± 7.5°). According to the literature data [32–35], the adhesion effect of various hydrophilic bacteria, including *Escherichia coli*, is usually enhanced on hydrophilic surfaces, but at a different extent. Bacterial cells show a higher affinity to surfaces with moderate wettability as compared with extremely hydrophobic or hydrophilic surfaces [34]. Thus, it was expected that *Escherichia coli* should exhibit a higher affinity towards Pt-coated glass than to bare one.

As the potential effects of surfaces roughness and hydrophilicity on the attachment of bacteria were ambiguous—and a layer of platinum could lead to the decrease (basing on surface roughness data) or to the increase (basing on its hydrophilic character) in bacterial adhesion—there was a need to carry out biologic investigations on the behavior of a selected bacterial strain colonizing both types of surfaces.

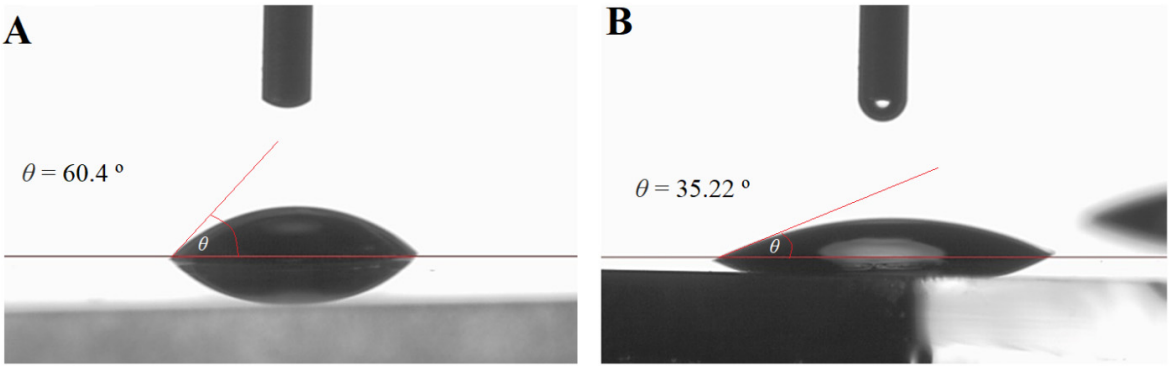

Figure 2. Surface hydrophilicity of investigated surfaces. (**A**) Behavior of a drop of water on the surface of a bare glass slide and (**B**) a Pt-coated glass slide.

3.2. Bacterial Colonization of Materials Surface

To assess the ability of bacteria to attach and grow on bare and Pt-coated glass slides, *Escherichia coli*, as a common pathogen, was cultured on the surface of materials for 48 h. After specified time, samples were investigated using SEM, and the micrographs were used to visualize the interactions between bacteria and investigated surfaces (Figure 3A). Consecutive stages of bacterial growth were monitored by assessing the bacterial cell density after 3 h, 24 h and 48 h of incubation. Accordingly, the results obtained after 3 h of culturing were related to the initial phase of bacteria growth, in which the bacteria tendency to attach to the surface could be investigated. As observed in Figure 3B, the density of bacteria on bare glass (15.3 ± 1.6 cells/200 μm^2) was slightly higher than on a Pt-coated glass slide (12.9 ± 2.1 cells/200 μm^2), what was consistent with the literature data [27,32], indicating a better adhesion of bacteria to more rough surface, although obtained data don't show statistically significant differences. These results may also suggest that the effect of roughness dominates over the effect of hydrophilicity, making the surface of a Pt-coated glass slide less prone to bacterial attachment.

Comparing to the first stage of bacterial growth (3 h of culture), where bacteria were irreversibly bound to the surface, the next phase (24 h) represented the multiplication stage of bacteria that occurred after their attachment to the surface. At this time, the bacterial cells multiplied and started spreading over the surface of specimens. In this phase, significantly increased number of bacteria was observed on both types of surfaces, namely 28.9 ± 2.5 cells/200 μm^2 and 29.5 ± 3.0 cells/200 μm^2 for bare and Pt-coated glass slides, respectively (Figure 3B). Since the bacteria density on both types of surfaces was almost identical, it could be concluded that the initial inconsiderable

decrease in the rate of adhesion observed on the surface of Pt was only a short-term effect, overcame by the ability of bacteria to proliferate.

After 48 h, a significant decrease in bacterial density on both surfaces was evident. This time point indicated a death phase of bacterial growth since the bacteria did not receive a new portion of fresh culture medium during this experiment. Therefore, many bacterial cells observed in the micrographs possessed deformed shapes (Figure 3A—insets). From the distorted surface of bacterial cells, it could be concluded that the growth and reproduction of bacteria were disrupted. Due to this, dead bacteria underwent lysis, released cells debris, and were easily detached from the surface. For this reason, only few healthy cells were observed on the surface of samples, and the bacterial density reached the values even lower than in the initial phase, i.e., 11.3 ± 1.6 cells/200 μm² and 11.4 ± 2.3 cells/200 μm² for a bare glass and a Pt-coated glass slide, respectively. These identical results pointed to the high similarity of both surfaces in terms of material characteristics influencing the adhesion of bacteria.

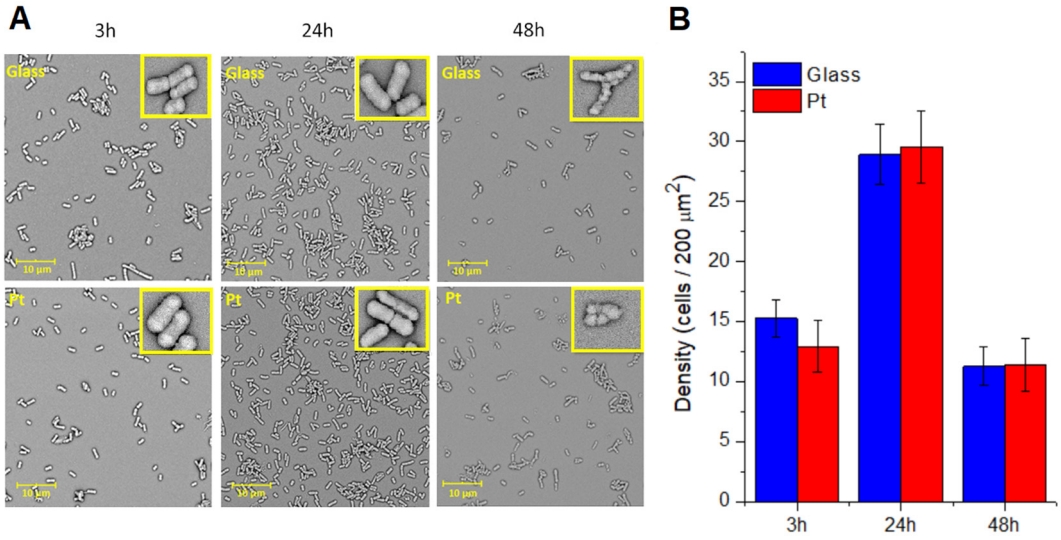

Figure 3. Colonization of *Escherichia coli* on the surfaces of bare and Pt-coated glass slides. (**A**) SEM micrographs presenting bacterial populations grown for 3 h, 24 h and 48 h on the surface of samples; (**B**) bacterial cells density (number of bacterial cells per 200 μm²) calculated from SEM images.

3.3. Dimensions of Bacterial Cells

Escherichia coli has already been extensively analyzed, becoming one of the best-known models of Gram-negative and relatively anaerobic bacteria. *Escherichia coli* is a rod-shaped bacterium with the average cell length of 1–2 μm and width of 0.5–1.0 μm. These dimensions depend on the bacterial metabolism and intensity of growth, since *Escherichia coli* can easily modulate its size to maintain vitality and reproductive capacity depending on the availability of nutrient-rich medium [36,37].

Therefore, to analyze the growth of bacteria on the surfaces of both materials (Figure 4A), their dimensions (length and width) were assessed (Table 1). To numerically describe the shape of the bacteria independently of their sizes, the dimensionless aspect ratio was introduced and calculated as a function of width and length. The values of the aspect ratio approached zero for very elongated bacteria and were close to unity for circular cells. In general, the investigated bacteria possessed average dimensions of rod-shaped *Escherichia coli* cells, namely the average length between 1.79 μm and 2.04 μm, and the average width between 0.66 μm and 0.77 μm. Although having similar shape, the bacteria cells cultured on the surface of bare glass were longer and wider (length of 1.95–2.04 μm, width of 0.70–0.77 μm) than the cells grown on the surface of Pt-coated glass (length of 1.79–1.95 μm, width of 0.66–0.75 μm).

Table 1. Average dimensions of bacterial cells. Comparison of average values of length, width and aspect ratio of bacteria cultured on bare and Pt-coated glass slides for 3 h, 24 h and 48 h; * = $p < 0.05$, n = 150.

Surface	Glass			Platinum		
Time, h	3	24	48	3	24	48
Length, µm	2.00 ± 0.04 *	1.94 ± 0.03	2.04 ± 0.04 *	1.79 ± 0.03 *	1.95 ± 0.03	1.90 ± 0.03 *
Width, µm	0.77 ± 0.01	0.70 ± 0.01 *	0.71 ± 0.01	0.75 ± 0.01	0.66 ± 0.01 *	0.71 ± 0.01
Aspect ratio	0.40 ± 0.01 *	0.37 ± 0.01	0.37 ± 0.01	0.43 ± 0.01 *	0.35 ± 0.01	0.39 ± 0.01

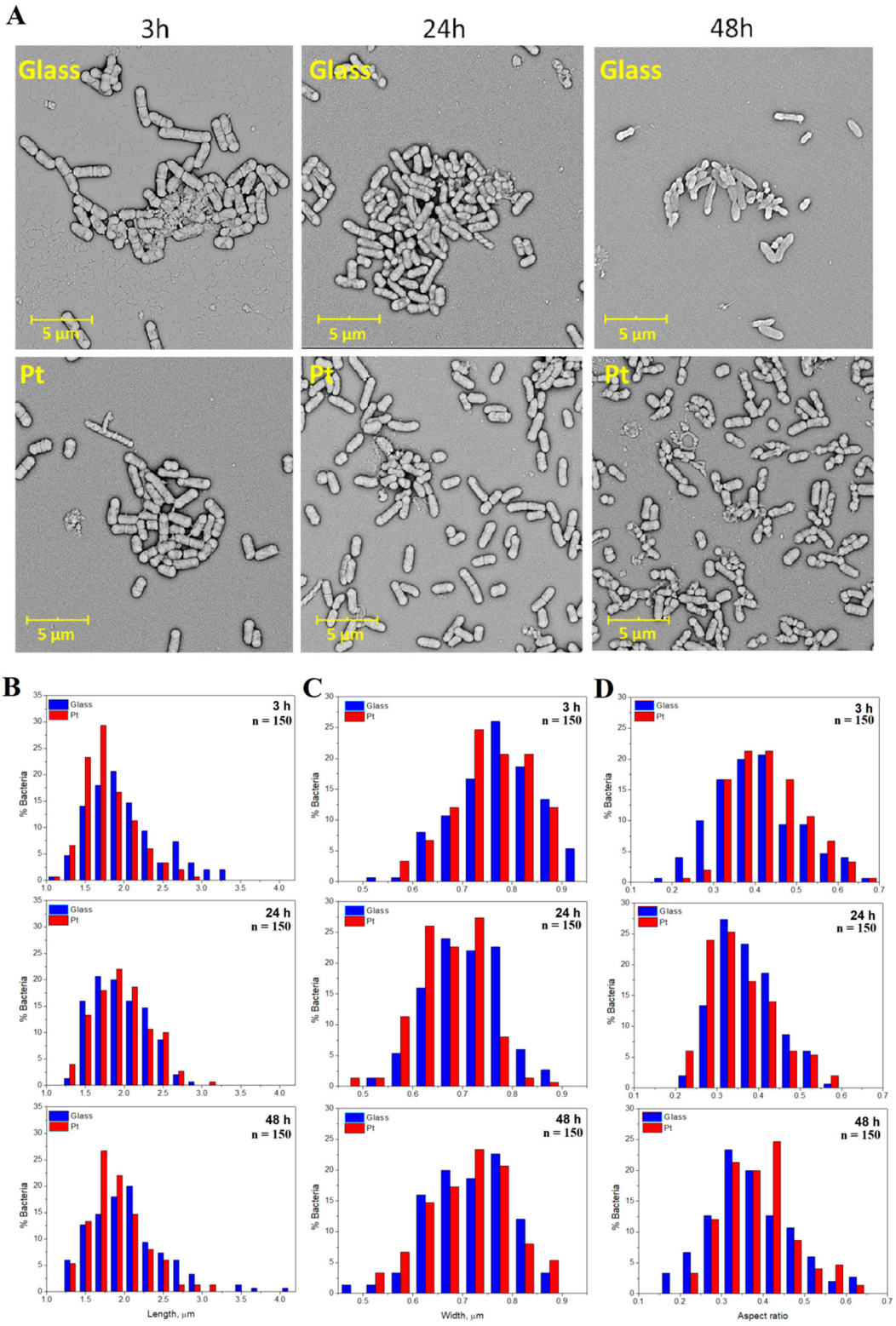

Figure 4. Size distribution of bacterial cells on bare and Pt-coated glass slides. (**A**) SEM micrographs presenting bacterial populations grown for 3 h, 24 h and 48 h on bare and Pt-coated glass; (**B**) histograms of the bacterial cells percentage in terms of specified values of (**C**) length, width and (**D**) aspect ratio, calculated from SEM images; n = 150.

The analysis of histograms showing the variations in length, width and aspect ratio (Figure 4B–D) was performed to provide more information and to assess the cycle of bacterial proliferation. Changes in the average length of bacterial cells, observed in Figure 4B after 3 h of incubation on both bare glass and Pt-coated glass, suggested that the cells remained still in the lag phase. After 24 h, bacteria cultured on glass were longer than in case of bacteria cultured on Pt, suggesting that their metabolic activity was enhanced. In addition, the bacteria cultured on glass were thicker than bacteria cultured on Pt (Figure 4C), confirming preferential growth of bacteria on glass. Furthermore, the bacteria were the widest after the first 3 h of incubation, while in subsequent time points (24 h and 48 h) they were longer in order to divide into daughter cells. After 24 h, all bacteria were found to grow actively (an increase in length was noted), which allowed them to enter the division phase and to significantly increase their population. A significant increase in length of bacterial cells was observed on the Pt-coated glass, for which the average value exceeded the result observed on bare glass.

However, after 48 h the length of cells was found to decrease. This effect, together with a significant decrease in cell density (Figure 3), suggested that bacteria entered the death phase. At this stage, the higher number of shorter cells was observed on bare glass as compared with the Pt-coated glass. However, the opposite effect was observed for cells being 1.4–2.0 mm long. In addition, the distribution of cells with lengths in the range of 1.4–2.2 mm (comprising lengths characteristic for *Escherichia coli*) was similar to that noted in the first phase. Some bacterial cells occupying the surface of bare glass were considerably longer than bacteria on Pt-coated glass. Comparing the aspect ratio of cells (Figure 4D), more frequently lower values were observed for bacteria growing for 24 h on both bare and Pt-coated glass, indicating intensive cell proliferation at that time.

3.4. LIVE/DEAD Analysis

To assess bacterial viability, a LIVE/DEAD analysis based on confocal fluorescent microscopic images was carried out at each time point (Figure 5A). The set of data (Figure 5B) indicated that, despite the higher density of bacteria on the surface of bare glass after first 3 h of culture, a significant part of them (79.5% ± 1.7%) was dead. The percentage of dead bacteria was significantly lower (61.1% ± 2.0%) during bacteria growth on Pt-coated glass. This result showed that a thin film of Pt deposited on a surface did not exhibit any antibacterial effects but seemed to be more compatible towards bacteria than a glass control surface. The percentage of live bacteria was twice as high on the surface of a Pt-coated glass than a glass control (38.9% ± 2.0% and 20.5% ± 1.7%, respectively).

This tendency partially vanished at the subsequent time point (after 24 h of incubation) representing the growth phase of bacterial culture. Now, live bacteria that adhered to the surface during the initial phase started to multiply, leading to a significant increase in cell density. After 24 h of incubation, the increased percentage of live bacteria on both types of surfaces was also observed. This effect was more pronounced in the case of Pt-coated glass than bare glass (61.8% ± 1.3% and 56.8% ± 0.6%, respectively).

Despite the fact that there were only a few bacteria remaining on the slides after 48 h, most of them were alive. The number of live bacteria was almost identical for both bare and Pt-coated glass slides (62.5% ± 1.1% and 62.1% ± 0.7%, respectively). On platinum, the percentage of live bacteria remained similar as in the previous time point. The 3D reconstruction of bacteria cultured on the surface of a Pt-coated glass slide for 48 h (Supplementary file) indicated that some cells were attached perpendicularly to the investigated surface, which should be associated with hydrophilicity of the substrate [38].

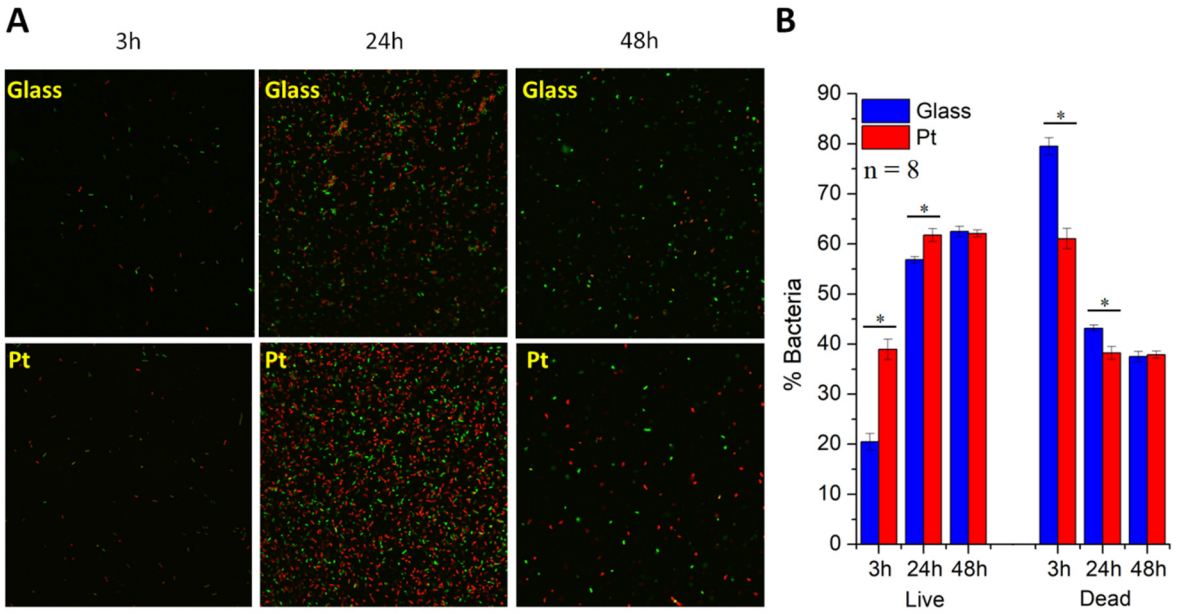

Figure 5. Viability of *Escherichia coli* on surfaces of glass and Pt-coated glass slides. (**A**) Confocal fluorescent microscopic images and (**B**) percentage values of live and dead bacteria after 3 h, 24 h and 48 h; * = $p < 0.05$, n = 8.

Since previous studies reported the antibacterial effect of sputter-coated layers of copper and silver [17,18], it was expected that also sputter-coated layer of platinum should possess similar biocidal character. This hypothesis was supported by the fact that both Pt ions and Pt nanoparticles are known for their antibacterial activity. Pt ions, due to their electronegativity, are supposed to be highly attracted to the negatively charged bacteria [2]. As a consequence, the increase in the bacterial-metal ion interactions is observed, leading to cell death. Small Pt nanoparticles, on the other way, are supposed to easily pass through the pores of the bacterial membrane, affecting cell growth and viability [14]. We expected similar results for a sputtered layer of Pt since the sputter-coating process should produce a platinum film with the grain size of about 2 nm. However, our results revealed opposite observations to those expected, as a thin layer of sputtered Pt was not shown to exhibit any antibacterial effect.

The lack of antibacterial properties of sputter-coated Pt layer should be correlated with the physicochemical stability of deposited film, preventing Pt ions and nanoparticles from release. In contrast, the mechanism of antimicrobial activity of sputter-coated silver and copper films was based on the release of Ag or Cu, respectively [17]. In the case of a mixed layer of Ag–Cu, the antibacterial effect could also arise from the galvanic action and small electrical field generated by the Ag–Cu electrochemical couple, as suggested by Blenkinsopp et al. [39]. For a thin film made purely of Pt, electric field could not be generated without external stimulation.

Thus, high physicochemical stability of platinum being its great advantage is also responsible for the lack of biocidal character of a sputter-coated layer against a model Gram-negative bacterial strain, *Escherichia coli*. Therefore, the surface of thin Pt film may be easily colonized by bacterial population, leading to an increased risk of infections, including nosocomial infections. For this reason, there is an urgent need for the development of new methods of surface modification that will reduce the risk of its colonization by bacteria and subsequent infections.

4. Conclusions

In this study, bare glass and Pt-coated glass slides were used to investigate the antibacterial activity of sputter-coated Pt films against a model bacterial strain, *Escherichia coli*. It was shown that the interactions between bacteria and both materials were similar. Although the examined materials were found to differ in hydrophilic character, roughness had a stronger effect on the adhesion of

bacteria than wettability. Therefore, the surface of a Pt-coated glass slide was less prone to bacterial attachment than a bare glass slide. Unfortunately, the lower number of bacterial cells adhering to the Pt-coated glass observed initially was only a short-term effect. The density of bacteria on both types of surfaces increased considerably after 24 h of culture. Consequently, it was shown that a thin layer of sputtered Pt was not sufficient to cause any antibacterial effects.

The lack of expected biocidal character of sputter-coated Pt layer against *Escherichia coli* seems to be correlated with the high physicochemical stability of such thin film, preventing Pt ions and Pt nanoparticles from release. Therefore, even though platinum is a metal exhibiting high biocompatibility and superior electrochemical properties and has a great importance and potential in biomedical applications, this study shows its serious limitation in the context of colonization by bacterial population, particularly *Escherichia coli*. For this reason, there is an urgent need for the development of new methods of surface modification that will reduce the risk of surface colonization by bacteria and subsequent infections, but will maintain high physicochemical stability and electroactivity of Pt.

Supplementary Materials: The following are available online at https://www.mdpi.com/1996-1944/13/12/2674/s1, Video S1: E.coli-on-sputter-coated-Pt-film_48h.

Author Contributions: Conceptualization, K.K. and B.C.; methodology, K.K. and D.C.-G.; investigation, D.C.-G., W.P., E.Z.-G and S.S.; writing—original draft preparation, D.C.-G; writing—review and editing, K.K and B.C.; supervision, K.K. and M.Ł.; funding acquisition, K.K. All authors have read and agreed to the published version of the manuscript.

Funding: This research was funded by the National Science Center in Poland in the framework of Sonata 2016/23/D/ST5/01306.

Conflicts of Interest: The authors declare no conflicts of interest.

References

1. Elsome, A.M.; Hamilton-Miller, J.M.T.; Brumfitt, W.; Noble, W.C. Antimicrobial activities in vitro and in vivo of transition element complexes containing gold (I) and osmium (VI). *J. Antimicrob. Chemother.* **1996**, *37*, 911–918, doi:10.1093/jac/37.5.911.
2. Vaidya, M.Y.; McBain, A.J.; Butler, J.; Banks, C.E.; Whitehead, K.A. Antimicrobial Efficacy and Synergy of Metal Ions against Enterococcus faecium, Klebsiella pneumoniae and Acinetobacter baumannii in Planktonic and Biofilm Phenotypes. *Sci. Rep.* **2017**, *7*, 5911, doi:10.1038/s41598-017-05976-9.
3. Rai, M.; Ingle, A.P.; Medici, S. *Biomedical Applications of Metals*; Springer: Berlin/Heidelberg, Germany, 2018; ISBN 9783319748146.
4. Kenny, J. Platinum in Cardiac Pacemakers. *Platin. Met. Rev.* **1973**, *17*, 64–65.
5. Hudak, E.M.; Kumsa, D.W.; Martin, H.B.; Mortimer, J.T. Electron transfer processes occurring on platinum neural stimulating electrodes: Calculated charge-storage capacities are inaccessible during applied stimulation. *J. Neural Eng.* **2017**, *14*, 046012, doi:10.1088/1741-2552/aa6945.
6. Ramos, A.P.; Cruz, M.; Tovani, C.B.; Ciancaglini, P. Biomedical applications of nanotechnology. *Biophys. Rev.* **2017**, *9*, 79–89, doi:10.1007/s12551-016-0246-2.
7. Marassi, V.; Di Cristo, L.; Smith, S.; Ortelli, S.; Blosi, M.; Costa, A.L.; Reschiglian, P.; Volkov, Y.; Prina-Mello, A. Silver nanoparticles as a medical device in healthcare settings: A five-step approach for candidate screening of coating agents. *R. Soc. Open Sci.* **2018**, *5*, 171113, doi:10.1098/rsos.171113.
8. Hashimoto, M.; Yanagiuchi, H.; Kitagawa, H.; Honda, Y. Inhibitory effect of platinum nanoparticles on biofilm formation of oral bacteria. *Nano Biomed.* **2017**, *9*, 77–82, doi:10.11344/nano.9.77.
9. Wang, L.; Hu, C.; Shao, L. The antimicrobial activity of nanoparticles: Present situation and prospects for the future. *Int. J. Nanomed.* **2017**, *12*, 1227–1249, doi:10.2147/IJN.S121956.
10. Morones, J.R.; Elechiguerra, J.L.; Camacho, A.; Holt, K.; Kouri, J.; Ramírez, J.T.; Yacaman, M.J. The bactericidal effect of silver nanoparticles. *Nanotechnology* **2005**, *16*, 2346–2353, doi:10.1088/0957-4484/16/10/059.
11. Sondi, I.; Salopek-Sondi, B. Silver nanoparticles as antimicrobial agent: A case study on E. coli as a model for Gram-negative bacteria. *J. Colloid Interface Sci.* **2004**, *275*, 177–182, doi:10.1016/j.jcis.2004.02.012.

12. Sano, K.; Kanematsu, H.; Hirai, N.; Ogawa, A.; Kougo, T.; Tanaka, T. The development of the anti-biofouling coating agent using metal nanoparticles and analysis by Raman spectroscopy and FIB system. *Surf. Coat. Technol.* **2017**, *325*, 715–721, doi:10.1016/j.surfcoat.2017.04.015.
13. Ren, J.; Han, P.; Wei, H.; Jia, L. Fouling-Resistant Behavior of Silver Nanoparticle-Modified Surfaces against the Bioadhesion of Microalgae. *ACS Appl. Mater. Interfaces* **2014**, *6*, 3829–3838, doi:10.1021/am500292y.
14. Gopal, J.; Hasan, N.; Manikandan, M.; Wu, H. Bacterial toxicity/compatibility of platinum nanospheres, nanocuboids and nanoflowers. *Sci. Rep.* **2013**, *3*, 1–8, doi:10.1038/srep01260.
15. Huang, X.; Bao, X.; Liu, Y.; Wang, Z.; Hu, Q.-L. Catechol-Functional Chitosan/Silver Nanoparticle Composite as a Highly Effective Antibacterial Agent with Species-Specific Mechanisms. *Sci. Rep.* **2017**, *7*, 1860, doi:10.1038/s41598-017-02008-4.
16. Kummala, R.; Brobbey, K.J.; Haapanen, J.; Mäkelä, J.M.; Gunell, M.; Eerola, E.; Huovinen, P.; Toivakka, M.; Saarinen, J.J. Antibacterial activity of silver and titania nanoparticles on glass surfaces. *Adv. Nat. Sci. Nanosci. Nanotechnol.* **2019**, *10*, 015012, doi:10.1088/2043-6254/ab0882.
17. McLean, R.J.; Hussain, A.A.; Sayer, M.; Vincent, P.J.; Hughes, D.J.; Smith, T.J.N. Antibacterial activity of multilayer silver–copper surface films on catheter material. *Can. J. Microbiol.* **1993**, *39*, 895–899, doi:10.1139/m93-134.
18. Wang, H.B.; Wei, Q.; Wang, J.Y.; Hong, J.H.; Zhao, X.Y. Sputter deposition of nanostructured antibacterial silver on polypropylene non-wovens. *Surf. Eng.* **2008**, *24*, 70–74, doi:10.1179/174329408x277493.
19. Musil, J. Flexible Antibacterial Coatings. *Molecules* **2017**, *22*, 813, doi:10.3390/molecules22050813.
20. Weinstein, R.A.; Gaynes, R.; Edwards, J.R.; System, N.N.I.S. Overview of Nosocomial Infections Caused by Gram-Negative Bacilli. *Clin. Infect. Dis.* **2005**, *41*, 848–854, doi:10.1086/432803.
21. Vihta, K.-D.; Stoesser, N.; Llewelyn, M.J.; Quan, T.P.; Davies, T.J.; Fawcett, N.J.; Dunn, L.; Jeffery, K.; Butler, C.C.; Hayward, G.; et al. Trends over time in Escherichia coli bloodstream infections, urinary tract infections, and antibiotic susceptibilities in Oxfordshire, UK, 1998–2016: A study of electronic health records. *Lancet Infect. Dis.* **2018**, *18*, 1138–1149, doi:10.1016/s1473-3099(18)30353-0.
22. Garrett, T.R.; Bhakoo, M.; Zhang, Z. Bacterial adhesion and biofilms on surfaces. *Prog. Nat. Sci.* **2008**, *18*, 1049–1056, doi:10.1016/j.pnsc.2008.04.001.
23. Skarstad, K.; Steen, H.B.; Boye, E. Cell cycle parameters of slowly growing Escherichia coli B/r studied by flow cytometry. *J. Bacteriol.* **1983**, *154*, 656–662, doi:10.1128/jb.154.2.656-662.1983.
24. Zwietering, M.; Jongenburger, I.; Rombouts, F.M.; Riet, K.V.T. Modeling of the Bacterial Growth Curve. *Appl. Environ. Microbiol.* **1990**, *56*, 1875–1881, doi:10.1128/aem.56.6.1875-1881.1990.
25. An, Y.H.; Friedman, R.J. Concise review of mechanisms of bacterial adhesion to biomaterial surfaces. *J. Biomed. Mater. Res.* **1998**, *43*, 338–348, doi:10.1002/(SICI)1097-4636(199823)43:33.0.CO;2-B.
26. Li, B.; Logan, B.E. Bacterial adhesion to glass and metal-oxide surfaces. *Colloids Surf. B Biointerfaces* **2004**, *36*, 81–90, doi:10.1016/j.colsurfb.2004.05.006.
27. Han, A.; Li, X.; Huang, B.; Tsoi, J.K.-H.; Matinlinna, J.P.; Chen, Z.; Deng, D.M. The effect of titanium implant surface modification on the dynamic process of initial microbial adhesion and biofilm formation. *Int. J. Adhes. Adhes.* **2016**, *69*, 125–132, doi:10.1016/j.ijadhadh.2016.03.018.
28. Wu, S.; Zhang, B.; Liu, Y.; Suo, X.; Li, H. Influence of surface topography on bacterial adhesion: A review (Review). *Biointerphases* **2018**, *13*, 060801, doi:10.1116/1.5054057.
29. Satou, N.; Satou, J.; Shintani, H.; Okuda, K. Adherence of Streptococci to Surface-modified Glass. *Microbiology* **1988**, *134*, 1299–1305, doi:10.1099/00221287-134-5-1299.
30. Fletcher, M.; Loeb, G.I. Influence of Substratum Characteristics on the Attachment of a Marine Pseudomonad to Solid Surfaces. *Appl. Environ. Microbiol.* **1979**, *37*, 67–72, doi:10.1128/aem.37.1.67-72.1979.
31. Shebl, R.I.; Farouk, F.; Azzazy, H.M. Effect of Surface Charge and Hydrophobicity Modulation on the Antibacterial and Antibiofilm Potential of Magnetic Iron Nanoparticles. *J. Nanomater.* **2017**, *2017*, 1–15, doi:10.1155/2017/3528295.
32. Bayoudh, S.; Othmane, A.; Bettaieb, F.; Bakhrouf, A.; Ben Ouada, H.; Ponsonnet, L. Quantification of the adhesion free energy between bacteria and hydrophobic and hydrophilic substrata. *Mater. Sci. Eng. C* **2006**, *26*, 300–305, doi:10.1016/j.msec.2005.10.045.
33. Bruinsma, G.M.; Van Der Mei, H.C.; Busscher, H.J. Bacterial adhesion to surface hydrophilic and hydrophobic contact lenses. *Biomaterials* **2001**, *22*, 3217–3224, doi:10.1016/s0142-9612(01)00159-4.

34. Daffonchio, D.; Thaveesri, J.; Verstraete, W. Contact angle measurement and cell hydrophobicity of granular sludge from upflow anaerobic sludge bed reactors. *Appl. Environ. Microbiol.* **1995**, *61*, 3676–3680, doi:10.1128/aem.61.10.3676-3680.1995.
35. Yuan, Y.; Hays, M.P.; Hardwidge, P.R.; Kim, J. Surface characteristics influencing bacterial adhesion to polymeric substrates. *RSC Adv.* **2017**, *7*, 14254–14261, doi:10.1039/C7RA01571B.
36. Reshes, G.; Vanounou, S.; Fishov, I.; Feingold, M. Cell Shape Dynamics in Escherichia coli. *Biophys. J.* **2008**, *94*, 251–264, doi:10.1529/biophysj.107.104398.
37. Westfall, C.S.; Levin, P.A. Bacterial Cell Size: Multifactorial and Multifaceted. *Annu. Rev. Microbiol.* **2017**, *71*, 499–517, doi:10.1146/annurev-micro-090816-093803.
38. Marshall, K.C.; Cruickshank, R.H. Cell surface hydrophobicity and the orientation of certain bacteria at interfaces. *Arch. Microbiol.* **1973**, *91*, 29–40, doi:10.1007/bf00409536.
39. Blenkinsopp, S.A.; Khoury, A.E.; Costerton, J.W. Electrical enhancement of biocide efficacy against Pseudomonas aeruginosa biofilms. *Appl. Environ. Microbiol.* **1992**, *58*, 3770–3773, doi:10.1128/aem.58.11.3770-3773.1992.

Materials Science & Engineering C 123 (2021) 112017

Contents lists available at ScienceDirect

Materials Science & Engineering C

journal homepage: www.elsevier.com/locate/msec

Electrically-responsive antimicrobial coatings based on a tetracycline-loaded poly(3,4-ethylenedioxythiophene) matrix

Dominika Czerwińska-Główka [a], Wioletta Przystaś [b,c], Ewa Zabłocka-Godlewska [b,c], Sebastian Student [c,d], Beata Cwalina [b,c], Mieczysław Łapkowski [a,e], Katarzyna Krukiewicz [a,*]

[a] Department of Physical Chemistry and Technology of Polymers, Silesian University of Technology, Gliwice, Poland
[b] Department of Environmental Biotechnology, Faculty of Energy and Environmental Engineering, Silesian University of Technology, Gliwice, Poland
[c] Biotechnology Centre, Silesian University of Technology, Krzywoustego 8, 44-100 Gliwice, Poland
[d] Department of Systems Biology and Engineering, Faculty of Automatic Control, Electronics and Computer Science, Silesian University of Technology, Gliwice, Poland
[e] Centre of Polymer and Carbon Materials, Polish Academy of Sciences, M. Curie-Sklodowskiej 34, Zabrze, Poland

ARTICLE INFO

Keywords:
Antimicrobial activity
Bacterial growth
Conjugated polymers
Escherichia coli
Poly(3,4-ethylenedioxythiophene)
Tetracycline

ABSTRACT

The growth of bacteria and the formation of complex bacterial structures on biomedical devices is a major challenge in modern medicine. The aim of this study was to develop a biocompatible, conducting and antibacterial polymer coating applicable in biomedical engineering. Since conjugated polymers have recently aroused strong interest as controlled delivery systems for biologically active compounds, we decided to employ a poly(3,4-ethylenedioxythiophene) (PEDOT) matrix to immobilize a powerful, first-line antibiotic: tetracycline (Tc). Drug immobilization was carried out simultaneously with the electrochemical polymerization process, allowing to obtain a polymer coating with good electrochemical behaviour (charge storage capacity of 19.15 ± 6.09 mC/cm^2) and high drug loading capacity (194.7 ± 56.2 μg/cm^2). Biological activity of PEDOT/Tc matrix was compared with PEDOT matrix and a bare Pt surface against a model Gram-negative bacteria strain of *Escherichia coli* with the use of LIVE/DEAD assay and SEM microscopy. Finally, PEDOT/Tc was shown to serve as a robust electroactive coating exhibiting antibacterial activity.

1. Introduction

Up to now, no surface is fully resistant to bacterial colonization. For this reason, many scientific investigations concern the formation of bacterial structures, such as colonies and biofilms, as well as the ways of preventing their growth [1]. This problem has become one of major challenges in modern medicine and biomedical engineering. Numerous reports demonstrated that bacterial biofilms often lead to severe infections due to their development on medical devices like prosthetic heart valves [2], central venous catheters [3], urinary catheters [4], etc. Some bacterial species prefer to grow in the form of biofilms, which are complex structures consisting of microbial cells enclosed in a matrix of extracellular polymeric substances (EPS) [5]. This type of microbial growth provides a considerable hardiness of cells to many unfavourable factors in the external environment, protects microorganisms from mechanical, chemical and other damages, as well as ensures a high degree of biofilm adhesion [6]. A very important feature of microorganisms growing in biofilms is their resistance to antibiotics, disinfectants and other germicides, particularly when compared with freely floating single cells. The antimicrobial agents cannot reach the full depth of the biofilm, as EPS significantly reduce their diffusion capacity [1]. In addition, the ability of cells to communicate through an exchange of chemical signals and plasmids coupled with the quorum-sensing mechanism [7], as well as through electrical signalling [8,9], makes microorganisms growing in biofilms an extremely developed form of a community with social intelligence [10].

Over the years, it has been observed that surface morphology influences its interactions with bacterial cells [11]. The surface topography determines the ease of microbial colonization, and it is possible to achieve a control in bacterial attachment and biofilm formation through surface modification. On the other hand, bacteria are sensitive to electrical impulses [12]. Thus, it seems that electroactive materials comprising specific chemical compounds could be the ones allowing to control a growth of bacterial biofilms. Conjugated polymers, particularly, are unique multifunctional compounds that combine electrical activity, in terms of high charge capacity, low impedance and effective

* Corresponding author.
E-mail address: katarzyna.krukiewicz@polsl.pl (K. Krukiewicz).

https://doi.org/10.1016/j.msec.2021.112017
Received 13 December 2020; Received in revised form 9 February 2021; Accepted 2 March 2021
Available online 9 March 2021

charge transfer [13–15], with biocompatibility. Due to their unusual nature, they have found a number of versatile applications as materials for solar cells [16,17] or light emitting diodes [18,19]. Demonstrated biocompatibility and the ability of serving as carriers for biologically active compounds, make conjugated polymers potentially applicable in biomedical engineering [20–23]. One of the most investigated conjugated polymers is poly(3,4-ethylenedioxytiophene) (PEDOT), exhibiting environmental and electrochemical stability making it attractive both as a material for implants [24,25], drug delivery systems [26–28], as well as tissue scaffolds [29,30]. Due to its in vitro and in vivo biocompatibility [31], PEDOT is believed as an ideal candidate for various bioengineering applications [31]. In addition, the possibility of using PEDOT as a carrier for many chemical compounds with specific activities, including anti-inflammatory [28,32,33], antibacterial [34,35] or anticancer functions [36–38], allows expanding the applicability of polymer matrices towards multifunctional electroactive systems.

Conducting polymers, particularly PEDOT, have been already used in bacteriology to detect and modulate bacterial colonization [39,40], diagnose bacterial infections [41], as well as to prevent biofilm formation [42]. Interestingly, the interactions between bacteria and PEDOT were found to be greatly influenced by the electrochemical redox state of conducting polymer [40]. When oxidized, PEDOT was found to promote bacteria adhesion and growth, and to facilitate the formation of biofilm, and this behaviour was expected to arise from the presence of available sites (electron holes) for bacterial electron transfer. In contrary, reduced PEDOT films were shown to express antibacterial effects, most probably due to the electron-saturation of the surface preventing bacterial electron transfer. Besides, experiments revealed that bacteria occupying the surface of PEDOT induced the electrochemical reduction of conducting polymer, allowing PEDOT to exhibit antibacterial effects without external electrical stimulation.

In this study, the application of an electrically-responsive PEDOT-based matrix as a surface able to control the bacterial growth was presented. As the surface of interest, sputter-coated platinum films were chosen, mainly because of their wide applicability in biomedical engineering [43], particularly cardiac and neural tissue engineering, and their vulnerability towards bacterial colonization [44]. PEDOT coating was formed on a platinum-coated substrate in the course of an electrochemical polymerization process, and was used as a carrier of tetracycline (Tc). The choice of Tc was dictated by the fact that it is a powerful antibiotic with a broad antibacterial spectrum, exhibiting a bactericidal effect through disrupting protein biosynthesis [45]. The mechanism of action of Tc ensures effectiveness against almost all medically relevant aerobic and anaerobic bacteria, both Gram-positive and Gram-negative, as well as atypical organisms such as protozoan parasites [46,47]. The physicochemical properties of PEDOT and PEDOT/Tc matrices were analyzed with the use of following methods: electrochemical (cyclic voltammetry), spectroscopic (UV–Vis, infrared spectroscopy) and microscopic (scanning electron microscopy). To assess biological activity of PEDOT and PEDOT/Tc matrices, a selected strain of Gram-negative bacteria, *Escherichia coli*, was cultured on their surfaces. Examination of bacterial attachment and growth was carried out by means of a scanning electron microscopy (bacterial dimensions), as well as confocal fluorescent microscopy (LIVE/DEAD assay).

2. Materials and methods

2.1. Electrochemical polymerization and drug immobilization

Electrochemical polymerization of 3,4-ethylenedioxythiophene, EDOT (Sigma-Aldrich, 97%) and immobilization of tetracycline hydrochloride, Tc (Sigma-Aldrich, 98.0%–102.0%) were carried out in a standard three-electrode arrangement, in which a Pt sputter-coated (automatic, rotary-pump coating system, Q150R Quorum Technologies, 30 mA, 120 s, giving a 4.8 nm thick layer of Pt) glass slide (microscopic slide, Labglass) was employed as a working electrode (0.283 cm^2), Ag/AgCl (3 M KCl) as a reference electrode and a platinum foil (1 cm^2) as a counter electrode. The electrochemical deposition of PEDOT on a Pt-coated glass slide was performed by means of cyclic voltammetry (CV) (CH instruments 400c) in aqueous solution of 10 mM EDOT based on phosphate-buffered saline (PBS, composed of 0.14 M NaCl, 0.0027 M KCl, 0.01 M $Na_2HPO_4{\cdot}2H_2O$, 0.002 M KH_2PO_4, pH = 7.4) being an isotonic, physiologically relevant solution, in the potential range from −0.9 V to 1.27 V (vs. Ag/AgCl), at a scan rate of 0.1 V/s for 25 CV cycles. Tetracycline-loaded polymer matrices (PEDOT/Tc) were obtained during electrochemical polymerization of 10 mM EDOT in PBS solution supplemented with Tc (from 0.5 mM to 50 mM). Similarly as in the case of pristine PEDOT, the electrochemical polymerization was achieved in the potential range from −0.9 V to 1.27 V (vs. Ag/AgCl), at a scan rate of 0.1 V/s for 25 CV cycles.

2.2. Material characterization

Surface morphology of PEDOT and PEDOT/Tc films was examined by means of a scanning electron microscope, SEM (Phenom ProX) operating at 10 kV. The 3D Roughness Reconstruction software (Phenom ProSuits) enabled the assessment of surface roughness and film thickness. Wettability of polymers was determined through contact angle measurements by means of DataPhysic OCA15 goniometer at room temperature (T ≈ 20 °C) using deionized water. In all measurements, three sample sites were analyzed on three different sample surfaces, giving $n = 9$. Chemical structure of PEDOT and PEDOT/Tc matrices was characterized by FTIR spectroscopy by using IR Perkin Elmer Spectrum Two spectrometer. IR spectra were recorded in the range between 500 cm^{-1} and 1800 cm^{-1} for 16 scans using a Diamond UATR accessory. Charge storage capacity (CSC) was calculated from CV curves, as the electric charge integrated under a corresponding CV curve.

2.3. Drug release

To assess the maximum amount of Tc that could be released from PEDOT/Tc, a chronoamperometric potential jump from −0.6 V (applied for 2 s) to −0.5 V (applied for 600 s) vs. Ag/AgCl was used to PEDOT/Tc electrodes immersed in PBS. The amount of released Tc was controlled by an UV–Vis Hewlett Packard 8453 UV/Vis Spectrophotometer. Concentrations of the drug were evaluated using a calibration curve: $y = 3.0461{\cdot}x + 0.0326$ ($R^2 = 0.9969$), where y is the absorbance value at 363 nm, and x is the concentration of Tc expressed in mM.

To assess the reference amount of Tc released with and without an electrical trigger in the absence of bacteria, PEDOT/Tc electrodes were placed into quartz cuvettes and immersed in PBS. UV–Vis spectra were recorded at specific time points, and Tc concentration was evaluated using a calibration curve, in which the absorbance value determined for peak at 363 nm was normalized to the baseline absorbance (determined at 420 nm).

2.4. Preparation of bacterial suspension and culture

A model Gram-negative bacteria strain *Escherichia coli* (DSM 30083, U5/41) was used to assess the antimicrobial properties of PEDOT and PEDOT/Tc matrices with respect to a bare Pt-coated glass slide. Bacteria were cultured at agar broth (BTL) slants at 35 °C for 48 h. After this time, a suspension of bacterial biomass in physiological saline (0.85% NaCl aqueous solution) (Acros) was prepared. The turbidity of suspension was established between 3 and 4 according to the McFarland scale (≈$10.5{\cdot}10^8$ CFU/ml).

PEDOT, PEDOT/Tc and Pt-coated glass slides were sterilized by leaving them under UVC radiation (253.7 nm) for an hour. Next, sterilized surfaces were placed in sterile 12 well plates. The portions of 0.1 ml of bacterial suspension mixed with 2 ml of growth medium (10 g/l Tryptone (BTL), 5 g/l yeast extract (BTL) and 10 g/l NaCl (Acros), pH =

7) were added into each well. Cultivation of bacteria on the surfaces was carried out in incubator for 48 h at 35 °C, and the samples were analyzed after 3 h, 24 h and 48 h.

In order to obtain reliable results, the experiments were done in triplicate for all materials, for each timepoint, under the same conditions. The results were presented as mean values ± standard deviation. A *t*-test was performed to determine statistical significance ($p < 0.05$).

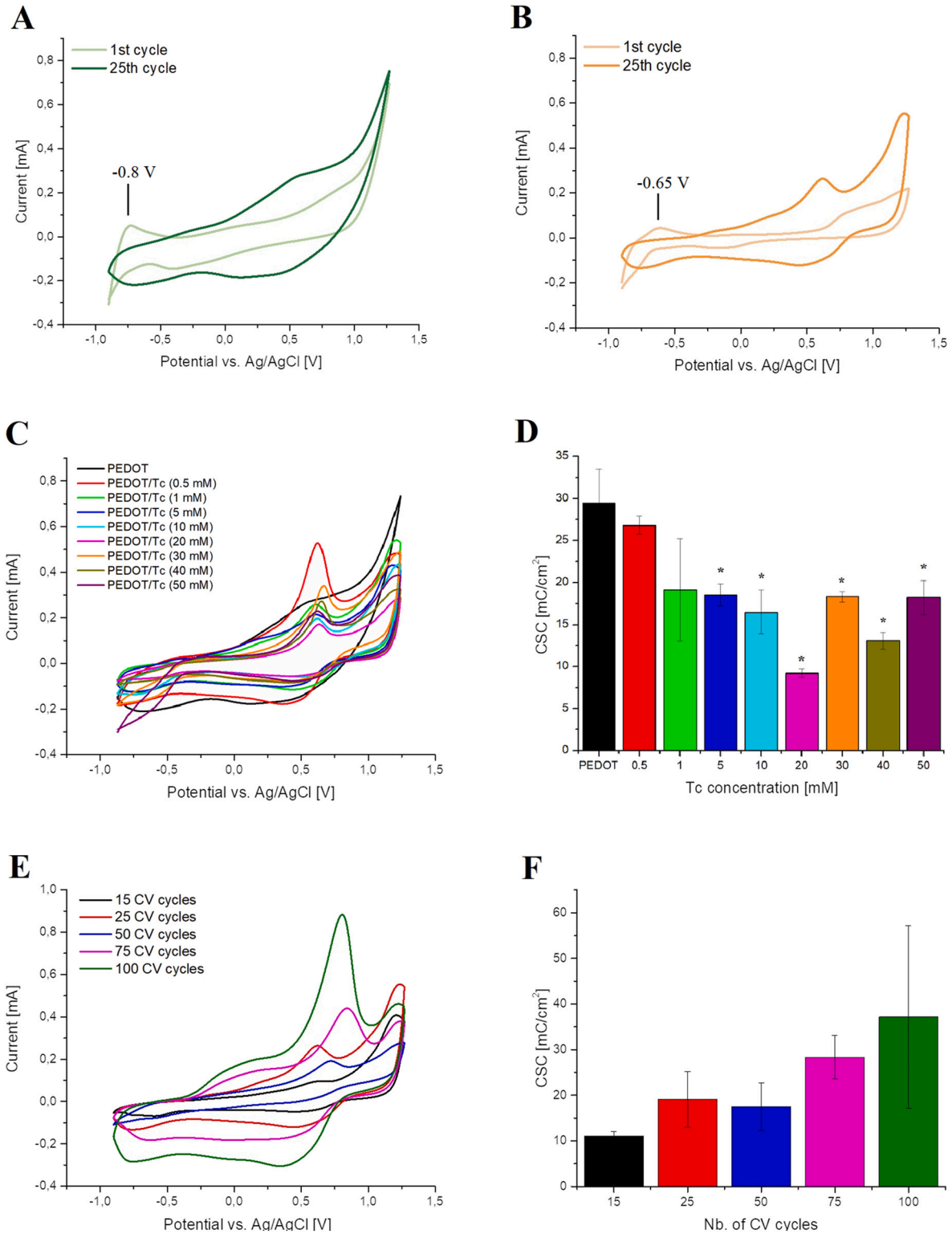

Fig. 1. Electrochemical polymerization and drug loading capacity of different PEDOT/Tc formulations. A) CV curves showing the electropolymerization process of 10 mM EDOT in PBS, and B) 10 mM EDOT in PBS in the presence of 1 mM Tc; scan rate = 0.1 V/s. C) CV curves of the 25th cycle of electropolymerization process of 10 mM EDOT in PBS, in the presence of 0.5 mM, 1 mM, 5 mM 10 mM, 20 mM, 30 mM, 40 mM and 50 mM Tc, and D) CSC of corresponding PEDOT/Tc matrices; * = $p < 0.05$ (vs. PEDOT), $n = 3$. E) CV curves of the 15, 25, 50, 75 and 100 CV cycles of electropolymerization process of 10 mM EDOT solution in PBS, in the presence of 1 mM Tc, and F) CSC of corresponding PEDOT/Tc matrices.

2.5. Staining and imaging bacterial cells attached to test surfaces

LIVE/DEAD® BacLight Bacterial Viability Kit (Life Technologies) together with confocal fluorescent microscopy (Olympus FluoView FV1000) were used to assess the viability of bacteria growing on PEDOT, PEDOT/Tc and Pt-coated glass slides. Staining alive bacteria in green with SYTO9 and dead bacteria in red with D-propidium iodide allowed to analyse the percentage of alive and dead bacterial cells on selected surfaces. Image analysis was accomplished using ImageJ (NIH) software.

Morphology of *E.coli* cells cultured on the surfaces of PEDOT, PEDOT/Tc and Pt-coated glass was observed by scanning electron microscopy (Phenom ProX). Before the samples could be visualized, materials were fixed using 3% glutaraldehyde (Fisher BioReagents) for 24 h. Consequently, samples were washed three times with sterile distilled water and dehydrated by immersing successively in the solutions of ethanol (99.8%, Acros Organics) with increasing concentrations (30%, 50%, 70%, 80%, 90%, 95%, 99.8%), each time for 10 min. After drying (24 h, 50 °C), samples were sputter-coated with a gold layer for better image quality (20 min, 20 mA; Q150R Quorum Technologies). SEM images were taken with an accelerating voltage of 15 kV at the magnifications of 5000×. The average length and width of bacterial cells, as well as their density (number of bacteria per 200 μm^2) were calculated using the ImageJ (NIH) software.

3. Results and discussion

3.1. Electrochemical polymerization and drug immobilization

The results of electrochemical investigations, involving electropolymerization of EDOT, Tc immobilization and characterization of different PEDOT/Tc formulations, were shown in Fig. 1. The course of an electrochemical polymerization process of EDOT could be tracked through the cyclic voltammetric (CV) curves, as shown in Fig. 1A&B. The irreversible oxidation peak at 1.27 V vs. Ag/AgCl for EDOT and EDOT/Tc, observed in the first CV cycle, corresponded to the electrochemical oxidation of monomer. For both data sets, gradually increasing currents confirmed the formation of a conducting film typical for electropolymerization process. Besides, a redox signal characteristic for Tc (−0.65 V vs. Ag/AgCl, Fig.S1) was present in the 1st polymerization cycle of EDOT/Tc, hindering the redox signal associated with electrochemical reactions of hydrogen [48] (−0.8 V vs. Ag/AgCl) as seen in the 1st polymerization cycle of EDOT. The differences between pristine PEDOT (Fig. 1A) and PEDOT/Tc (Fig. 1B) films were evident when comparing both 25th polymerization cycles, representing fully developed polymeric forms. Firstly, it could be clearly observed that the currents flowing through the polymer films were higher in the case of PEDOT as compared with PEDOT/Tc, indicating a more developed surface area of the electrode coated with a pristine polymer. On the other hand, a sharp oxidation peak at approx. 0.6 V (vs. Ag/AgCl) was observed in the CV curve of PEDOT/Tc. The presence of broad waves in CV curves is usually associated with many redox processes occurring during reduction/oxidation of a conjugated polymer [49], and narrowing of anodic band in the case of PEDOT/Tc may suggest formation of a structure more sensitive to redox processes. Besides, small dopants stimulate more effective polymerization process than larger ones [50]. Thus, bulky Tc molecules could hinder the process of electrochemical polymerization of EDOT, which could result in less developed polymer structures. Due to the bulky nature of Tc, it is expected that the process of drug immobilization relies on physical entrapment rather than ionic interactions.

To describe the maximum amount of charge that can be stored within a polymer matrix, a charge storage capacity (CSC) was calculated from CV curves for both PEDOT and PEDOT/Tc (Fig. 1D). CSC was chosen as a measure of the electrochemical quality of polymer mainly because it is a common practice to characterize electroactive, tissue interface materials by determining their CSC [51]. The results showed that the incorporation of Tc had a deteriorating effect on the capacitance of polymer film, since average value of CSC calculated for PEDOT/Tc (19.15 ± 6.09 mC/cm^2) was found to be lower than CSC value calculated for pristine PEDOT (29.49 ± 4.05 mC/cm^2). Nevertheless, both coatings outperformed bare noble metals electrodes, since the average CSC values determined for Pt and Au were 1.5 mC/cm^2 and 7.4 mC/cm^2, respectively [50,52]. Even though the careful choice of doping ions could elevate CSC of PEDOT to the values of 44.9 mC/cm^2 (doping with $LiClO_4$ [28]) or 58.83 mC/cm^2 (doping with p-toluene sulfonate [53]), biofunctionalized PEDOT is typically characterized by moderate values of CSC, such as 3.2 mC/cm^2 (functionalization with tauroursodeoxycholic acid [27]), 2.6 mC/cm^2 (functionalization with dexamethasone phosphate[27]) and approx. 3.5 mC/cm^2 (functionalization with laminin-derived peptides [54]).

To assess the effect of drug concentration on the efficiency of electrochemical polymerization, eight polymer matrices were fabricated from electropolymerization solutions containing various concentrations of Tc (0.5–50 mM), and were electrochemically characterized through cyclic voltammetry (Fig. 1C). When comparing capacitances of coatings (Fig. 1D), a significant decrease in CSC values was noticed for Tc (especially at concentrations above 10 mM) when compared with pristine PEDOT, further confirming the deteriorating effect of Tc on the electrochemical polymerization of EDOT. Taking into account the variability of CV curves, the values of CSC calculated for PEDOT formed in the presence of 0.5 mM and 1 mM Tc seemed to be not statistically different from CSC values determined for a pristine polymer.

To examine the effect of electropolymerization time on film capacitance, electrochemical polymerization of 10 mM EDOT in the presence of 1 mM Tc was performed with an increasing number of polymerization cycles (from 15 to 100 CV cycles) (Fig. 1E). Even though longer polymerization times typically result in the deposition of thicker polymer layers, a maximum thickness of 68 ± 4 μm was observed for PEDOT/Tc grown during 50 CV cycles (Fig.S2). CSC, however, was found to be the highest for PEDOT/Tc formed in the course of 100 CV cycles (37.14 ± 20.01 mC/cm^2). It should be kept in mind that the measurement of thickness was conducted for dry matrices. Since thick matrices are fragile, unstable and prone to the process of swelling [50], it is expected that their structure could be affected by the process of drying, and the acquired results might not well represent their thickness in a wet state. To avoid this problem, polymer films of moderate thickness, obtained during 25 CV cycles, were chosen for further experiments.

3.2. Material characterization

Chemical structures of PEDOT and PEDOT/Tc were confirmed using FTIR spectroscopy (Fig. 2A). Both PEDOT and PEDOT/Tc spectra showed typical bands for PEDOT [55–58]. The bands at approximately 1474 cm^{-1}, 1422 cm^{-1}, 1362 cm^{-1} were assigned to asymmetric stretching mode of C═C and inter-ring stretching mode of C—C. The signals at around 1208 cm^{-1} and 1070 cm^{-1} were related to C—O—C, while the signals at 986 cm^{-1}, 848 cm^{-1} and 697 cm^{-1} were characteristic for stretching vibrations of C—S—C bond. Similarly, several bands characteristic for Tc (Fig. 2B) [59–61] were observed in the FTIR spectra of PEDOT/Tc, including signals at 1616 cm^{-1} and 1580 cm^{-1} typical for C═O stretching of aromatic ring, bands at approximately 1448 cm^{-1} and 1176 cm^{-1} typical for C—N stretching mode. Bands at 1310 cm^{-1} assigned to deformation band for OH, a signal at 1034 cm^{-1} characteristic for stretching C—O and a signal at 742 cm^{-1} typical for C—H band in aromatic ring. The presence of bands characteristic for Tc in the spectrum of PEDOT/Tc proved that the process of electrochemical polymerization led to the immobilization of Tc on the surface and/or in the bulk of a polymer matrix.

SEM analysis was used to compare surface morphology of PEDOT and PEDOT/Tc, as shown in Fig. 3. PEDOT was characterized by more regular grains compared to PEDOT/Tc, which surface revealed a

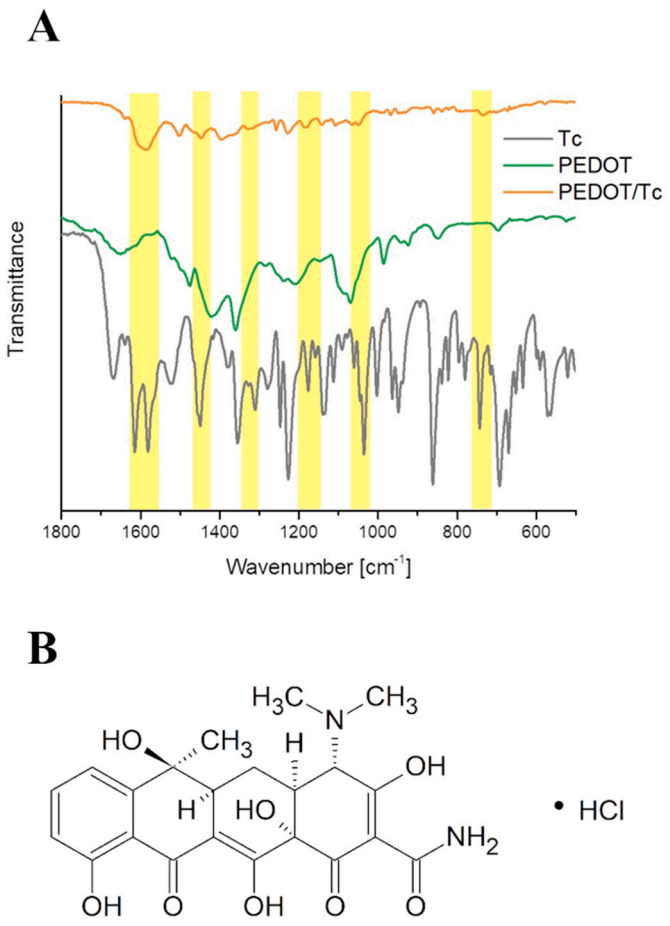

Fig. 2. Chemical characterization of polymer matrices. A) FTIR spectra of Tc, PEDOT and PEDOT/Tc (yellow bands indicate signals characteristic for Tc), and B) a chemical structure of tetracycline hydrochloride. (For interpretation of the references to colour in this figure legend, the reader is referred to the web version of this article.)

presence of distinct, irregular drug-loaded surface structures. These structures were similar to structures found during examination of another drug-loaded system, namely poly(3,4-ethylenedioxypyrrole) doped with ibuprofen [62], and are supposed to arise from a growth of polymer film around drug agglomerates occurring at the surface of the electrode. Even though a visual observation of both types of surfaces suggested different surface morphology, these surfaces exhibited a similar value of a roughness parameter expressed by the arithmetical mean height (S_a). For PEDOT, the value of S_a was estimated to equal 0.62 ± 0.03 μm, and for PEDOT/Tc to equal 0.63 ± 0.06 μm. Both values of S_a were significantly different when compared with a bare substrate, namely Pt-coated glass ($S_a = 0.21 \pm 0.01$ μm). Literature data indicate that surface topography has a significant impact on the mutual interaction between bacterial cells and surface [11,63]. As higher roughness promotes adhesion of bacteria, the analysis of PEDOT and PEDOT/Tc surface morphology suggested that the attachment of bacteria on both surfaces may be preferential when related to a surface of bare Pt-coated glass.

The differences in wettability between PEDOT, PEDOT/Tc and Pt-coated slides were investigated by determining the contact angle (θ) at room temperature ($T \approx 20$ °C) using deionized water. The results showed that the surface of PEDOT/Tc was slightly more hydrophilic ($\theta = 26.2° \pm 3.5°$) than a surface of PEDOT ($\theta = 31.5° \pm 2.6°$), and they were both more hydrophilic than a surface of glass sputter-coated with Pt ($\theta = 35.2° \pm 10.5°$). Literature data [64–66] showed that hydrophilic bacteria such as *Escherichia coli* can adhere easily to hydrophilic surfaces. Therefore, wettability studies suggested that bacteria should attach effectively to all investigated surfaces, namely Pt, PEDOT and PEDOT/Tc.

3.3. Drug release studies

To assess the maximum amount of Tc that could be released from PEDOT/Tc, an electrochemical reduction of a polymer matrix was performed in PBS as a physiologically relevant solution. It is known that when oxidized/reduced, conjugated polymers are able to capture/release doping ions, resulting in a change in a polymer volume [62]. Consequently, the shrinkage of conducting polymer matrix as the effect of applying sufficiently low potential is responsible for the release of Tc from PEDOT/Tc into the solution. Due to the presence of chromophores, the release of Tc could be easily monitored by UV–Vis spectrophotometry. As it was shown in Fig.S3, the absorption spectrum of Tc exhibited a multiplet with maximum absorption peaks at 276 nm and 363 nm, corresponding mainly to $\pi \rightarrow \pi^*$ transition [67]. The absorption peak at 363 nm remained stable in a wide range of Tc concentrations, thus a peak at this wavelength was used for the calculations of the amount of released Tc.

Literature reports [62] have shown that drug loading capacity of a conjugated polymer matrix is not in a linear relationship with the concentration of drug in a polymerization solution. Therefore, also in our study the fabrication of a polymer matrix was carried out using a series of drug concentrations (Tc, 0.5–50 mM). Even though the concentration of Tc released from PEDOT/Tc was dependent on the initial Tc concentration during the polymerization process (Fig.S4A), a maximum concentration of released Tc was noted for a polymer matrix formed in the presence of 1 mM and 5 mM Tc (38.2 ± 11.03 μM and 45.5 ± 12.2 μM, respectively) (Fig. 4A). Interestingly, higher Tc concentrations in the polymerization solution did not lead to the increase in drug loading capacity, which could be the consequence of the deteriorating effect of

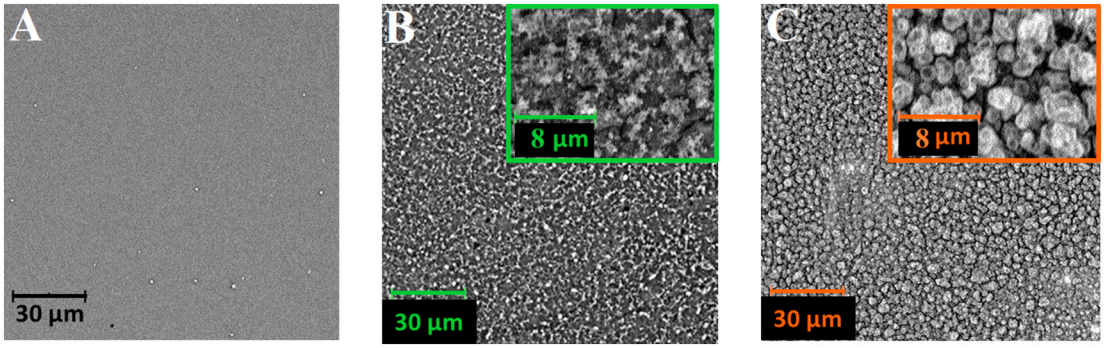

Fig. 3. Surface characterization of polymer matrices. SEM micrographs of A) Pt-coated glass, B) PEDOT, and C) PEDOT/Tc; scale bars are 30 μm for main images and 8 μm for insets.

Tc on the electrochemical polymerization of EDOT. As shown earlier, electrochemical properties of a PEDOT/Tc matrix formed in the presence of 1 mM Tc resembled pristine PEDOT matrix. Besides, the application of a reduction potential allowed PEDOT/Tc (1 mM) matrix to be efficiently contracted, leading to the release of substantial amounts of Tc in a controlled manner (Fig.S5A).Since the UV–Vis spectrum of released Tc was identical to the spectrum of untreated Tc (Fig.S6), the chemical structure of Tc was not expected to be changed during electrochemical immobilization and release processes.

Apart from the maximum Tc loading efficiency, the release profile of Tc without electrical stimulation was also determined (Fig.S5B). A rapid release was observed within first 15 min of the experiment, then reached the plateau that was observed for the next 6 h. A maximum Tc concentration released in this way reached 61.4 ± 10.5 μg/cm^2 (5.7 mg/l), which value was much above the minimum therapeutic dose of Tc (minimum inhibitory concentration of 16 μg/l) [68]. Therefore, it is expected that the initial burst release of Tc will be sufficient to avoid possible risk or potential of resistance and tolerance of bacteria to Tc, which could occur in a constantly low Tc-releasing environment. The maximum concentration of Tc achieved by spontaneous release was 31.5% of the maximum amount of immobilized Tc, therefore, it should be expected that the presence of bacteria that are able to reduce the polymer will be sufficient to release further portions of immobilized drug [40].

The analysis of Tc release from PEDOT/Tc formed with increasing number of polymerization cycles (from 15 to 100 CV cycles) (Fig. 4B) revealed the maximum efficiency of drug release for the matrix formed during 25 CV cycles (Fig.S4B). Similarly as for other drug-loaded conjugated polymer matrices [62,69], PEDOT/Tc matrices formed during few CV cycles possessed limited drug capacity, and PEDOT/Tc matrices formed during ≥50 CV cycles were harder to be fully reduced. An increase in the amount of released Tc observed with the increase in the number of CV cycles should be related to the instability of a matrix and its possible electrochemical degradation. Consequently, by extending the time of electropolymerization, it was not possible to maximize neither drug loading capacity nor the amount of released drug.

3.4. Antimicrobial activity

Escherichia coli is commonly found to contaminate medical devices and to cause nosocomial infections [70–72], therefore, it can serve as a model organism for different studies in biological engineering and industrial microbiology [73]. Also in our study, the antibacterial properties of PEDOT and PEDOT/Tc in relation to Pt-coated glass slides were investigated against this bacteria strain. To characterize the growth of *E.coli* strain cultured on different surfaces, the density of bacterial cells (number of bacterial cells per 200 μm^2) as well as their dimensions (length, width and aspect ratio) were analyzed using SEM after 3 h, 24 h and 48 h of bacterial culture (Fig. 5). These three time points were selected based on the progression of growth curves of bacterial cultures in a closed system batch cultivation (without food supplementation and removing metabolites). In the initial phase (lag phase, 3 h), the bacteria in nutrient-rich medium adapt to the new conditions, attach reversibly to the surface and grow in mass. Subsequently, in the logarithmic growth phase (24 h), bacteria attached to the surface significantly increase their dimensions (length and width), achieving the ability to divide. The bacterial cell divides to form two identical daughter cells. At this stage, biological processes begin to dominate over the physical and chemical processes of attachment to the surface. In the stationary phase (48 h), population growth begins to decline as nutrients are consumed and wastes (metabolites) are accumulated. Cells become less metabolically active and lose their ability to divide. Finally in the death phase the inaccessibility of nutrients and the excess of metabolites, in this also toxic substances, cause a rapid decline in the number of living bacterial cells in the population [74,75].

Calculated average values of bacterial cells density were shown in Fig. 6. After 3 h of culture, cells density (Fig. 6A) was much lower on the PEDOT (21.5 ± 1.4 cells/200 μm^2), and in particular on PEDOT/Tc (13.2 ± 2.8 cells/200 μm^2), when related to Pt-coated glass (27.9 ± 3.8 cells/200 μm^2). The decrease in the density of bacterial cells (Fig. 6B) was equal to 22.9% for PEDOT, and was as high as 52.7% for PEDOT/Tc. In the next phase of bacterial growth (24 h), the average density of bacterial cells did not change significantly, and was equal to 25.1 ± 5.2 cells/200 μm^2 for Pt-coated glass, 22.7 ± 4.8 cells/200 μm^2 for PEDOT and 15.0 ± 2.0 cells/200 μm^2 for PEDOT/Tc. Therefore, it might be seen that the antibacterial effect of PEDOT (9.6% decrease in bacterial cells density when compared with a control) and particularly PEDOT/Tc (40.2% decrease in bacterial cells density when compared with a control) was maintained. In the last phase of bacterial growth (48 h), the bacterial density on Pt-coated glass slides began to increase (28.0 ± 4.0 cells/200 μm^2), while a significant decrease was observed on the surfaces of both polymers, namely PEDOT (12.7 ± 1.8 cells/200 μm^2, 40.2% decrease in bacterial cells density when compared with a control) and PEDOT/Tc (10.1 ± 1.5 cells/200 μm^2, 54.6% decrease in bacterial cells density when compared with a control).

The adhesion of bacterial cells to the surface of a substrate, which is

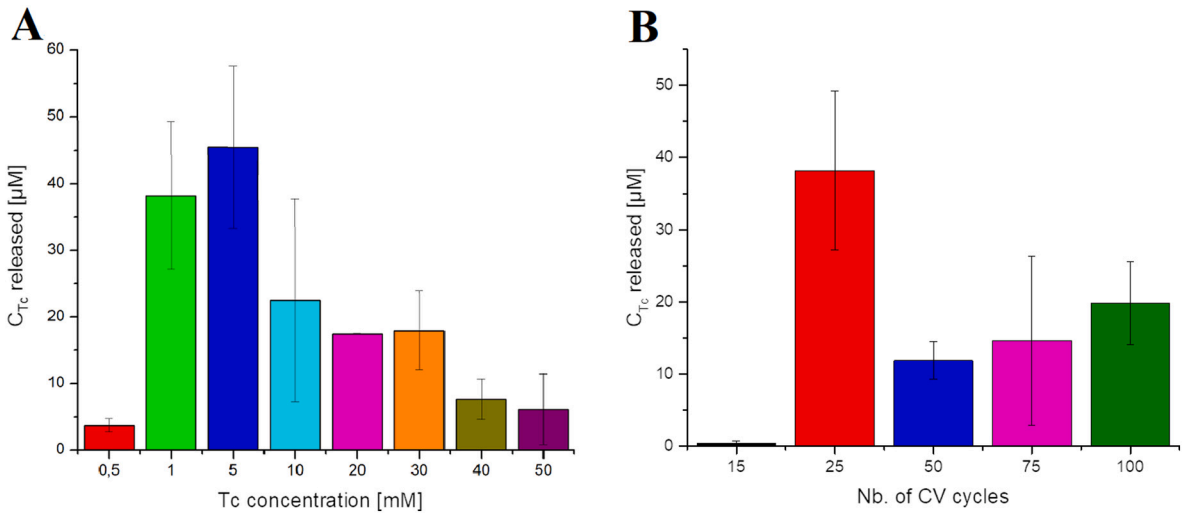

Fig. 4. The results of drug release studies. Concentrations of Tc released from PEDOT/Tc matrix A) formed in the presence of 0.5–50 mM Tc, and B) formed during 15–100 CV cycles.

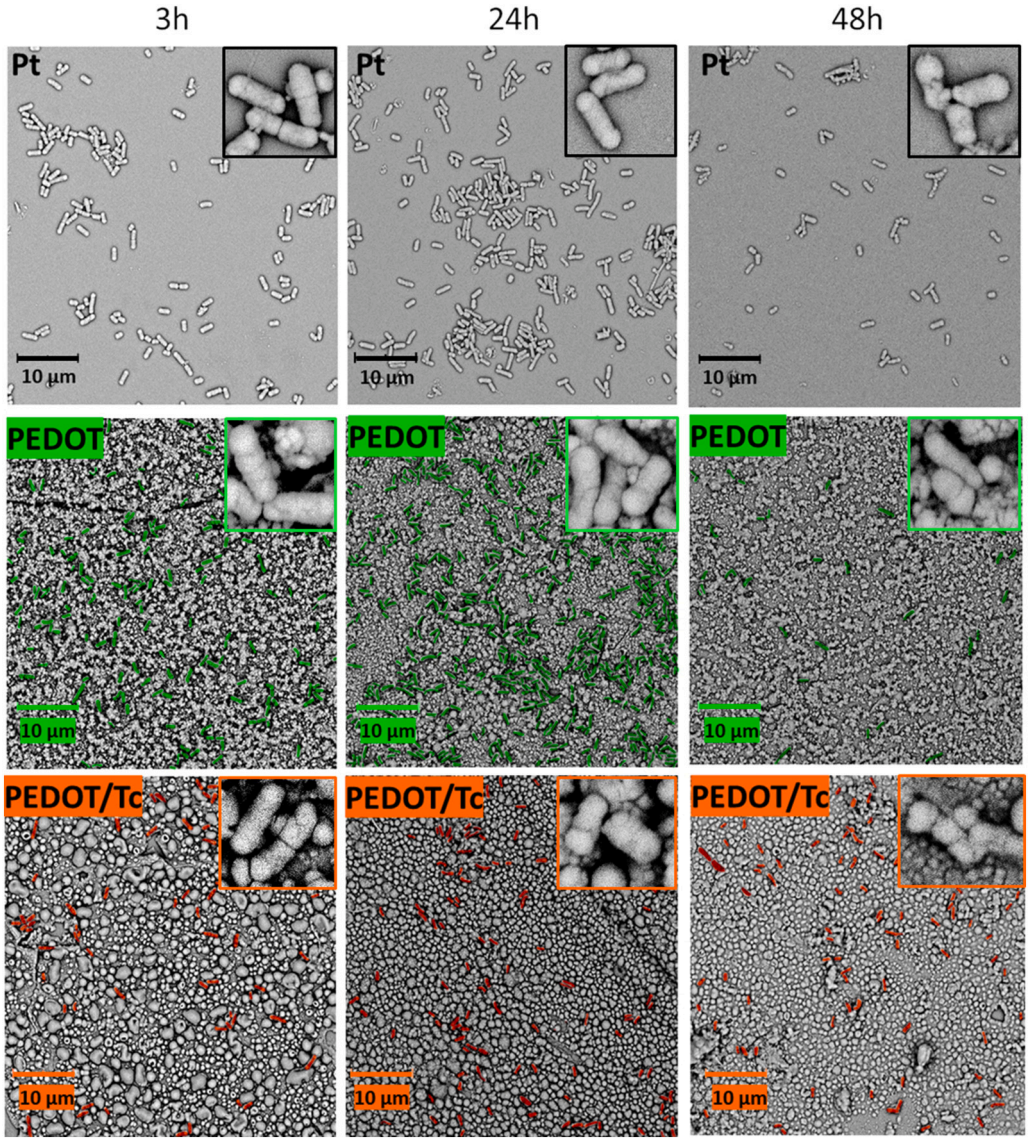

Fig. 5. Morphology of bacterial cells. SEM micrographs presenting *E.coli* cultured on Pt-coated glass, PEDOT and PEDOT/Tc after 3 h, 24 h and 48 h of culturing; scale bars are 10 µm each; false colours indicate bacterial cells present on the surface of PEDOT (green) and PEDOT/Tc (orange). (For interpretation of the references to colour in this figure legend, the reader is referred to the web version of this article.)

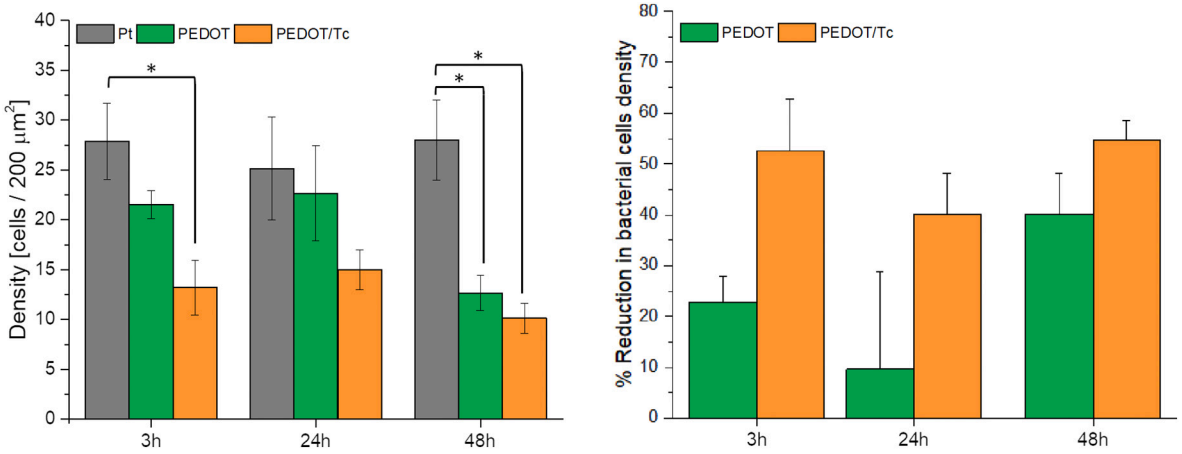

Fig. 6. Bacterial surface colonization analysis. A) Bacterial cells density (number of bacterial cells per 200 µm^2) calculated from SEM images after 3 h, 24 h and 48 h of culturing *E.coli* on the surface of Pt-coated glass, PEDOT and PEDOT/Tc; * = $p < 0.05$, $n = 3$, and B) corresponding percentage decrease in *E.coli* cells density on PEDOT and PEDOT/Tc in relation to Pt-coated glass.

the first stage of bacterial biofilm formation, depends mainly on the surface properties. Our previous observations showed that both PEDOT and PEDOT/Tc possessed favourable roughness and were hydrophilic in nature, so the adhesion of bacteria on these polymer matrices should be facilitated when related to a Pt-coated glass slide. The results of biological investigations showed, however, that both PEDOT and PEDOT/Tc exhibited antibacterial effects. It is expected that the antibacterial activity of pristine PEDOT arose from the electron-saturation of conducting polymer surface, due to its spontaneous reduction in time and/or electrochemical reduction induced by the presence of bacteria, as reported elsewhere [40]. Still, the reduction in bacterial cells density was the highest for PEDOT/Tc, and this effect was maintained for the whole time of the experiment indicating the effectiveness of drug entrapped in the polymer matrix against *E.coli*. Interestingly, the reduction of bacterial cells density was not constant in time for a pristine PEDOT matrix. Particularly, the significant decrease in bacterial cells density when compared with a control was noted at the last time point (48 h), possibly indicating facilitated detachment of dead bacterial cells from a surface of PEDOT.

3.5. Bacterial cell dimensions

The shape of bacterial cells is significantly influenced by the availability and composition of the culture medium and appropriate culture conditions. If they are provided, new proteins and other structural elements of bacterial cells may be produced. Consequently, bacteria grow until they reach a certain size, and then they are able to divide into two daughter cells. Their size at the stage of division is not constant, but is typically distributed over a narrow range [76]. The length of a cell has a significant impact on its functioning. Too short cells do not have adequate reproductive resources, while too long ones have problems with a transport of nutrients. Bacterial cells growing under constant and certain culture conditions add the same volume regardless of the initial size obtained after cell division, keeping their aspect ratio (a ratio of width to length) at the same level [77]. In this regard, bacterial cells modulate size to maximize viability and reproductive efficiency [78].

The average bacterial cell length and width (Fig. 7) were calculated based on SEM micrographs. In the initial phase (3 h), bacteria were still relatively short on Pt-coated glass (1.77 ± 0.04 μm), PEDOT (1.64 ± 0.03 μm) as well as on PEDOT/Tc matrices (1.73 ± 0.03 μm) (Fig. 7A). Their average width was represented as 0.70 ± 0.01 μm for Pt surfaces, 0.62 ± 0.01 μm for PEDOT and 0.64 ± 0.01 μm for PEDOT/Tc (Fig. 7B). To more accurately compare the shape of bacterial cells, an aspect ratio was calculated (Fig. 7C), allowing to assess whether the cells were more elongated or oval. After 3 h, bacterial cells cultured on Pt expressed slightly more circular shapes (0.42 ± 0.01) than for both PEDOT (0.39 ± 0.01) and PEDOT/Tc (0.37 ± 0.01), the latest being slightly more elongated than others.

After 24 h, the bacterial cell length increased on all investigated surfaces, namely bare Pt (2.02 ± 0.03 μm), PEDOT (1.80 ± 0.03 μm) and PEDOT/Tc (1.91 ± 0.03 μm). The bacteria became longer, but slightly reduced their width. The average width was equal to 0.66 ± 0.01 μm for bare Pt, 0.60 ± 0.01 μm for PEDOT and 0.60 ± 0.01 μm for PEDOT/Tc. After 24 h, a change in shape was observed: bacteria became more rod-shaped and elongated on each surfaces, and the aspect ratios were equal to 0.34 ± 0.01 for bare Pt, 0.35 ± 0.01 for PEDOT and 0.33 ± 0.01 for PEDOT/Tc.

After 48 h, a slight increase in length was observed, but only for bacteria cultured on Pt-coated glass (2.17 ± 0.06 μm). For PEDOT (1.84 ± 0.04 μm) and PEDOT/Tc (1.97 ± 0.03 μm), the values practically did not change. However, narrowing of bacterial cells was observed, especially in the case of PEDOT (0.51 ± 0.01 μm) and PEDOT/Tc (0.52 ± 0.01 μm) when compared to bare Pt (0.63 ± 0.01 μm). At the same time, the aspect ratio of bacteria was equal to 0.31 ± 0.01 for bare Pt, 0.30 ± 0.01 for PEDOT and 0.28 ± 0.01 for PEDOT/Tc.

At all time points, the longest and the widest bacterial cells were observed on Pt-coated glass. Both polymeric surfaces were found to inhibit the growth of bacterial cells, and the strongest impact of surface was observed after 48 h of culture. Interestingly, the shape of bacterial cells, in terms of their aspect ratio, was similar on all investigated surfaces, even though it changed in time. The observed homeostasis of aspect ratio at the single cell level was a good example of how bacteria were able to control their dimensions through maintaining a constant ratio between the accumulation of division proteins and the rate of cell elongation [79]. A slow growth of bacteria observed on the surfaces of PEDOT and PEDOT/Tc might indicate that they became dormant, similarly as when bacteria were starved for nutrients [80]. Since the amount and content of culture medium were the same for all investigated samples, it may be supposed that PEDOT and PEDOT/Tc could have inhibitory impact on bacterial cells growth and/or could limit the accessibility of nutrients, e.g. by the interactions between biologically active compounds and polymeric surface.

3.6. LIVE/DEAD assay

The viability of *E.coli* on the surface of Pt-coated glass, PEDOT and PEDOT/Tc was assessed with the use of the LIVE/DEAD assay allowing to count the number of live (green coloured) and dead (red coloured) bacterial cells by fluorescent microscopy (Fig. 8). After 3 h of culture, the highest percentage of live bacterial cells was observed on the surface of Pt-coated glass slides (74.8 ± 2.2%). On the surface of polymer matrices, both PEDOT (44.7 ± 2.3%) and PEDOT/Tc (42.7 ± 0.7%), the number of viable cells was less than a half of a total bacterial population (live and dead cells). When bacteria were in the logarithmic growth phase (24 h),

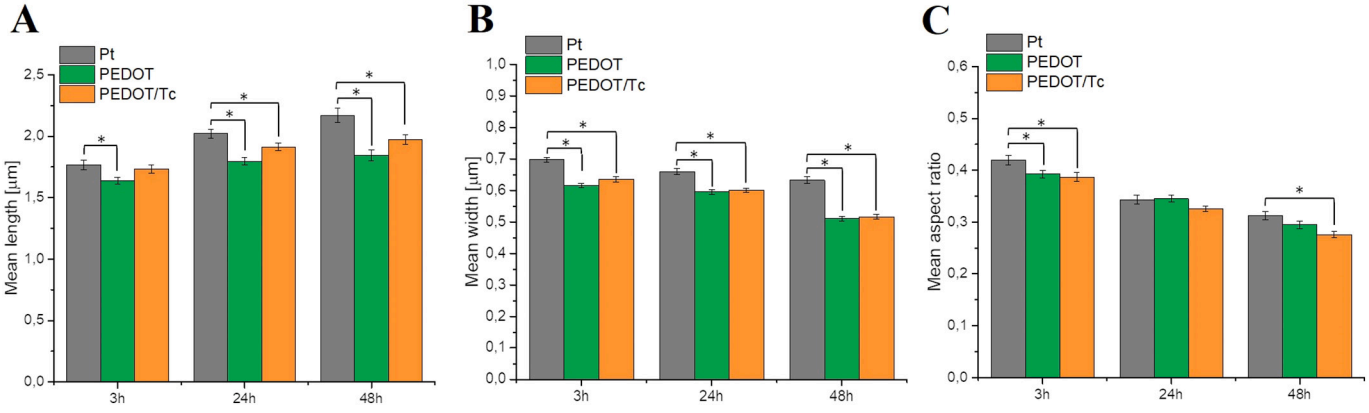

Fig. 7. Bacterial cell dimension analysis. The average values of A) length, B) width, and C) aspect ratio of bacterial cells on the Pt, PEDOT and PEDOT/Tc at three time points: 3 h, 24 h and 48 h; * = $p < 0.05$, $n = 3$.

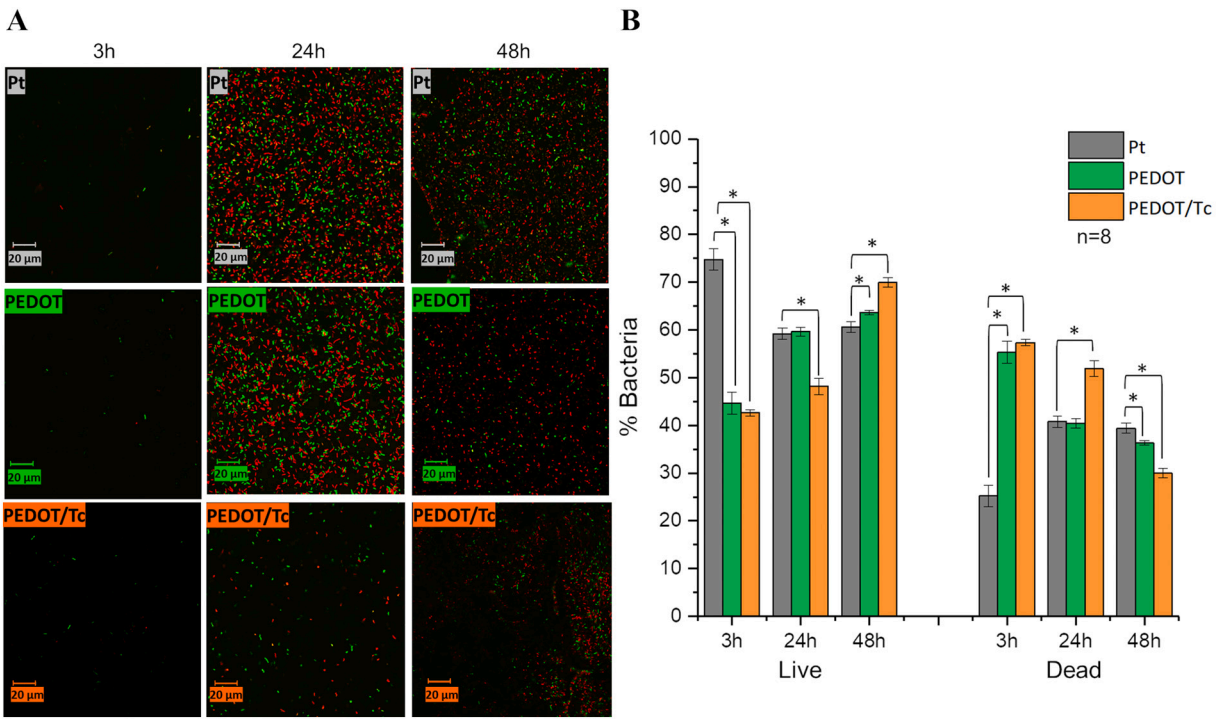

Fig. 8. The results of a LIVE/DEAD assay. A) Confocal fluorescent microscope images of *E.coli* on the surface of Pt-coated glass, PEDOT and PEDOT/Tc at three time points: 3 h, 24 h and 48 h; green colour denotes live bacteria, while red colour denotes dead bacteria; scale bars are 20 µm each. B) Percentage of live and dead bacteria on the surface of Pt, PEDOT and PEDOT/Tc at three time points: 3 h, 24 h and 48 h; * = $p < 0.05$, $n = 8$. (For interpretation of the references to colour in this figure legend, the reader is referred to the web version of this article.)

a decrease in the percentage of live cells to 59.2 ± 1.2% was observed on the surface of Pt. However, they still constituted more than half of a total bacterial population. On the contrary, the percentage of live cells on the surface of PEDOT increased and equalled with bacteria counted on the Pt-coated glass slides (59.6 ± 1.0%). Still, only a slight increase in the percentage of live cells was observed on the surface of PEDOT/Tc (48.2 ± 1.7%). The percentage of live cells on the Pt-coated surface after 48 h did not change, and the number of live cells remained at a constant level (60.6 ± 1.1%). However, in the case of PEDOT and PEDOT/Tc, despite a significant decrease in cell density, their viability increased significantly. More than a half of total bacterial population was still alive (63.7 ± 0.5%) on the surface of PEDOT. Live bacterial cells prevailed (70.0 ± 1.0%) also on the surface of PEDOT/Tc. This observation may indicate that dead bacterial cells were more liable to lysis and/or were more easily detached from the polymer layers than Pt-coated glass slides, what was already suggested above and impacted on the obtained percentage results concerning the viability of bacteria.

Although the results of the LIVE/DEAD assay may suggest weak antibacterial effects of PEDOT and PEDOT/Tc, since the percentage of live bacterial cells after 48 h was the highest for these samples, acquired data must be coupled with the surface coverage by bacterial cells. Similarly as in the case of SEM micrographs (Fig. 5), also fluorescent images (Fig. 8A) confirmed that the total number of bacterial cells was significantly lower on the surface of PEDOT/Tc when compared with the surface of bare Pt or pristine PEDOT. In this way, the efficiency of PEDOT as a potent Tc carrier was confirmed. The process of electrochemical immobilization was shown not to interfere with antibacterial properties of Tc, and the amounts of released Tc were appropriate to have a desired biological response towards *E.coli*. Also, PEDOT/Tc was shown to exhibit antibacterial activity without an electrical trigger, although electrical stimulation could further enhance the antibacterial performance of this material [42]. Even though the antibacterial effect of PEDOT/Tc was mainly associated with Tc, the application of a conjugated polymer as a matrix allows using PEDOT/Tc to modulate the metabolism of bacteria by changing electrochemical redox state of electroactive surface, similarly as reported by Gomez-Carretero et al. [40]. Therefore, PEDOT/Tc could serve as a robust coating with tunable antibacterial characteristics.

4. Conclusions

In summary, we fabricated a robust antibacterial coating by incorporating an antibiotic (tetracycline, Tc) into poly(3,4-ethylenedioxythiophene) (PEDOT) matrix. Optimization procedure allowed the selection of the appropriate Tc concentration (1 mM) during immobilization and the most effective polymerization conditions, so that the resulting matrix was characterized simultaneously by superior electrochemical properties (CSC of 19.15 ± 6.09 mC/cm^2) and high drug loading capacity (194.7 ± 56.2 µg/cm^2). Even though a pristine PEDOT matrix exhibited antimicrobial activity against a model Gram-negative bacteria strain (*Escherichia coli*), the presence of Tc evidently enhanced the antimicrobial activity of PEDOT, leading to a three-fold decrease in the number of bacteria after 48 h when compared with a control Pt surface. Smaller dimensions of bacteria growing on both PEDOT and PEDOT/Tc surfaces when compared with a bare Pt surface might indicate that their metabolic activity was decreased (they became dormant), possible due to some negative effects resulting from the interactions between nutrients and polymeric surface. The application of a conjugated polymer as the carrier of Tc allowed designing a robust antibacterial system with electrically-triggered biological performance, providing solid basis for further application, particularly in implantology. Still, to fully evaluate the antibacterial activity of PEDOT/Tc, it will be required to assess its effects on Gram-positive bacteria, including sporulating and non-sporulating bacterial strains. Nevertheless, it is expected that electroactive PEDOT/Tc systems, combining good electrochemical performance with antibacterial characteristics, would serve as multifunctional coatings for biomedical devices used in cardiac and neural tissue engineering.

Authors contribution

Dominika Czerwińska-Główka: Methodology, Investigation, Writing—original draft preparation. **Wioletta Przystaś**: Supervision. **Ewa Zabłocka-Godlewska**: Supervision. **Sebastian Student**: Investigation. **Beata Cwalina**: Conceptualization, Writing—review and editing. **Mieczysław Łapkowski**: Supervision. **Katarzyna Krukiewicz**: Conceptualization, Methodology, Investigation, Writing—review and editing, Supervision, Funding acquisition.

All authors have read and agreed to the published version of the manuscript.

Declaration of competing interest

The authors declare that they have no known competing financial interests or personal relationships that could have appeared to influence the work reported in this paper.

Acknowledgements

This research was funded by the National Science Center in Poland in the framework of SONATA 2016/23/D/ST5/01306 and OPUS 2019/35/B/ST5/00995, and by the Silesian University of Technology, Poland (04/040/BK_20/0113, 04/040/BK_21/0145 and 04/040/BKM20/0118).

Appendix A. Supplementary data

Supplementary data to this article can be found online at https://doi.org/10.1016/j.msec.2021.112017.

References

[1] R.M. Donlan, J.W. Costerton, Biofilms: survival mechanisms of clinically relevant microorganisms, Clin. Microbiol. Rev. 15 (2002) 167–193. doi:https://doi.org/10.1128/CMR.15.2.167-193.2002.
[2] A. Nagpal, M.R. Sohail, J.M. Steckelberg, Prosthetic valve endocarditis: state of the heart, Clin, Investig. (Lond). 2 (2012) 803–817, https://doi.org/10.4155/cli.12.70.
[3] K. Nishikawa, A. Takasu, K. Morita, H. Tsumori, T. Sakamoto, Deposits on the intraluminal surface and bacterial growth in central venous catheters, J. Hosp. Infect. 75 (2010) 19–22, https://doi.org/10.1016/j.jhin.2009.11.005.
[4] L.E. Nicolle, Catheter associated urinary tract infections, Antimicrob. Resist. Infect. Control. 3 (2014) 23, https://doi.org/10.1186/2047-2994-3-23.
[5] H.C. Flemming, J. Wingender, U. Szewzyk, P. Steinberg, S.A. Rice, S. Kjelleberg, Biofilms: an emergent form of bacterial life, Nat. Rev. Microbiol. 14 (2016) 563–575, https://doi.org/10.1038/nrmicro.2016.94.
[6] W.M. Dunne Jr., Bacterial adhesion: seen any good biofilms lately? Clin. Microbiol. Rev. 15 (2002) 155–166, https://doi.org/10.1128/CMR.15.2.155.
[7] S.T. Rutherford, B.L. Bassler, Bacterial quorum sensing: its role in virulence and possibilities for its control, cold spring, Harb. Perspect. Med. 2 (2012) 1–25, https://doi.org/10.1101/cshperspect.a012427.
[8] J. Humphries, L. Xiong, J. Liu, A. Prindle, F. Yuan, H.A. Arjes, L. Tsimring, G. M. Süel, Species-independent attraction to biofilms through electrical signaling, Cell. 168 (2017), https://doi.org/10.1016/j.cell.2016.12.014, 200-209.e12.
[9] A. Prindle, J. Liu, M. Asally, S. Ly, J. Garcia-Ojalvo, G.M. Süel, Ion channels enable electrical communication in bacterial communities, Nature. 527 (2015) 59–63, https://doi.org/10.1038/nature15709.
[10] E. Ben Jacob, I. Becker, Y. Shapira, H. Levine, Bacterial linguistic communication and social intelligence, Trends Microbiol. 12 (2004) 366–372, https://doi.org/10.1016/j.tim.2004.06.006.
[11] S. Wu, B. Zhang, Y. Liu, X. Suo, H. Li, Influence of surface topography on bacterial adhesion: a review (review), Biointerphases. 13 (2018), 060801, https://doi.org/10.1116/1.5054057.
[12] D. Czerwińska-Główka, K. Krukiewicz, A journey in the complex interactions between electrochemistry and bacteriology: from electroactivity to electromodulation of bacterial biofilms, Bioelectrochemistry. 131 (2020), 107401, https://doi.org/10.1016/j.bioelechem.2019.107401.
[13] S. Wilks, Poly(3,4-ethylene dioxythiophene) (PEDOT) as a micro-neural interface material for electrostimulation, Front. Neuroeng. 2 (2009) 1–8, https://doi.org/10.3389/neuro.16.007.2009.
[14] M.R. Abidian, D.-H. Kim, D.C. Martin, Conducting-polymer nanotubes for controlled drug release, Adv. Mater. 18 (2006) 405–409, https://doi.org/10.1002/adma.200501726.
[15] K. Krukiewicz, A. Kowalik, D. Czerwińska-Główka, M. Biggs, Electrodeposited poly (3,4-ethylenedioxypyrrole) films as neural interfaces: Cytocompatibility and electrochemical studies, Electrochim. Acta 302 (2019) 21–30, https://doi.org/10.1016/j.electacta.2019.02.023.
[16] X. Liu, W. Wen, G.C. Bazan, Post-deposition treatment of an arylated-carbazole conjugated polymer for solar cell fabrication, Adv. Mater. 24 (2012) 4505–4510, https://doi.org/10.1002/adma.201201567.
[17] D. Liu, B. Yang, B. Jang, B. Xu, S. Zhang, C. He, H.Y. Woo, J. Hou, Molecular design of a wide-band-gap conjugated polymer for efficient fullerene-free polymer solar cells, Energy Environ. Sci. 10 (2017) 546–551, https://doi.org/10.1039/C6EE03489F.
[18] Z. Hu, K. Zhang, F. Huang, Y. Cao, Water/alcohol soluble conjugated polymers for the interface engineering of highly efficient polymer light-emitting diodes and polymer solar cells, Chem. Commun. 51 (2015) 5572–5585, https://doi.org/10.1039/C4CC09433F.
[19] K. Bai, S. Wang, L. Zhao, J. Ding, L. Wang, Highly emissive carbazole-functionalized homopoly(spirobifluorene) for deep-blue polymer light-emitting diodes, Polym. Chem. 8 (2017) 2182–2188, https://doi.org/10.1039/C7PY00216E.
[20] C.A.R. Chapman, E.A. Cuttaz, J.A. Goding, R.A. Green, Actively controlled local drug delivery using conductive polymer-based devices, Appl. Phys. Lett. 116 (2020), 010501, https://doi.org/10.1063/1.5138587.
[21] B. Alshammary, F.C. Walsh, P. Herrasti, C. Ponce de Leon, Electrodeposited conductive polymers for controlled drug release: polypyrrole, J. Solid State Electrochem. 20 (2016) 839–859, https://doi.org/10.1007/s10008-015-2982-9.
[22] S. Zips, L. Grob, P. Rinklin, K. Terkan, N.Y. Adly, L.J.K. Weiß, D. Mayer, B. Wolfrum, Fully printed μ-needle electrode Array from conductive polymer ink for bioelectronic applications, ACS Appl. Mater. Interfaces 11 (2019) 32778–32786, https://doi.org/10.1021/acsami.9b11774.
[23] A. Fallahi, S. Mandla, T. Kerr-Phillip, J. Seo, R.O. Rodrigues, Y.A. Jodat, R. Samanipour, M.A. Hussain, C.K. Lee, H. Bae, A. Khademhosseini, J. Travas-Sejdic, S.R. Shin, Flexible and stretchable PEDOT-embedded hybrid substrates for bioengineering and sensory applications, ChemNanoMat. 5 (2019) 729–737, https://doi.org/10.1002/cnma.201900146.
[24] A. Madhan Kumar, A.Y. Adesina, M.A. Hussein, S. Ramakrishna, N. Al-Aqeeli, S. Akhtar, S. Saravanan, PEDOT/FHA nanocomposite coatings on newly developed Ti-Nb-Zr implants: biocompatibility and surface protection against corrosion and bacterial infections, Mater. Sci. Eng. C. 98 (2019) 482–495, https://doi.org/10.1016/j.msec.2019.01.012.
[25] C. Bodart, N. Rossetti, J. Hagler, P. Chevreau, D. Chhin, F. Soavi, S.B. Schougaard, F. Amzica, F. Cicoira, Electropolymerized poly(3,4-ethylenedioxythiophene) (PEDOT) coatings for implantable deep-brain-stimulating microelectrodes, ACS Appl. Mater. Interfaces 11 (2019) 17226–17233, https://doi.org/10.1021/acsami.9b03088.
[26] C. Kleber, K. Lienkamp, J. Rühe, M. Asplund, Electrochemically controlled drug release from a conducting polymer hydrogel (PDMAAp/PEDOT) for local therapy and bioelectronics, Adv. Healthc. Mater. 8 (2019), e1801488, https://doi.org/10.1002/adhm.201801488.
[27] S. Carli, G. Fioravanti, A. Armirotti, F. Ciarpella, M. Prato, G. Ottonello, M. Salerno, A. Scarpellini, D. Perrone, E. Marchesi, D. Ricci, L. Fadiga, A new drug delivery system based on Tauroursodeoxycholic acid and PEDOT, Chem. – A Eur. J. 25 (2018), chem.201805285, https://doi.org/10.1002/chem.201805285.
[28] K. Krukiewicz, A. Kruk, R. Turczyn, Evaluation of drug loading capacity and release characteristics of PEDOT/naproxen system: effect of doping ions, Electrochim. Acta 289 (2018) 218–227, https://doi.org/10.1016/j.electacta.2018.09.011.
[29] A.K. Jayaram, C. Pitsalidis, E. Tan, C.-M. Moysidou, M.F.L. De Volder, J.-S. Kim, R. M. Owens, 3D hybrid scaffolds based on PEDOT:PSS/MWCNT composites, Front. Chem. 7 (2019) 1–9, https://doi.org/10.3389/fchem.2019.00363.
[30] S. Wang, S. Guan, Z. Zhu, W. Li, T. Liu, X. Ma, Hyaluronic acid doped-poly(3,4-ethylenedioxythiophene)/chitosan/gelatin (PEDOT-HA/Cs/Gel) porous conductive scaffold for nerve regeneration, Mater. Sci. Eng. C. 71 (2017) 308–316, https://doi.org/10.1016/j.msec.2016.10.029.
[31] S.C. Luo, E.M. Ali, N.C. Tansil, H.H. Yu, S. Gao, E.A.B. Kantchev, J.Y. Ying, Poly (3,4-ethylenedioxythiophene) (PEDOT) nanobiointerfaces: thin, ultrasmooth, and functionalized PEDOT films with in vitro and in vivo biocompatibility, Langmuir. 24 (2008) 8071–8077, https://doi.org/10.1021/la800333g.
[32] K. Krukiewicz, J.K. Zak, Conjugated polymers as robust carriers for controlled delivery of anti-inflammatory drugs, J. Mater. Sci. 49 (2014) 5738–5745, https://doi.org/10.1007/s10853-014-8292-2.
[33] R. Wadhwa, C.F. Lagenaur, X.T. Cui, Electrochemically controlled release of dexamethasone from conducting polymer polypyrrole coated electrode, J. Control. Release 110 (2006) 531–541, https://doi.org/10.1016/j.jconrel.2005.10.027.
[34] D. Esrafilzadeh, J.M. Razal, S.E. Moulton, E.M. Stewart, G.G. Wallace, Multifunctional conducting fibres with electrically controlled release of ciprofloxacin, J. Control. Release 169 (2013) 313–320, https://doi.org/10.1016/j.jconrel.2013.01.022.
[35] S. Sirivisoot, R. Pareta, T.J. Webster, Electrically controlled drug release from nanostructured polypyrrole coated on titanium, Nanotechnology. 22 (2011), 085101, https://doi.org/10.1088/0957-4484/22/8/085101.
[36] K. Krukiewicz, T. Jarosz, J.K. Zak, M. Lapkowski, P. Ruszkowski, T. Bobkiewicz-Kozlowska, B. Bednarczyk-Cwynar, Advancing the delivery of anticancer drugs: conjugated polymer/triterpenoid composite, Acta Biomater. 19 (2015) 158–165, https://doi.org/10.1016/j.actbio.2015.03.006.
[37] K. Krukiewicz, M. Cichy, P. Ruszkowski, R. Turczyn, T. Jarosz, J.K. Zak, M. Lapkowski, B. Bednarczyk-Cwynar, Betulin-loaded PEDOT films for regional chemotherapy, Mater. Sci. Eng. C. 73 (2017) 611–615, https://doi.org/10.1016/j.msec.2016.12.115.

[38] N. Alizadeh, E. Shamaeli, Electrochemically controlled release of anticancer drug methotrexate using nanostructured polypyrrole modified with cetylpyridinium: release kinetics investigation, Electrochim. Acta 130 (2014) 488–496, https://doi.org/10.1016/j.electacta.2014.03.055.
[39] S. Löffler, H. Antypas, F.X. Choong, K. Peter, A. Richter-Dahlfors, Conjugated oligo- and polymers for bacterial sensing, Front. Chem. 7 (2019) 265, https://doi.org/10.3389/fchem.2019.00265.
[40] S. Gomez-Carretero, B. Libberton, M. Rhen, A. Richter-Dahlfors, K. Svennersten, K. Persson, E. Jager, M. Berggren, M. Rhen, A. Richter-Dahlfors, Redox-active conducting polymers modulate Salmonella biofilm formation by controlling availability of electron acceptors, Npj Biofilms Microbiomes. 3 (2017) 19, https://doi.org/10.1038/s41522-017-0027-0.
[41] K. Butina, S. Löffler, M. Rhen, A. Richter-Dahlfors, Electrochemical sensing of bacteria via secreted redox active compounds using conducting polymers, Sensors Actuators B Chem. 297 (2019), 126703, https://doi.org/10.1016/j.snb.2019.126703.
[42] S. Gomez-Carretero, R. Nybom, A. Richter-Dahlfors, Electroenhanced antimicrobial coating based on conjugated polymers with covalently coupled silver nanoparticles prevents Staphylococcus aureus biofilm formation, Adv. Healthc. Mater. 6 (2017), 1700435, https://doi.org/10.1002/adhm.201700435.
[43] A. Petrossians, J.J. Whalen III, J.D. Weiland, F. Mansfeld, Electrodeposition and characterization of thin-film platinum-iridium alloys for biological interfaces, J. Electrochem. Soc. 158 (2011) D269, https://doi.org/10.1149/1.3559477.
[44] D. Czerwińska-Główka, W. Przystaś, E. Zabłocka-Godlewska, S. Student, B. Cwalina, M. Łapkowski, K. Krukiewicz, Bacterial surface colonization of sputter-coated platinum films, Materials (Basel). 13 (2020) 2674. https://doi.org/10.3390/ma13122674.
[45] T.R. Tritton, Ribosome-tetracycline interactions, Biochemistry. 16 (1977) 4133–4138, https://doi.org/10.1021/bi00637a029.
[46] I. Chopra, M. Roberts, Tetracycline antibiotics: mode of action, applications, molecular biology, and epidemiology of bacterial resistance, Microbiol. Mol. Biol. Rev. 65 (2001) 232–260. doi:https://doi.org/10.1128/MMBR.65.2.232-260.2001.
[47] C.U. Chukwudi, rRNA binding sites and the molecular mechanism of action of the tetracyclines, Antimicrob. Agents Chemother. 60 (2016) 4433–4441, https://doi.org/10.1128/AAC.00594-16.
[48] S. Li, A. Thomas, Emerged carbon nanomaterials from metal-organic precursors for electrochemical catalysis in energy conversion, in: Adv. Nanomater. Electrochem. Energy Convers. Storage, Elsevier, 2020, https://doi.org/10.1016/B978-0-12-814558-6.00012-5.
[49] X. Chen, O. Inganäs, Three-step redox in polythiophenes: evidence from electrochemistry at an ultramicroelectrode, J. Phys. Chem. 100 (1996) 15202–15206, https://doi.org/10.1021/jp9601779.
[50] U.A. Aregueta-Robles, A.J. Woolley, L.A. Poole-Warren, N.H. Lovell, R.A. Green, Organic electrode coatings for next-generation neural interfaces, Front. Neuroeng. 7 (2014) 15, https://doi.org/10.3389/fneng.2014.00015.
[51] S.F. Cogan, Neural stimulation and recording electrodes, Annu. Rev. Biomed. Eng. 10 (2008) 275–309, https://doi.org/10.1146/annurev.bioeng.10.061807.160518.
[52] K. Krukiewicz, M. Chudy, C. Vallejo-Giraldo, M. Skorupa, D. Więcławska, R. Turczyn, M. Biggs, Fractal form PEDOT/Au assemblies as thin-film neural interface materials, Biomed. Mater. 13 (2018), 54102. http://stacks.iop.org/1748-605X/13/i=5/a=054102.
[53] H.-C. Tian, J.-Q. Liu, X.-Y. Kang, Q. He, B. Yang, X. Chen, C.-S. Yang, Flexible multi-channel microelectrode with fluidic paths for intramuscular stimulation and recording, Sensors Actuators A Phys. 228 (2015) 28–39, https://doi.org/10.1016/j.sna.2015.02.035.
[54] N. Bhagwat, R.E. Murray, S.I. Shah, K.L. Kiick, D.C. Martin, Biofunctionalization of PEDOT films with laminin-derived peptides, Acta Biomater. 41 (2016) 235–246, https://doi.org/10.1016/j.actbio.2016.05.016.
[55] A.P. Sandoval, M.F. Suárez-Herrera, J.M. Feliu, IR and electrochemical synthesis and characterization of thin films of PEDOT grown on platinum single crystal electrodes in [EMMIM]Tf_2N ionic liquid, Beilstein J. Org. Chem. 11 (2015) 348–357, https://doi.org/10.3762/bjoc.11.40.
[56] Q. Zhao, R. Jamal, L. Zhang, M. Wang, T. Abdiryim, The structure and properties of PEDOT synthesized by template-free solution method, Nanoscale Res. Lett. 9 (2014) 557, https://doi.org/10.1186/1556-276X-9-557.
[57] F. Kuralay, S. Demirci, M. Kiristi, L. Oksuz, A.U. Oksuz, Poly(3,4-ethylenedioxythiophene) coated chitosan modified disposable electrodes for DNA and DNA–drug interaction sensing, Colloids Surfaces B Biointerfaces. 123 (2014) 825–830, https://doi.org/10.1016/j.colsurfb.2014.10.021.
[58] C. Li, T. Imae, Electrochemical and optical properties of the poly(3,4-ethylenedioxythiophene) film Electropolymerized in an aqueous sodium dodecyl sulfate and Lithium Tetrafluoroborate medium, Macromolecules. 37 (2004) 2411–2416, https://doi.org/10.1021/ma035188w.
[59] E.E. Ozseker, A. Akkaya, Development of a new antibacterial biomaterial by tetracycline immobilization on calcium-alginate beads, Carbohydr, Polym. 151 (2016) 441–451, https://doi.org/10.1016/j.carbpol.2016.05.073.
[60] H.J. Haroosh, Y. Dong, K.-T. Lau, Tetracycline hydrochloride (TCH)-loaded drug carrier based on PLA:PCL nanofibre mats: experimental characterisation and release kinetics modelling, J. Mater. Sci. 49 (2014) 6270–6281, https://doi.org/10.1007/s10853-014-8352-7.
[61] Z. Li, V.M.K. Kolb, W.-T. Jiang, H. Hong, FTIR and XRD investigations of tetracycline intercalation in smectites, Clay Clay Miner. 58 (2010) 462–474, https://doi.org/10.1346/CCMN.2010.0580402.
[62] K. Krukiewicz, P. Zawisza, A.P. Herman, R. Turczyn, S. Boncel, J.K. Zak, An electrically controlled drug delivery system based on conducting poly(3,4-ethylenedioxypyrrole) matrix, Bioelectrochemistry. 108 (2016) 13–20, https://doi.org/10.1016/j.bioelechem.2015.11.002.
[63] A. Han, X. Li, B. Huang, J.K.H. Tsoi, J.P. Matinlinna, Z. Chen, D.M. Deng, The effect of titanium implant surface modification on the dynamic process of initial microbial adhesion and biofilm formation, Int. J. Adhes. Adhes. 69 (2016) 125–132, https://doi.org/10.1016/j.ijadhadh.2016.03.018.
[64] S. Bayoudh, A. Othmane, F. Bettaieb, A. Bakhrouf, H. Ben Ouada, L. Ponsonnet, Quantification of the adhesion free energy between bacteria and hydrophobic and hydrophilic substrata, Mater. Sci. Eng. C. 26 (2006) 300–305, https://doi.org/10.1016/j.msec.2005.10.045.
[65] G.M. Bruinsma, H.C. Van Der Mei, H.J. Busscher, Bacterial adhesion to surface hydrophilic and hydrophobic contact lenses, Biomaterials. 22 (2001) 3217–3224, https://doi.org/10.1016/S0142-9612(01)00159-4.
[66] Y. Yuan, M.P. Hays, P.R. Hardwidge, J. Kim, Surface characteristics influencing bacterial adhesion to polymeric substrates, RSC Adv. 7 (2017) 14254–14261, https://doi.org/10.1039/C7RA01571B.
[67] I. Bezruk, V. Vrakin, L. Savchenko, A. Materiienko, V. Georgiyants, Development and validation of tetracycline hydrochloride assay procedure by spectrophotometry in compounded ointment, Scr. Sci. Pharm. 4 (2017) 33, https://doi.org/10.14748/ssp.v4i1.2117.
[68] J. Bengtsson-Palme, D.G.J. Larsson, Concentrations of antibiotics predicted to select for resistant bacteria: proposed limits for environmental regulation, Environ. Int. 86 (2016) 140–149, https://doi.org/10.1016/j.envint.2015.10.015.
[69] M. Tomczykowa, M.E. Plonska-Brzezinska, Conducting polymers, hydrogels and their composites: preparation, properties and bioapplications, Polymers (Basel). 11 (2019) 350, https://doi.org/10.3390/polym11020350.
[70] L. Crémet, A. Broquet, C. Jacqueline, C. Caillou, K. Asehnoune, S. Corvec, N. Caroff, Innate immune evasion of Escherichia coli clinical strains from orthopedic implant infections, Eur. J. Clin. Microbiol. Infect. Dis. 35 (2016) 993–999, https://doi.org/10.1007/s10096-016-2628-6.
[71] E.J. Boll, J. Frimodt-Møller, B. Olesen, K.A. Krogfelt, C. Struve, Heat resistance in extended-spectrum beta-lactamase-producing Escherichia coli may favor environmental survival in a hospital setting, Res. Microbiol. 167 (2016) 345–349, https://doi.org/10.1016/j.resmic.2016.02.002.
[72] N. Mohd Daud, I.F. Saeful Bahri, N.A.N. Nik Malek, H. Hermawan, S. Saidin, Immobilization of antibacterial chlorhexidine on stainless steel using crosslinking polydopamine film: towards infection resistant medical devices, Colloids Surfaces B Biointerfaces. 145 (2016) 130–139, https://doi.org/10.1016/j.colsurfb.2016.04.046.
[73] G. Sharma, S. Sharma, P. Sharma, D. Chandola, S. Dang, S. Gupta, R. Gabrani, Escherichia coli biofilm: development and therapeutic strategies, J. Appl. Microbiol. 121 (2016) 309–319, https://doi.org/10.1111/jam.13078.
[74] K. Skarstad, H.B. Steen, E. Boye, Cell cycle parameters of slowly growing Escherichia coli B/r studied by flow cytometry, J. Bacteriol. 154 (1983) 656–662. doi:https://doi.org/10.1128/jb.154.2.656-662.1983.
[75] M.H. Zwietering, I. Jongenburger, F.M. Rombouts, van't Riet K., Modeling of the bacterial growth curve, Appl. Environ. Microbiol. 56 (1990) 1875–1881. doi: https://doi.org/10.1128/AEM.56.6.1875-1881.1990.
[76] G. Reshes, S. Vanounou, I. Fishov, M. Feingold, Cell shape dynamics in Escherichia coli, Biophys. J. 94 (2008) 251–264, https://doi.org/10.1529/biophysj.107.104398.
[77] A. Amir, Cell size regulation in Bacteria, Phys. Rev. Lett. 112 (2014), 208102, https://doi.org/10.1103/PhysRevLett.112.208102.
[78] C.S. Westfall, P.A. Levin, Bacterial cell size: multifactorial and multifaceted, Annu. Rev. Microbiol. 71 (2017) 499–517, https://doi.org/10.1146/annurev-micro-090816-093803.
[79] N. Ojkic, D. Serbanescu, S. Banerjee, Surface-to-volume scaling and aspect ratio preservation in rod-shaped bacteria, Elife. 8 (2019), e47033, https://doi.org/10.7554/eLife.47033.
[80] D.A. Gray, G. Dugar, P. Gamba, H. Strahl, M.J. Jonker, L.W. Hamoen, Extreme slow growth as alternative strategy to survive deep starvation in bacteria, Nat. Commun. 10 (2019) 890, https://doi.org/10.1038/s41467-019-08719-8.

Bioelectrochemistry 144 (2022) 108030

Contents lists available at ScienceDirect

Bioelectrochemistry

journal homepage: www.elsevier.com/locate/bioelechem

Bifunctional conducting polymer matrices with antibacterial and neuroprotective effects

Dominika Czerwińska-Główka [a], Magdalena Skonieczna [b,c], Adrian Barylski [d], Sylwia Golba [d], Wioletta Przystaś [c,e], Ewa Zabłocka-Godlewska [c,e], Sebastian Student [b,c], Beata Cwalina [c,f], Katarzyna Krukiewicz [a,*]

[a] Department of Physical Chemistry and Technology of Polymers, Silesian University of Technology, M.Strzody 9, 44-100 Gliwice, Poland
[b] Department of Systems Biology and Engineering, Faculty of Automatic Control, Electronics and Computer Science, Silesian University of Technology, Akademicka 16, 44-100 Gliwice, Poland
[c] Biotechnology Centre, Silesian University of Technology, B. Krzywoustego 8, 44-100 Gliwice, Poland
[d] Institute of Materials Engineering, University of Silesia, 75 Pulku Piechoty, 41-500 Chorzow, Poland
[e] Department of Air Protection, Faculty of Energy and Environmental Engineering, Silesian University of Technology, S. Konarskiego 22B, 44-100 Gliwice, Poland
[f] Department of Environmental Biotechnology, Faculty of Energy and Environmental Engineering, Silesian University of Technology, S.Konarskiego 18, 44-100 Gliwice, Poland

ARTICLE INFO

Article history:
Received 23 August 2021
Received in revised form 24 October 2021
Accepted 29 November 2021
Available online 4 December 2021

Keywords:
Antibacterial coating
Conducting polymer
Neural interface
Neuroprotective effect
Poly(3,4-ethylenedioxypyrrole)
Tetracycline

ABSTRACT

Current trends in the field of neural tissue engineering include the design of advanced biomaterials combining excellent electrochemical performance with versatile biological characteristics. The purpose of this work was to develop an antibacterial and neuroprotective coating based on a conducting polymer – poly(3,4-ethylenedioxypyrrole) (PEDOP), loaded with an antibiotic agent – tetracycline (Tc). Employing an electrochemical technique to immobilize Tc within a growing polymer matrix allowed to fabricate robust PEDOP/Tc coatings with a high charge storage capacity (63.65 ± 6.05 mC/cm^2), drug release efficiency (629.4 μg/cm^2 ± 62.7 μg/cm^2), and low charge transfer resistance (2.4 ± 0.1 kΩ), able to deliver a stable electrical signal. PEDOP/Tc were found to exhibit strong antimicrobial effects against Gram-negative bacteria *Escherichia coli*, expressed through negligible adhesion, reduction in viability, and a characteristic elongation of bacterial cells. Cytocompatibility and neuroprotective effects were evaluated using a rat neuroblastoma B35 cell line, and were analyzed using MTT, cell cycle, and Annexin-V apoptosis assays. The presence of Tc was found to enhance neural cell viability and neurite outgrowth. The results confirmed that PEDOP/Tc can serve as an efficient neural electrode coating able to enhance charge transfer, as well as to exhibit bifunctional biological characteristics, different for eukaryotic and prokaryotic cells.

1. Introduction

Neurodegenerative diseases are often associated with a progressive damage of neural cells leading to disorders related to mobility, memory, and a decrease in mental performance. The World Health Organization predicts that, due to the increasing life expectancy, the number of patients suffering from neurodegenerative diseases will increase intensively over the next years [1]. Therefore, the recent research efforts have been focused on designing biomaterials compatible with neural tissue, and able to be employed in a wide range of neurostimulation therapies, particularly electrostimulation [2–4]. Undoubtedly, neural implants have to meet many requirements, as the key elements for the efficiency of their performance are the interactions at the tissue/implant interface. Not only the chemical composition of the substrate, but also its physicochemical features, including surface topography, porosity, hydrophobicity, and surface charge, have an impact on cell behavior [5–7]. For proper functionality, neural implants should allow an efficient transfer of electrical charge, usually assessed in terms of low impedance and high capacitance [8,9]. Therefore, the most popular neural electrode materials comprise noble metals, especially platinum and its alloys [10]. Unfortunately, the mismatch between the soft living tissue and the hard surface of metal often leads to an exacerbation of the inflammatory response, increased expression of proinflammatory cytokines, glial cell activation, and neuronal degeneration [11,12]. The grand challenge to the design of a robust neural interface is to minimize scar

* Corresponding author.
E-mail address: katarzyna.krukiewicz@polsl.pl (K. Krukiewicz).

https://doi.org/10.1016/j.bioelechem.2021.108030
1567-5394/

tissue surrounding the implants, as the migration of astrocytes and microglia towards the implant can significantly decrease the rate of charge transfer [13].

Similarly to other implantable biomedical devices [14], neural implants are susceptible to bacterial colonization. For instance, a previous study [15] has shown that a surface of platinum may be easily colonized by bacteria. Besides, the process of implantation often leads to a localized inflammatory reaction [16], which reduces the ability of the organism to ward off bacteria [17]. It is clear that the development of a bacterial biofilm on the surface of neural implants is an extremely severe problem, leading to the increase in a number of revision surgeries, and, sometimes, fatality. Therefore, tailoring a biomaterial to exhibit antibacterial effects would be considered as an important benefit [18,19].

Combining low Young's modulus, excellent electrochemical and mechanical characteristics, as well as biocompatibility, conducting polymers are currently a competitive alternative to noble metals [20–28]. Besides, since the entrapment of bioactive molecules into the polymer matrix is an efficient drug immobilization method, conducting polymers can serve as robust electro-responsive drug delivery systems [29–31]. Recent studies [32,33] have shown that conducting polymers, either in their pristine form or loaded with antibacterial agents, can be used to modulate bacterial attachment and biofilm formation. Since bacterial biofilm growing on the surface of the implant limits the integration of neural cells with a device [34], antimicrobial coatings are supposed to indirectly increase the efficiency of electrical stimulation. Simultaneously, the increase in the capacitance and conductivity of the coated electrode is supposed to allow an application of lower stimulation currents, increasing the safety of the overall treatment.

The scope of this study was aimed to fabricate and characterize a bifunctional conducting polymer coating based on a poly(3,4-ethylenedioxypyrrole) (PEDOP) matrix loaded with tetracycline (Tc), combining antibacterial and neuroprotective functionalities. PEDOP is a conducting polymer belonging to the family of polypyrroles (PPy), known for their high biocompatibility towards neural cells [35]. The presence of an ethylenedioxy bridge in its structure increases the electrochemical stability of PEDOP [36], making it related to another conducting polymer with a great potential in bioelectronics, namely poly(3,4-ethylenedioxythiophene), PEDOT [37]. Although structurally similar to the most frequently applied conducting polymers, PEDOP has been long considered as a versatile but underutilized polymer [38]. Recently, our group has revealed the applicability of PEDOP as a drug carrier [39–41] and a neural interface [42,43], highlighting its advantages when compared with PPy and PEDOT, including low polymerization potential [40], high electrochemical stability [42] and the ability to provide controlled drug release [43].

Tc, on the other hand, is a potent bacteriostatic agent, able to bind to the 30S ribosomal subunit of bacteria and inhibit the synthesis of proteins, and is typically used as an antibiotic for humans [44]. It has been shown that Tc and its derivatives possess neuroprotective functions, as they can inhibit activation and proliferation of microglia [45], attenuate apoptosis and suppress the production of reactive oxygen species [46], influencing the mechanisms involved in the neurodegeneration processes compromising the performance of neural implants. Therefore, we have stated that by immobilizing Tc into PEDOP matrix, it will be possible to form an electroactive coating exhibiting simultaneously neuroprotective and antibacterial effects. This kind of a bifunctional behaviour has not been identified as yet neither for PEDOT nor PPy.

To form a Tc-loaded PEDOP coating on the surface of Pt-coated electrodes, the *in situ* drug immobilization in the course of electrochemical polymerization was employed. The extensive physicochemical characterization of as-formed PEDOP/Tc coatings involved the assessment of electrochemical performance (cyclic voltammetry, chronopotentiometry), charge transfer resistance (electrochemical impedance spectroscopy), surface characterization (infrared spectroscopy, contact angle measurements, scanning electron microscopy, atomic force microscopy), strength of adhesion (scratch test), as well as the estimate of drug release efficiency (UV–Vis spectroscopy). Antibacterial activity of PEDOP/Tc was evaluated against *Escherichia coli* and was examined using LIVE/DEAD fluorescent assay and morphometric analysis (scanning electron microscopy). Cytocompatibility and neuroprotective functions of PEDOP/Tc were verified towards a B35 rat neuroblastoma cell line using MTT, cell cycle, and Annexin V apoptosis assays.

2. Materials and methods

2.1. Electrochemical polymerization and drug immobilization

Electrochemical polymerization of conducting polymer matrices was carried out using a potentiostat (CH Instruments 400c) with the three-electrode arrangement, employing a Pt sputter-coated (automatic, rotary-pump coating system, Q150R Quorum Technologies, 30 mA, 120 s, giving a 4.8 nm thick layer of Pt) glass slide (microscopic slide, Labglass) as a working electrode (0.283 cm^2), Ag/AgCl (3 M KCl) as a reference electrode, and a platinum foil (1 cm^2) as a counter electrode. The choice of Pt-coated glass slides as the substrates was based on the applicability of glass in neural science [47–49], allowing to couple electrical stimulation with optogenetic and infrared stimulation [50]. Sputter-coating of a thin layer of Pt, on the other hand, was used to provide conductivity to the substrate while maintaining a certain level of transparency. Poly(3,4-ethylenedioxypyrrole), PEDOP, was electrochemically synthesized by means of a cyclic voltammetry (CV) in an aqueous solution of 10 mM EDOP (Sigma Aldrich, 2% (w/v) in THF) in a phosphate-buffered saline (PBS: 0.14 M NaCl, 0.0027 M KCl, 0.01 M $Na_2HPO_4{\cdot}2H_2O$, 0.002 M KH_2PO_4, pH = 7.4) in the potential range from −0.8 V to 1.0 V (vs. Ag/AgCl), at a scan rate of 0.1 V/s for 25 CV cycles. PBS was chosen as a physiologically-relevant medium able to prevent local pH changes induced by electrochemical processes. Tetracycline hydrochloride, Tc (Sigma-Aldrich, 98.0%-102.0%) was incorporated into a polymer matrix *via* an electrochemical polymerization process in an aqueous solution of PBS, monomer (10 mM of EDOP), and Tc (from 1 mM to 20 mM). To obtain a drug-loaded film (PEDOP/Tc), the polymerization was performed in the potential range from −0.8 V to 1.0 V (vs. Ag/AgCl), at a scan rate of 0.1 V/s for 15–100 CV cycles.

2.2. Material characterization

The chemical structure of PEDOP, PEDOP/Tc, and Tc was characterized by FTIR spectroscopy (IR Perkin Elmer Spectrum Two spectrometer) using a Diamond UATR accessory, in the range between 500 cm^{-1} and 1800 cm^{-1} for 16 scans. The surface morphology of polymer matrices was studied using a scanning electron microscope, SEM (Phenom ProX, Thermo Fisher Scientific) operating at an accelerating voltage of 10 kV. A surface roughness parameter (arithmetic mean height, S_a) was determined using 3D Roughness Reconstructions software associated with SEM (Phenom ProSuite), while a root mean square roughness (R_{rms}) was determined by means of atomic force microscopy (CoreAFM, Nanosurf) and a Gwyddion software. Contact angle (CA) measurements were performed using an optical goniometer (OCA15 DataPhysisc) at room temperature (T ∼ 20 °C) employing deionized water. The capacitance of investigated samples was presented in terms of a charge storage capacity (CSC), and was calculated as the electric charge

integrated under a corresponding CV curve according to the following equation:

$$CSC = \frac{1}{S}\int_{t_1}^{t_2} I(t)dt \quad (1)$$

where: S is geometrical area of the electrode (cm^2), t_1 denotes the beginning of a CV cycle, t_2 denotes the end of a CV cycle, and I is the current (A).

Electrochemical impedance spectroscopy (EIS) was performed in a PBS solution with an AC amplitude of 40 mV (vs. Ag/AgCl) and a DC potential of 0 V (vs. Ag/AgCl), within a frequency range from 100 mHz to 10 kHz. The results were presented on Bode plots and compared to those of a bare Pt electrode. EIS Spectrum Analyzer 1.0 software [51] and the Powell algorithm were used to fit the experimental data to an equivalent circuit model.

Voltage profiles during charge injeciton were determined basing on chronopotentiometric experiments performed with repetitive oxidation and reduction pulses of opposing polarity, but equal time (5 ms) and magnitude, being equivalent to a biphasic pulse with no interphase gap. The measurements were conducted in PBS using a three electrode setup, with a platinum wire counter electrode and Ag/AgCl reference electrode. Basing on literature studies, four charge densities were selected, namely 3 μC/cm^2 (typical minimum limit used for cochlear implants) [52], 10 μC/cm^2 (typical maximum limit used for cochlear implants) [52], 36 μC/cm^2 (used to evoke motor response in rats) [53] and 50 μC/cm^2 (used to establish charge injection limit). A complete biphasic pulse, comprising one oxidation and one reduction pulse, was repeated five times.

2.3. Drug release studies

A chronoamperometric potential jump from −0.6 V (2 s) to −0.5 V (600 s) was applied to trigger the release of Tc from PEDOP/Tc and to assess the total drug release efficiency of PEDOP/Tc. The amount of released Tc was measured by UV/Vis spectroscopy (Hewlett Packard 8453), with the use of a calibration curve: y = 3.0461x + 0.00326 (R^2 = 0.9969), where y is the absorbance value at 363 nm, and x is the concentration of Tc expressed in mM.

To measure the amount of Tc released spontaneously form PEDOT/Tc, three PEDOT/Tc-coated electrodes were put separately in three quartz cuvettes (optical path of 2 mm) filled with PBS (0.5 ml). UV–Vis spectra of the supernatants were taken at specific time points (1 h, 2 h, 4 h, 8 h, 24 h, 2 days, 3 days, 4 days and 7 days). Avrami's model was used to investigate the release kinetics of Tc from PEDOP/Tc following the equation [54–56]:

$$X = 1 - \exp(-kt^n) \quad (2)$$

rearranged to its linear form:

$$\ln(-\ln(1-X)) = \ln k + n\ln t \quad (3)$$

where: X is the fraction of a drug released at time t, n is the exponent of release, and k is the release rate constant. The fitting of the data describing the release kinetics was made with the use of two free parameters, namely n and k. The equilibrium concentration was determined experimentally.

2.4. Adhesion of the polymer coating

The adhesion forces of PEDOP and PEDOP/Tc to Pt-coated glass slides, and a layer of Pt to a glass slide were assessed using a scratch test method by means of a Micro-Combi Tester platform (Anton Paar) in accordance with the ISO 19252, ISO 20,502 and ASTM C1624 standards. During the test, a Rockwell diamond cone with a diameter of 100 μm was used to make a scratch. Every test was divided into three stages. In a pre-scan, a profile of sample was scanned with a constant loading of 0.03 N. An actual scan consisted of making a scratch with a gradual increase in the normal force loading from 0.03 N to 15 N for PEDOP and PEDOP/Tc, and from 0.03 N to 30 N for a bare Pt-coated glass slide, with the speed of 3 mm/min and the crack length of 3 mm. In a post-scan, a profile of sample was scanned with a constant loading of 0.03 N. Three measurements were taken on each sample.

2.5. Bacterial suspension and culture conditions

Microbiological analysis was performed using a bacterial strain of Gram-negative *Escherichia coli* (DSM 30083, U5/41). Bacteria were cultivated for 48 h in agar broth (BTL) at 35 °C. Next, the suspension of microorganisms in a physiological saline (0.85 % water solution of NaCl; Acros Organics) was prepared with the final concentration of approx. 10.5×10^8 CFU/ml. PEDOP, PEDOP/Tc, and Pt-coated glass slides were sterilized by UVC radiation (253.7 nm) for an hour and then placed in sterile 12-well plates. 0.1 ml of bacterial suspension and 2 ml of a sterile growth medium (10 g/l Tryptone (BTL), 5 g/l yeast extract (BTL), and 10 g/l NaCl (Acros), pH = 7) were added into each well. The samples were then incubated at 35 °C and analyzed after 3 h, 24 h, and 48 h.

2.6. Staining and imaging of bacterial cells

Assessing bacterial viability on PEDOP, PEDOP/Tc, and Pt-coated glass slides was performed using a LIVE/DEAD® BacLight Bacterial Viability Kit (Life Technologies, Thermo Fisher Scientific) together with an Olympus FV 1000 confocal fluorescent microscope. Bacteria labeled with SYTO9 stain (live bacterial cells) were observed as green, and bacteria stained with D-propidium iodide (dead bacterial cells) were observed as red. Image analysis was accomplished using ImageJ software (Fiji, NIH).

SEM microscopy (Phenom ProX) was employed to visualize the morphology of bacteria on investigated surfaces. Firstly, bacteria on PEDOP, PEDOP/Tc, and Pt-coated glass slides were fixed using 3 % glutaraldehyde (Fisher BioReagents) for 24 h, then washed three times with sterile distilled water. Subsequently, samples were dehydrated by immersing them for 10 min in the solutions of ethanol (Acros Organics) with increasing concentrations (30 %, 50 %, 70 %, 80 %, 90 %, 95 %, 99.8 %), then dried for 24 h at 50 °C. To enhance the quality of imaging, dehydrated samples were sputter-coated with a gold layer (20 min, 20 mA; Q150R Quorum Technologies). Images were taken with an accelerating voltage of 15 kV at the magnifications of 1 000 ×, 5 000 × and 10 000 × . ImageJ software (NIH) was used to quantify the size distribution of *E. coli* cells (length, width, aspect ratio), as well as their density (number of bacteria per 200 μm^2).

2.7. Cell line and culture conditions

A rat neuroblastoma cell line B35 (ATCC® CRL-2754™) was used to analyze cell viability on PEDOP, PEDOP/Tc, and Pt-coated glass slides. Cells were cultured in 75 cm^2 bottles (Nunc) in 15 ml Dulbecco's Modified Eagle Medium/Nutrient Mixture F-12 (DMEM/F12, Sigma-Aldrich) supplemented with 10 % fetal bovine serum (FBS, Gibco) and gentamicin (40 mg/ml, Krka Poland Sp. z o.o.) in constant 80 % humidity atmospheres and 5 % carbon dioxide concentration at 37 °C (Heracell™ 150i, Thermo Scientific). The cells for experiments were prepared by trypsinization with a 0.25 % trypsin-EDTA solution (Sigma-Aldrich) in PBS. Then, trypsin was neutralized by the addition of an equal amount of culture medium, and cells were counted in a Bürker chamber. 2×10^5 cells in 2 ml medium were seeded per each well of 12-well plates (Biologix) on

PEDOP, PEDOP/Tc and Pt-coated glass slides, and were cultured for 48 h. After that time, 1 ml of 0.25 % trypsin-EDTA solution (Sigma-Aldrich) was added to each well. The resulting cell suspensions were centrifuged at 1500 rpm for 3 min.

2.8. MTT viability assay

For cytotoxicity analysis, MTT (3-[4,5-dimethylthiazol-2-yl]-2, 5-diphenyltetrazolium bromide) assay based on mitochondrial dehydrogenase enzyme activity was performed. 50 μl of MTT solution (0.05 mg/ml in phenol red and FBS free DMEM-F12; PAA) was added to centrifuged cells previously grown on the surfaces of PEDOP, PEDOP/Tc, Pt-coated glass slide and in the empty well of 12-well plates. After 1–2 h in a CO_2 incubator, MTT solution was removed and formazan crystals were dissolved in 400 μl acidic isopropanol. The absorbance of solutions was measured spectrophotometrically at 570 nm, using a multi-well plate reader SYNERGY4 (BioTek Instruments, USA).

2.9. Assessment of a cell cycle

To analyze the cell cycle of B35 neuroblastoma cells, a flow cytometer (Becton Dickinson Aria III) was employed. Cells after centrifugation were washed with 500 μl PBS and centrifuged again. Finally, the cells were stained with 250 μl of hypotonic buffer (comprising 100 μg/mL PI in PBS, 5 mg/L citric acid, 1:9 Triton-X solution, 100 μg/mL RNase in PBS, from Sigma, Poznan, Poland), DNA levels were assessed by fluorescence measurements using BD FACSAriaTM III sorter (Becton, Dickinson and Company, Franklin Lakes, NJ, USA) at a PE configuration (547 nm excitation laser line; emission: 585 nm).

2.10. Apoptosis analysis

FITC Annexin-V Apoptosis Detection Kit with PI (Bio Legend) was used to assess the number of necrotic and apoptotic cells cultured on PEDOP, PEDOP/Tc, Pt-coated glass slides, and an empty well. 50 μl of Annexin V Binding Buffer, 2.5 μl of FITC Annexin V and 10 μl propidium iodide (100 μg/ml) were added to cells collected after 48 h of culture. Next, the samples were vortexed gently and incubated in dark for 20 min at room temperature (25 °C). Before measurement, 250 μl of Annexin-V Binding Buffer was added to each tube. The fluorescence of PI (necrotic cells) was detected at the configuration for PE channel, and for Annexin-V FITC-conjugated antibody (apoptotic cells) at FITC channel configuration (488 nm excitation laser line; emission: LP mirror 503, BP filter 530/30).

2.11. Imaging of rat neuroblastoma cells

To visualize the morphology of cells cultured on PEDOP, PEDOP/Tc, and Pt-coated glass, SEM microscopy (Phenom ProX) was used. Similarly as for imaging of bacteria, neuroblastoma cells were fixed using 3 % glutaraldehyde (Fisher BioReagents) for 24 h. Analogously, cells were washed three times with deionized water and dehydrated by immersing the samples in the solutions of ethanol (Acros Organics) with increasing concentrations (30 %, 50 %, 70 %, 80 %, 90 %, 95 %, 99.8 %) for 10 min each, and dried 24 h at 50 °C. Then, samples were sputter-coated with a gold layer (20 min, 20 mA; Q150R Quorum Technologies) and images were taken at 10 kV at the magnifications of 3000 × .

2.12. Statistical analysis

The statistical analysis was based on a *t*-test and a p-value < 0.05 was considered as statistically significant. All tests were performed in triplicate for all materials in all timepoints under the same conditions. The results were expressed as a mean value ± standard deviation.

3. Results

3.1. Electrochemical polymerization and drug immobilization

CV curves presenting the process of electrochemical polymerization of EDOP in the absence and presence of Tc were shown in Fig. 1. In both datasets, an irreversible oxidation peak associated with monomer oxidation was observed in the first potential cycle at the potential of approx. 0.7 V vs. Ag/AgCl. The increasing currents observed for both matrices during consecutive CV cycles exemplified the formation of conducting polymer films. It could be noticed that after completing 25 CV cycles, different areas under CV curves for PEDOP and PEDOP/Tc were achieved, giving slightly higher charge transferred in PEDOP/Tc when compared with a pristine PEDOP.

3.2. Drug release efficiency

To estimate a total amount of reversibly immobilized drug, PEDOP/Tc matrix was subjected to a reduction potential sufficiently low to cause polymer shrinkage and release of Tc. Analyzing the effect of different Tc concentrations (1–20 mM) on drug release efficiency of PEDOP/Tc matrices (Fig. 2A), it was found that the highest amount of released Tc was related to PEDOP/Tc electropolymerized for 25 CV cycles from a solution containing 5 mM of Tc (123.48 ± 12.31 μM). Both the decrease in the initial Tc concentration and its further increase did not increase drug release efficiency.

Also the number of CV cycles of an electrodeposition process played a key role in tailoring drug release efficency. The dependence of the drug release efficiency on the polymer films grown at a constant Tc concentration of 5 mM for 15–100 CV cycles (Fig. 2B) indicated that the lowest amount of drug was released from a polymer layer grown for 15 cycles (7.83 ± 2.29 μM), and this amount was much lower as compared with the drug release efficiency from a layer of PEDOP/Tc grown for 25 CV cycles (123.48 ±

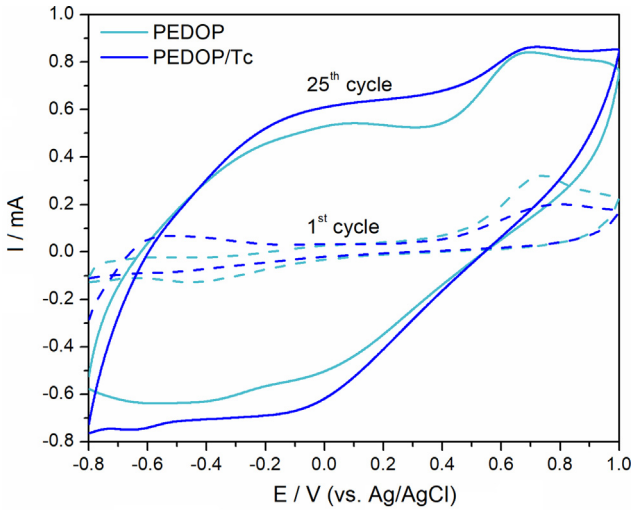

Fig. 1. Electrochemical fabrication of PEDOP and PEDOP/Tc. Current (I/mA) vs. potential (E/V vs. Ag/AgCl) curves showing 1st (dashed line) and 25th (solid line) cycle of an electropolymerization process of 10 mM EDOP in PBS (teal line), and 10 mM EDOP in PBS in the presence of 5 mM Tc (blue line); scan rate = 0.1 V/s.

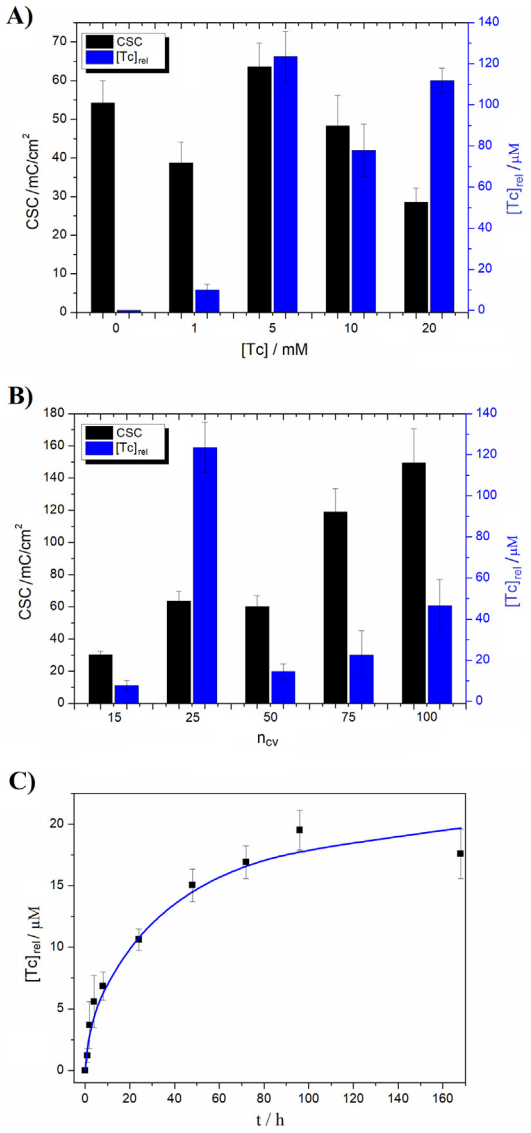

Fig. 2. Evaluation of capacitive properties and drug release efficiency of PEDOP/Tc. Charge storage capacity (CSC/mC/cm^2) values and concentrations of Tc released from PEDOP/Tc matrices ([Tc]$_{rel}$/µM) formed for 25 CV cycles in the presence of different concentrations of Tc ([Tc]/mM) (A), and formed at [Tc] = 5 mM for different number of CV cycles (n_{CV}) (B), n = 3. Drug elution profile of spontaneous Tc release from PEDOP/Tc ([Tc] = 5 mM, n_{CV} = 25); dots are the experimental values, and lines represent the corresponding fitting curve calculated basing on Avrami's kinetic model (C).

12.31 µM). However, a further increase in the number of CV cycles was not associated with the increase in drug release efficiency.

Consequently, an optimised protocol of PEDOP/Tc fabrication was developed, and it consisted on the electropolymerization of EDOT in the presence of 5 mM Tc for 25 CV cycles. A spontaneous Tc elution profile from optimized PEDOP/Tc matrix (Fig. 2C) indicated a rapid increase in Tc concentration during first 4 h of release, followed by its gradual increase until day 4, when a maximum Tc concentration was noted (19.5 ± 1.6 µM). Tc release profile was found to match the Avrami's kinetic model (R^2 = 0.95), exhibiting a rate constant (k) of 0.095 1/h and the exponent of release (n) of 0.66.

3.3. Electrochemical characterization

Analyzing the effect of different initial Tc concentrations (1–20 mM) on the capacitance of PEDOP/Tc matrices (Fig. 2A & **Figure S1A**), it was found that a maximum value of a charge storage capacity, CSC, was achieved for PEDOP/Tc polymerized from the solution containing 5 mM Tc (63.65 ± 6.05 mC/cm^2), and this value was not statistically different from CSC of a pristine polymer (54.22 ± 5.76 mC/cm^2). With a further increase in Tc concentration, CSC values of PEDOP/Tc decreased, reaching 48.35 ± 7.88 mC/cm^2 for 10 mM Tc and 28.51 ± 3.76 mC /cm^2 for 20 mM Tc, respectively.

CSC was also found to vary with the number of CV cycles used for the process of electropolymerization (Fig. 2B & **Figure S1B**), starting from CSC of 30.28 ± 2.12 mC/cm^2 for PEDOP/Tc grown for 15 CV cycles, and reaching the value of 149.54 ± 21.04 mC/cm^2 for PEDOP/Tc grown for 100 CV cycles.

EIS analysis (Fig. 3A) indicated that covering a Pt-coated electrode with a PEDOP layer decreased the impedance of the system by one order of magnitude, particularly in a low frequency region (<100 Hz). Although PEDOP/Tc was also found to decrease the impedance of the electrode, this change was not as notable as for pristine PEDOP. Upon the analysis of a phase angle profile (Fig. 3B), a shift in the frequency peak was observed from 2 Hz for Pt, to 15 Hz for PEDOP. By fitting the experimental data to the equivalent electrical circuit model (Randles circuit) [42], it was possible to calculate electrical properties of Pt-coated electrode, PEDOP and PEDOP/Tc, including solution resistance (R_S), charge transfer resistance (R_{CT}), Warburg element (A_w) associated with the diffusion of charge through electrode, and constant phase element (comprising of two parameters, P and n) of the electrode/-

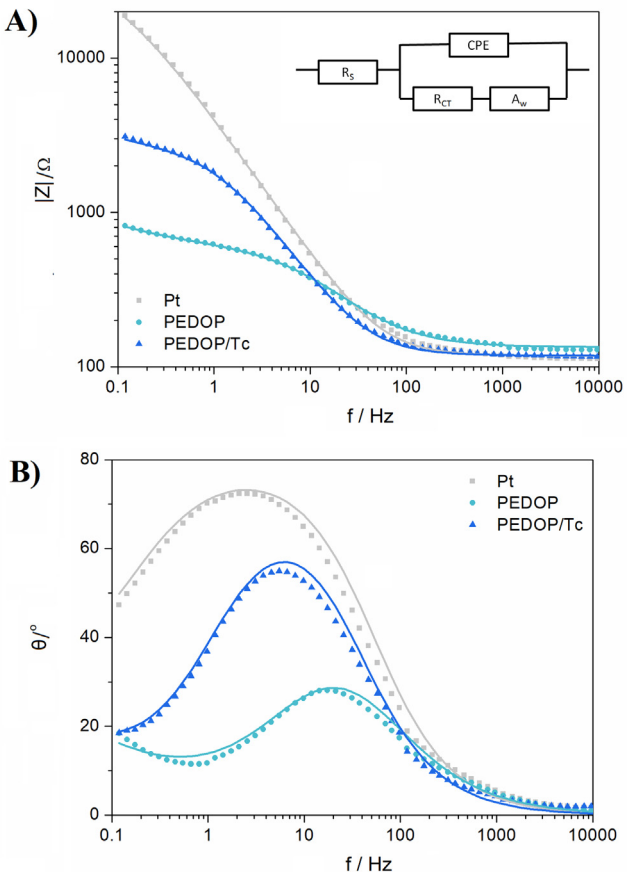

Fig. 3. Impedance behaviour of PEDOP and PEDOP/Tc, compared with a Pt-coated glass slide. EIS results in the form of Bode plots of impedance modulus (|Z|/Ω) vs. frequency (f/Hz) (A) and a phase angle (θ/°) vs. frequency (f/Hz) (B) for PEDOP and PEDOP/Tc, as well as a bare Pt electrode; dots represent experimental data, while lines represent simulated results. Equivalent circuit model used for the fitting of EIS data is presented as an inset.

solution interface (**Table S1**). The model resulted in a good fit between the experimental and simulated data ($\chi^2 < 0.005$).

Even though the solution resistance was almost identical for all the samples, a significant decrease in the charge transfer resistance was noted when a Pt-coated electrode (R_{CT} = 24.8 ± 3.9 kΩ) was covered with a layer of PEDOP/Tc (R_{CT} = 2 416 ± 141 Ω) or PEDOP (R_{CT} = 488 ± 11 Ω). Also a Warburg diffusion element was found to decrease greatly for polymer-coated electrodes. The analysis of constant phase element parameters revealed the decrease in n value and the increase in P value when a Pt-coated electrode was covered with a layer of PEDOP/Tc or PEDOP.

When subjected to the recurrent biphasic potential pulse (Fig. 4), both PEDOP and PEDOP/Tc were found to decrease the polarizaiton of the electrode when compared with a Pt-coated control for all investigated charge densities (**Figure S2**). For the charge density of 36 μm/cm^2, for instance, the maximum anodic potential reached 0.6 V for Pt, and only 0.35 V and 0.25 V for PEDOP/Tc and PEDOP, respectively. Also, the voltage profile within a single pulse was found to be flat for both polymers. In contrast, a voltage profile of a Pt-coated electrode displayed an initial ohmic drop followed by a more gradual polarization of the interface. However, the balance between the magnitude of cathodic and anodic pulse was evidently disturbed for Pt electrode, for which more charge was transferred within an oxidation pulse. For PEDOP and PEDOP/Tc, the amount of charge injected during a negative and a positive pulse was approximately the same.

3.4. Surface characterization

FTIR spectrum of PEDOP/Tc (Fig. 5**A**) exhibited typical bands for PEDOP, including the band at approximately 1476 cm^{-1} assigned to the asymmetric stretching bond of C = C. The absorption bands at 1436 cm^{-1} and 1370 cm^{-1} were related to the inter-ring stretching bond of C-C. The typical band at around 1077 cm^{-1} was assigned to C-O-C, while 1240 cm^{-1} belonged to stretching of C–N [57,58]. Also the signals characteristic for Tc (Fig. 5**B**) were visible in the spectrum of PEDOP/Tc, including a band at 1449 cm^{-1} which was assigned to the amide bonds. Besides, 1640 cm^{-1} and 1580 cm^{-1} bands were observed as typical to the C = O stretching in Tc rings, while a band at 1310 cm^{-1} was related to the deformation of OH [59].

The surface morphology of PEDOP, PEDOP/Tc, and a Pt-coated glass slide was characterized by scanning electron microscopy (Fig. 6) and atomic force microscopy (**Figure S3**). Both polymers

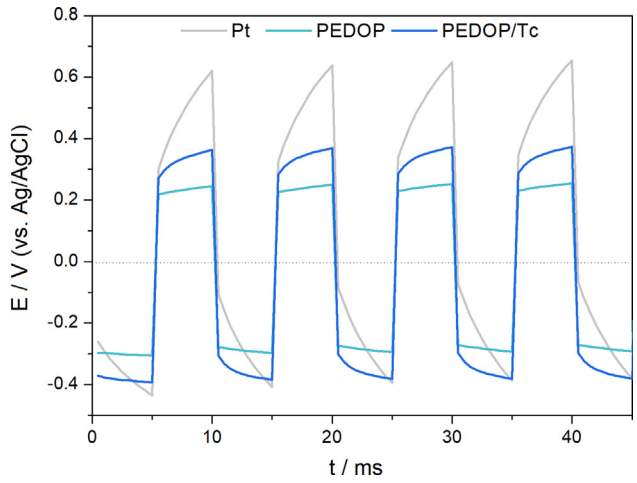

Fig. 4. Voltage profile during charge injection. Potential (E/V vs. Ag/AgCl)) vs. time (t/ms) curves recorded for a current density of 36 μC/cm^2 in PBS for PEDOP, PEDOP/Tc and Pt-coated electrodes.

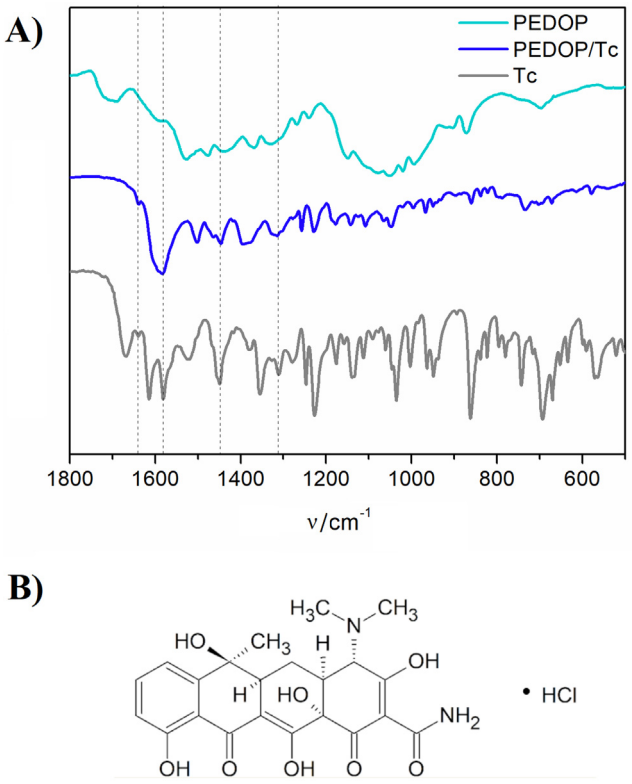

Fig. 5. Chemical characterization of polymer surface. Transmittance vs. wavenumber (ν/cm^{-1}) FTIR spectra of PEDOP, PEDOP/Tc, and Tc; marked regions correspond to bands characteristic for Tc (A), and a chemical structure of tetracycline hydrochloride (B).

exhibited a spongy-like, highly porous morphology, with an arithmetic mean height (S_a) of 4.36 ± 0.52 μm and 4.13 ± 0.90 μm for PEDOP and PEDOP/Tc, respectively – much higher than S_a of a Pt-coated glass slide (S_a = 0.21 ± 0.01 μm). An AFM-derived roughness (R_{rms}), was much smaller than S_a, with the values of 5.1 ± 0.5 nm, 1. 5 ± 0.2 nm, and 2.0 ± 0.3 nm noted for a Pt-coated glass slide, PEDOP and PEDOP/Tc, respectively, The wettability of the investigated surfaces was determined by contact angle (θ) measurements. The results indicated that Pt-coated glass slides exhibited the most hydrophilic character (θ = 35.2° ± 10.5°). The rough surface of the polymers slightly increased the contact angle values reaching θ of 38.2° ± 4.3° and 45.8° ± 8.5° for PEDOP and PEDOP/Tc, respectively.

3.5. Adhesion strength

The adhesion forces of PEDOP and PEDOP/Tc to the Pt-coated glass slide, as well as a layer of Pt to a glass substrate, were analysed by means of a scratch test. The investigation of cracks (**Figure S4**) allowed to identify two critical loadings, LC2 (Pt) – loading at which Pt layer was completely damaged, and LC (P) – loading at which a polymer layer (either PEDOP or PEDOP/Tc) was damaged entirely (Table 1). The strength of adhesion of both PEDOP and PEDOP/Tc was found to be similar (approx 1.5 N), and was three times lower than the strength of adhesion between a layer of sputter-coated Pt and a glass slide.

3.6. Antimicrobial activity

Antimicrobial activity of PEDOP/Tc was determined against *E.coli* as a model bacterial strain, and was based on SEM

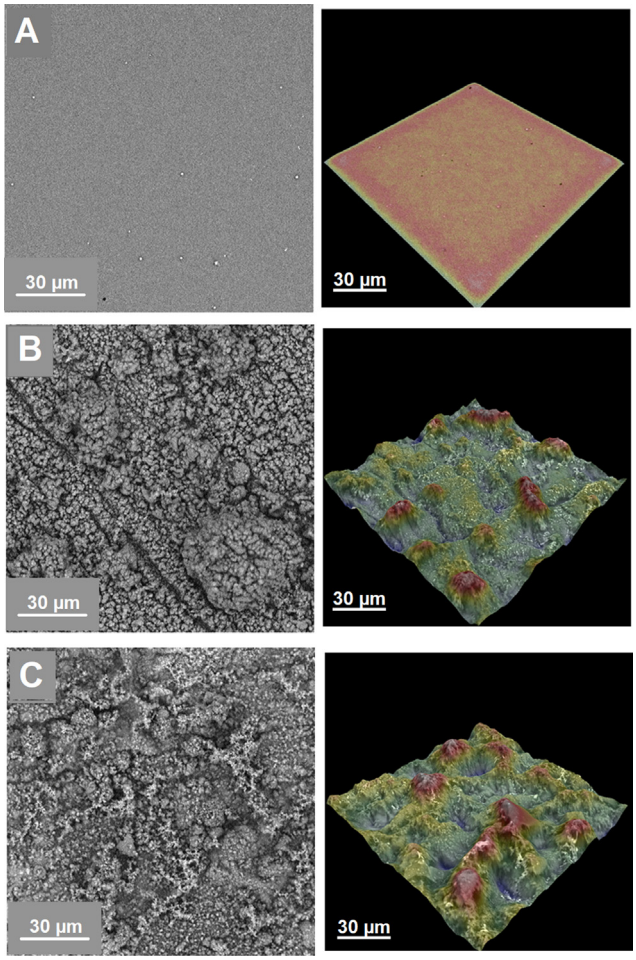

Fig. 6. Surface morphology. 2D SEM micrographs and 3D SEM profiles of Pt-coated glass slide (A), PEDOP (B), and PEDOP/Tc (C), scale bar is 30 μm.

Table 1
The strength of adhesion of PEDOP and PEDOP/Tc to the Pt-coated glass slide; LC2(Pt) – loading at which Pt layer was damaged, LC(P) – loading at which a polymer layer was damaged; n = 3.

Critical loading	Pt-coated glass slide	PEDOP	PEDOP/Tc
LC2(Pt), N	4.1 ± 0.5	4.9 ± 1.6	3.3 ± 0.5
LC(P), N	–	1.5 ± 0.1	1.3 ± 0.2

measurements (Fig. 7A-C), by a quantitative analysis of bacterial density (number of bacterial cells per 200 μm^2) (Fig. 7D) and bacterial dimensions (length (**Figure S5A**), width (**Figure S5B**), and aspect ratio (Fig. 7E)) after 3 h, 24 h and 48 h of culture. Even though the high roughness of PEDOP and PEDOP/Tc could potentially obstruct the observation of bacteria within the pores of the coating, the use of high magnification (10 000 ×) SEM images and confocal fluorescent microscope images of different layers allowed to provide a reliable analysis.

In the initial lag phase (after 3 h of culture in a closed batch system), when bacteria attached to the surface, the density of *E.coli* adhering to PEDOP/Tc was lower than that for a Pt-coated control and stayed at a similar level in each time point. The presence of Tc limited the adherence of bacterial cells in the initial lag phase (0.7 ± 0.1 cells/200 μm^2 related to 11.5 ± 1.0 cells/200 μm^2 noted for control) and their subsequent multiplication after 24 h (0.9 ± 0.3 cells/200 μm^2) and 48 h (1.9 ± 0.5 cells/200 μm^2). Interestingly, pristine PEDOP was not found to inhibit bacterial growth, seeming to support the expansion of bacteria. After 3 h, the density of bacterial cells on PEDOP (10.7 ± 0.9 cells/200 μm^2) was similar to the density of bacterial cells on a Pt-coated glass slide. After 24 h, however, in the exponential growth phase, bacterial density on PEDOP noticeably increased reaching 17.4 ± 2.0 cells/200 μm^2 (while the density of 9.7 ± 1.4 cells/200 μm^2 was noted for a control). After 48 h (death phase), a decrease in bacterial density was observed on both PEDOP (4.9 ± 0.7 cells/200 μm^2) and Pt (3.8 ± 0.5 cells/200 μm^2).

SEM microscopy allowed for a more detailed investigation of cell morphology. In general, dimensions of spherocylindrical *E.coli* vary in a range from 0.8 to 1 μm in diameter and from 2 to 4 μm in length depending on available nutrition [60]. In our study, after the first 3 h and 24 h, an average length (**Figure S5A**) and width (**Figure S5B**) of adhered bacterial cells depended on the investigated surfaces, with the longest and widest cells observed on a Pt-coated glass slide. However, after 48 h of culture, a significant increase in both length and width on PEDOP/Tc was observed. Also, the calculation of an aspect ratio, determining the circularity of bacterial cells, indicated a significant bacterial cell elongation on PEDOP/Tc.

LIVE/DEAD assay allowed to assess the viability of *E.coli* cells on Pt-coated glass slides, PEDOP and PEDOP/Tc after 3 h, 24 h and 48 h (**Figure S6** & Fig. 7F). After 3 h of incubation, the highest percentage of live bacterial cells was noted on the surface of a Pt-coated glass slide (61.8 ± 6.4 %), then less than half of bacterial population on PEDOP/Tc (45.6 ± 2.4 %) and pristine PEDOP (25.8 ± 4.0 %). Subsequently, after 24 h PEDOP/Tc presented the highest percentage of live cells (53.4 ± 1.2 %) despite the very low density of bacteria. A gradual increase in viability of bacterial cells was observed on pristine PEDOP (36.7 ± 2.6 %), which was 42.2 % higher than in the adhesion phase (3 h). However, a decrease in the percentage of live cells to 43.8 ± 5.8 % was observed on a Pt-coated glass slide. 48 h of culture was the time when a further increase in cell viability on the surface of pristine PEDOP was noticed, reaching the value of 48.8 ± 0.5 %. The viability of bacteria on a Pt-coated glass slide did not change significantly, remaining at a constant level (47.4 ± 0.8 % of live cells). Simultaneously, a notable decrease in the percentage of live cells concerning previous stages was determined for PEDOP/Tc (21.4 ± 2.4 %).

3.7. Neural cell cytocompatibility

Cytocompatibility of PEDOP and PEDOP/Tc concerning a Pt-coated glass slide and an empty well as control was determined towards rat neuroblastoma cell line (B35) using MTT assay, in which the amount of reduced MTT was proportional to the metabolic activity of the cell's mitochondria, and to the number of metabolically active cells in the population. As shown in Fig. 8A, PEDOP/Tc exhibited similar cell viability (83.7 % ± 4.3 %) as a Pt-coated glass slide (86.2 % ± 4.4 %), both fulfilling the criteria of biocompatibility [61]. Simultaneously, for pristine PEDOP the viability of B35 cells was lower (59.3 % ± 3.6 %), and could be indicative of moderate cytotoxicity of this material.

Flow cytometry was employed to evaluate the effects of PEDOP, PEDOP/Tc, and Pt-coated glass slide on the B35 cell cycle after 48 h of treatment. The cell cycle (Fig. 8B) is the process of generating genetically identical daughter cells. It consists of two stages, including the G0, sub-G1, G1, S, G2 interphase, and M mitosis during which karyokinesis and cytokinesis take place. The sub-G1 phase includes cells that are dead as a result of apoptosis or necrosis. In the G1 phase, the cells are metabolically active and the synthesis of lipids and proteins takes place. While in the G0 phase cells are metabolically active but do not divide. S phase launches DNA replication and histone synthesis, and G2 contains the synthesis of lipids and proteins necessary in mitosis. Finally, in the M phase

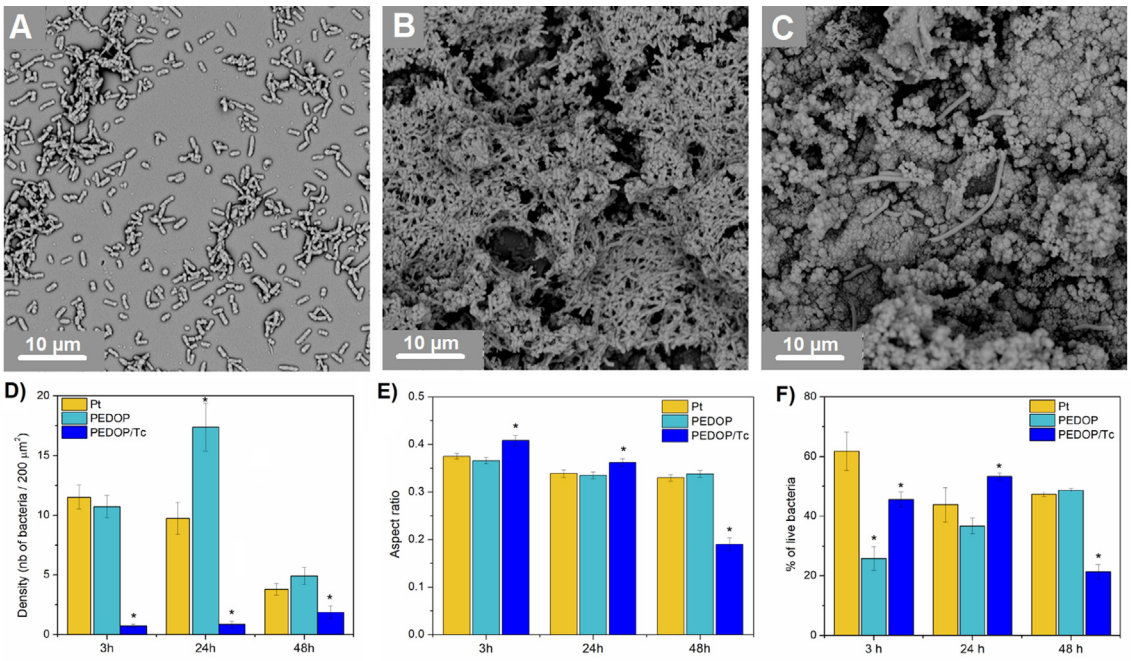

Fig. 7. Antibacterial activity of PEDOP and PEDOP/Tc. SEM micrographs of *E.coli* on the surface of a Pt-coated glass slide (A), PEDOP (B) and PEDOP/Tc (C) after 48 h of culture; density of *E.coli* (number of bacterial cells per 200 μm^2), * = $p < 0.05$, n = 3 (D), and average aspect ratio calculated from corresponding SEM micrographs, * = $p < 0.05$, n = 80 (E). Percentage of live bacterial cells on Pt-coated glass slides, PEDOP and PEDOP/Tc after 3 h, 24 h and 48 h, * = $p < 0.05$, n = 8 (F).

cell's growth and final division take place. As shown in Fig. 8C, no significant differences in the distribution of the cell cycle phases were observed when compared to the untreated cells. For all samples, the highest number of cells (over 60 %) were placed in the G0/G1 phase, about 20 % in the G2/M phase, and about 10 % in the other two phases (sub-G1 and S). Also, the results for the Pt-coated glass slide were almost identical to the control in each phase of the cell cycle. For PEDOP, the results were also similar, however, for PEDOP/Tc the obtained data were slightly more varied especially in sub-G1 and G2/M phases. Cells were not arrested in the G0/G1 phase, indicating their normal development on the surfaces. Analysis of the sub-G1 fraction showed a slightly higher number of damaged cells for PEDOP/Tc.

As cell cycle analysis indicated a presence of damaged cells in a population, it was necessary to distinguish apoptosis as programmed, physiological cell death, from necrosis which acts as an uncontrolled effect caused by external agents. The use of Annexin-V apoptosis assay and flow cytometry enabled the observation and differentiation of normal, early-stage apoptotic, late apoptotic, and necrotic cells on PEDOP, PEDOP/Tc, and a Pt-coated glass slide as well as a control well after 48 h of culture (Fig. 8D & **Figure S7**). The experimental results showed that normal cells were the most abundant on control samples: an empty well (82.4 % ± 0.4 %) and a Pt-coated glass slide (74.0 % ± 0.7 %). The highest percentage of early apoptotic cells was observed for PEDOP (6.7 % ± 1.8 %), and significantly less for a Pt-coated glass slide (2.9 % ± 0.6 %) and PEDOP/Tc (1.9 % ± 0.1 %). For late apoptosis, again, the highest percentage was observed for PEDOP (30.8 % ± 0.4 %), and lower for PEDOP/Tc (23.9 % ± 1.8 %) and Pt-coated glass slide (19.8 % ± 1.3 %). Necrotic cells were scarce in each case, with only 5.3 % ± 1.7 % observed for PEDOP/Tc and 1.1 % ± 0.4 % for pristine PEDOP.

SEM micrographs of B35 rat neuroblastoma cells cultured on a Pt-coated glass slide, PEDOP, as well as PEDOP/Tc were presented in Fig. 9A-C. It could be noticed, that neural cells, when cultured on different substrates, differed in size as well as the level of networking (Fig. 9C-D). Due to the favourable surface roughness of polymeric substrates, cells were found to be anchored on both PEDOP and PEDOP/Tc (as marked with a rectangular shape in Fig. 9-B-C). A close interaction of neurons with polymers was observed, with neurites climbing the surface of PEDOP and PEDOP/Tc and penetrating their structure. Notably, neurons cultured on PEDOP/Tc exhibited highly complex and evenly distributed neurites creating interconnected networks. On the other hand, neurons cultured on pristine PEDOP were found to form clusters with shorter neurites (Fig. 9D) and limited branching (Fig. 9E).

4. Discussion

Identifying the major limitations of noble metal-based neural interfaces as an exacerbation of the inflammatory response and an easy surface colonization by bacterial cells, we aimed to provide a coating combining neuroprotective and antibacterial functionalities with excellent electrochemical characteristics. Basing on our previous experience in designing protective neural coatings [33,39,40,42,43], we have hypothesised that PEDOP should serve as an excellent electroactive carrier for Tc, an antibiotic known from its neuroprotective functions [44,62–64]. To verify our hypothesis, we have fabricated Tc-loaded PEDOP matrices, and extensively examined their properties, including electrochemical performance, surface morphology, adhesion strength, antibacterial effects against *E.coli* and neuroprotective effects towards B35 cells.

Electrochemical oxidation process enabled to obtain a pristine polymer matrix (PEDOP) as well as a polymer with immobilized antibiotic – tetracycline (PEDOP/Tc). In both cases, the oxidation of EDOP occurred at the potential of 0.7 V, which was approx. 0.5 V lower than the potential typically observed for the oxidation of its more famous "relative", EDOT [33], confirming that the electron-rich structure of EDOP facilitates the process of electropolymerization [65]. As polymerization medium consisted of a phosphate-buffered saline (PBS), it is expected that PEDOP was primarily doped with chlorides, and co-doped with phosphates. Since PBS is known to simulate physiological conditions, it has been

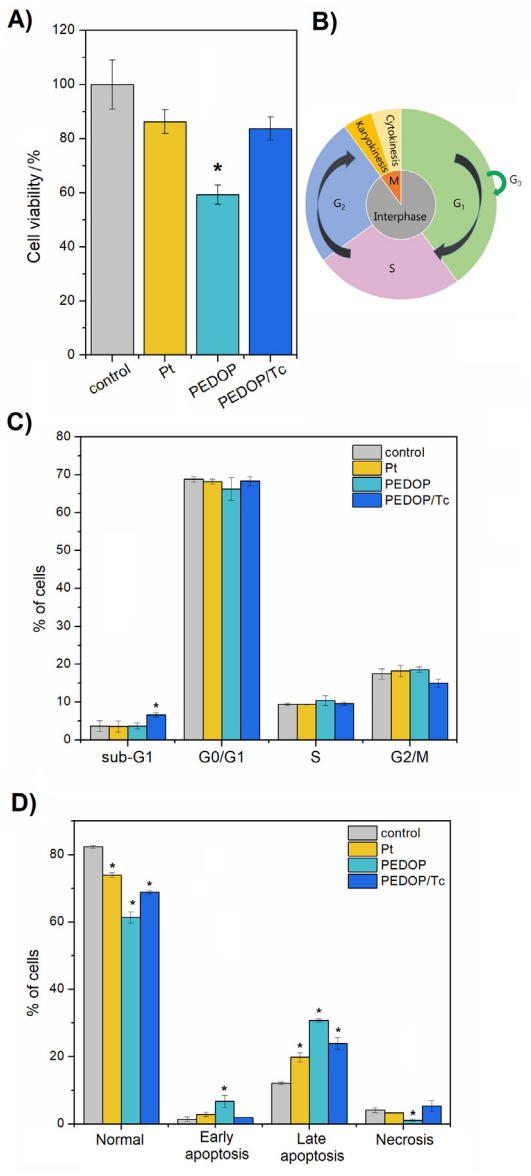

Fig. 8. Neuroprotective effects of PEDOP and PEDOP/Tc. Cells viability assessed through a MTT assay (after 48 h of culturing B35 cells in an empty well (untreated control), as well as on the surface of Pt-coated glass slide, PEDOP and PEDOP/Tc (A), a diagram representing a typical cell cycle (B), cell cycle analysis (C), and percentage of cells in each phase (D); for each * = $p < 0.05$ (vs. control), n = 9.

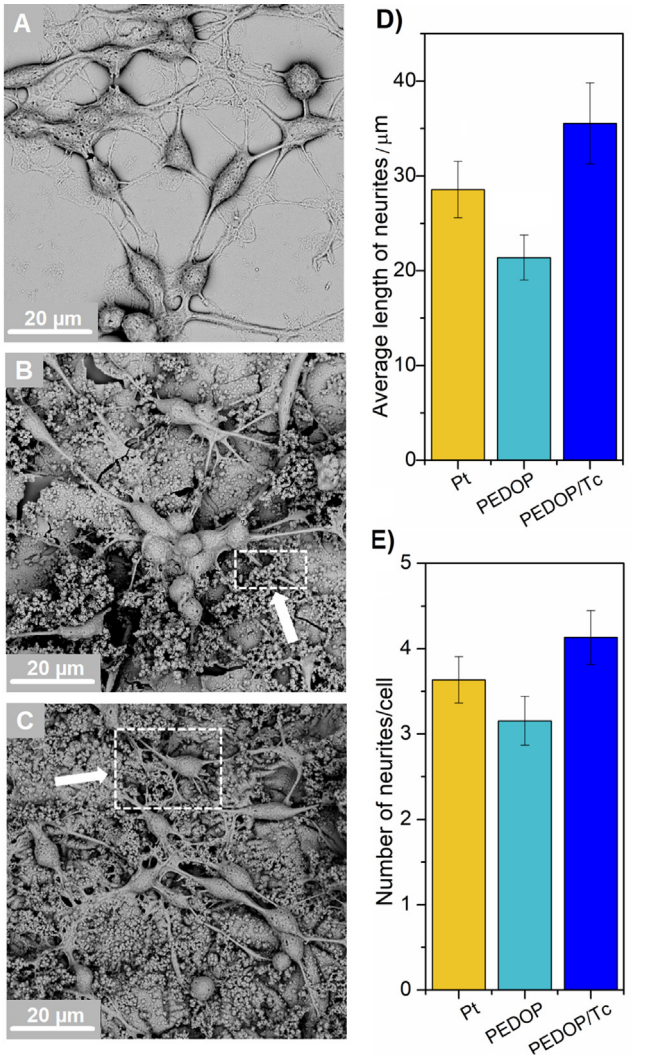

Fig. 9. Interactions between B35 cells and polymer surface. SEM micrographs of B35 cells on a Pt-coated glass slide (A), PEDOP (B) and PEDOP/Tc (C) after 48 h of culturing; the average length of neurites (D), and an average number of neurites/cell (E).

hypothesized that PEDOP electrodeposited in the presence of PBS should be stable upon implantation. Although Tc was present in the polymerization solution in a form of a hydrochloride salt, it is supposed that due to its bulky nature, the immobilization of Tc relied on physical entrapment rather than ionic interactions, as shown previously [33].

The fact that at the final CV cycle higher charges were transferred through PEDOP/Tc than PEDOP suggested that the presence of Tc affected the capacitance of PEDOP. This effect could be associated with a high molecular size of Tc, since large molecules can affect polymer density and thus modify its physicochemical properties [66]. To further investigate this issue, a parameter called a charge storage capacity (CSC) was calculated, since it allows to determine the maximum amount of charge stored in a polymer matrix. Noticeably, materials possessing high CSC values are found to enhance neural stimulation and recording [67,68]. Intrestingly, the highest CSC was achieved for PEDOP/Tc deposited from a solution containing 5 mM Tc (63.65 ± 6.05 mC/cm^2), and this sample outperformed pristine PEDOP, as well as other previously studied drug-loaded conducting materials, such as PEDOP/ciprofloxacin (20.7 ± 1.6 mC/cm^2), PEDOP/quercetin (41.9 ± 3.5 mC/cm^2) [40], PEDOP/ibuprofen (13.7 mC/cm^2) [39], or PEDOT/Tc (19.15 ± 6.09 mC/cm^2) [33]. Nevertheless, higher Tc concentration did not lead to further increase in CSC values. A similar trend was described previously in the literature, e.g. in the works examining the effect of ibuprofen concentration on the electropolymerization of pyrrole [56] as well as EDOP [39]. In both cases, the inhibition of a polymerization process and a decrease in release efficiency was observed for drug concentration exceeding 15 mM, and was explained by the steric effects of drug molecules used as dopants.

Similarly to the results presented in other works [69,70], CSC values were found to steadily increase with the number of CV cycles. Therefore, electrochemical polymerization of EDOP could be considered as living polymerization, where the amount of formed polymer is determined by the accessibility of monomer and electrical charge. Still, it must be kept in mind that while CSC describes the electroactivity of a conducting polymer coating, it does not fully reflect its ability to immobilize and release drug molecules.

When immobilizing a drug into the polymer structure, it is necessary to determine the actual amount of trapped biomolecules that can be released. Previous studies [29] reported that non-optimized electropolymerization conditions may lead to the formation of a so-called "dead volume" – the situation when conducting polymer matrix is too thick to allow the release of drug. In this study, the use of a polymerization solution containing 5 mM Tc enabled to fabricate a material able to carry the highest amount of Tc (up to 59.4 mg/l), which significantly exceeded the minimum inhibitory concentration (16 μg/l) predicted for resistant bacteria [71]. Moreover, this concentration was achieved for the polymer layer deposited during 25 CV cycles, and a further increase in the number of cycles was not associated with the increase in drug release efficiency, probably due to the aforementioned "dead volume" effect.

PEDOP/Tc was also found to release Tc spontaneously, in the absence of an electrical trigger. Even though the achievable Tc concentrations (9.4 mg/l) were lower than in case of an electrically-triggered release, they were much above a therapeutic level. Fitting the experimental data to the Avrami's kinetic model, which is frequently used to describe the release kinetics of conducting polymer-based drug delivery systems [43,54,72], revealed a relatively low value of drug release constant (0.095 1/h), suggesting prolonged time of release. The fact that the exponent of release (n) was close to 0.5 indicated that the release of Tc from PEDOP/Tc has a diffusive character [73,74], which is consistent with previous studies on conducting polymer-based drug delivery systems working under open circuit conditions [73].

Although the presence of PEDOP/Tc was found to greatly decrease the impedance and charge transfer resistance of Pt-coated electrodes, the effect was much more evident for pristine PEDOP, suggesting hindered electron transfer in the presence of Tc. Still, the charge transfer resistance of PEDOP/Tc was low enough to consider it as an interface able to enhance the performance of neural electrodes [75,76] and the detection of electrophysiological signals [77]. The analysis of a phase angle profile and constant phase element parameters indicated that particularly PEDOP acted as an imperfect capacitor (a decrease in n-value) exhibiting high capacitance (an increase in P value). A significant decrease in the value of a Warburg parameter suggested limited diffusion of faradaic current in the case of both PEDOP and PEDOP/Tc [78].

Ideally, neural electrodes should allow to deliver a stable, constant electrical signal for the whole duration of a stimulating pulse [79]. Voltage profiles recorded during a charge injection event equivalent to a biphasic pulse used in the treatment of neural disorders highlighted the non-ideality of a platinum-based neural interface. Pt electrode was found to deliver signal that was variable in time and consisted of an initial ohmic drop followed by a gradual polarization. Besides, enhanced interface polarization noted for a Pt-coated electrode could be considered as a sign of a low charge injection capacity of this material [52]. In contrast, both PEDOP and PEDOP/Tc displayed a stable performance with much lower initial ohmic voltage drop, which was not followed by additional polarization. Therefore, by using both polymers, and particularly PEDOP, it was possible to inject more charge without exceeding the electrochemical water window for the electrodes, which is a typical benefit of using conducting polymers as neural interfaces [80].

While designing neural interfaces it is crucial to consider mechanical interactions between the implant and the brain. The mechanobiology of brain function involves cellular processes generating the forces in the order of pN [81]. The major challenge for any neural interface would be, however, to maintain its integrity during the implantation. Although the insertion force is dependent on several parameters, including implant geometry, mechanical properties, and insertion speed, the typical forces applied during insertion are in the order of mN [82]. With the adhesion force of approx. 1.5 N, both PEDOP and PEDOP/Tc are expected to "survive" the process of implantation and remain stable in the body afterwards.

Apart from beneficial electrochemical characteristics, mechanical robustness and high drug content, antibacterial and neuroprotective interfaces should exhibit defined surface morphology. High roughness has a significant impact on neural applications, since it is known to lead to high effective surface area and lower electrode impedance [83]. Also, roughness is a crucial factor for cell attachment, because rough structures favor neuronal anchorage [84]. At the same time, rough surfaces could increase bacterial attachment and biofilm formation [85]. The issue of surface roughness is, therefore, a double-edged sword. Recent studies have suggested that by a careful manipulation with surface roughness, it is possible to fabricate surfaces facilitating cell attachment and limiting bacterial adhesion. Diaz et al [86] noticed that bacteria prefer to adhere to nanopatterned surfaces than smooth ones. Interestingly, the same bacteria were not found to adhere easily to micro-rough structures. Sorkin et al [84], on the other hand, demonstrated that cell attachment is favored if surface roughness matches the sizes of neurons. PEDOP and PEDOP/Tc were found to exhibit a complex microstructure with considerable smooth polymer aggregates densely located on the electrode, giving rise to highly rough surface. Because of the variability in surface roughness at different levels of magnification, it should be expected that PEDOP and PEDOP/Tc would be susceptible to the attachment of neural cells while preventing the adhesion of bacterial cells.

Also the evaluation of wettability plays a crucial role in material comparison. Based on previous reports [87–92], it is known that the hydrophilicity of the material is an important factor contributing to both cell adhesion as well as biofilm formation. In general, substrates with extremely hydrophobic or hydrophilic properties limit interactions between *E.coli* and surface. It is also known that hydrophobic bacteria are repelled by the hydrophilic surface due to electrostatic interactions [93]. Consequently, hydrophilic bacteria like *E.coli* should be more attracted to hydrophilic surfaces [94–96]. For instance, Yuan et al [87] demonstrated that moderate hydrophobicity (θ of 90°) facilitates bacterial cell adhesion. Also, neural cells were observed to exhibit the strongest adhesion to hydrophilic surfaces (θ of 55°) [97]. On the other hand, Wang et al [98], decided to cover PLGA/MWNCT scaffolds with poly-L-lysine to provide a hydrophilic environment, which resulted in effective attachment and proliferation of PC-12 and Schwann cells. As both PEDOP, PEDOP/Tc and Pt-coated glass slides are typically hydrophilic surfaces, they seem to serve as an extremely favourable environment for both neural cell attachment and bacterial biofilm development.

For the assessment of antimicrobial activity of PEDOP and PEDOP/Tc, *E.coli* was selected as a Gram-negative bacterial strain commonly inhabiting biomedical devices and causing nosocomial infections [99–102]. Microscopic observations of bacterial adhesion enabled us to perceive that pristine PEDOP exhibited promoting effect for bacterial attachment, while PEDOP/Tc showed a bacteriostatic effect. Moreover, bacterial dimensions (length, width and aspect ratio) calculated basing on SEM micrographs revealed significantly elongated cells on the surface of PEDOP/Tc. The change in bacterial dimensions was expected to be the result of the action of released Tc. Under constant conditions, bacteria usually maintain a uniform rod shape with an approximately permanent width and varying length during the cell cycle [103,104]. The presence of external factors, such as antibiotics, often leads to the occurrence of bacterial stresses causing disturbances in cell division. It can be observed as an elongation of bacterial cells which was described previously [105–107]. An inadequate amount of protein initiating the division process results in the formation of

filamentous cells while maintaining a constant width, which is reflected in the aspect ratio [108,109]. These observations, together with the results of bacterial density and dimension analysis, indicated that PEDOP/Tc exhibited a long-term antimicrobial activity.

In the first stage, the release of Tc led to the reduction in cell adhesion to the surface, elongation of bacterial cells, and a visible decrease in their viability. On contrary, pristine PEDOP strongly promoted bacterial cell adherence with a steady increase in their viability. The rough surface of PEDOP together with its hydrophilicity, as assumed, turned out to be favourable for bacterial colonization, especially when compared with a smooth surface of Pt-coated glass slide. Due to its ability to prevent the association of aminoacyl-tRNA with the bacterial ribosome, the incorporation of Tc into a conducting polymer matrix allowed to switch the bacterial growth promoting nature of PEDOP to bacteriostatic characteristics of PEDOP/Tc. Even though Tc is considered as bacteriostatic, it exhibits a slow bactericidal effect when its concentration exceeds 10–500 times the minimal inhibitory concentration (MIC) [110]. This was found to be a case for PEDOP/Tc, for which the maximum amount of released Tc was 3000 higher than MIC.

Neuroprotective functions of PEDOP/Tc were evaluated using a rat neuroblstoma B35 cell line, which exhibits almost normal karyotype and neuronal properties [111] and is frequently used as a model to analyse CNS neurons in culture, particularly in the research aimed to study signalling pathways that guide axonal outgrowth and cell motility [111–113], as well as neuroprotective activity [114,115]. The results of biological assays and SEM imaging clearly showed that the presence of Tc in PEDOP matrix had a beneficial effect on neural cell proliferation. As described previously [116–118], tetracyclines are a group of antibiotics with large therapeutic effects extended in a wide range of diseases, also possessing anti-inflammatory and neuroprotective functions [44,45,62,119]. The presence of Tc allowed diminishing the moderate cytotoxic effects of PEDOP matrix on B35 cells, highlighting neuroprotective effects of this antibiotic. Indeed, numerous *in vitro* and in *vivo models* [44–46,120,121] have shown that tetracyclines are able to prevent neural cell death by at least two mechanisms. The first one considers the ability of tetracyclines to attenuate innate and adaptive immunity through the inhibition of microglial activation and proliferation, induction of caspase-1 and inducible nitric oxide synthase, as well as induction of cyclooxygenase 2 [44]. Another proposed mechanism states that tetracyclines target mitochondrium and block the release of pro-apoptopic factors: cytochrome *c*, SMAC and an apoptosis-inducing factor [120,121]. Since in our study we used a single cell line, we expect that the observed neuroprotectice effects of PEDOP/Tc resulted from the blockage of the apoptopic cascades.

Besides, a close integration of neurons with PEDOP/Tc was observed through SEM analysis, with neurites climbing the surface of PEDOP and PEDOP/Tc and penetrating their structure. A similar effect observed previously for a bioinspired microcone-array-based living biointerface [122] was the consequence of the rough micro- and nanostructure of the surface, which should also play a key role in the case of neuronal anchorage to PEDOP/Tc. Another study [84] highlighted that a high level of integration can be realized particularly for surfaces for which roughness matches the diameter of neuronal processes. Although the diameter of a human neuron cell body (10–50 μm) is considerably larger than polymer structures present on the surface of PEDOP, the diameters of axon (1–25 μm) and neurite (fraction of a micrometer) [123] are comparable with polymer roughness. Consequently, neurons cultured on PEDOP/Tc were found to exhibit highly complex and evenly distributed neurites creating interconnected networks, which are essential for proper brain functionality [122,124]. Because a close integration between the electrode and tissue allows facilitating charge transfer enhancing the efficiency of treatment [125], PEDOP/Tc was shown as a perfect candidate to serve as a polymer coating for biomedical devices.

5. Conclusions

In this work, a conducting, antibacterial and neuroprotective polymer coating for biomedical devices was developed by immobilizing tetracycline into the poly(3,4-ethylenedioxypyrrole) matrix. Optimized material presented prominent electrochemical properties (CSC of 63.65 ± 6.05 mC/cm^2, low charge transfer resistance, and ability to deliver a stedy electrical signal), as well as high drug release efficiency (629.4 μg/cm^2 ± 62.7 μg/cm^2) and mechanical stability. PEDOP/Tc demonstrated a strong antimicrobial effect expressed through negligible adhesion, reduction in viability, and characteristic elongation of bacterial cells. In contrast, pristine PEDOP appeared to greatly promote bacterial attachment and development by providing favourable growth conditions. The protective effect of PEDOP/Tc film on neural cells was demonstrated by MTT, cell cycle, and apoptosis assay with the use of a rat neuroblastoma B35 cell line. Cell viability was significantly increased due to the presence of Tc, making PEDOP/Tc suitable for neural applications. What is more, PEDOP/Tc proved to lead to the increase in the number of neurites per cell as well as neurites length when compared with cells grown on Pt-coated glass slides and a pristine PEDOP layer. Consequently, PEDOP/Tc was shown as an appropriate candidate for neural interface applications, possessing advanced electrochemical properties coupled with effective antibacterial effect and high cytocompatibility.

Funding sources

This research was supported by the National Science Centre, Poland (SONATA 2016/23/D/ST5/01306, OPUS 2019/35/B/ST5/00995 and SONATA 2019/35/D/ST5/01136) and by the Silesian University of Technology, Poland (04/040/BK_21/0145 and 04/040/BKM20/0118, 04/040/BKM21/0178 and 04/040/RGJ21/0147).

CRediT authorship contribution statement

Dominika Czerwińska-Główka: Methodology, Investigation, Writing – original draft. **Magdalena Skonieczna:** Methodology, Investigation. **Adrian Barylski:** Investigation. **Sylwia Golba:** Investigation. **Wioletta Przystaś:** Supervision. **Ewa Zabłocka-Godlewska:** Supervision. **Sebastian Student:** Investigation. **Beata Cwalina:** Conceptualization, Writing – review & editing. **Katarzyna Krukiewicz:** Conceptualization, Methodology, Writing – review & editing, Supervision, Funding acquisition.

Declaration of Competing Interest

The authors declare that they have no known competing financial interests or personal relationships that could have appeared to influence the work reported in this paper.

Appendix A. Supplementary data

Supplementary data to this article can be found online at https://doi.org/10.1016/j.bioelechem.2021.108030.

References

[1] World Health Organisation, Neurological Disorders: Public Health Challenges, Switzerland, Geneva, 2006.
[2] B. Rubehn, T. Stieglitz, In vitro evaluation of the long-term stability of polyimide as a material for neural implants, Biomaterials. 31 (13) (2010) 3449–3458, https://doi.org/10.1016/j.biomaterials.2010.01.053.

[3] M. Asplund, H. von Holst, O. Inganäs, Composite biomolecule/PEDOT materials for neural electrodes, Biointerphases. 3 (3) (2008) 83–93, https://doi.org/10.1116/1.2998407.
[4] M. Lv, Y. Zhang, L.e. Liang, M. Wei, W. Hu, X. Li, Q. Huang, Effect of graphene oxide on undifferentiated and retinoic acid-differentiated SH-SY5Y cells line, Nanoscale. 4 (13) (2012) 3861, https://doi.org/10.1039/c2nr30407d.
[5] S.P. Lacour, G. Courtine, J. Guck, Materials and technologies for soft implantable neuroprostheses, Nat. Rev. Mater. 1 (2016) 16063, https://doi.org/10.1038/natrevmats.2016.63.
[6] H.-Y. Lai, L.-D. Liao, C.-T. Lin, J.-H. Hsu, X. He, Y.-Y. Chen, J.-Y. Chang, H.-F. Chen, S. Tsang, Y.-Y. Shih, Design, simulation and experimental validation of a novel flexible neural probe for deep brain stimulation and multichannel recording, J. Neural Eng. 9 (3) (2012) 036001, https://doi.org/10.1088/1741-2560/9/3/036001.
[7] A.E. Hess, J.R. Capadona, K. Shanmuganathan, L. Hsu, S.J. Rowan, C. Weder, D.J. Tyler, C.A. Zorman, Development of a stimuli-responsive polymer nanocomposite toward biologically optimized, MEMS-based neural probes, J. Micromech. Microeng. 21 (5) (2011) 054009, https://doi.org/10.1088/0960-1317/21/5/054009.
[8] E. Castagnola, A. Ansaldo, E. Maggiolini, T. Ius, M. Skrap, D. Ricci, L. Fadiga, Smaller, softer, lower-impedance electrodes for human neuroprosthesis: A pragmatic approach, Front. Neuroeng. 7 (2014) 1–17, https://doi.org/10.3389/fneng.2014.00008.
[9] M.R. Abidian, D.C. Martin, Experimental and theoretical characterization of implantable neural microelectrodes modified with conducting polymer nanotubes, Biomaterials. 29 (9) (2008) 1273–1283, https://doi.org/10.1016/j.biomaterials.2007.11.022.
[10] S.F. Cogan, Neural Stimulation and Recording Electrodes, Annu. Rev. Biomed. Eng. 10 (1) (2008) 275–309, https://doi.org/10.1146/bioeng.2008.10.issue-1.
[11] Z.J. Du, C.L. Kolarcik, T.D.Y. Kozai, S.D. Luebben, S.A. Sapp, X.S. Zheng, J.A. Nabity, X.T. Cui, Ultrasoft microwire neural electrodes improve chronic tissue integration, Acta Biomater. 53 (2017) 46–58, https://doi.org/10.1016/j.actbio.2017.02.010.
[12] J.K. Nguyen, D.J. Park, J.L. Skousen, A.E. Hess-Dunning, D.J. Tyler, S.J. Rowan, C. Weder, J.R. Capadona, Mechanically-compliant intracortical implants reduce the neuroinflammatory response, J. Neural Eng. 11 (5) (2014) 056014, https://doi.org/10.1088/1741-2560/11/5/056014.
[13] G. Lind, C.E. Linsmeier, J. Schouenborg, The density difference between tissue and neural probes is a key factor for glial scarring, Sci. Rep. 3 (2013) 2942, https://doi.org/10.1038/srep02942.
[14] F. Jahanmard, F.M. Dijkmans, A. Majed, H.C. Vogely, B.C.H. van der Wal, D.A.C. Stapels, S.M. Ahmadi, T. Vermonden, S. Amin Yavari, Toward Antibacterial Coatings for Personalized Implants, ACS Biomater, Sci. Eng. 6 (10) (2020) 5486–5492, https://doi.org/10.1021/acsbiomaterials.0c00683.
[15] D. Czerwińska-Główka, W. Przystaś, E. Zabłocka-Godlewska, S. Student, B. Cwalina, M. Łapkowski, K. Krukiewicz, Bacterial Surface Colonization of Sputter-Coated Platinum Films, Materials (Basel). 13 (2020) 2674, https://doi.org/10.3390/ma13122674.
[16] C. Vallejo-Giraldo, A. Kelly, M.J.P. Biggs, Biofunctionalisation of electrically conducting polymers, Drug Discov. Today. 19 (1) (2014) 88–94, https://doi.org/10.1016/j.drudis.2013.07.022.
[17] J. Kzhyshkowska, A. Gudima, V. Riabov, C. Dollinger, P. Lavalle, N.E. Vrana, Macrophage responses to implants: prospects for personalized medicine, J. Leukoc. Biol. 98 (6) (2015) 953–962, https://doi.org/10.1189/jlb.5VMR0415-166R.
[18] Z. Zhang, J. Nong, Y. Zhong, Antibacterial, anti-inflammatory and neuroprotective layer-by-layer coatings for neural implants, J. Neural Eng. 12 (4) (2015) 046015, https://doi.org/10.1088/1741-2560/12/4/046015.
[19] L.D. Soule, N. Pajares Chomorro, K. Chuong, N. Mellott, N. Hammer, K.D. Hankenson, X. Chatzistavrou, Sol-Gel-Derived Bioactive and Antibacterial Multi-Component Thin Films by the Spin-Coating Technique, ACS Biomater, Sci. Eng. 6 (10) (2020) 5549–5562, https://doi.org/10.1021/acsbiomaterials.0c01140.
[20] A.o. Zhuang, Q. Pan, Y. Qian, S. Fan, X. Yao, L. Song, B.o. Zhu, Y. Zhang, Transparent Conductive Silk Film with a PEDOT-OH Nano Layer as an Electroactive Cell Interface, ACS Biomater. Sci. Eng. 7 (3) (2021) 1202–1215, https://doi.org/10.1021/acsbiomaterials.0c01665.
[21] M.R. Abidian, D.-H. Kim, D.C. Martin, Conducting-polymer nanotubes for controlled drug release, Adv. Mater. 18 (4) (2006) 405–409, https://doi.org/10.1002/(ISSN)1521-4095.
[22] A. Magaz, B.F. Spencer, J.G. Hardy, X.u. Li, J.E. Gough, J.J. Blaker, Modulation of Neuronal Cell Affinity on PEDOT-PSS Nonwoven Silk Scaffolds for Neural Tissue Engineering, ACS Biomater. Sci. Eng. 6 (12) (2020) 6906–6916, https://doi.org/10.1021/acsbiomaterials.0c01239.
[23] J. Qu, L. Ouyang, C.C. Kuo, D.C. Martin, Stiffness, strength and adhesion characterization of electrochemically deposited conjugated polymer films, Acta Biomater. 31 (2016) 114–121, https://doi.org/10.1016/j.actbio.2015.11.018.
[24] M. Khorrami, M. Antensteiner, F. Fallahianbijan, A. Borhan, M.R. Abidian, Conducting polymer microcontainers for biomedical applications, in: Proc. Annu. Int. Conf. IEEE Eng. Med. Biol. Soc. EMBS, Annu Int Conf IEEE Eng Med Biol Soc, 2017: pp. 1869–1872. doi:10.1109/EMBC.2017.8037211.
[25] C.L. Kolarcik, K. Catt, E. Rost, I.N. Albrecht, D. Bourbeau, Z. Du, T.D.Y. Kozai, X. Luo, D.J. Weber, X. Tracy Cui, Evaluation of poly(3,4-ethylenedioxythiophene)/carbon nanotube neural electrode coatings for stimulation in the dorsal root ganglion, J. Neural Eng. 12 (1) (2015) 016008, https://doi.org/10.1088/1741-2560/12/1/016008.
[26] D. Khodagholy, J.N. Gelinas, T. Thesen, W. Doyle, O. Devinsky, G.G. Malliaras, G. Buzsáki, NeuroGrid: recording action potentials from the surface of the brain, Nat. Neurosci. 18 (2) (2015) 310–315, https://doi.org/10.1038/nn.3905.
[27] D. Khodagholy, T. Doublet, M. Gurfinkel, P. Quilichini, E. Ismailova, P. Leleux, T. Herve, S. Sanaur, C. Bernard, G.G. Malliaras, Highly Conformable Conducting Polymer Electrodes for In Vivo Recordings, Adv. Mater. 23 (36) (2011) H268–H272, https://doi.org/10.1002/adma.201102378.
[28] M. Antensteiner, M.R. Abidian, Tunable nanostructured conducting polymers for neural interface applications, in: Proc. Annu. Int. Conf. IEEE Eng. Med. Biol. Soc. EMBS, NIH Public Access, 2017: pp. 1881–1884. doi:10.1109/EMBC.2017.8037214.
[29] K. Krukiewicz, T. Jarosz, J.K. Zak, M. Lapkowski, P. Ruszkowski, T. Bobkiewicz-Kozlowska, B. Bednarczyk-Cwynar, Advancing the delivery of anticancer drugs: Conjugated polymer/triterpenoid composite, Acta Biomater. 19 (2015) 158–165, https://doi.org/10.1016/j.actbio.2015.03.006.
[30] K. Krukiewicz, A. Stokfisz, J.K. Zak, Two approaches to the model drug immobilization into conjugated polymer matrix, Mater. Sci. Eng. C. Mater. Biol. Appl. 54 (2015) 176–181, https://doi.org/10.1016/j.msec.2015.05.017.
[31] M. Antensteiner, M. Khorrami, F. Fallahianbijan, A. Borhan, M.R. Abidian, Conducting Polymer Microcups for Organic Bioelectronics and Drug Delivery Applications, Adv. Mater. 29 (39) (2017) 1702576, https://doi.org/10.1002/adma.201702576.
[32] S. Gomez-Carretero, B. Libberton, K. Svennersten, K. Persson, E. Jager, M. Berggren, M. Rhen, A. Richter-Dahlfors, Redox-active conducting polymers modulate Salmonella biofilm formation by controlling availability of electron acceptors, Npj Biofilms Microbiomes. 3 (2017) 19, https://doi.org/10.1038/s41522-017-0027-0.
[33] D. Czerwińska-Główka, W. Przystaś, E. Zabłocka-Godlewska, S. Student, B. Cwalina, M. Łapkowski, K. Krukiewicz, Electrically-responsive antimicrobial coatings based on a tetracycline-loaded poly(3,4-ethylenedioxythiophene) matrix, Mater. Sci. Eng. C. 123 (2021) 112017, https://doi.org/10.1016/j.msec.2021.112017.
[34] S. Glage, S. Paret, A. Winkel, M. Stiesch, A. Bleich, J.K. Krauss, K. Schwabe, A new model for biofilm formation and inflammatory tissue reaction: intraoperative infection of a cranial implant with Staphylococcus aureus in rats, Acta Neurochir. (Wien) 159 (9) (2017) 1747–1756, https://doi.org/10.1007/s00701-017-3244-7.
[35] P.M. George, A.W. Lyckman, D.A. LaVan, A. Hegde, Y. Leung, R. Avasare, C. Testa, P.M. Alexander, R. Langer, M. Sur, Fabrication and biocompatibility of polypyrrole implants suitable for neural prosthetics, Biomaterials. 26 (17) (2005) 3511–3519, https://doi.org/10.1016/j.biomaterials.2004.09.037.
[36] T.A. Skotheim, J.R. Reynolds, Conjugated polymers: Theory, synthesis, properties, and characterization, CRC Press, 2007.
[37] C. Boehler, Z. Aqrawe, M. Asplund, Applications of PEDOT in bioelectronic medicine, Bioelectron. Med. 2 (2) (2019) 89–99, https://doi.org/10.2217/bem-2019-0014.
[38] R.M. Walczak, J.R. Reynolds, Poly(3,4-alkylenedioxypyrroles): The PXDOPs as versatile yet underutilized electroactive and conducting polymers, Adv. Mater. 18 (9) (2006) 1121–1131, https://doi.org/10.1002/(ISSN)1521-4095.
[39] K. Krukiewicz, P. Zawisza, A.P. Herman, R. Turczyn, S. Boncel, J.K. Zak, An electrically controlled drug delivery system based on conducting poly(3,4-ethylenedioxypyrrole) matrix, Bioelectrochemistry. 108 (2016) 13–20, https://doi.org/10.1016/j.bioelechem.2015.11.002.
[40] K. Krukiewicz, B. Gniazdowska, T. Jarosz, A.P.A.P. Herman, S. Boncel, R. Turczyn, Effect of immobilization and release of ciprofloxacin and quercetin on electrochemical properties of poly(3,4-ethylenedioxypyrrole) matrix, Synth. Met. 249 (2019) 52–62, https://doi.org/10.1016/j.synthmet.2019.02.001.
[41] K. Krukiewicz, Tailorable drug capacity of dexamethasone-loaded conducting polymer matrix, IOP Conf. Ser. Mater. Sci. Eng. 369 (2018) 012002, https://doi.org/10.1088/1757-899X/369/1/012002.
[42] K. Krukiewicz, A. Kowalik, D. Czerwińska-Główka, M. Biggs, Electrodeposited poly(3,4-ethylenedioxypyrrole) films as neural interfaces: Cytocompatibility and electrochemical studies, Electrochim. Acta. 302 (2019) 21–30, https://doi.org/10.1016/j.electacta.2019.02.023.
[43] K. Krukiewicz, A. Kowalik, R. Turczyn, M.J.P. Biggs, In vitro attenuation of astrocyte activation and neuroinflammation through ibuprofen-doping of poly(3,4-ethylenedioxypyrrole) formulations, Bioelectrochemistry. 134 (2020) 107528, https://doi.org/10.1016/j.bioelechem.2020.107528.
[44] M. Domercq, C. Matute, Neuroprotection by tetracyclines, Trends Pharmacol. Sci. 25 (12) (2004) 609–612, https://doi.org/10.1016/j.tips.2004.10.001.
[45] T. Tikka, B.L. Fiebich, G. Goldsteins, R. Keinänen, J. Koistinaho, Minocycline, a tetracycline derivative, is neuroprotective against excitotoxicity by inhibiting activation and proliferation of microglia, J. Neurosci. 21 (8) (2001) 2580–2588, https://doi.org/10.1523/JNEUROSCI.21-08-02580.2001.
[46] D. Orsucci, V. Calsolaro, M. Mancuso, G. Siciliano, Neuroprotective Effects of Tetracyclines: Molecular Targets, Animal Models and Human Disease, CNS Neurol. Disord. - Drug Targets. 8 (2012) 222–231, https://doi.org/10.2174/187152709788680689.
[47] K.M. Szostak, L. Grand, T.G. Constandinou, Neural interfaces for intracortical recording: Requirements, fabrication methods, and characteristics, Front. Neurosci. 11 (2017) 665, https://doi.org/10.3389/fnins.2017.00665.

[48] C.-W. Lin, Y.-T. Lee, C.-W. Chang, W.-L. Hsu, Y.-C. Chang, W. Fang, Novel glass microprobe arrays for neural recording, Biosens. Bioelectron. 25 (2) (2009) 475–481, https://doi.org/10.1016/j.bios.2009.08.006.
[49] Y.-T. Lee, C.-W. Lin, C.-M. Lin, S.-R. Yeh, Y.-C. Chang, W. Fang, A pseudo 3D glass microprobe array: Glass microprobe with embedded silicon for alignment and electrical interconnection during assembly, J. Micromechanics Microengineering. 20 (2) (2010) 025014, https://doi.org/10.1088/0960-1317/20/2/025014.
[50] T.V.F. Abaya, S. Blair, P. Tathireddy, L. Rieth, F. Solzbacher, A 3D glass optrode array for optical neural stimulation, Biomed. Opt. Express. 3 (12) (2012) 3087, https://doi.org/10.1364/BOE.3.003087.
[51] A.S. Bondarenko, G.A. Ragoisha, EIS Spectrum Analyser, in: Prog. Chemom. Res., 2005: pp. 89–102.
[52] A.R. Harris, C. Newbold, P. Carter, R. Cowan, G.G. Wallace, Using Chronopotentiometry to Better Characterize the Charge Injection Mechanisms of Platinum Electrodes Used in Bionic Devices, Front. Neurosci. 13 (2019) 380, https://doi.org/10.3389/FNINS.2019.00380.
[53] E.K. Brunton, B. Winther-Jensen, C. Wang, E.B. Yan, S. Hagh Gooie, A.J. Lowery, R. Rajan, S.H. Gooie, A.J. Lowery, R. Rajan, In vivo comparison of the charge densities required to evoke motor responses using novel annular penetrating microelectrodes, Front. Neurosci. 9 (2015) 265, https://doi.org/10.3389/fnins.2015.00265.
[54] E. Shamaeli, N. Alizadeh, Kinetic studies of electrochemically controlled release of salicylate from nanostructure conducting molecularly imprinted polymer, Electrochim. Acta. 114 (2013) 409–415, https://doi.org/10.1016/j.electacta.2013.10.119.
[55] Ehsan Shamaeli, Naader Alizadeh, Nanostructured biocompatible thermal/electrical stimuli-responsive biopolymer-doped polypyrrole for controlled release of chlorpromazine: Kinetics studies, Int. J. Pharm. 472 (1-2) (2014) 327–338, https://doi.org/10.1016/j.ijpharm.2014.06.036.
[56] B. Alshammary, N. Casillas, R.B. Cook, J. Swingler, C. Ponce de León, F.C. Walsh, The importance of the film structure during self-powered ibuprofen salicylate drug release from polypyrrole electrodeposited on AZ31 Mg, J. Solid State Electrochem. 20 (12) (2016) 3375–3382, https://doi.org/10.1007/s10008-016-3288-2.
[57] E.Y. Thiam, A. Dramé, A. Sene, S.Y. Dieng, F. Guittard, T. Darmanin, Designing bioinspired parahydrophobic surfaces by electrodeposition of poly(3,4-ethylenedioxypyrrole) and poly(3,4-propylenedioxypyrrole) with mixed hydrocarbon and fluorocarbon chains, Eur. Polym. J. 110 (2019) 76–84, https://doi.org/10.1016/j.eurpolymj.2018.11.003.
[58] B. Narsimha Reddy, Melepurath Deepa, Electrochromic switching and nanoscale electrical properties of a poly(5-cyano indole)-poly(3,4-ethylenedioxypyrrole) device with a free standing ionic liquid electrolyte, Polym. (United Kingdom) 54 (21) (2013) 5801–5811, https://doi.org/10.1016/j.polymer.2013.08.016.
[59] Zhaohui Li, Vera M. Kolb, Wei-Teh Jiang, Hanlie Hong, FTIR and XRD Investigations of Tetracycline Intercalation in Smectites, Clays Clay Miner. 58 (4) (2010) 462–474, https://doi.org/10.1346/CCMN.2010.0580402.
[60] Rosalind J Allen, Bartlomiej Waclaw, Bacterial growth: a statistical physicist's guide, Reports Prog. Phys. 82 (1) (2019) 016601, https://doi.org/10.1088/1361-6633/aae546.
[61] ISO10993-5, Biological Evaluation of Medical devices-Part 5: Tests for in vitro Cytotoxicity, Int. Stand. Organ. (2009).
[62] Emanuela Paldino, Claudia Balducci, Pietro La Vitola, Luisa Artioli, Vincenza D'Angelo, Carmela Giampà, Vladimiro Artuso, Gianluigi Forloni, Francesca R. Fusco, Neuroprotective Effects of Doxycycline in the R6/2 Mouse Model of Huntington's Disease, Mol. Neurobiol. 57 (4) (2020) 1889–1903, https://doi.org/10.1007/s12035-019-01847-8.
[63] K. Hashimoto, T. Ishima, A novel target of action of minocycline in NGF-induced neurite outgrowth in PC12 cells: Translation initiator factor eIF4AI, PLoS One. 5 (2010), https://doi.org/10.1371/journal.pone.0015430.
[64] D. Orsucci, M. Mancuso, M. Filosto, G. Siciliano, Tetracyclines and Neuromuscular Disorders, Curr. Neuropharmacol. 10 (2012) 134–138, https://doi.org/10.2174/157015912800604498.
[65] C.L. Gaupp, K. Zong, P. Schottland, B.C. Thompson, C.A. Thomas, J.R. Reynolds, Poly(3,4-ethylenedioxypyrrole): Organic Electrochemistry of a Highly Stable Electrochromic Polymer, Macromolecules. 33 (2000) 1132–1133, https://doi.org/10.1021/ma9916180.
[66] T.-H.H. Le, Y. Kim, H. Yoon, Electrical and electrochemical properties of conducting polymers, Polymers (Basel). 9 (2017) 150, https://doi.org/10.3390/polym9040150.
[67] S. Shin, J. Kim, J. Jeong, T.M. Gwon, G.J. Choi, S.E. Lee, J. Kim, S.B. Jun, J.W. Chang, S.J. Kim, High Charge Storage Capacity Electrodeposited Iridium Oxide Film on Liquid Crystal Polymer-Based Neural Electrodes, Sensors Mater. 28 (2016) 243–260, https://doi.org/10.18494/SAM.2016.1175.
[68] A. Cisnal, J.-C. Fraile, J. Pérez-Turiel, V. Muñoz-Martinez, C. Müller, F.R. Ihmig, A Measurement Setup and Automated Calculation Method to Determine the Charge Injection Capacity of Implantable Microelectrodes, Sensors. 18 (2018) 4152, https://doi.org/10.3390/s18124152.
[69] C. Boehler, F. Oberueber, M. Asplund, Tuning drug delivery from conducting polymer films for accurately controlled release of charged molecules, J. Control. Release. 304 (2019) 173–180, https://doi.org/10.1016/j.jconrel.2019.05.017.
[70] Reecha Wadhwa, Carl F. Lagenaur, Xinyan Tracy Cui, Electrochemically controlled release of dexamethasone from conducting polymer polypyrrole coated electrode, J. Control. Release. 110 (3) (2006) 531–541, https://doi.org/10.1016/j.jconrel.2005.10.027.
[71] J. Bengtsson-Palme, D.G.J. Larsson, Concentrations of antibiotics predicted to select for resistant bacteria: Proposed limits for environmental regulation, Environ. Int. 86 (2016) 140–149, https://doi.org/10.1016/j.envint.2015.10.015.
[72] E. Shamaeli, N. Alizadeh, Functionalized gold nanoparticle-polypyrrole nanobiocomposite with high effective surface area for electrochemical/pH dual stimuli-responsive smart release of insulin, Colloids Surfaces B Biointerfaces. 126 (2015) 502–509, https://doi.org/10.1016/j.colsurfb.2015.01.003.
[73] N. Alizadeh, E. Shamaeli, Electrochemically controlled release of anticancer drug methotrexate using nanostructured polypyrrole modified with cetylpyridinium: Release kinetics investigation, Electrochim. Acta. 130 (2014) 488–496, https://doi.org/10.1016/j.electacta.2014.03.055.
[74] Yao Fu, Weiyuan John Kao, Drug release kinetics and transport mechanisms of non-degradable and degradable polymeric delivery systems, Expert Opin. Drug Deliv. 7 (4) (2010) 429–444, https://doi.org/10.1517/17425241003602259.
[75] Reem M. Almasri, Walid AlChamaa, Ali Reza Tehrani-Bagha, Massoud L. Khraiche, Highly Flexible Single-Unit Resolution All Printed Neural Interface on a Bioresorbable Backbone, ACS Appl. Bio Mater. 3 (10) (2020) 7040–7051, https://doi.org/10.1021/acsabm.0c00895.
[76] M. Vafaiee, R. Mohammadpour, M. Vossoughi, E. Asadian, M. Janahmadi, P. Sasanpour, Carbon Nanotube Modified Microelectrode Array for Neural Interface, Front. Bioeng. Biotechnol. 8 (2021) 1465, https://doi.org/10.3389/FBIOE.2020.582713.
[77] Jessamyn A. Fairfield, Nanostructured Materials for Neural Electrical Interfaces, Adv. Funct. Mater. 28 (12) (2018) 1701145, https://doi.org/10.1002/adfm.v28.12.
[78] K. Krukiewicz, J. Britton, D. Więcławska, M. Skorupa, J. Fernandez, J.R. Sarasua, M.J.P. Biggs, Electrical percolation in extrinsically conducting, poly(ε-decalactone) composite neural interface materials, Sci. Rep. 11 (2021) 1295, https://doi.org/10.1038/s41598-020-80361-7.
[79] Katarzyna Krukiewicz, Dawid Janas, Catalina Vallejo-Giraldo, Manus J.P. Biggs, Self-supporting carbon nanotube films as flexible neural interfaces, Electrochim. Acta. 295 (2019) 253–261, https://doi.org/10.1016/j.electacta.2018.10.157.
[80] S. Wilks, S. Richardson-Burns, J. Hendricks, D.C. Martin, K. Otto, Poly(3,4-ethylene dioxythiophene) (PEDOT) as a micro-neural interface material for electrostimulation, Front. Neuroeng. 2 (2009) 1–8, https://doi.org/10.3389/neuro.16.007.2009.
[81] William J. Tyler, The mechanobiology of brain function, Nat. Rev. Neurosci. 13 (12) (2012) 867–878, https://doi.org/10.1038/nrn3383.
[82] D. Prodanov, J. Delbeke, Mechanical and biological interactions of implants with the brain and their impact on implant design, Front. Neurosci. 10 (2016) 11, https://doi.org/10.3389/fnins.2016.00011.
[83] T Chung, J Q Wang, J Wang, B Cao, Y Li, S W Pang, Electrode modifications to lower electrode impedance and improve neural signal recording sensitivity, J. Neural Eng. 12 (5) (2015) 056018, https://doi.org/10.1088/1741-2560/12/5/056018.
[84] Raya Sorkin, Alon Greenbaum, Moshe David-Pur, Sarit Anava, Amir Ayali, Eshel Ben-Jacob, Yael Hanein, Process entanglement as a neuronal anchorage mechanism to rough surfaces, Nanotechnology. 20 (1) (2009) 015101, https://doi.org/10.1088/0957-4484/20/1/015101.
[85] Garth A. James, Laura Boegli, John Hancock, Lisa Bowersock, Albert Parker, Brian M. Kinney, Bacterial Adhesion and Biofilm Formation on Textured Breast Implant Shell Materials, Aesthetic Plast. Surg. 43 (2) (2019) 490–497, https://doi.org/10.1007/s00266-018-1234-7.
[86] Carolina Díaz, María Cecilia Cortizo, Patricia Laura Schilardi, Sandra Gabriela Gómez de Saravia, Mónica Alicia Fernández Lorenzo de Mele, Influence of the nano-micro structure of the surface on bacterial adhesion, Mater. Res. 10 (1) (2007) 11–14, https://doi.org/10.1590/S1516-14392007000100004.
[87] Yue Yuan, Michael P. Hays, Philip R. Hardwidge, Jooyoun Kim, Surface characteristics influencing bacterial adhesion to polymeric substrates, RSC Adv. 7 (23) (2017) 14254–14261, https://doi.org/10.1039/C7RA01571B.
[88] M.T. Khorasani, H. Mirzadeh, S. Irani, Plasma surface modification of poly (l-lactic acid) and poly (lactic-co-glycolic acid) films for improvement of nerve cells adhesion, Radiat. Phys. Chem. 77 (3) (2008) 280–287, https://doi.org/10.1016/j.radphyschem.2007.05.013.
[89] Matteo Solazzo, Katarzyna Krukiewicz, Ainur Zhussupbekova, Karsten Fleischer, Manus J. Biggs, Michael G. Monaghan, PEDOT:PSS interfaces stabilised using a PEGylated crosslinker yield improved conductivity and biocompatibility, J. Mater. Chem. B. 7 (31) (2019) 4811–4820, https://doi.org/10.1039/C9TB01028A.
[90] Lingyan Yang, Ziyun Jiang, Linhong Zhou, Keli Zhao, Xun Ma, Guosheng Cheng, Hydrophilic cell-derived extracellular matrix as a niche to promote adhesion and differentiation of neural progenitor cells, RSC Adv. 7 (72) (2017) 45587–45594, https://doi.org/10.1039/C7RA08273H.
[91] I. Sousa, A. Mendes, R.F. Pereira, P.J. Bártolo, Collagen surface modified poly(ε-caprolactone) scaffolds with improved hydrophilicity and cell adhesion properties, Mater. Lett. 134 (2014) 263–267, https://doi.org/10.1016/j.matlet.2014.06.132.
[92] K. Webb, V. Hlady, P.A. Tresco, Relative importance of surface wettability and charged functional groups on NIH 3T3 fibroblast attachment, spreading, and cytoskeletal organization, J. Biomed. Mater. Res. 41 (1998) 422–430, https://

doi.org/10.1002/(SICI)1097-4636(19980905)41:3<422::AID-JBM12>3.0.CO;2-K.
[93] Yea-Ling Ong, Anneta Razatos, George Georgiou, Mukul M. Sharma, Adhesion Forces between E. c oli Bacteria and Biomaterial Surfaces, Langmuir. 15 (8) (1999) 2719–2725, https://doi.org/10.1021/la981104e.
[94] Kestutis Kurselis, Roman Kiyan, Victor N. Bagratashvili, Vladimir K. Popov, Boris N. Chichkov, 3D fabrication of all-polymer conductive microstructures by two photon polymerization, Opt. Express. 21 (25) (2013) 31029, https://doi.org/10.1364/OE.21.031029.
[95] Xiaoxue Zhang, Ling Wang, Erkki Levänen, Superhydrophobic surfaces for the reduction of bacterial adhesion, RSC Adv. 3 (30) (2013) 12003, https://doi.org/10.1039/c3ra40497h.
[96] Xiao-Qiu Dou, Di Zhang, Chuanliang Feng, Lei Jiang, Bioinspired Hierarchical Surface Structures with Tunable Wettability for Regulating Bacteria Adhesion, ACS Nano. 9 (11) (2015) 10664–10672, https://doi.org/10.1021/acsnano.5b04231.
[97] S.J. Lee, G. Khang, Y.M. Lee, H.B. Lee, The effect of surface wettability on induction and growth of neurites from the PC-12 cell on a polymer surface, J. Colloid Interface Sci. 259 (2003) 228–235, https://doi.org/10.1016/S0021-9797(02)00163-7.
[98] J. Wang, L. Tian, N. Chen, S. Ramakrishna, X. Mo, The cellular response of nerve cells on poly-L-lysine coated PLGA-MWCNTs aligned nanofibers under electrical stimulation, Mater. Sci. Eng. C. 91 (2018) 715–726, https://doi.org/10.1016/j.msec.2018.06.025.
[99] Anton Y. Peleg, David C. Hooper, Hospital-Acquired Infections Due to Gram-Negative Bacteria, N. Engl. J. Med. 362 (19) (2010) 1804–1813, https://doi.org/10.1056/NEJMra0904124.
[100] N. Mohd Daud, I.F. Saeful Bahri, N.A.N. Nik Malek, H. Hermawan, S. Saidin, Immobilization of antibacterial chlorhexidine on stainless steel using crosslinking polydopamine film: Towards infection resistant medical devices, Colloids Surfaces B Biointerfaces. 145 (2016) 130–139, https://doi.org/10.1016/j.colsurfb.2016.04.046.
[101] D. Nagarjuna, G. Mittal, R.S. Dhanda, P.K. Verma, R. Gaind, M. Yadav, Faecal Escherichia coli isolates show potential to cause endogenous infection in patients admitted to the ICU in a tertiary care hospital, New Microbes New Infect. 7 (2015) 57–66, https://doi.org/10.1016/j.nmni.2015.05.006.
[102] W. Bereket, K. Hemalatha, B. Getenet, T. Wondwossen, A. Solomon, A. Zeynudin, S. Kannan, Update on bacterial nosocomial infections, Eur. Rev. Med. Pharmacol. Sci. 16 (2012) 1039–1044, https://doi.org/10.1155/2018/2127814.
[103] Leigh K. Harris, Julie A. Theriot, Surface Area to Volume Ratio: A Natural Variable for Bacterial Morphogenesis, Trends Microbiol. 26 (10) (2018) 815–832, https://doi.org/10.1016/j.tim.2018.04.008.
[104] Jens Möller, Tessa Luehmann, Heike Hall, Viola Vogel, The Race to the Pole: How High-Aspect Ratio Shape and Heterogeneous Environments Limit Phagocytosis of Filamentous Escherichia coli Bacteria by Macrophages, Nano Lett. 12 (6) (2012) 2901–2905, https://doi.org/10.1021/nl3004896.
[105] Luciana Calheiros Gomes, Filipe José Mergulhão, SEM analysis of surface impact on biofilm antibiotic treatment, Scanning. 2017 (2017) 1–7, https://doi.org/10.1155/2017/2960194.
[106] L.C. Gomes, L.N. Silva, M. Simões, L.F. Melo, F.J. Mergulhão, Escherichia coli adhesion, biofilm development and antibiotic susceptibility on biomedical materials, J. Biomed. Mater. Res. Part A. 103 (4) (2015) 1414–1423, https://doi.org/10.1002/jbm.a.35277.
[107] M. Jacques, A. Lebrun, B. Foiry, M. Dargis, F. Malouin, Effects of antibiotics on the growth and morphology of Pasteurella multocida, J. Gen. Microbiol. 137 (11) (1991) 2663–2668, https://doi.org/10.1099/00221287-137-11-2663.
[108] N. Ojkic, D. Serbanescu, S. Banerjee, Surface-to-volume scaling and aspect ratio preservation in rod-shaped bacteria, Elife. 8 (2019) e47033. doi:10.7554/eLife.47033.
[109] Hai Zheng, Po-Yi Ho, Meiling Jiang, Bin Tang, Weirong Liu, Dengjin Li, Xuefeng Yu, Nancy E. Kleckner, Ariel Amir, Chenli Liu, Interrogating the Escherichia coli cell cycle by cell dimension perturbations, Proc. Natl. Acad. Sci. 113 (52) (2016) 15000–15005, https://doi.org/10.1073/pnas.1617932114.
[110] J. Carleton, J.P. Phair, The Slow Bactericidal Effect of Tetracycline and Minocycline on Wall-Defective Staphylococcus, J. Infect. Dis. 126 (4) (1972) 457–459, https://doi.org/10.1093/infdis/126.4.457.
[111] C.A. Otey, M. Boukhelifa, P. Maness, B35 neuroblastoma cells: An easily transfected, cultured cell model of central nervous system neurons, Methods Cell Biol. 2003 (2003) 287–304, https://doi.org/10.1016/s0091-679x(03)01013-6.
[112] N.M. Curthoys, H. Freittag, A. Connor, M. Desouza, M. Brettle, A. Poljak, A. Hall, E. Hardeman, G. Schevzov, P.W. Gunning, T. Fath, Tropomyosins induce neuritogenesis and determine neurite branching patterns in B35 neuroblastoma cells, Mol. Cell. Neurosci. 58 (2014) 11–21, https://doi.org/10.1016/j.mcn.2013.10.011.
[113] Malika Boukhelifa, Mana M. Parast, Juli G. Valtschanoff, Anthony S. LaMantia, Rick B. Meeker, Carol A. Otey, David Drubin, A role for the cytoskeleton-associated protein palladin in neurite outgrowth, Mol. Biol. Cell. 12 (9) (2001) 2721–2729, https://doi.org/10.1091/mbc.12.9.2721.
[114] D.J.R. Croslan, M.C. Schoell, G.D. Ford, J.V. Pulliam, A. Gates, C.M. Clement, A.E. Harris, B.D. Ford, Neuroprotective effects of neuregulin-1 on B35 neuronal cells following ischemia, Brain Res. 1210 (2008) 39–47, https://doi.org/10.1016/j.brainres.2008.02.059.
[115] Long Tai Zheng, Geun-Mu Ryu, Byoung-Mog Kwon, Won-Ha Lee, Kyoungho Suk, Anti-inflammatory effects of catechols in lipopolysaccharide-stimulated microglia cells: Inhibition of microglial neurotoxicity, Eur. J. Pharmacol. 588 (1) (2008) 106–113, https://doi.org/10.1016/j.ejphar.2008.04.035.
[116] F. Bahrami, D.L. Morris, M.H. Pourgholami, Tetracyclines: Drugs with Huge Therapeutic Potential, Mini-Reviews, Med. Chem. 12 (2012) 44–52, https://doi.org/10.2174/138955712798868977.
[117] Ioana Inta, Georg F Hoffmann, Markus Bettendorf, Pediatric use of tetracyclines: focus on neurodevelopmental effects, Pediatr. Res. 82 (5) (2017) 725–726, https://doi.org/10.1038/pr.2017.167.
[118] Ozhan Merzuk Uckun, Fatih Alagoz, Mehmet Secer, Oguz Karakoyun, Ayhan Ocakcioglu, Ali Erdem Yildirim, Fevzi Yılmaz, Mert Sahinoglu, Denizhan Divanlioglu, Ali Dalgic, Ergun Daglioglu, Ahmet Deniz Belen, Neuroprotective effects of tetracyclines on blunt head trauma: An experimental study on rats, J. Neurosci. Rural Pract. 6 (01) (2015) 027–032, https://doi.org/10.4103/0976-3147.143186.
[119] D.C. Baptiste, K.J. Powell, C.A.B. Jollimore, C. Hamilton, T.L. Levatte, M.L. Archibald, B.C. Chauhan, G.S. Robertson, M.E.M. Kelly, Effects of minocycline and tetracycline on retinal ganglion cell survival after axotomy, Neuroscience. 134 (2) (2005) 575–582, https://doi.org/10.1016/j.neuroscience:2005.04.011.
[120] Shan Zhu, Irina G. Stavrovskaya, Martin Drozda, Betty Y.S. Kim, Victor Ona, Mingwei Li, Satinder Sarang, Allen S. Liu, Dean M. Hartley, Du Chu Wu, Steven Gullans, Robert J. Ferrante, Serge Przedborski, Bruce S. Kristal, Robert M. Friedlander, Minocycline inhibits cytochrome c release and delays progression of amyotrophic lateral sclerosis in mice, Nat. 417 (6884) (2002) 74–78, https://doi.org/10.1038/417074a.
[121] X. Wang, S. Zhu, M. Drozda, W. Zhang, I.G. Stavrovskaya, E. Cattaneo, R.J. Ferrante, B.S. Kristal, R.M. Friedlander, Minocycline inhibits caspase-independent and -dependent mitochondrial cell death pathways in models of Huntington's disease, Proc. Natl. Acad. Sci. U. S. A. 100 (18) (2003) 10483–10487, https://doi.org/10.1073/pnas.1832501100.
[122] H. Chen, L. Wang, Y. Lu, X. Du, Bioinspired microcone-array-based living biointerfaces: enhancing the anti-inflammatory effect and neuronal network formation, Microsystems Nanoeng. 6 (2020) 58, https://doi.org/10.1038/s41378-020-0172-0.
[123] M.F. Bear, B.W. Connors, M.A. Paradiso, Neuroscience: Exploring the brain, Fourth edition, 2015.
[124] Qin Tu, Long Pang, Yun Chen, Yanrong Zhang, Rui Zhang, Bingzhang Lu, Jinyi Wang, Effects of surface charges of graphene oxide on neuronal outgrowth and branching, Analyst. 139 (1) (2014) 105–115, https://doi.org/10.1039/C3AN01796F.
[125] D.-H. Kim, S.M. Richardson-Burns, L.K. Povlich, M.R. Abidian, S. Spanninga, J.L. Hendricks, D.C. Martin, Soft, fuzzy and bioactive conducting polymers for improving the chronic performance of neural prosthetic devices, in: W.M. Reichert (Ed.), Indwelling Neural Implant. Strateg. Contend. with Vivo Environ., CRC Press, 2007: p. 21204405. doi:10.1201/9781420009309.ch7.

cells

MDPI

Review

Guidelines for a Morphometric Analysis of Prokaryotic and Eukaryotic Cells by Scanning Electron Microscopy

Dominika Czerwińska-Główka and Katarzyna Krukiewicz *

Department of Physical Chemistry and Technology of Polymers, Silesian University of Technology, 44-100 Gliwice, Poland; dominika.czerwinska-glowka@polsl.pl
* Correspondence: katarzyna.krukiewicz@polsl.pl; Tel.: +48-32-237-1312

Abstract: The invention of a scanning electron microscopy (SEM) pushed the imaging methods and allowed for the observation of cell details with a high resolution. Currently, SEM appears as an extremely useful tool to analyse the morphology of biological samples. The aim of this paper is to provide a set of guidelines for using SEM to analyse morphology of prokaryotic and eukaryotic cells, taking as model cases *Escherichia coli* bacteria and B-35 rat neuroblastoma cells. Herein, we discuss the necessity of a careful sample preparation and provide an optimised protocol that allows to observe the details of cell ultrastructure ($\geq$ 50 nm) with a minimum processing effort. Highlighting the versatility of morphometric descriptors, we present the most informative parameters and couple them with molecular processes. In this way, we indicate the wide range of information that can be collected through SEM imaging of biological materials that makes SEM a convenient screening method to detect cell pathology.

Keywords: *Escherichia coli*; image analysis; morphological analysis; morphometry; neuroblastoma; scanning electron microscopy

Citation: Czerwińska-Główka, D.; Krukiewicz, K. Guidelines for a Morphometric Analysis of Prokaryotic and Eukaryotic Cells by Scanning Electron Microscopy. *Cells* **2021**, *10*, 3304. https://doi.org/10.3390/cells10123304

Academic Editors: Francesco Pezzella, Kingsley Micklem and Alexander E. Kalyuzhny

Received: 16 September 2021
Accepted: 24 November 2021
Published: 25 November 2021

1. Introduction

A continuous development of biological research is possible due to the constant improvement in experimental techniques. The classical observational and descriptive methods in light microscopy allowed for the visualisation of objects invisible to the naked eye, constituting a breakthrough in microbiology and medicine. The invention of an electron microscopy enabled to observe cell details, including the smallest cell organelles, with a high resolution [1]. Thanks to the continuous advances in scanning electron microscopy (SEM), the observation of the micro world and a deep interpretation of observed images have become achievable.

The first SEM image was taken in 1935 by Max Knoll [2], and now SEM is an extremely useful method in biomedical engineering, allowing a comprehensive observation of isolated microorganisms or cells at a significant magnification [3]. To create a SEM image, an electron beam is emitted from a cathode, accelerated and attracted by a positively charged anode. When accelerated electrons hit the specimen, their kinetic energy is dissipated, which is a source of secondary electrons (typically used to create a SEM image), reflected or backscattered electrons, characteristic X-rays (used for elemental analysis by means of an energy dispersive spectroscopy), light, heat, and transmitted electrons. The resolution of obtained image depends on electron wavelength, which is much shorter than the wavelength of visible light providing much higher resolution (typically approx. 10 nm) than in traditional light microscopy (about 200–250 nm). New generations of high resolution SEM allow to achieve image resolution of 1 nm, approaching the resolution typical for a transmission electron microscopy, TEM, but without requiring high accelerating potentials (100–200 kV) [4]. Nevertheless, since the best instrumentation is only as good as the best specimen [5], sample preparation should be performed under favourable conditions.

The aim of this paper is to provide a set of guidelines for using a scanning electron microscopy to analyse morphology of prokaryotic and eukaryotic cells, taking as model cases *Escherichia coli* bacteria (known as a molecular biologist tool box [6]) and B-35 rat neuroblastoma cells (an easily transfected, cultured cell model of central nervous system neurons [7]). We discuss the necessity of a careful sample preparation and provide an optimised protocol that allowed to observe the details of ultrastructure ($\geq$ 50 nm) of model cells with a minimum processing effort. Highlighting the versatility of morphometric descriptors that can be used to analyse prokaryotic and eukaryotic cells, we present the most valuable parameters and couple them with molecular processes, such as cell division, mobility, growth dynamics, apoptosis, and necrosis. In this way, we indicate the wide range of information that can be collected through SEM imaging of biological materials.

2. Sample Preparation

To obtain a high resolution SEM image of small objects, such as bacteria and eukaryotic cells, proper preparation of a sample is essential. Since it is crucial to maintain a vacuum of at least 10^{-4} Pa and to prevent contamination, biological samples must be carefully processed and dehydrated. An inadequate preparation of a specimen may result in shrinkage and deformation of cells, leading to incorrect results and misleading interpretations [8]. The process of preparing biological samples for SEM imaging consists of several stages, and the main ones include fixation, dehydration and drying. In addition, specimens are typically sputter-coated with a conducting film, since the investigated surface should be conductive to prevent image distortion caused by an electron charging effect [9].

2.1. Fixation

In the first stage of sample preparation (fixation), biological samples are treated with protein and/or lipid crosslinking reagents. The aim of this process is to keep the structure of a biological material unchanged, thus enabling the imaging of a natural state of an object. Fixation should also prevent autolysis and decomposition of cells. Many fixatives are known [10], however in practice the most commonly used are glutaraldehyde, osmium tetroxide or their mixtures with other compounds, e.g., paraformaldehyde—the comparison of their properties is presented in Table 1. Generally, the penetration of a fixative into the cell membrane is a long-term process lasting from several to several dozen hours, requiring the use of an appropriately selected pH, temperature, and osmolarity. The basic fixative with the strongest protein crosslinking character is undoubtedly glutaraldehyde. Its effectiveness is related to its multicomponent nature, where at a given pH several forms are present in a reagent solution [11–13]. Osmium tetroxide is the second most commonly used biological fixative that crosslinks lipids. However, it penetrates into the cell structure slower than glutaraldehyde. Moreover, its vapours are harmful to eyes, respiratory and digestive systems. Osmium tetroxide is also a strong oxidising agent, and can cause undesirable damage or shrinkage of membrane components during the fixation process [14]. Sometimes paraformaldehyde in combination with glutaraldehyde is used due to faster penetration into the tissue, but this mixture exhibits a weaker fixing effect.

Table 1. Comparison of the most popular fixatives used for processing of biological materials for SEM imaging; where dH_2O is deionised water, CAC is a cacodylate buffer; PB is a phosphate buffer.

Fixing Agent	Fixing Conditions	Fixing Time	Rinsing Conditions	Major Risks	Ref.
Osmium tetroxide	1% OsO4 in dH2O or 0.1 M CAC	30–60 min	1 × 2 min with 0.1 M CAC or dH2O, and 2 × 2 min with dH2O	Causes eye and skin burns. Causes digestive and respiratory tract burns. Aspiration hazard if swallowed. Can enter lungs and cause damage. May cause adverse reproductive effects. **Target organs**: kidneys.	[9,15–17]
	0.5% OsO4 and 0.8% K4Fe(CN)6 in dH2O or 0.1M CAC (reduced osmium)	30–60 min	1 × 2 min with 0.1 M CAC or dH2O, and 2 × 2 min with dH2O	Causes eye and skin burns. Causes digestive and respiratory tract burns. Aspiration hazard if swallowed. Can enter lungs and cause damage. May cause adverse reproductive effects. **Target organs**: kidneys.	[9,15–17]
Glutaraldehyde	1.5–4% in 0.1 M CAC or PB, pH 6.8–7.4	20–60 min for animal cells, 1–48 h for bacterial cells	3 × 2 min with 0.1–0.2 M CAC or PB	Causes eye and skin burns. Causes digestive and respiratory tract burns. May cause allergic respiratory and skin reaction. Harmful if swallowed, inhaled, or absorbed through the skin. Aspiration hazard if swallowed. Can enter lungs and cause damage. Dangerous for the environment. **Target organs**: central nervous system, lungs, respiratory system, eyes, skin.	[9,14–16,18]
Paraformaldehyde	4% in 0.1 M CAC or PB, pH 6.8–7.4	30–60 min for animal cells, 48 h for bacterial cells	4 × 5 min with 0.1 M CAC or PB	Harmful if swallowed. Causes skin irritation. May cause an allergic skin reaction. Causes serious eye damage. Harmful if inhaled. May cause respiratory irritation. Suspected of causing cancer. **Target organs**: respiratory system.	[9,16,19]
Methacarn	methanol/ chloroform/ acetic acid 6:3:1	48 h for bacterial cells	4 × 5 min with 0.1 M CAC	May cause irritation to the eyes, nose, throat, headache, dizziness, nausea. **Target organs**: eyes, skin, respiratory system, central nervous system, gastrointestinal tract.	[16,20]

2.2. Dehydration

Living organisms are largely composed of water, and it is necessary to dry them properly before placing them in a vacuum. Therefore, another important step in the preparation of biological samples for SEM analysis is dehydration, in which water present in cells is gradually removed. The dehydration process is carried out by immersing samples for several minutes in water solutions of increasing concentrations of ethanol or acetone, until reaching ethanol/acetone concentration of 100%. Ethanol is preferable as a dehydrating agent due to the fact that anhydrous acetone absorbs water more strongly from the atmosphere than from a specimen [9,14]. Additionally, it has been shown that ethanol dehydration causes only a minimal reduction in a cell size [21].

An interesting approach is the application of an organosilicon compound, hexamethyldisilazane (HMDS), as a drying agent exhibiting a reduced surface tension and an ability to crosslink proteins. HMDS treatment is supposed to improve a mechanical stability of

a specimen, which is beneficial in the next steps of sample processing and imaging [22]. HMDS is typically used as a final dehydrating solution in the course of an ethanol/acetone dehydration process [23]. After the last HMDS wash, specimens are left in HMDS until the complete evaporation of the solution. Numerous studies confirmed that HMDS treatment prevents the occurrence of imaging artifacts, allows a specimen to preserve surface details, as well as preserves cell microstructure without shrinkage [24]. Therefore, this drying method can be successfully employed for the visualisation of delicate samples, for instance pollen grains [25], but also hepatic endothelial cells [22], porcine retina [23] and bacteria (*P. fluorescens*) [26]. The risk of changing surface properties of a specimen as a result of silanization [27], however, restricts the application of HMDS treatment for high resolution imaging. Another drawback of HMDS is its acute toxicity [28].

An alternative to conventional SEM imaging performed under reduced pressure is the use of an environmental scanning electron microscopy (ESEM), in which the pressure around the sample is increased to 10–20 torr. In this method, gas particles in the chamber are ionised facilitating a free flow of current, which in turn allows for imaging of wet and non-conductive samples. The obvious advantage of imaging biological materials with ESEM is the ability to collect an image with minimal sample preparation [29,30]. However, a negative effect of humidity is still observed at higher pressures, and the presence of condensed water layer on a sample can result in low contrast and poor visibility of fine details of cells. Moreover, applied conditions are at a burden for biological materials, therefore it is generally accepted that a single ESEM sample can be only viewed once [31]. According to these limitations, the major challenge associated with ESEM is to dry the samples while preventing structural damage to investigated materials. Common drying methods include critical point drying, freeze-drying and direct air-drying after dehydration with alcohol.

Critical point drying (CPD) takes advantage of the fact that at the critical point the liquid turns into gas, and this phenomenon is not accompanied by distorting forces. A previously used dehydrating agent is displaced with a liquid (carbon dioxide or freon) brought to a critical point at elevated temperature and pressure. Once the critical point is reached, the heat is kept at the critical temperature and steam is slowly released from the chamber until the vessel reaches atmospheric pressure [14]. CPD procedure allows to reduce surface charging and improve contrast of observed materials, however it is not devoid of drawbacks. CPD requires the use of an additional equipment, and some types of samples may show artifacts, cracks, and undergo significant shrinkage upon processing [8,32]. Although CPD was found to cause a 25–30% reduction in the diameter of dehydrated cells, high resolution SEM studies demonstrated that all structural components of cells retained their usual relationship [21].

In a freeze-drying method, a specimen in the aqueous phase is quickly frozen and transferred to a special chamber where the temperature is kept below −80 °C. The frozen substance sublimates to the gas phase and then is absorbed or removed by vacuum. The process of freeze-drying can take from several hours to several days depending on sample size, temperature, and pressure. The major advantage of this method is limited shrinkage, especially when compared with CPD. However, some disadvantages include the need for a special equipment, problems with rapid freezing and transfer of the sample, long time needed to dry biological samples, and the presence of a sediment remaining on the sample surfaces. Additionally, freeze-drying can cause distortions and damage due to the formation of ice crystals [8,32–34].

The above-mentioned drying techniques, although giving excellent results for certain biological samples, are not always suitable for examining every microorganism or tissue. Moreover, they require complex, specialised, and expensive equipment. Therefore, the easiest and most effective way for drying of biological samples is a simple air-drying [35,36]. Although air-drying carries the risk of an excessive shrinkage, cracking, and collapse of fragile structures such as cilia and flagella, the use of solvents such as ethanol or HMDS in the dehydration phase enables to apply air-drying without damaging tested materials [34].

2.3. Sputter-Coating

Being non-conductive materials, dehydrated biological samples usually cause charging problems in SEM. The charge accumulated on the sample disrupts the primary electron beam leading to image distortion and low contrast. Therefore, it is essential to cover the sample with a thin layer of a conducting material, thus increasing its surface conductivity [37]. Consequently, a dried sample is placed in a vacuum sputter-coater. The pressure in chamber is lowered by means of a vacuum pump, and an inert gas is introduced. Then, gas molecules are ionised and strike a charged heavy metal target. Thereby, some of the atoms are knocked out and can coat the sample. The preferred sputtering metals are gold, gold-palladium, platinum, iridium, and chromium, while the three latter are usually selected for a high resolution imaging. Iridium, particularly, is preferably chosen as a coating material for high magnification applications [38], mainly due to its stability, resistance to oxidation, and the ability to provide a virtually grain-less coating layer [39]. Apart from metals, also a carbon layer can be used to increase surface conductivity of samples, particularly those amenable for X-ray microanalysis [38]. This material, however, should be deposited by either ion-beam sputtering or vacuum evaporation, since in conventional direct current magnetron sputter coaters it tends to form non-conducting diamond-like carbon films.

2.4. Optimised Protocol for Sample Preparation

Obviously, different research groups have developed their own sample preparation protocols, suitable for the visualisation of particular biological samples with a resolution degree matching specific needs. The majority of current SEM protocols [40–42] involves two fixation steps, one with paraformaldehyde and/or glutaraldehyde, and the other one with osmium tetroxide. Washing of specimen is followed by ethanol or acetone dehydration, critical point drying and metal sputter-coating. When adopted, these protocols may allow for the visualisation of biological objects with a resolution of 5 nm. Undoubtedly, this level of detail is high enough to thoroughly investigate a cell's ultrastructure. Still, the majority of morphometric descriptors, as described later in this review paper, do not require such a high resolution.

The complexity of aforementioned approach inspired researchers to investigate how the modification of a sample preparation protocol would influence the quality of imaging. For instance, Moran et al. [23] studied numerous sample preparation methodologies for imaging the ultrastructure of porcine retina, representing a delicate biological tissue. It was shown that the additional fixation with osmium tetroxide did not improve the quality of imaging, providing that samples were first fixed in a formalin solution. Additionally, a careful dehydration of specimens with ethanol and HMDS was found to provide similar results as CPD, with an additional benefit of no specialised equipment required, lower costs and time commitment [23]. In the light of the above, we decided to further investigate whether simplifications of a sample preparation protocol could allow for collecting SEM images with an acceptable image quality.

In our research, we used SEM imaging to visualise the morphology of two types of biological samples representing prokaryotic and eukaryotic cells: a model Gram-negative bacterial strain *Escherichia coli* (DSM 30083, U5/41), and a cultured cell model of central nervous system neurons, namely rat neuroblastoma cell line B-35 (ATCC® CRL-2754™). The details of culturing both types of cells can be found in our previous reports [43–45]. According to the optimised sample preparation protocol [43–45], cells were fixed using 3% glutaraldehyde for 24 h, then washed three times with sterile distilled water. Subsequently, samples were dehydrated by immersing them for 10 min in the solutions of ethanol with increasing concentrations (30%, 50%, 70%, 80%, 90%, 95%, 99.8%), then dried for 24 h at 50 °C. To enhance the quality of imaging, dehydrated samples were sputter-coated with a gold layer to produce a 5 nm thick conducting film. The developed protocol is depicted in Figure 1. Although this processing method is not recommended for collecting high resolution SEM images (resolution < 5 nm), it allows for imaging the details of cell

ultrastructure larger than 50 nm, which is enough to carry on a morphometric analysis as described further in this paper.

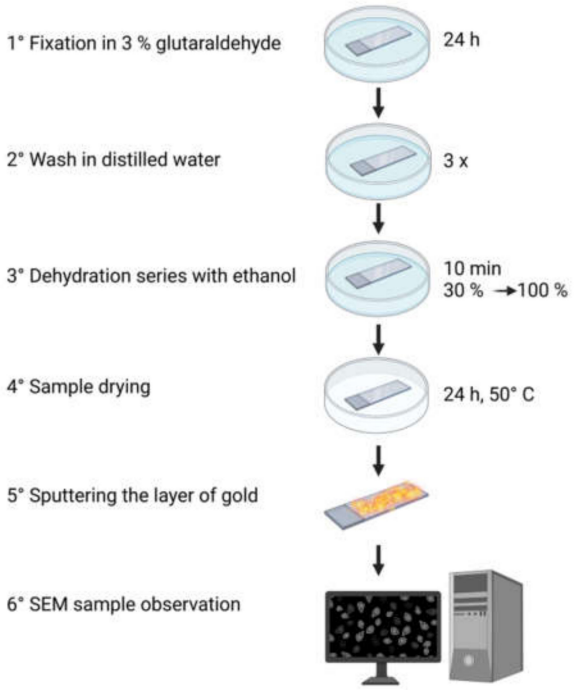

Figure 1. Schematic representation of the optimised protocol for the preparation of *Escherichia coli* and B-35 cells for SEM imaging.

3. Morphometric Analysis of Model Prokaryotic Cells: *Escherichia coli*

As prokaryotic cells, bacteria represent a maximally simplified structure consisting of cell organelles and DNA loosely embedded in the cytoplasm, surrounded by a cytoplasmic membrane and a rigid cell wall [30,46]. It has been shown that although various species of bacteria may differ significantly in shape or size, the variation in cell dimensions (length, width, aspect ratio, volume, etc.) may carry useful information about their growth phase, growth rate, and nutritional conditions. Moreover, shape is a selectable feature that helps cells survive under various conditions. Bacteria react to the surrounding environment to adopt size and shape that are optimal for current environmental conditions.

SEM is widely used in microbiological analysis to assess the morphology of bacterial cells, their adhesion to the surface, as well as their tendency to form bacterial biofilms [43–45]. Moreover, SEM allows to estimate the number and distribution of microorganisms on the investigated surface [43]. The versatility of results that can be collected by SEM analysis makes this type of microscopy favourable for the evaluation of antimicrobial character of medical surfaces [43], effectiveness of new antibiotic agents [47] or bioactive materials [44,45]. What is more, a high resolving power of SEM allows obtaining reliable information on the state of microorganisms in their natural environment [47–49].

Cell length and cell width can be easily measured from SEM images by manually tracing the dimensions of individual cells (Figure 2A,B). Results are usually reported as the mean value of multiple measurements. Dividing bacterial width by length allows to determine aspect ratio, which is close to unity for circular cells and decreases when bacterial cells become elongated. The values of bacterial length (L) and width (W) can be used to calculate cell volume (V) using the following equation [50]:

$$V = \frac{\pi W^2}{4\left(L - \frac{W}{3}\right)} \quad (1)$$

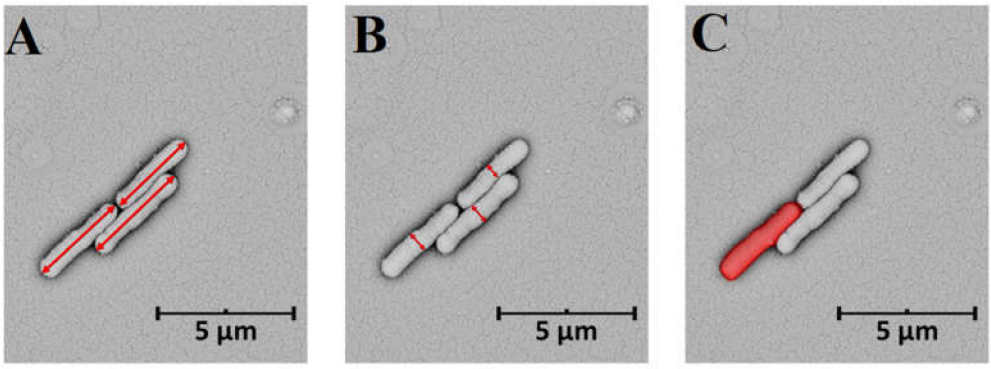

Figure 2. Morphometric descriptors of bacteria on the example of *Escherichia coli* cells: (**A**) length, (**B**) width, (**C**) cell surface area. SEM micrographs were collected by means of a Phenom ProX scanning electron microscope operating at 15 kV.

By looking at cell morphology, it is possible to distinguish critical elements of the control of the cell cycle and the viability of microorganisms [51]. For instance, *E. coli* mutants lacking in binding proteins are also known from their inability to produce enough septation proteins to accommodate their increasing diameter. Therefore, instead of dividing, they continue to grow in length and girth until they lyse [52]. The cell shape of many rod-shaped bacteria is determined by the cytoskeleton MreB protein, actin homolog, and ftsZ, tibulin homolog. It has been found that lowering the mreB level results in an increase in cell width, while decreasing the ftsZ level leads to an increase in cell length [53,54].

It has also been shown that many bacterial species exhibit a surface-to-volume (S/V) homeostasis. Bacteria tightly control their cell cycles to adjust their size and the proper time of division. The shape of most bacteria is constant, and their growth is associated mainly with a change in volume. For example, volume changes in *E. coli* cells occur at a different rate, but usually cells keep the same shape—a rod with a constant aspect ratio (approx. 0.25). Disturbances in a normal bacterial growth including genetic alterations, lack of nutrition, and the effects of pharmacological agents disrupt homeostasis, and often lead to a change in cell width or length, and thus also S/V. For instance, increasing the length of cells reduces the S/V ratio. Although the cells become thinner, they tend to maintain homeostasis by reducing their width [55,56].

4. Morphometric Analysis of Model Eukaryotic Cells: B35 Neuroblastoma Cells

Imaging of various types of animal cells is increasingly applied in both medical research and diagnostics, since the shape of a cell is closely related to its biological properties [57]. The morphological analysis of cells has many applications, including the elucidation of numerous physiological mechanisms. For instance, SEM imaging is used to study morphological changes during the cell cycle, to analyse the phenomenon of cell division, mobility and growth dynamics, as well as the apoptosis and necrosis [58,59]. Microscopic images of cells are extensively analysed in clinical applications, especially in oncology, due to the fact that the morphology of cancer cells differs significantly from that of healthy ones [60,61]. The use of a morphometric analysis makes it possible to correlate the shape of analysed cells with the progression of a disease, identify abnormalities enabling early detection of cancer cells, and predict the course of a disease. Therefore, the use of microscopic techniques is an effective method of assessing the pharmacological effects of many drugs, including anti-cancer agents. Much information can be obtained by observing the behaviour of cells under specific stress conditions. Shape analysis can also assist to identify certain pathologies in many tissues, as well as the transition of cells towards drug-resistant phenotype [62]. Analysing cell morphology also provides an opportunity to assess the progress in cell differentiation and correlate cell shape with its functionality [57]. As a consequence, SEM analysis is commonly employed in cytotoxicity and biocompatibility studies, enabling the characterisation of new biomaterials [61,63,64].

Morphometric analysis is particularly useful in neuroscience, since the analysis of neural cell morphology, branching or formation of complex cell networks is important in assessing the state and proper functioning of the brain [64,65]. Moreover, SEM imaging is also used to assess the ability to control regeneration, replacement, and stimulation of neural cells—features that are extremely important for the diagnostics and treatment of neurodegenerative diseases, such as Parkinson's or Alzheimer's disease. The degeneration and death of neural cells have enormous health consequences prompting a lot of innovative research in the field of neural engineering [66,67].

When designing new solutions for cellular applications, it should be borne in mind that cells are extremely susceptible to many environmental factors. For instance, external electrical stimulation with direct current has been shown to selectively increase the growth rate of neurites towards the anode [68]. Aside from electrical and biochemical signals, there are increasing numbers of studies pointing to equally important physical parameters of the extracellular environment during the development of the nervous system. These include physical forces, mechanical factors, substrate flexibility, nanotopography, scaffold geometry and stiffness. All of these signals act as physical and chemical cues for the formation and reconstruction of neural tissue, hence may significantly affect cell shape [69,70].

The topography of an extracellular microenvironment has been shown to influence cell morphology, but also provide guidance and affect cell differentiation. Therefore, a widely studied trend among biomaterials is the inclusion of topographic cues to control the behaviour of neural cells and support their regeneration. Until now, cells of the neuronal type have been grown on isotropic (microfilars) and anisotopic (meshes, microchannels, electrospun fibres) surfaces, as well as undefined random topographies that may better reflect natural conditions in tissues [71]. To relate topographic cues to specific cell responses, surface must be well analysed with respect to width, depth of the grooves and microgrids, the length or diameter of the fibres, and the shapes of the holes, etc. Moreover, not only the topography but also the dimensions of individual features play a significant role in the development of cells, since surface features which are similar in size to neurons can enhance cell–substrate interactions [66,70,72]. Consequently, SEM imaging of neural cells on the surface of biomaterials enables to predict and control cell adhesion, spreading, alignment, and morphological changes.

4.1. Conventional Morphometric Descriptors

A neuronal cell is characterised by the presence of elongated neurites, from which axons and dendrites can be distinguished as forming branched structures. The morphological complexity of the branches largely determines the functional capacity of cells. When neural cells are connected to each other, they form networks that serve as the basis of neural function. Shape development is determined both by genetic factors and interactions with a surrounding tissue. To fully describe the morphology of neural cells, a number of metric parameters are used, including soma size, neurite diameter, neurite length, cell area, cell volume, and correlations between them [73]. Another set of parameters is used to assess the development of neural network (branching descriptors), namely neurite density, neurite alignment, number of cells forming neurites, etc. [70,72,74,75].

Neurite number is defined as the number of neurites exiting a single cell body [76] (Figure 3A). In the case of branched cells, a typical descriptor is an average neurite length, defined as the sum of the lengths of all neurites in a single cell divided by the total number of neurites [75,77,78]. The measurement of neurite length, which affects networking and signal transmission, can be made by a manual tracing of the entire neurite from the base to its edge with the use of an image analysis software, for example ImageJ (NIH) (Figure 3B). When describing neural length, one can also use a maximum neurite length defined as the length of the longest neurite in each cell. By determining a radial distance (the minimum length from the cell to the ends of the neurite), it is also possible to assess the straightness of the branches by defining the difference between the length of the neurite and the radial distance [79].

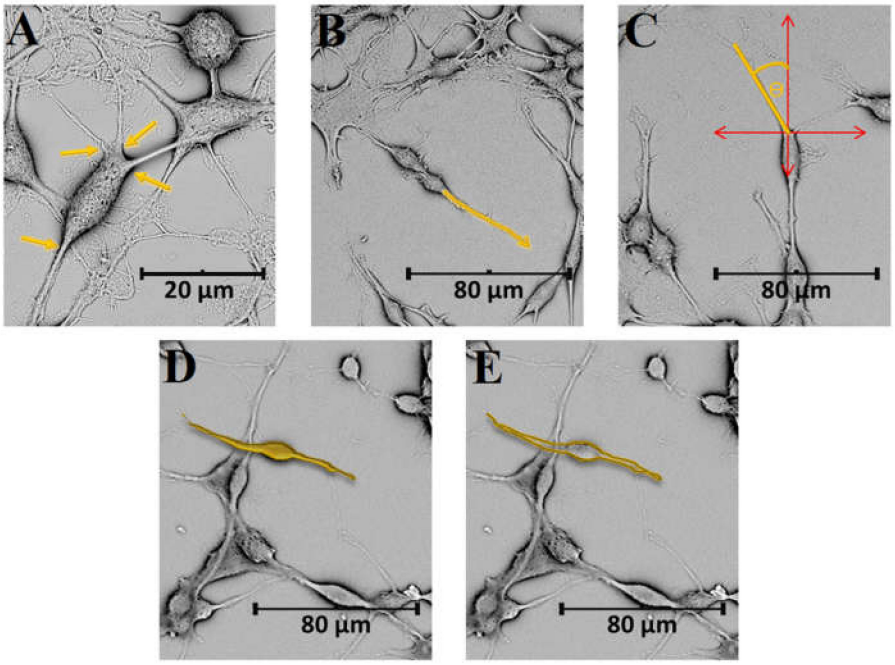

Figure 3. Morphometric descriptors for neural cells on the example of rat neuroblastoma B35 cells: (**A**) number of neuritis, (**B**) length of neuritis, (**C**) angle, (**D**) cell area, (**E**) perimeter. SEM micrographs were collected by means of a Phenom ProX scanning electron microscope operating at 10 kV.

Angular measurements are usually used to analyse the alignment of neurites on the surface of topographically modified material (Figure 3C). The purpose of such materials is to specifically target neural cells, thereby proposing a therapeutic solution for the regeneration of damaged cells. To estimate a directionality of the neurons, a straight line is drawn from one end of the neurite to the other one, and an angle is determined with respect to the grid axis. When the measured value of the angle is less than 15°, the neurite is considered parallel to the designated grids. On the other hand, when it is greater than 75°, the neurite is scored as perpendicular to the cues. In the case of substrates without a topographic pattern, a random direction can be selected as the axis [71,80].

SEM visualisation of neural cells is a preliminary indicator of interactions allowing the assessment of surface adhesion, which is crucial for cell survival and development. Subsequently, it is possible to assess the number of differentiated cells on tested biomaterials. This can be done by visually examining the field and counting cells that have at least one neurite equal to the diameter of a cell body [73]. The formation of neural networks, lengthening and branching of neurites is a reliable indicator of the functioning of neurons, therefore this analysis is widely used in the assessment of biological functionality of biomaterials. Moreover, it is also possible to evaluate the geometric complexity of the cells by expressing inter cell area, perimeter, or circularity [60,62,81]. An area of the cell is calculated as the area defined by the closed curve and presented by counting all pixels (Figure 3D). A perimeter is measured by the shape of the cell defined by the outline and by counting pixels (Figure 3E), and a circularity (C) is expressed as a function of cell area (A) and perimeter (P) with the use of the following formula [61,82]:

$$C = \frac{4\pi A}{P^2} \quad (2)$$

Circularity of 1 is typical for round cells, and it decreases for cells with irregular shapes. The analysis of these morphometric descriptors was found to be suitable to differentiate between different types of microglial cells present in the neocortex of an injured rat brain [81]. For instance, circularity was useful to discriminate bushy cells from all other cell groups, including ramified and hypertrophied microglia. Additionally, the analysis

of circularity allowed for the detection of significant differences between hypertrophied and ramified cells from injured brains. Interestingly, changes in cell perimeter and cell area were found to be more informative than circularity. Numerous studies report on the changes of a microglia perimeter as a result of phagocytosis [83] or pathological situations, including traumatic brain injury or inflammatory reaction induced by neuraminidase [82].

4.2. Fractal Analysis

Apart from conventional descriptors of cell morphology, fractal analysis has recently become a recognised technique to characterise neural tissue [84,85]. Introduced by Mandelbrot in 1977 [86], fractals are characterised by a scale-invariant and self-similar behaviour. This type of geometry is abundant in nature, with numerous examples in anatomy, including cardiovascular, respiratory, and neural systems [84]. Since fractal connectivity is known to be a basis for brain organisation and complexity, fractal analysis allows to quantify complex patterns found in neuroscience and to make predictions about clinical outcomes [85]. The most frequently used fractal descriptors are fractal dimension, D (defined as a statistical index of complexity comparing how a detail in a cell changes with the scale at which it is measured) and lacunarity, L (defined as a measure of how cells fill the available space).

Fractal analysis can be performed with the use of different types of images, including SEM micrographs [84], confocal micrographs [84], fluorescence images [87], magnetic resonance images [88], etc. The starting point for a typical fractal analysis consists of thresholding the image to eliminate background noise and is followed by converting the image to a binary format and outlining the shape of a cellular network. As-formed binary silhouettes of the neurons, as depicted in Figure 4, are further quantified with the use of different algorithms. Depending on the magnification, fractal analysis could be performed either for a single neuron or for a neural network. Even though fractal analysis of a neural network could be done using optical imaging, this method would not be useful to visualise features on optically nontransparent materials. The use of SEM allows to perform fractal analysis of cells on a variety of substrates, regardless of their degree of transparency [34].

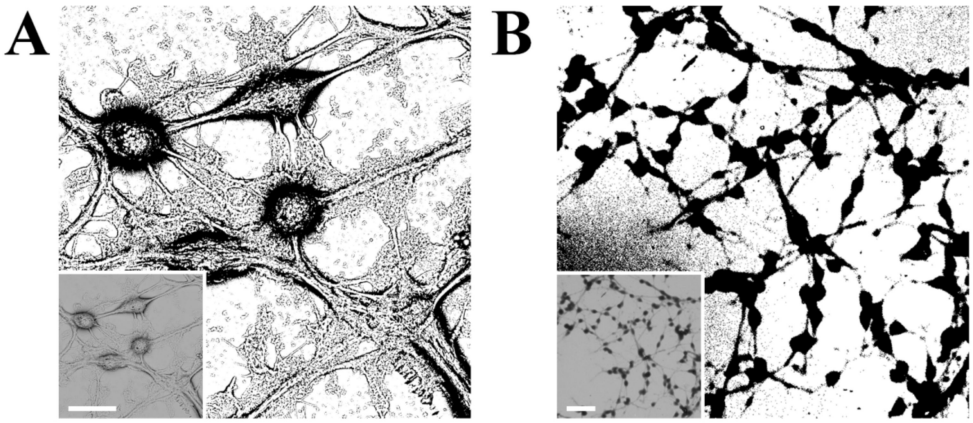

Figure 4. Binary images of B35 cells in (**A**) high magnification (scale bar is 20 µm), and (**B**) low magnification (scale bar is 100 µm), with source SEM micrographs (Phenom ProX, 10 kV) as the insets.

Fractal analysis is particularly suitable for the investigation of dendritic arborisation, which is defined as a process in which neurons create new synapses by forming new dendritic trees and branches [89]. In this context, a small value of D should be correlated with cells exhibiting a simple, uncomplicated structure, for example those in the early stage of development [90]. On the other hand, cells exhibiting complex structures with a high level of branching exhibit a large value of D. In a recent work, Smith et al. [84] analysed three-dimensional SEM images of rat neurons to investigate the degree to which

neurons resemble fractals, as well as the origins of this fractality and its impact on neuron functionality. The results showed that different types of neuron were characterised by different values of D, and, in general, D was higher for neurons with a greater need for connectivity, for example hyperbranched Purkinje cells [91]. D was also found to be affected by pathological states of neural tissue, for example those associated with Alzheimer's disease [92]. The disturbances in fractal branching decreased the degree of interconnections between neighbouring neurons and limited transfer of nutrients and energy.

Although D is suitable for detecting the changes in branching structure, it is not sensitive to some features that are hard to visually recognise, e.g., the relation of soma size to process length [93]. In this case, L can be used to distinguish similarly looking microglial morphologies with the same D. In fact, the term lacunarity was introduced to describe the gaps between various features of fractal objects, allowing to distinguish between different texture details [94]. Therefore, L is suitable to assess the degree of clustering within a neural network, as well as to distinguish between dense structures and scattered/non-connected objects [88]. Different values of L calculated basing on SEM images of two neural cell populations may indicate that either these cells originate from different parts of the brain, or one group represents damaged cells. For instance, L was found to be an indicator of Alzheimer's disease, as this pathology was manifested through the presence of lacunar formations in the brain [95]. Additionally, L was found to increase with the development of a disease, resulting in an anomalous functioning of the brain.

4.3. Textural Descriptors

Recent advances in digital imaging and computing allowed for the development of imaging processing tools aimed to quantify the perceive texture of an image. In a general meaning, image texture provides information about spatial arrangement of intensities (grey bands) in an image [96] and can be qualitatively described with the use of following descriptors: regularity, directionality, fineness, coarseness, smoothness, granulation, randomness, lineation, being mottled, irregular, or hummocky [97,98]. The use of these descriptors is usually called "perceptual characterisation" and is useful for a coarse classification of textures [98]. A quantitative description of a texture requires the use of advanced computational methods, for instance a multiresolution decomposition using Gabor wavelets [98], artificial neural networks [99], as well as a textural analysis based on a gray-level co-occurrence matrix (GLCM) [100].

Since SEM enables to capture fine shapes of biological objects, this technique has been routinely used to collect images suitable for the analysis of textural descriptors [99–102]. Still, it should be borne in mind that the processing method could affect the texture of a sample. For instance, too harsh dehydration could result in the formation of defects in the plasma membrane of mammalian cells. The presence of cracks and crinkles has been previously noted for samples after freeze-drying, particularly those not treated with a fixing agent [34]. Actually, using glutaraldehyde and ethanol dehydration strengthens the surface of a cell through cross-linking the collagen present in the extracellular matrix.

To perform a quantitative analysis, however, a high number of SEM micrographs should be collected and processed point by point [99]. The most popular texture analysis method, GLCM, allows to present surface details of a sample with a mathematical function (procedural texture), and to extract the following texture descriptors: angular second moment, entropy, correlation, contrast, and inverse different moment [99,103]. A set of texture descriptors can be then applied as a base for a high efficiency classification tool that will allow to recognise elements of an SEM image on the basis of the texture of image pixel.

So far, there are only few literature studies reporting the application of textural analysis in biological sciences, including the detection of polysaccharide in raspberry powders [99], and cervical precancerous [102]. Nevertheless, the presence of different textures in SEM images of B35 cells, associated with a cell's body, an extracellular matrix, neurites, etc. (Figure 5), suggests that the textural analysis should be also suitable for the analysis of neural cells.

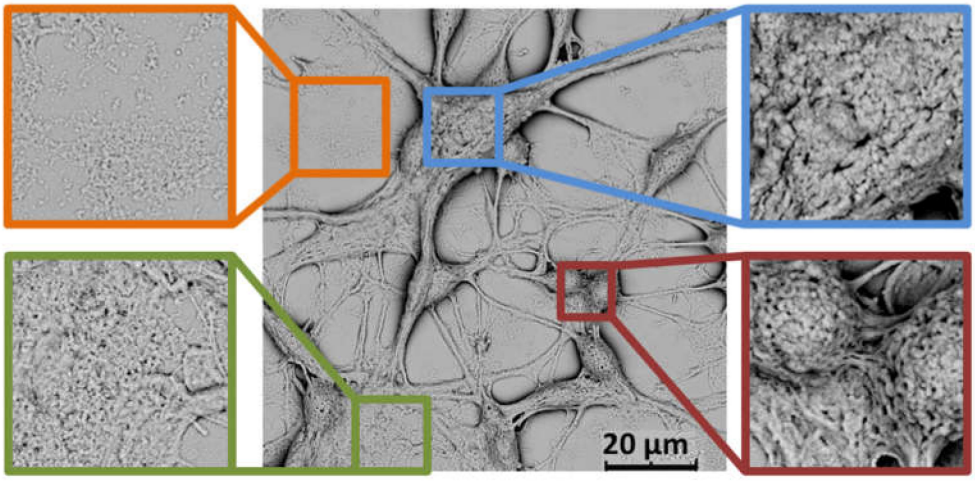

Figure 5. SEM images showing different textures typical for neural cells on the example of rat neuroblastoma B35 cells. The defects present on the surface of cells should be related to a dehydration process. SEM micrographs were collected by means of a Phenom ProX scanning electron microscope operating at 10 kV.

5. Conclusions

Scanning electron microscopy appears as an extremely useful tool to analyse morphology of different types of cells, including prokaryotic and eukaryotic ones. Providing that a biological sample is prepared with special care, for instance using the optimised protocol presented in this study, SEM allows to achieve the resolution of 50 nm, which is more than enough to investigate cell morphology in detail. Therefore, SEM can be efficiently used to monitor even slight variations in cell dimensions and morphology, which could be related with the onset of important changes in the state of cells. Due to the versatility of morphometric descriptors and their relation with molecular processes, it is possible to apply SEM as a convenient screening method to detect cell pathology.

Funding: This research was funded by the National Science Centre, Poland [OPUS 2019/35/B/ST5/00995] and the Silesian University of Technology, Poland [04/040/SDU/10-22-03, 04/040/SDU/10-21-01, 04/040/BKM21/0178, and 04/040/RGJ21/0147].

Conflicts of Interest: The authors declare no conflict of interest.

References

1. Vihinen, H.; Belevich, I.; Jokitalo, E. Three dimensional electron microscopy of cellular organelles by serial block face SEM and ET. *Microsc. Anal.* **2013**, *27*, 7–10.
2. Smith, K.C.A.; Wells, O.C.; McMullan, D. The fiftieth anniversary of the first applications of the scanning electron microscope in materials research. *Phys. Procedia* **2008**, *1*, 3–12. [CrossRef]
3. Dokland, T.; Hutmacher, D.W.; Ng, M.M.-L.; Schantz, J.-T. *Techniques in Microscopy for Biomedical Applications*; World Scientific: Singapore, 2006; Volume 2. [CrossRef]
4. Goldstein, A.; Soroka, Y.; Frušić-Zlotkin, M.; Popov, I.; Kohen, R. High resolution SEM imaging of gold nanoparticles in cells and tissues. *J. Microsc.* **2014**, *256*, 237–247. [CrossRef] [PubMed]
5. Schatten, H. Low voltage high-resolution SEM (LVHRSEM) for biological structural and molecular analysis. *Micron* **2011**, *42*, 175–185. [CrossRef]
6. Idalia, V.-M.N.; Bernardo, F. Escherichia coli as a Model Organism and Its Application in Biotechnology. In *Escherichia coli—Recent Advances on Physiology, Pathogenesis and Biotechnological Applications*; IntechOpen: London, UK, 2017; ISBN 978-953-51-3330-8.
7. Otey, C.A.; Boukhelifa, M.; Maness, P. B35 neuroblastoma cells: An easily transfected, cultured cell model of central nervous system neurons. *Methods Cell Biol.* **2003**, *2003*, 287–304. [CrossRef]
8. Rahmah Aid, S.; Nur Anis Awadah Nik Zain, N.; Nadhirah Mohd Rashid, N.; Hara, H.; Shameli, K.; Koji, I. A Study on Biological Sample Preparation for High Resolution Imaging of Scanning Electron Microscope. *J. Phys. Conf. Ser.* **2020**, *1447*, 012034. [CrossRef]
9. Fischer, E.R.; Hansen, B.T.; Nair, V.; Hoyt, F.H.; Dorward, D.W. Scanning Electron Microscopy. *Curr. Protoc. Microbiol.* **2012**, *25*, 2B.2.1–2B.2.47. [CrossRef]

10. Singh, H.; Bishen, K.A.; Garg, D.; Sukhija, H.; Sharma, D.; Tomar, U. Fixation and Fixatives: Roles and Functions—A Short Review. *Dent. J. Adv. Stud.* **2019**, *7*, 51–55. [CrossRef]
11. Migneault, I.; Dartiguenave, C.; Bertrand, M.J.; Waldron, K.C. Glutaraldehyde: Behavior in aqueous solution, reaction with proteins, and application to enzyme crosslinking. *Biotechniques* **2004**, *37*, 790–802. [CrossRef]
12. Hopwood, D. Theoretical and practical aspects of glutaraldehyde fixation. *Histochem. J.* **1972**, *4*, 267–303. [CrossRef]
13. Hopwood, D. Some aspects of fixation with glutaraldehyde. A biochemical and histochemical comparison of the effects of formaldehyde and glutaraldehyde fixation on various enzymes and glycogen, with a note on penetration of glutaraldehyde into liver. *J. Anat.* **1967**, *101*, 83–92.
14. Zhang, Y.; Huang, T.; Jorgens, D.M.; Nickerson, A.; Lin, L.-J.; Pelz, J.; Gray, J.W.; López, C.S.; Nan, X. Quantitating morphological changes in biological samples during scanning electron microscopy sample preparation with correlative super-resolution microscopy. *PLoS ONE* **2017**, *12*, e0176839. [CrossRef]
15. Wisse, E.; Braet, F.; Duimel, H.; Vreuls, C.; Koek, G.; Damink, S.W.O.; van den Broek, M.A.; De Geest, B.; Dejong, C.H.; Tateno, C.; et al. Fixation methods for electron microscopy of human and other liver. *World J. Gastroenterol.* **2010**, *16*, 2851. [CrossRef]
16. Dassanayake, R.P.; Falkenberg, S.M.; Stasko, J.A.; Shircliff, A.L.; Lippolis, J.D.; Briggs, R.E. Identification of a reliable fixative solution to preserve the complex architecture of bacterial biofilms for scanning electron microscopy evaluation. *PLoS ONE* **2020**, *15*, e0233973. [CrossRef]
17. Fischer Scientific Osmium(VIII)-Tetroxide, 99.9+% MSDS. Available online: https://fscimage.fishersci.com/msds/96359.htm (accessed on 16 August 2021).
18. Mhatre, S.; Singh, N.K.; Wood, J.M.; Parker, C.W.; Pukall, R.; Verbarg, S.; Tindall, B.J.; Neumann-Schaal, M.; Venkateswaran, K. Description of Chloramphenicol Resistant Kineococcus rubinsiae sp. nov. Isolated From a Spacecraft Assembly Facility. *Front. Microbiol.* **2020**, *11*, 1957. [CrossRef]
19. Fischer Scientific Paraformaldehyde MSDS. Available online: https://fscimage.fishersci.com/msds/18000.htm (accessed on 16 August 2021).
20. Cancer Diagnostics Inc Methacarn MSDS. Available online: https://www.msdsdigital.com/methacarn-msds (accessed on 16 August 2021).
21. Gusnard, D.; Kirschner, R.H. Cell and organelle shrinkage during preparation for scanning electron microscopy: Effects of fixation, dehydration and critical point drying. *J. Microsc.* **1977**, *110*, 51–57. [CrossRef]
22. Braet, F.; De Zanger, R.; Wisse, E. Drying cells for SEM, AFM and TEM by hexamethyldisilazane: A study on hepatic endothelial cells. *J. Microsc.* **1997**, *186*, 84–87. [CrossRef]
23. Moran, P.; Coats, B. Biological Sample Preparation for SEM Imaging of Porcine Retina. *Micros. Today* **2012**, *20*, 28–31. [CrossRef]
24. Nikara, S.; Ahmadi, E.; Nia, A.A. Effects of different preparation techniques on the microstructural features of biological materials for scanning electron microscopy. *J. Agric. Food Res.* **2020**, *2*, 100036. [CrossRef]
25. Chissoe, W.F.; Vezey, E.L.; Skvarla, J.J. Hexamethyldisilazane as a Drying Agent for Pollen Scanning Electron Microscopy. *Biotech. Histochem.* **2009**, *69*, 192–198. [CrossRef]
26. Hazrin-Chong, N.H.; Manefield, M. An alternative SEM drying method using hexamethyldisilazane (HMDS) for microbial cell attachment studies on sub-bituminous coal. *J. Microbiol. Methods* **2012**, *90*, 96–99. [CrossRef] [PubMed]
27. Grate, J.W.; Warner, M.G.; Pittman, J.W.; Dehoff, K.J.; Wietsma, T.W.; Zhang, C.; Oostrom, M. Silane modification of glass and silica surfaces to obtain equally oil-wet surfaces in glass-covered silicon micromodel applications. *Water Resour. Res.* **2013**, *49*, 4724–4729. [CrossRef]
28. Sigma Aldrich Hexamethyldisilazane MSDS. Available online: https://www.sigmaaldrich.com/RS/en/substance/hexamethyldisilazane16139999973 (accessed on 16 August 2021).
29. Tai, S.S.W.; Tang, X.M. Manipulating biological samples for environmental scanning electron microscopy observation. *Scanning* **2001**, *23*, 267–272. [CrossRef] [PubMed]
30. Bergmans, L.; Moisiadis, P.; Van Meerbeek, B.; Quirynen, M.; Lambrechts, P. Microscopic observation of bacteria: Review highlighting the use of environmental SEM. *Int. Endod. J.* **2005**, *38*, 775–788. [CrossRef]
31. Muscariello, L.; Rosso, F.; Marino, G.; Giordano, A.; Barbarisi, M.; Cafiero, G.; Barbarisi, A. A critical overview of ESEM applications in the biological field. *J. Cell. Physiol.* **2005**, *205*, 328–334. [CrossRef]
32. Bennett, P.C.; Engel, A.S.; Roberts, J.A. Counting and Imaging Bacteria on Mineral Surfaces. In *Methods for Study of Microbe—Mineral Interactions*; Clay Minerals Society: Chantilly, VA, USA, 2006; Volume 14, pp. 37–77. ISBN 188120815X.
33. Korpa, A.; Trettin, R. The influence of different drying methods on cement paste microstructures as reflected by gas adsorption: Comparison between freeze-drying (F-drying), D-drying, P-drying and oven-drying methods. *Cem. Concr. Res.* **2006**, *36*, 634–649. [CrossRef]
34. Lee, J.T.Y.; Chow, K.L. SEM sample preparation for cells on 3D scaffolds by freeze-drying and HMDS. *Scanning* **2012**, *34*, 12–25. [CrossRef]
35. Velasco, D.; Benito, L.; Fernández-Gutiérrez, M.; San Román, J.; Elvira, C. Preparation in supercritical CO2 of porous poly(methyl methacrylate)-poly(l-lactic acid) (PMMA-PLA) scaffolds incorporating ibuprofen. *J. Supercrit. Fluids* **2010**, *54*, 335–341. [CrossRef]
36. Rai, B.; Lin, J.L.; Lim, Z.X.H.; Guldberg, R.E.; Hutmacher, D.W.; Cool, S.M. Differences between in vitro viability and differentiation and in vivo bone-forming efficacy of human mesenchymal stem cells cultured on PCL–TCP scaffolds. *Biomaterials* **2010**, *31*, 7960–7970. [CrossRef]

37. Golding, C.G.; Lamboo, L.L.; Beniac, D.R.; Booth, T.F. The scanning electron microscope in microbiology and diagnosis of infectious disease. *Sci. Rep.* **2016**, *6*, 26516. [CrossRef]
38. Heu, R.; Shahbazmohamadi, S.; Yorston, J.; Capeder, P. Target Material Selection for Sputter Coating of SEM Samples. *Micros. Today* **2019**, *27*, 32–36. [CrossRef]
39. Fichtman, B.; Shaulov, L.; Harel, A. Imaging Metazoan Nuclear Pore Complexes by Field Emission Scanning Electron Microscopy. *Methods Cell Biol.* **2014**, *122*, 41–58. [CrossRef]
40. Hover, T.; Maya, T.; Ron, S.; Sandovsky, H.; Shadkchan, Y.; Kijner, N.; Mitiagin, Y.; Fichtman, B.; Harel, A.; Shanks, R.M.Q.; et al. Mechanisms of Bacterial (Serratia marcescens) Attachment to, Migration along, and Killing of Fungal Hyphae. *Appl. Environ. Microbiol.* **2016**, *82*, 2585–2594. [CrossRef]
41. Goldberg, M.W.; Allen, T.D. High resolution scanning electron microscopy of the nuclear envelope: Demonstration of a new, regular, fibrous lattice attached to the baskets of the nucleoplasmic face of the nuclear pores. *J. Cell Biol.* **1992**, *119*, 1429–1440. [CrossRef]
42. Bray, D. Critical Point Drying of Biological Specimens for Scanning Electron Microscopy. *Supercrit. Fluid Methods Protoc.* **2003**, 235–243. [CrossRef]
43. Czerwińska-Główka, D.; Przystaś, W.; Zabłocka-Godlewska, E.; Student, S.; Cwalina, B.; Łapkowski, M.; Krukiewicz, K. Bacterial Surface Colonization of Sputter-Coated Platinum Films. *Materials (Basel).* **2020**, *13*, 2674. [CrossRef]
44. Czerwińska-Główka, D.; Przystaś, W.; Zabłocka-Godlewska, E.; Student, S.; Cwalina, B.; Łapkowski, M.; Krukiewicz, K. Electrically-responsive antimicrobial coatings based on a tetracycline-loaded poly(3,4-ethylenedioxythiophene) matrix. *Mater. Sci. Eng. C* **2021**, *123*, 112017. [CrossRef]
45. Skorupa, M.; Więcławska, D.; Czerwińska-Główka, D.; Skonieczna, M.; Krukiewicz, K. Dopant-dependent electrical and biological functionality of pedot in bioelectronics. *Polymers* **2021**, *13*, 1948. [CrossRef]
46. Guzev, V.S.; Byzov, B.A. Morphometric analysis of bacteria associated with soil millipedes. *Microbiology* **2006**, *75*, 219–225. [CrossRef]
47. Gomes, L.C.; Mergulhão, F.J. SEM analysis of surface impact on biofilm antibiotic treatment. *Scanning* **2017**, *2017*, 2960194. [CrossRef]
48. Kim, K.W. High-resolution imaging of the microbial cell surface. *J. Microbiol.* **2016**, *54*, 703–708. [CrossRef] [PubMed]
49. Hannig, C.; Follo, M.; Hellwig, E.; Al-Ahmad, A. Visualization of adherent micro-organisms using different techniques. *J. Med. Microbiol.* **2010**, *59*, 1–7. [CrossRef] [PubMed]
50. Dai, X.; Zhu, M. High Osmolarity Modulates Bacterial Cell Size through Reducing Initiation Volume in Escherichia coli. *mSphere* **2018**, *3*, 17. [CrossRef] [PubMed]
51. Young, K.D. The Selective Value of Bacterial Shape. *Microbiol. Mol. Biol. Rev.* **2006**, *70*, 660–703. [CrossRef]
52. Varma, A.; Young, K.D. FtsZ Collaborates with Penicillin Binding Proteins To Generate Bacterial Cell Shape in Escherichia coli. *J. Bacteriol.* **2004**, *186*, 6768–6774. [CrossRef]
53. Ursell, T.; Lee, T.K.; Shiomi, D.; Shi, H.; Tropini, C.; Monds, R.D.; Colavin, A.; Billings, G.; Bhaya-Grossman, I.; Broxton, M.; et al. Rapid, precise quantification of bacterial cellular dimensions across a genomic-scale knockout library. *BMC Biol.* **2017**, *15*, 1–15. [CrossRef]
54. Zheng, H.; Ho, P.-Y.; Jiang, M.; Tang, B.; Liu, W.; Li, D.; Yu, X.; Kleckner, N.E.; Amir, A.; Liu, C. Interrogating the Escherichia coli cell cycle by cell dimension perturbations. *Proc. Natl. Acad. Sci. USA* **2016**, *113*, 15000–15005. [CrossRef]
55. Harris, L.K.; Theriot, J.A. Surface Area to Volume Ratio: A Natural Variable for Bacterial Morphogenesis. *Trends Microbiol.* **2018**, *26*, 815–832. [CrossRef]
56. Ojkic, N.; Serbanescu, D.; Banerjee, S. Surface-to-volume scaling and aspect ratio preservation in rod-shaped bacteria. *Elife* **2019**, *8*, e47033. [CrossRef]
57. Paluch, E.; Heisenberg, C.-P. Biology and Physics of Cell Shape Changes in Development. *Curr. Biol.* **2009**, *19*, R790–R799. [CrossRef]
58. Abdel Wahab, S.I.; Abdul, A.B.; Alzubairi, A.S.; Mohamed Elhassan, M.; Mohan, S. In vitro ultramorphological assessment of apoptosis induced by Zerumbone on (HeLa). *J. Biomed. Biotechnol.* **2009**, *2009*, 769568. [CrossRef]
59. Toth, S.R. Cell Cycle-related Morphological Changes of Feline Lymphoid Cells as Revealed by Electron Microscopy. *Cancer Res.* **1981**, *41*, 4727–4736.
60. Pasqualato, A.; Palombo, A.; Cucina, A.; Mariggiò, M.A.; Galli, L.; Passaro, D.; Dinicola, S.; Proietti, S.; D'Anselmi, F.; Coluccia, P.; et al. Quantitative shape analysis of chemoresistant colon cancer cells: Correlation between morphotype and phenotype. *Exp. Cell Res.* **2012**, *318*, 835–846. [CrossRef]
61. Chen, S.; Zhao, M.; Wu, G.; Yao, C.; Zhang, J. Recent advances in morphological cell image analysis. *Comput. Math. Methods Med.* **2012**, *2012*, 101536. [CrossRef]
62. Venkatesan, P.; Das, S.; Krishnan, M.M.R.; Chakraborty, C.; Chaudhury, K.; Mandal, M. Effect of AEE788 and/or Celecoxib on colon cancer cell morphology using advanced microscopic techniques. *Micron* **2010**, *41*, 247–256. [CrossRef]
63. Timashev, P.S.; Vedunova, M.V.; Guseva, P.D.; Ponimaskin, E.; Deiwick, A.; Mishchenko, T.; Mitroshina, E.V.; Koroleva, A.V.; Pimashkin, A.S.; Mukhina, I.V.; et al. 3D in vitro platform produced by two-photon polymerization for the analysis of neural network formation and function. *Biomed. Phys. Eng. Express* **2016**, *2*, 035001. [CrossRef]

64. Lobo, J.; See, E.Y.S.; Biggs, M.; Pandit, A. An insight into morphometric descriptors of cell shape that pertain to regenerative medicine. *J. Tissue Eng. Regen. Med.* **2016**, 539–553. [CrossRef]
65. Pincus, Z.; Theriot, J.A. Comparison of quantitative methods for cell-shape analysis. *J. Microsc.* **2007**, *227*, 140–156. [CrossRef]
66. Yang, C.-Y.; Huang, W.-Y.; Chen, L.-H.; Liang, N.-W.; Wang, H.-C.; Lu, J.; Wang, X.; Wang, T.-W. Neural tissue engineering: The influence of scaffold surface topography and extracellular matrix microenvironment. *J. Mater. Chem. B* **2021**, *9*, 567–584. [CrossRef]
67. Vishwakarma, S.K.; Bardia, A.; Lakkireddy, C.; Paspala, S.A.B.; Khan, A.A. Bioengineering Human Neurological Constructs Using Decellularized Meningeal Scaffolds for Application in Spinal Cord Injury. *Front. Bioeng. Biotechnol.* **2018**, *6*, 1–19. [CrossRef]
68. Lynch, K.; Skalli, O.; Sabri, F. Growing Neural PC-12 Cell on Crosslinked Silica Aerogels Increases Neurite Extension in the Presence of an Electric Field. *J. Funct. Biomater.* **2018**, *9*, 30. [CrossRef] [PubMed]
69. Zychowicz, M.; Mehn, D.; Ruiz, A.; Frontczak-Baniewicz, M.; Rossi, F.; Buzanska, L. Patterning of human cord blood-derived stem cells on single cell posts and lines: Implications for neural commitment. *Acta Neurobiol. Exp. (Wars).* **2012**, *72*, 325–336. [PubMed]
70. Simitzi, C.; Ranella, A.; Stratakis, E. Controlling the morphology and outgrowth of nerve and neuroglial cells: The effect of surface topography. *Acta Biomater.* **2017**, *51*, 21–52. [CrossRef] [PubMed]
71. Chua, J.S.; Chng, C.-P.; Moe, A.A.K.; Tann, J.Y.; Goh, E.L.K.; Chiam, K.-H.; Yim, E.K.F. Extending neurites sense the depth of the underlying topography during neuronal differentiation and contact guidance. *Biomaterials* **2014**, *35*, 7750–7761. [CrossRef]
72. Park, M.; Oh, E.; Seo, J.; Kim, M.-H.; Cho, H.; Choi, J.Y.; Lee, H.; Choi, I.S. Control over Neurite Directionality and Neurite Elongation on Anisotropic Micropillar Arrays. *Small* **2016**, *12*, 1148–1152. [CrossRef]
73. Das, K.P.; Freudenrich, T.M.; Mundy, W.R. Assessment of PC12 cell differentiation and neurite growth: A comparison of morphological and neurochemical measures. *Neurotoxicol. Teratol.* **2004**, *26*, 397–406. [CrossRef]
74. Chen-Yang, Y.; Feng, Z.V.; Chen, W.S.; Keratithamkul, K.; Stoick, M.; Kapala, B.; Johnson, E.; Huang, A.-C.; Chin, T.Y.; Yang, M.-L. Degradation of the electrospun silica nanofiber in a biological medium for primary hippocampal neuron–effect of surface modification. *Int. J. Nanomedicine* **2016**, *11*, 729. [CrossRef]
75. Su, W.-T.; Liao, Y.-F.; Wu, T.-W.; Wang, B.-J.; Shih, Y.-Y. Microgrooved patterns enhanced PC12 cell growth, orientation, neurite elongation, and neuritogenesis. *J. Biomed. Mater. Res. Part. A* **2013**, *101A*, 185–194. [CrossRef]
76. Haq, F.; Anandan, V.; Keith, C.; Zhang, G. Neurite development in PC12 cells cultured on nanopillars and nanopores with sizes comparable with fi lopodia. *Int. J. Nanomedicine* **2007**, *2*, 107–115. [CrossRef]
77. Repić, T.; Madirazza, K.; Bektur, E.; Sapunar, D. Characterization of dorsal root ganglion neurons cultured on silicon micro-pillar substrates. *Sci. Rep.* **2016**, *6*, 39560. [CrossRef]
78. Radotić, V.; Braeken, D.; Drviš, P.; Mattotti, M.; Kovačić, D. Advantageous environment of micro-patterned, high-density complementary metal–oxide–semiconductor electrode array for spiral ganglion neurons cultured in vitro. *Sci. Rep.* **2018**, *8*, 7446. [CrossRef]
79. Rocchi, M.B.L.; Sisti, D.; Albertini, M.C.; Teodori, L. Current trends in shape and texture analysis in neurology: Aspects of the morphological substrate of volume and wiring transmission. *Brain Res. Rev.* **2007**, *55*, 97–107. [CrossRef]
80. Tonazzini, I.; Masciullo, C.; Savi, E.; Sonato, A.; Romanato, F.; Cecchini, M. Neuronal contact guidance and YAP signaling on ultra-small nanogratings. *Sci. Rep.* **2020**, *10*, 3742. [CrossRef]
81. Sołtys, Z.; Ziaja, M.; Pawliński, R.; Setkowicz, Z.; Janeczko, K. Morphology of reactive microglia in the cerebral cortex. Fractal analysis and complementary quantitative methods. *J. Neurosci. Res.* **2001**, *63*, 90–97. [CrossRef]
82. Fernández-Arjona, M. del M.; Grondona, J.M.; Granados-Durán, P.; Fernández-Llebrez, P.; López-Ávalos, M.D. Microglia Morphological Categorization in a Rat Model of Neuroinflammation by Hierarchical Cluster and Principal Components Analysis. *Front. Cell. Neurosci.* **2017**, *11*, 1–22. [CrossRef]
83. Perez-Pouchoulen, M.; VanRyzin, J.W.; McCarthy, M.M. Morphological and Phagocytic Profile of Microglia in the Developing Rat Cerebellum. *eNeuro* **2015**, *2*, 36–51. [CrossRef]
84. Smith, J.H.; Rowland, C.; Harland, B.; Moslehi, S.; Montgomery, R.D.; Schobert, K.; Watterson, W.J.; Dalrymple-Alford, J.; Taylor, R.P. How neurons exploit fractal geometry to optimize their network connectivity. *Sci. Reports 2021 111* **2021**, *11*, 1–13. [CrossRef]
85. John, A.M.; Elfanagely, O.; Ayala, C.A.; Cohen, M.; Prestigiacomo, C.J. The utility of fractal analysis in clinical neuroscience. *Rev. Neurosci.* **2015**, *26*, 633–645. [CrossRef]
86. Mandelbrot, B. *Fractals: Form, chance, and dimension*; W.H. Freeman: San Francisco, CA, USA, 1977; ISBN 9780716704737.
87. Jakubowicz-Gil, J.; Rzeski, W.; Zdzisinska, B.; Dobrowolski, P.; Gawron, A. Cell death and neuronal arborization upon quercetin treatment in rat neurons. *Acta Neurobiol. Exp.* **2008**, *68*, 139–146.
88. Katsaloulis, P.; Verganelakis, D.A.; Provata, A. Fractal dimension and lacunarity of tractography images of the human brain. *Fractals* **2009**, *17*, 181–189. [CrossRef]
89. Wang, S.; Tanzi, R.E.; Li, A. Quantitative Analysis of Neuronal Dendritic Arborization Complexity in Drosophila. *JoVE (J. Vis. Exp.* **2019**, *2019*, e57139. [CrossRef] [PubMed]
90. Smith, T.G.; Marks, W.B.; Lange, G.D.; Sheriff, W.H.; Neale, E.A. A fractal analysis of cell images. *J. Neurosci. Methods* **1989**, *27*, 173–180. [CrossRef]
91. Takeda, T.; Ishikawa, A.; Ohtomo, K.; Kobayashi, Y.; Matsuoka, T. Fractal dimension of dendritic tree of cerebellar Purkinje cell during onto- and phylogenetic development. *Neurosci. Res.* **1992**, *13*, 19–31. [CrossRef]

92. Mufson, E.J.; Mahady, L.; Waters, D.; Counts, S.E.; Perez, S.E.; DeKosky, S.T.; Ginsberg, S.D.; Ikonomovic, M.D.; Scheff, S.W.; Binder, L.I. Hippocampal plasticity during the progression of Alzheimer's disease. *Neuroscience* **2015**, *309*, 51–67. [CrossRef]
93. Nichita, M.V.; Paun, M.A.; Paun, V.A.; Paun, V.P. Fractal analysis of brain glial cells. Fractal dimension and lacunarity. *UPB Sci. Bull. Ser. A Appl. Math. Phys.* **2019**, *81*, 273–284.
94. Armatas, G.S.; Kolonia, K.M.; Pomonis, P.J. Morphometry of porous solids: Lacunarity, fractal dimensions, connectivity, and some topological similarities with neurons. *Langmuir* **2002**, *18*, 10421–10429. [CrossRef]
95. Bordescu, D.; Paun, M.A.; Paun, V.A.; Paun, V.P. Fractal analysis of neuroimagistics. Lacunarity degree, a precious indicator in the detection of Alzheimer's disease. *UPB Sci. Bull. Ser. A Appl. Math. Phys.* **2018**, *80*, 309–320.
96. Shapiro, L.G.; Stockman, G. . *Computer Vision*; Prentice Hall: Upper Saddle River, NJ, USA, 2001.
97. Haralick, R.M. Statistical and Structural Approaches to Texture. *Proc. IEEE* **1979**, *67*, 786–804.
98. Wu, P.; Manjunath, B.S.; Newsam, S.; Shin, H.D. A texture descriptor for browsing and similarity retrieval. *Signal. Process. Image Commun.* **2000**, *1–2*, 33–43. [CrossRef]
99. Przybył, K.; Koszela, K.; Adamski, F.; Samborska, K.; Walkowiak, K.; Polarczyk, M. Deep and Machine Learning Using SEM, FTIR, and Texture Analysis to Detect Polysaccharide in Raspberry Powders. *Sensors 2021, Vol. 21, Page 5823* **2021**, *21*, 5823. [CrossRef]
100. Tsutsui, K.; Terasaki, H.; Uto, K.; Maemura, T.; Hiramatsu, S.; Hayashi, K.; Moriguchi, K.; Morito, S. A methodology of steel microstructure recognition using SEM images by machine learning based on textural analysis. *Mater. Today Commun.* **2020**, *25*, 101514. [CrossRef]
101. Zhang, H.; He, C.; Yu, M.; Fu, J. Texture feature extraction and classification of SEM images of wheat straw/polypropylene composites in accelerated aging test. *Adv. Mater. Sci. Eng.* **2015**, *2015*, 1–10. [CrossRef]
102. Jusman, Y.; Ng, S.-C.; Hasikin, K.; Kurnia, R.; Osman, N.A.A.; Teoh, K.H. A system for detection of cervical precancerous in field emission scanning electron microscope images using texture features. *J. Innov. Opt. Health Sci.* **2017**, *10*, 10. [CrossRef]
103. Haralick, R.M.; Dinstein, I.; Shanmugam, K. Textural Features for Image Classification. *IEEE Trans. Syst. Man Cybern.* **1973**, *6*, 610–621. [CrossRef]